

**UNIVERSIDADE FEDERAL DO RIO GRANDE DO SUL  
INSTITUTO DE GEOCIÊNCIAS  
PROGRAMA DE PÓS-GRADUAÇÃO EM GEOCIÊNCIAS**

**Lu-Hf EM ZIRCÃO POR LA-MC-ICP-MS**

**ANELISE LOSANGELA BERTOTTI**

**ORIENTADOR – Prof. Dr. Farid Chemale Jr.**

**Volume I**

**Porto Alegre – 2012**

**UNIVERSIDADE FEDERAL DO RIO GRANDE DO SUL  
INSTITUTO DE GEOCIÊNCIAS  
PROGRAMA DE PÓS-GRADUAÇÃO EM GEOCIÊNCIAS**

**Lu-Hf EM ZIRCÃO POR LA-MC-ICP-MS**

**ANELISE LOSANGELA BERTOTTI**

**ORIENTADOR – Prof. Dr. Farid Chemale Jr.**

**BANCA EXAMINADORA**

Prof. Dr. Massimo Matteini – Instituto de Geociências, Universidade de  
Brasília

Prof. Dr. Miguel A. S. Basei - Instituto de Geociências, Universidade de São  
Paulo

Prof. Dr. Márcio M. Pimentel – Instituto de Geociências, Universidade Federal  
do Rio Grande do Sul

Tese de Doutorado apresentada como  
requisito parcial para a obtenção do  
Título de Doutor em Ciências.

Porto Alegre – 2012

Bertotti, Anelise Losangela

Lu-Hf EM ZIRCÃO POR LA-MC-ICP-MS / Anelise  
Losangela Bertotti. – Porto Alegre: IGEO/UFRGS, 2012.  
[162f.] il.

Tese (Doutorado) - Universidade Federal do Rio Grande  
do Sul. Programa de Pós-Graduação em Geociências, Porto  
Alegre, RS - BR, 2012.

Orientador: Prof. Dr. Farid Chemale Júnior.

1. Metodologia de Lu-Hf. 2. LA-ICP-MS. 3. Zircão. I. Título.

---

Catalogação na Publicação  
Biblioteca do Instituto de Geociências - UFRGS  
Alexandre Ribas Semeler CRB 10/1900

**Dedico esta tese aos amores da minha vida**

**Giselda, Nei e Luiza.**

## **AGRADECIMENTOS**

Agradeço o CNPq, pelo fomento da bolsa de doutorado, e a Universidade Federal do Rio Grande do Sul pela oportunidade de inserção na dinâmica científica desta renomada instituição.

Agradeço o Programa de Pós-Graduação em Geociências, ao secretário Roberto M. Pereira e ao Prof. Dr. Elírio Toldo Jr. pela acolhida e o permanente apoio proporcionado.

Agradeço o orientador Prof. Dr. Farid Chemale Jr., pela oportunidade de trabalho no LGI e por sua orientação na trajetória investigativa de quatro anos.

Agradeço o Prof. Dr. Márcio M. Pimentel pela confiança em mim depositada e pela compreensão e gratuidade evidenciada em relação à ressignificação do objeto de investigação em questão.

Agradeço os professores Dra. Carla C. Porcher, Dr. Edinei Koester e Prof. Dr. Rommulo V. Conceição pela atenção, pelos diálogos e lições constantes.

Agradeço os colegas do LGI pelas conversas diárias, companhias no RU, jantas,...: Ana, André, Cris K., Eduardo, Fernanda, Fernando, Gisela, Larissa, Léo, Maria Luiza, Mariana, Renato, Ronei, Tiago. Obrigada pela amizade proporcionada!

Agradeço os colegas da graduação de Geologia e da pós-graduação do Instituto de Geociências da UFRGS que de alguma forma me auxiliaram e me apoiaram nesta caminhada.

Agradeço, obviamente, em especial, o Prof. Dr. Koji Kawashita, que, atualmente, mesmo distante, me auxilia e, por isso, influencia significativamente a minha vida acadêmica.

Agradeço o Prof. Dr. Paul J. Sylvester pela oportunidade de estágio no laboratório de microanálises da Memorial University of Newfoundland e a todos os amigos e colegas de trabalho que me auxiliaram durante a minha estada no Canadá.

Agradeço aos meus familiares pelo apoio e incentivo, em especial aos meus irmãos Suzi e Paulo, a minha carinhosa Tia Tea, às primas, companheiras em potencial, Ingrid e Mônica.

E, fundamentalmente agradeço às pessoas que sempre me compreenderam, me apoiaram e acreditaram em mim no decorrer destes quatro anos de busca e que demonstram, cotidianamente, a imprescindibilidade do amor fraternal: minha mãe Giselda, meu esposo Valdonei e minha princesa Luiza. Obrigada pela afetividade consagrada!

Por fim, não menos importante agradeço a Deus, meu amparo, meu guia, minha força nos momentos de alegria e tristeza. Dou graças a Ti Senhor por esta conquista!

## RESUMO

Atualmente a metodologia de Lu-Hf é um dos métodos mais utilizados na geocronologia, principalmente nas análises *in situ* em zircão por LA-ICP-MS. O interesse na aplicação desta metodologia, quando se dispõe de um sistema como o LA-ICP-MS, deve ser consignado à relativa simplicidade, sensibilidade e rapidez da análise. A alta concentração e a baixa mobilidade do Hf no zircão propiciam razões isotópicas e idades modelos bastante precisas, que podem subsidiar importantes inferências não só quanto à idade de extração mantélica, mas também quanto à sua possível história evolutiva, proveniência e estudos afins. Assim, o projeto de tese foi elaborado com base nos principais objetivos, o aprendizado, a implementação e a aplicação da metodologia de Lu-Hf em zircão por ICP-MS. Zircões de três diferentes áreas, previamente datados pela metodologia U-Pb, foram analisados: Anortosito de Capivarita (Brasil), Ofiolito de Aburrá (Colômbia) e a Bacia de Camamu (Brasil). As análises foram feitas utilizando equipamentos como o ICP-MS Neptune (ThermoFinnigan), e os lasers Excimer 193 nm (ArF, GeoLas) e o 213 UP (Nd:YAG, New Wave). O ofiolito estudado consiste de rochas maficas e ultramáficas. Análises de 12 grãos revelaram  $\varepsilon_{\text{Hf}}(t)$  entre +2,01 e +5,35, enquanto as idades modelo  $T_{\text{DM}}$  resultaram valores em um intervalo entre 1,15 e 1,44 Ga, sugerindo a presença de um magma juvenil com possível contaminação crustal e forte afinidade com as rochas da Província Rondoniana - San Ignacio. Zircões magmáticos e metamórficos do Anortosito de Capivarita, localizado na porção NE do Escudo Sul-Rio-Grandense, fizeram parte de um estudo de comparação para verificar a reprodutibilidade dos dados obtidos pela metodologia de Lu-Hf desenvolvida no LGI. As análises foram feitas primeiramente no LGI-UFGRS (Brasil) e depois no MAFIIC-MUN (Canadá). Os resultados dos dois laboratórios mostraram boa reprodutibilidade, as idades  $T_{\text{DM}}$  e os valores de  $\varepsilon_{\text{Hf}}$  obtidos foram concordantes dentro dos erros experimentais. Estes resultados forneceram informações sobre a proveniência do anortosito e sugeriram uma fonte juvenil para a fusão com algum grau de contaminação crustal Paleoproterozóica. A Bacia de Camamu está relacionada ao rompimento do Gondwana e pertence ao grupo de bacias sedimentares da margem leste brasileira. Zircões detriticos dos Grupos Brotas e Almada, relacionados às fases pré-rifte e rifte da bacia, foram analisados por U-Pb e Lu-Hf. No Grupo Brotas, 70% dos zircões analisados são de idade Cambriana-Vendiana, provenientes do Orógeno Araçuaí-Congo Ocidental levando em conta as medidas de paleocorrente de S-SW para N-NE. No Grupo Almada, as principais fontes dos zircões são Paleoproterozóica e Arqueana, de proveniência direta do embasamento adjacente a Oeste da Bacia de Camamu, consistente com as medidas de paleocorrente de oeste para leste das unidades estudadas. Os zircões paleoproterozóicos e arqueanos analisados, mesmo os Neoproterozóicos e os Eopaleozóicos mostram um forte componente crustal retrabalhado com menor contribuição de crosta juvenil. Contudo, a metodologia de Lu-Hf por LA-ICP-MS aplicada em zircões de diferentes áreas mostrou o potencial em fornecer dados precisos e confiáveis para estudos de proveniência e de crescimento crustal, de modo a redimensionar cada vez mais a geocronologia.

## ABSTRACT

Currently the methodology of Lu-Hf is one of the most widely used in geochronology, especially in *in situ* analysis in zircon by LA-ICP-MS. The interest in the application of this methodology, when it has a system like LA-ICP-MS, should be consigned to relative simplicity, sensitivity and speed of analysis. The high concentration and low mobility of Hf in zircon, provide isotopic ratios and model ages highly accurate that can support not only important inferences about the age of mantle extraction, but also as to its possible evolutionary history, provenance and related studies. Thus, the thesis project was elaborated based on main objectives, learning, implementation and application of Lu-Hf methodology in zircon by ICP-MS. Zircons from three different areas, previously dated by U-Pb method, were analyzed: Capivarita Anorthosite (Brazil), Aburrá Ophiolite (Colombia) and Camamu Basin (Brazil). The Lu-Hf *in situ* analyses were performed using equipments such as Neptune ICP-MS (ThermoFinnigan), and lasers Excimer 193 nm (ArF, GeoLas) and UP 213 (Nd: YAG, New Wave). The studied ophiolite consists of ultramafic and mafic rocks. Analyses of 12 grains revealed  $\epsilon_{\text{Hf}}(t)$  between +2.01 and +5.35, while the  $T_{\text{DM}}$  model ages values resulted in a range between 1.15 and 1.44 Ga, suggesting the presence of a juvenile magma with possible crustal contamination and strong affinity with the rocks of the Rondonian-San Ignacio Province. Magmatic and metamorphic zircons from Capivarita Anorthosite, located in the NE portion of the Sul-Rio-Grandense Shield, were part of a comparison study to verify the reproducibility of obtained data by Lu-Hf methodology developed in the LGI. Analyses were performed first in the LGI-UFGRS (Brazil) and then at MAFIIC-MUN (Canada). Results from both laboratories show good reproducibility,  $T_{\text{DM}}$  ages and  $\epsilon_{\text{Hf}}(t)$  values obtained are in agreement within experimental errors. These results provide information on the origin of anorthosite and suggested a juvenile source for the melt with some degree of Paleoproterozoic crustal contamination. Camamu Basin is related to the breakup of Gondwana and belongs to the group of sedimentary basins on the eastern Brazilian margin. Detrital zircons of Brotas and Almada Groups, related to the pre-rift and rift phases of the basin, were analyzed by U-Pb and Lu-Hf. In Brotas Group, 70% of analyzed zircons are Vendian-Cambrian age, from the Araçuaí-West Congo Belt taking into account the paleocurrent measurements from S-SW to N-NE. In Almada Group, the main sources of the zircons are Paleoproterozoic and Archean, with direct provenance from the basement adjacent to West Camamu Basin which is consistent with the paleocurrent measurements from west to east of the studied units. The analyzed Paleoproterozoic and Archean zircons, even the Neoproterozoic and Eopaleozoic show a strong reworked crustal component with small contribution of juvenile crust. However, the Lu-Hf methodology by LA-ICP-MS applied to zircons from different areas showed the potential to provide accurate and reliable data for provenance and crustal growth studies in order to resize increasingly the geochronology.

## SUMÁRIO

<b>Estrutura da Tese.....</b>	<b>09</b>
<b>1. Introdução.....</b>	<b>10</b>
<b>1.1 Objetivos e Estado da arte.....</b>	<b>11</b>
<b>1.2 Metodologias Empregadas.....</b>	<b>15</b>
<b>1.2.1 Método U-Pb.....</b>	<b>17</b>
<b>1.3 Texto Integrador dos Artigos.....</b>	<b>22</b>
<b>1.4 Referências.....</b>	<b>25</b>
<b>2. Corpo Principal – Artigos Submetidos.....</b>	<b>28</b>
<b>2.1 Primeiro Artigo.....</b>	<b>29</b>
<b>2.2 Segundo Artigo.....</b>	<b>50</b>
<b>2.3 Terceiro Artigo.....</b>	<b>85</b>
<b>Anexo A. Resumo Publicado no 45º Congresso Brasileiro de Geologia.....</b>	<b>01</b>
<b>Anexo B. Resumos Publicados no VII SSAGI.....</b>	<b>02</b>
<b>Anexo C. Artigo Publicado na Precambrian Research.....</b>	<b>10</b>

## ESTRUTURA DA TESE

Esta tese está estruturada em torno de artigos submetidos a periódicos durante o desenvolvimento do Doutorado. Conseqüentemente, sua organização compreende as seguintes partes principais:

- O Capítulo 1 refere-se à *Introdução* da Tese, que apresenta os objetivos e o estado da arte do tema da tese, os métodos de investigação utilizados para o desenvolvimento da mesma, seguidos de uma discussão integradora. (A discussão em foco sintetiza os resultados da pesquisa nas diferentes áreas geológicas da tese e, por fim, descrevem-se as referências dos trabalhos citados no texto do primeiro capítulo.)
- O Capítulo 2 compõe o *Corpo Principal* da Tese, assim compreendido integralmente em três artigos submetidos a diferentes periódicos escritos pelo autor durante o desenvolvimento do Doutorado, com as respectivas cartas de recebimentos dos artigos submetidos.
- Nos *Anexos* encontram-se dois resumos de participação em congresso durante o desenvolvimento do doutorado, um artigo no qual a autora é co-autora e está relacionado ao tema central da tese.

## **Capítulo 1**

### **INTRODUÇÃO**

## 1.1 Objetivos e Estado da Arte

Nas duas últimas décadas, a metodologia de Lu-Hf tornou-se um dos métodos mais utilizados na geocronologia, principalmente nas análises *in situ* em zircão por LA-ICP-MS (Laser Ablation – Ion Coupled Plasma – Mass Spectrometer). Tal fato ocorreu devido a este sistema isotópico complementar estudos de proveniência e de crescimento crustal, assim como pela qualidade e rapidez das análises dos MC-ICP-MS (MC – Multiplier Colector). Além da possibilidade de obter no mesmo grão de zircão a idade U-Pb e os dados de Hf.

Em virtude da necessidade e interesse em desenvolver esta metodologia de datação e pelo fato de contarmos com a qualificada e significativa infra-estrutura do Laboratório de Geologia Isotópica da Universidade Federal do Rio Grande do Sul (LGI-UFRGS) lançamos um olhar prospectivo sobre a viabilidade de um plano de tese. Assim, o presente projeto de tese de doutorado foi elaborado e teve desde o início os seguintes objetivos:

- Aprender a metodologia de Lu-Hf em zircão por LA-ICP-MS por meio de pesquisa bibliográfica para estudos da evolução crustal e de proveniência sedimentar;
- Implementar a metodologia de Lu-Hf em zircão por LA-ICP-MS no LGI-UFRGS a fim de possibilitar estas análises para a comunidade científica;
- Investigar e assimilar os cálculos necessários nesta metodologia para redução dos dados brutos obtidos nas análises *in situ*, e assim desenvolver uma planilha de cálculo do Excel;
- Desenvolver estudos da metodologia de Lu-Hf em zircões de diferentes áreas geológicas, avaliando e sistematizando as informações obtidas em cada amostra.

Para a elaboração dessa Tese de Doutorado, a pesquisa de trabalhos relacionados com a metodologia de Lu-Hf foi imprescindível para o conhecimento de seus principais fundamentos. Esse conhecimento auxiliou na implementação da metodologia no LGI-UFRGS, assim como nas demais etapas de desenvolvimento da tese.

No contexto investigativo, cabe enfatizar uma atenção especial aos trabalhos que combinam o método U-Pb ao de Hf no mesmo grão de zircão, os quais mostram o potencial desta técnica para estudos de proveniência como também para entender a história de crescimento crustal de um determinado terreno. Além disso, considerou-se essencial a constatação dos diferentes procedimentos analíticos e parâmetros operacionais adotados para a metodologia Lu-Hf de cada laboratório e/ou trabalho lido. Dessa forma, a revisão apresentada destaca os principais trabalhos que auxiliaram no presente estudo.

As análises de Lu-Hf no zircão podem ser feitas por TIMS (Thermal Ionization Mass Spectrometry), SIMS (Second Ion Mass Spectrometer) ou LA-MC-ICP-MS. Os dois últimos equipamentos são menos precisos, mas são mais efetivos no ponto de vista da maior quantidade de resultados quando comparados ao que se dispõe do TIMS e pela possibilidade de datar grãos de zircão com diferentes fases de crescimento (Gerdes & Zeh, 2006).

Os primeiros estudos isotópicos para Hf foram feitos com o uso do TIMS com quantidades em microgramas por digestão ácida e separação de Lu e Hf por colunas de troca catiônica (Patchett et al., 1981). Porém para que os resultados obtidos dessas análises fossem precisos é necessária uma quantidade de amostra muito grande, pois o TIMS apresenta baixa eficiência de ionização para o Hf (Blichert-Toft & Albarède, 1997). Apesar desta restrição, muitas análises puderam ser feitas, pelo fato de o zircão conter alta concentração de Hf.

Ao seguir nessa lógica de análise, inicialmente as medidas microanalíticas de Hf foram executadas no zircão com o auxílio do SIMS (Kinny et al., 1991). Destacando que a referida técnica microanalítica não foi mais adotada, pelo fato de o volume analítico ser pequeno, pela baixa eficiência de ionização do Hf e pelo SIMS dispor somente um coletor, o que resultava em uma baixa precisão na ordem de 0,05%.

Contudo, atualmente os equipamentos mais indicados e utilizados para a metodologia de Lu-Hf em zircão, são o laser e o ICP-MS. Os pioneiros nesta técnica foram Thirlwall & Walder (1995), posteriormente inúmeros trabalhos foram desenvolvidos. Trabalhos como os de Griffin et al. 2000, Woodhead et al. 2004, Izuka & Hirata 2005, Wu et al. 2006, Gerdes & Zeh 2006, Nebel et al. 2007, Gerdes & Zeh 2009, Kinny & Maas 2003, mostram que os efeitos do fracionamento nos processos de ablação dos minerais podem ser monitorados diariamente por padrões

internos e externos de zircões, que o uso de múltiplos coletores compensam a instabilidade do plasma com uma precisão que se aproxima da obtida pelo TIMS. Assim como a intensidade do sinal obtido nas análises *in situ* de Hf no zircão pode ser mais intensa do que o obtido no SIMS, pois a alta temperatura do plasma resulta em um número menor de moléculas interferentes se compararmos com as presentes no SIMS.

No que diz respeito à intensidade do sinal para as análises a laser, uma das formas mais direta e eficiente que se vislumbra para aumentar e melhorar a ionização, e por consequência melhorar o resultado do dado analítico, seria aumentar o tamanho do furo. Porém esta tática nem sempre pode ser colocada em prática, pois deve ser levado em conta o tamanho dos grãos que, por vezes são da ordem de 50 µm. Assim, para as análises de Lu-Hf no ICP-MS a adição de uma pequena quantidade de N<sub>2</sub> junto ao gás de Ar para suprimir a formação de óxidos no plasma, mostra-se eficiente no aumento do sinal (Louie & Soo, 1992).

Experimentos realizados por Izuka & Hirata (2005) no padrão de zircão 91500 demonstraram que a sensibilidade dos elementos de Hf, Lu e Yb foram intensificadas num fator de 2-3 vezes quando adicionado 4 mL/min de N<sub>2</sub>. Estes autores também demonstraram que modificações na célula de ablação, como a diminuição para 1/3 da original, causa uma maior eficiência no transporte do material da célula para o ICP.

Os padrões de zircão utilizados na metodologia Lu-Hf, conforme mencionado anteriormente servem para monitorar diariamente as análises de minerais por ablação. Segundo Woodhead & Herdt (2005) para um zircão ser assumido como padrão de referência internacional deve ser levado em conta sua homogeneidade isotópica, grande quantidade disponível deste material, o tamanho do grão e que sua razão Lu/Hf não seja muito baixa para não afetar a precisão das correções de interferências isobáricas. De acordo com os autores nenhum material de referência tem todas as características citadas acima, mas os dois padrões de zircão Temora-2 e Mud Tank são materiais que se complementam na questão da razão de Lu/Hf, tendo homogeneidade e abundância de material.

Nessa perspectiva, os trabalhos de Morel et al. (2008) e Slama et al. (2008) os padrões GJ-1 e Plešovice, respectivamente, são sugeridos como futuros promissores para materiais de referência em análises de Hf por Laser Ablation. As

concentrações de Lu e Hf do GJ-1 evidenciam uma correlação positiva e imagens de CL não apresentam nenhum zoneamento visível, implicando em uma homogeneidade bastante almejada. O zircão Plešovice também é isotopicamente homogêneo em Hf e apresenta uma ampla variedade nas razões de Lu/Hf e Yb/Hf. Em comparação com o padrão Temora 2, o zircão Plešovice possui a razão Yb/Hf mais baixa que é necessária para fazer as correções de interferências isobáricas utilizando o Hf.

Desse modo, embora seja possível alcançar sensibilidades altas e monitorar análises através de padrões de zircão, ainda assim correções de fracionamento e de interferência isobáricas são necessárias. Em outros termos, para obter a razão  $^{176}\text{Hf}/^{177}\text{Hf}$  do zircão com acuracidade os sinais dos isótopos livres de interferências  $^{171}\text{Yb}$ ,  $^{173}\text{Yb}$  e  $^{175}\text{Lu}$  são monitorados durante as análises, a fim de remover as interferências isobáricas de  $^{176}\text{Yb}$  e  $^{176}\text{Lu}$  no  $^{176}\text{Hf}$ . Os trabalhos de Patchett & Tatsumoto 1980, Chu et al. 2002, Segal et al. 2003, Iizuka & Hirata 2005, auxiliaram a definir as razões isotópicas de Hf, Lu e Yb a serem empregadas nas devidas correções.

Na presente abordagem, um aspecto complementar ainda não discutido e oportuno para abordar é a respeito do zircão. O zircão é um mineral com uma geoquímica em potencial, que faz com que ele seja facilmente datável por vários métodos radiométricos (Woodhead et al. 2004). Além do mais, o zircão apresenta alta resistência para eventos termais posteriores a sua cristalização, a temperatura de fechamento do Hf no zircão é de 200°C, mais alta do que a do Pb, mostrando que o Hf permanece isotopicamente fechado durante a maioria dos eventos termais (Faure, 1986).

Outras características a respeito do zircão se somam de forma vantajosa a esta metodologia. O zircão normalmente contém 0,5 a 2 % de Hf (Kinny & Maas, 2003), o que viabiliza sua análise no ICP-MS. Sua razão Lu-Hf é baixa, normalmente menor que 0,002, e possui baixo crescimento de  $^{176}\text{Hf}$  pelo decaimento de  $^{176}\text{Lu}$ . Assim, a razão  $^{176}\text{Hf}/^{177}\text{Hf}$  do zircão pode ser considerada o valor inicial do momento de sua cristalização.

Dentre os vários aspectos a serem abordados pelo Lu-Hf em zircão, destaca-se a sua aplicabilidade no uso combinado com a idade de cristalização do zircão (método U-Pb), pois define a fonte do material da formação do zircão, seja mantélica, crustal

ou mista. Inúmeros estudos mostraram que o uso combinado de diferentes sistemas isotópicos pode ser efetivo em obter informações sobre a evolução crustal, metamorfismo e proveniência de sedimentos.

O trabalho de Gerdes & Zeh (2006) em zircões detriticos do metasedimento Armórico do Complexo Cristalino Central da Alemanha (Mid-German Crystalline Rise - MGCR) combina os dados de U-Pb com novos dados isotópicos de Hf para estudos da proveniência. Os resultados obtidos forneceram evidências que alguns zircões detriticos do metasedimento Brotterode cristalizaram-se no magma juvenil, embora muitos grãos tenham se formado durante a reciclagem da crosta antiga. Este estudo de proveniência em zircões detriticos se mostrou essencial para o detalhamento da reconstrução paleogeográfica e interpretação da assinatura de cada rocha.

Por fim, há que mencionar neste estudo que, cada trabalho contribuiu para estabelecer os procedimentos e parâmetros adotados à metodologia a ser empregada. E primordialmente, fundamentar a autora para a produção dos artigos que compõem esta tese, e contribuir na ressignificação dos estudos geocronológicos.

## 1.2 Metodologias Empregadas

A metodologia de trabalho empregada nesta tese objetiva aprimorar os conhecimentos acerca da metodologia de Lu-Hf, utilizada na geocronologia, de modo a possibilitar a obtenção de dados adicionais do zircão e que seguiu diversas etapas:

- Revisão bibliográfica realizada no decorrer do desenvolvimento desta tese, que potencializou o aprendizado da metodologia Lu-Hf em zircão por meio do material pesquisado;
- Desenvolvimento da metodologia Lu-Hf em zircão por LA-MC-ICP-MS, no LGI-UFRGS, com a execução das medidas em padrões e testes com adição de nitrogênio durante as análises;

- Preparação de soluções com concentração de 200ppb de Yb, Lu e Hf e análises do padrão de Hf JMC-475 (200ppb) dopado em diferentes dosagens com as soluções preparadas, a fim de estabelecer as razões isotópicas da literatura que melhor se aplicam para as correções de fracionamento e interferência isobárica necessárias para a redução dos dados de Lu-Hf;
- Análises *in situ* de Lu-Hf em zircão de diferentes amostras previamente analisadas pelo método U-Pb, bem como análises dos padrões internacionais de zircão GJ-1, Mud Tank e Temora-2 para verificação da estabilidade e reproduzibilidade do equipamento durante as análises;
- Desenvolvimento de uma planilha de cálculo no programa Excel para a redução dos dados brutos obtidos nas análises que corrija o fracionamento e as interferências isobáricas, pois tal procedimento possibilita o cálculo das razões  $^{176}\text{Hf}/^{177}\text{Hf}(t)$ , idade modelo  $T_{\text{DM}}$  e o fator  $\varepsilon_{\text{Hf}}(t)$  da amostra em questão;
- Nesta lógica procedural inclui-se como etapa também o estágio de um ano realizado no Microanalysis Facilities Inco Innovation Centre (MAFCII) da MUN (Canadá), que redimensionou o conhecimento adquirido até então na metodologia de Lu-Hf e que posteriormente proporcionou um estudo de comparação de dados obtidos entre os dois laboratórios;
- Em desfecho foi realizada uma avaliação final da compilação dos dados obtidos para cada amostra e interpretação dos mesmos na implicação direta da área estudada.

Dessa forma, para o desenvolvimento desta tese, foi imprescindível o uso do MC-ICP-MS e de duas microssondas a laser para as análises *in situ* de Lu-Hf em zircão. O MC-ICPMS utilizado, tanto no laboratório da UFRGS quanto no da MUN, foi o Neptune da Thermo Finnigan. Este ICP-MS é um espectrômetro de massa multicoletor de alta resolução para medidas de razões isotópicas com uma configuração especial para detectar simultaneamente uma ampla gama de nuclídeos de elementos, utilizando 9 coletores Faraday e 6 contadores de íons (MIC's), que podem inclusive serem combinados em uma única configuração.

As microssondas a laser utilizadas foram a UP 213 (Nd: YAG, New Wave) e a Excimer 193nm (ArF, GeoLas) localizadas nos laboratórios da UFRGS e da MUN, respectivamente. Tais microssondas são utilizadas para as análises por ablação em minerais e emitem alta densidade de energia em vários tamanhos de crateras (aproximadamente 4 a 110  $\mu\text{m}$ ). Os seus comprimentos de onda de 213 nm e 193

nm produzem uma distribuição fina das partículas, o que otimiza a eficiência no transporte do material, resultando em mínima deposição no plasma. A principal diferença entre as duas reside no fato de que microssondas com comprimentos de onda menores, como a Excimer 193 nm, produz muito mais partículas pequenas devido à baixa profundidade de penetração, favorecendo um aumento da sensibilidade e um menor fracionamento dos elementos durante as análises (Guillong et al., 2003).

As amostras selecionadas para compor esta tese são de áreas fonte e idades distintas, as quais já estavam montadas em sessão polida, possuíam imagens de MEV dos grãos de zircão, bem como a determinação do conteúdo isotópico de U-Th-Pb. O método de datação U-Pb utilizado primeiramente para análise *in situ* dos zircões será descrito na próxima seção. A metodologia de Lu-Hf em zircão por LA-ICP-MS, por sua vez, será descrita detalhadamente nos artigos que compõe o corpo principal desta tese.

### 1.2.1 Método U-Pb

As análises de U-Pb das amostras desta tese foram executadas no LGI-UFRGS com o equipamento MC-ICP-MS (Neptune, ThermoFinnigan) e uma microssonda a laser acoplada (UP 213, Nd:YAG, New Wave) (Figura 1). A seguir, descreve-se o método de análise *in situ* em zircões com o equipamento LA-MC-ICP-MS.

A configuração mista dos coletores Faraday e multiplicadores de íons (MIC's) utilizada para as medidas simultâneas dos isótopos de Th, U, Pb e Hg é apresentada na tabela 1.

MIC3	MIC4	L4	MIC6	L3	Axial	H2	H4
$^{202}\text{Hg}$	$^{204}\text{Hg+}$	$^{206}\text{Pb}$	$^{207}\text{Pb}$	$^{208}\text{Pb}$		$^{232}\text{Th}$	$^{238}\text{U}$
		$^{204}\text{Pb}$					

Tabela 1 - Configuração dos coletores Faraday e MIC's adotada para as análises de U-Th-Pb.

A calibração de ganho dos coletores Faraday é realizada rotineiramente antes da realização da seção de análises, enquanto a calibração cruzada (cross calibration) envolvendo um dos Faraday de referência e os 3 MICs só é efetuada quando a sensibilidade de um deles é afetada de forma significativa, tornando necessário, por exemplo, a mudança da voltagem de operação ou mesmo uma troca. Para o fator de ganho para calibração dos copos Faraday, aplica-se um sinal constante de 33 volts. Para a calibração cruzada, ou cálculo do fator de conversão das leituras em volts (Faraday) para contagens por segundo (cps) dos MICs envolvidos, utiliza-se uma solução diluída e própria para o Neptune com concentração da ordem de 220 ppt acrescida de Th. O valor teórico para a conversão é de 62.440 cps/mV quando se usa um resistor de  $10^{11}$  ohms nos medidores Faraday.



Figura 1 – Ilustração do MC-ICP-MS Neptune (ThermoFinnigan) com a microssonda a laser UP213 (New Wave) acoplada, utilizados para as análises *in situ* de U-Pb em zircão no LGI-UFRGS.

No ICP, os íons são muito abundantes e sofrem repulsão eletrostática em que os elementos leves são mais repelidos que os pesados, e também os elementos com massas até da ordem de 90 são menos ionizados, causando fracionamento isotópico. Deve-se acrescer ainda ao processo de fracionamento o que se verifica durante o processo de ablação no laser por envolver elementos como Pb e U com volatilidades muito distintas. Assim, as razões isotópicas são afetadas por estes

processos, mas podem ser corrigidas utilizando-se um padrão internacional cujas concentrações e razões foram aferidas pelo clássico método de diluição isotópica e utilizando espectrômetros de ionização térmica (TIMS).

O presente método U-Pb utilizou o zircão GJ-1, padrão internacional do GEMOC ARC National Key Center, Austrália, para as correções nas razões isotópicas. Os teores de U, Th e Pb variam consideravelmente, mas trata-se de um padrão muito homogêneo em termos de razão entre os radiogênicos e respectivos isótopos pais, da mesma forma que razões  $(^{207}\text{Pb}/^{206}\text{Pb})^*$  (onde \* refere a fração radiogênica).

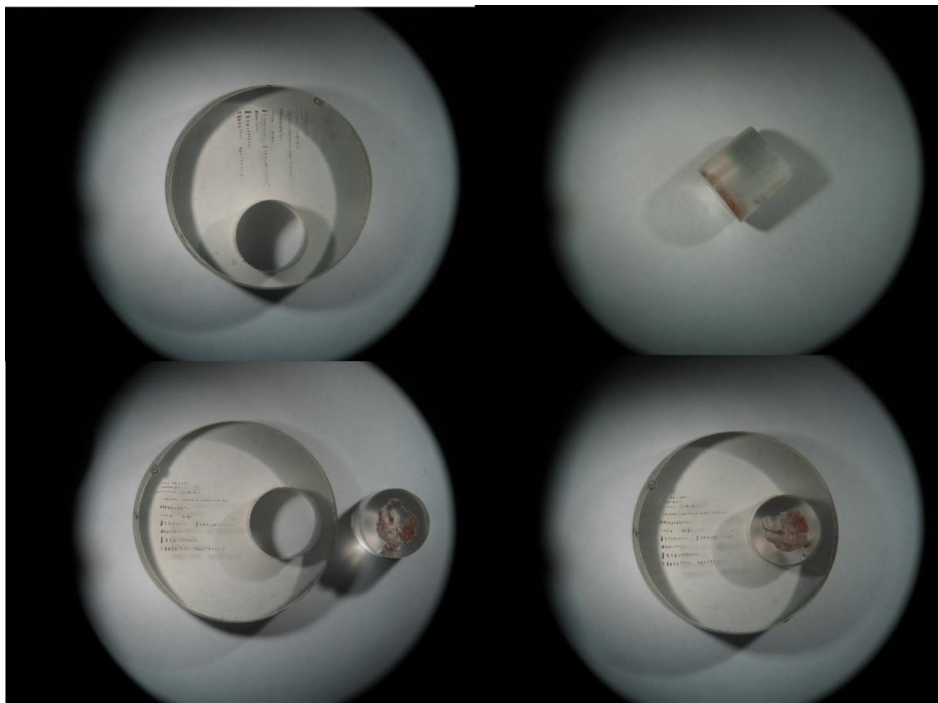


Figura 2 - Imagens da seção com zircões e padrão. A) Seção com zircões das diferentes famílias em fileiras verticais; B) Detalhe do padrão embutido em um cilindro 8mm de diâmetro; C) Seção da amostra e padrão GJ-1 separados; D) Seção da amostra com o padrão GJ-1 prontos para análises.

Esta sistemática de correção conhecida como “bias” é, pois, uma correção externa, não interna como acontece nas análises isotópicas utilizando TIMS. As correções são estimadas após a análise. As análises pontuais são procedidas em grupo de 4 até 10 determinações intercalados com o padrão acima. O número de pontos ou “spots” varia em função da homogeneidade dos zircões em estudo e também dos teores de U e Pb nas áreas selecionadas. Para um melhor controle e utilização de mesmas condições analíticas, os cristais são montados em várias

fileiras sobre a superfície de uma pastilha de araldite com cerca de 2,0 cm de diâmetro (Figura 2). Após a fixação, são cuidadosamente polidas até a exposição de superfície fresca para os procedimentos posteriores.

O tamanho dos grãos deve ter ao menos 20 µm, pois os spots podem ser de 10, 25, 40 ou até de 60 µm. O tamanho é muitas vezes estabelecido no momento, tendo como base as intensidades dos sinais. Neste quesito o sinal correspondente ao  $^{207}\text{Pb}$  é o determinante principal. Quando este for menor que 10.000 cps, é necessário aumentar o tamanho do spot ou a intensidade da potência do laser. A amostra padrão é montada sobre um cilindro pequeno também de epóxi e é inserido na cavidade apropriadamente feito em cada pastilha, conforme pode ser observado na figura 2.

Os parâmetros usuais do laser aparecem na tabela 2. A aquisição de dados de forma simultânea é procedida em 50 ciclos de 1,049 segundos de integração e sem tempo de espera entre os ciclos. Com este tempo de ablação o laser chega a “escavar” cerca de 20 µm de profundidade. Para cada conjunto de medidas do padrão e amostras são adquiridos também os valores de branco nas mesmas condições analíticas. Os valores de branco são subtraídos das leituras do conjunto. O valor do  $^{204}\text{Pb}$  é corrigido para  $^{204}\text{Hg}$ , para estimar o chumbo comum, assumindo-se que a razão de  $^{202}\text{Hg}/^{204}\text{Hg}$  é igual 4,355.

O método contumazmente utilizado para correção de Pb comum em zircões, baseia-se na presença do isótopo de  $^{204}\text{Pb}$ . No caso do laser, o sinal do  $^{204}\text{Pb}$  varia intensamente e é afetado fortemente pela presença do  $^{204}\text{Hg}$  proveniente dos gases de AR e He, o que resulta em uma estimativa imprecisa do Pb comum. Uma das maneiras de minimizar tais incertezas é realizar o cálculo da fração do Pb comum na amostra, de modo a utilizar as seguintes equações (Williams, 1998):

$$f_{206} = [^{206}\text{Pb}/^{204}\text{Pb}]_c/[^{206}\text{Pb}/^{204}\text{Pb}]_s$$

$$f_{207} = [^{207}\text{Pb}/^{204}\text{Pb}]_c/[^{207}\text{Pb}/^{204}\text{Pb}]_s$$

Para as razões isotópicas do Pb comum, utiliza-se a curva de evolução proposta por Stancey e Kramers (1975) em que é requerida uma idade estimada inicial. As

razões de  $^{207}\text{Pb}^*/^{206}\text{Pb}^*$  e  $^{206}\text{Pb}^*/^{238}\text{U}$  (onde \* refere a fração radiogênica) são corrigidas a partir das equações de  $f_{206}$  e  $f_{207}$  para ciclos individuais. Em termos gerais, os ciclos com valores de  $f_{206}$  acima de 0.0025 (i.e., 0.25% de presença de Pb comum) não são incluídos no cálculo, pois resultam em idades discordantes e não se dispõem junto a curva concórdia. Áreas esbranquiçadas (alteradas por algum processo) ou metamitizadas (escuras neste caso) e áreas cortadas por microfissuras preenchidas no zircão revelam quase sempre alto teor de Pb comum. Assim, é adotado nesta metodologia, evitar tais áreas para efetuação do spot valendo-se de imagens de retro-espalhamento ou catodo-luminescência.

---

### MC-ICPMS

---

Instrumento	Neptune (ThermoFinnigan)
<b>Fonte de íon</b>	
Potência	1200 W
Fluxo de gás	Ar Resfriador: 15 L/min
	Ar Auxiliar: 0,73 L/min
	Ar Transporte: ~0,75 L/min
Extração	-2000 V
Modo de Análise	Estático
Detecção	Coletores Faraday e MIC's
<b>Aquisição de Dados</b>	
Tempo de integração	1,049s
Nº de integrações	1

---

### Laser Ablation

---

Instrumento	UP-213 (Nd:YAG) New Wave
Diâmetro do furo	15, 25 e 40 µm
Energia	4-6 J/cm <sup>2</sup>
Freqüência	10 Hz
Total da ablação	50s
Fluxo de He	~0,45 L/min

---

Tabela 2 - Condições de operação do laser e do MC-ICP-MS.

As razões isotópicas necessárias para o cálculo de idades convencionais ou elaboração de diagramas tipo concórdia seguem um procedimento sistemático envolvendo primeiramente correção para branco. Após as correções de branco as razões de interesse são calculadas e podem variar devido a processos de fracionamento conforme comentado anteriormente. Neste aspecto, as razões  $^{206}\text{Pb}^*/^{238}\text{U}$  variam visivelmente durante os 50 ciclos de medição. As razões aumentam em razão do Pb (mais volátil) condensar progressivamente nas paredes do tubo de ablação à medida que o laser vai aprofundando.

Na maior parte dos casos o fracionamento que ocorre é linear. Como razão real da amostra utiliza-se o intercepto da melhor reta em que os 6 primeiros pontos são geralmente descartados, de acordo com a formulação proposta por Youden (1951) e também adotada por Košler et al. (2002). Em geral calcula-se a média aritmética dos valores, eliminando valores discrepantes (ao nível de 2SD). Nos casos em que  $^{207}\text{Pb}^*/^{206}\text{Pb}^*$  e, também  $^{232}\text{Th}/^{238}\text{U}$ , apresentam fracionamento inverso, utiliza-se o mesmo método do fracionamento induzido por ablação a laser e aplicado para obtenção da razão  $^{206}\text{Pb}/^{238}\text{U}$ . A etapa seguinte envolve correções devidas a Pb comum e cálculos de razões corrigidas e respectivos erros (1SD). As idades individuais ou construção de diagramas tipo concórdia são obtidas valendo-se do Isoplot (Ludwig, 1998). O software para a execução de toda esta sistemática acha descrita em Chemale Jr. et al. (2009).

### **1.3 Texto Integrador dos Artigos**

Como já nos referimos anteriormente, o objeto de investigação da presente tese intencionou potencializar o aprendizado, a implementação e a aplicação da metodologia de Lu-Hf em zircão por ICP-MS. Os três artigos que compõem o corpo principal refletem a proposta inicial apresentando a metodologia de Lu-Hf em zircões empregada nas análises e os resultados obtidos em zircões de três áreas geológicas distintas. Assim, uma análise integradora destes trabalhos se faz necessária a fim de sistematizar os temas discutidos entre si, de modo a evidenciar seu interrelacionamento no que diz respeito ao aperfeiçoamento da metodologia de Lu-Hf em zircão por ICP-MS.

O primeiro artigo que compõe o corpo principal desta tese descreve sucintamente a metodologia Lu-Hf em zircão por LA-ICP-MS implantada no LGI-UFRGS e exemplifica sua aplicação em zircões ígneos do Ofiolito Aburrá, Colômbia. Também é apresentada a geoquímica deste sistema isotópico e resultados de análises de Hf em padrões de zircão com adição de nitrogênio.

O ofiolito estudado consiste de rochas maficas e ultramáficas: o Dunito de Medellín e os Metagabros de El Picacho. Os zircões deste ofiolito são cristais grandes que medem em torno de 500 µm, bem formados e homogêneos. Análises de Hf *in situ* em 12 destes grãos revelaram valores variáveis positivos de  $\epsilon_{\text{Hf}}(t)$  sugerindo a presença de um magma juvenil com possível contaminação crustal.

A metodologia Lu-Hf aplicada aos zircões do Ofiolito de Aburrá forneceu novos dados isotópicos e contribui para a história geológica da borda NW da América do Sul. Os dados combinados de U-Pb e Lu-Hf são ainda muito escassos para maiores interpretações, mas pode se antever como um potencial instrumento para robustecer as idéias e novos conhecimentos sobre a evolução crustal da área.

No segundo artigo, é apresentado um estudo de comparação em zircões magmáticos e metamórficos do Anortosito de Capivarita com objetivo de verificar a reproduutibilidade dos dados obtidos pela metodologia de Lu-Hf desenvolvida no LGI. O Anortosito Capivarita está situado na localidade Pantano Grande, na porção NE do Escudo Sul-Rio-Grandense, Rio Grande do Sul, Brasil. Este anortosito faz parte do Cinturão Dom Feliciano (DFB) formado durante o Neoproterozóico (860-550 Ma).

As análises *in situ* de Lu-Hf nos zircões do Anortosito foram feitas primeiramente no LGI da UFGRS (Brasil) e depois no MAFIIC da MUN (Canada). Ambos laboratórios utilizaram o mesmo modelo de MC-ICP-MS, o Neptune da Thermo Finnigan, mas diferentes lasers assim como diferentes metodologias de trabalho. As principais diferenças, além de diferentes lasers, residem no fato de ter sido utilizado durante as análises no LGI um diâmetro maior para o furo do laser e nitrogênio que originaram intensidades 30-50% mais intensas. A medida das razões isotópicas  $^{176}\text{Hf}/^{177}\text{Hf}$  em ambos os laboratórios são similares, geralmente diferem na sexta casa depois da vírgula.

Assim, os resultados dos dois laboratórios mostraram significativa reproduutibilidade nas análises de Hf. As idades  $T_{\text{DM}}$  e os valores de  $\epsilon_{\text{Hf}}$  obtidos são

concordantes dentro dos erros experimentais. Estes resultados permitiram que os isótopos de Hf pudessem contribuir na interpretação das idades dos zircões, fornecer informações sobre a proveniência do anortosito e sugerir uma fonte juvenil para a fusão com algum grau de contaminação crustal Paleoproterozóica.

O outro estudo, que compõe o terceiro artigo, foi desenvolvido com zircões detriticos da Bacia de Camamu. Esta bacia está relacionada com o rompimento do Gondwana e pertence ao grupo de bacias sedimentares que compõem a margem leste brasileira. Neste artigo, foi realizada uma investigação petrográfica das unidades fluviais e eólicas dos Grupos Brotas e Almada, pertencentes respectivamente a fase pré-rifte e rifte da bacia. Análises isotópicas de U-Pb e Lu-Hf também foram executadas a fim de obter informações sobre a proveniência dos sedimentos originais. Primeiramente foram realizadas análises *in situ* nos grãos de zircão para obter a idade U-Pb, seguidos pelas análises de Hf.

Os resultados da petrografia indicaram que os sedimentos são derivados de um bloco continental. As amostras da Formação Sergi, Grupo Brotas, mostraram um grupo principal de idade U-Pb de 480-600 Ma relacionado à aglutinação do Orógeno Araçuaí e sua fase pós-orogênica. Outros quatro subordinados grupos de idades U/Pb: 900-1000 Ma, 1900-2100 Ma, 2500-2800 Ma e 3000-3200 Ma; estão relacionados ao rifteamento Neoproterozóico, Ciclo Transmazônico (Paleoproterozóico), Ciclo Jequié (Neoarqueano) e Ciclo Mesoarqueano, presentes no Cráton do São Francisco, respectivamente.

A distribuição das idades dos zircões detriticos das amostras do Grupo Almada, é bastante diferente das amostras do Grupo Brotas. Os picos principais são de idade Paleoproterozóica relacionados com os ciclos Transamazônico e Jequié, portanto diretamente ligados a rochas do embasamento cristalino adjacente à Bacia de Camamu. Os dados de Hf mostram valores bastante variáveis da idade modelo  $T_{DM}$  e do fator  $\epsilon_{Hf}$  das amostras, evidenciando que alguns grãos de zircão da Bacia de Camamu cristalizaram em um magma juvenil, enquanto a maioria dos grãos foi formada durante a reciclagem ou contaminada com a crosta antiga.

Tais dados apontam que a principal fonte da Bacia de Camamu das unidades estudadas pode ser caracterizada. Na formação Sergi, 60 a 70% dos zircões analisados são de idade Cambriana-Vendiana, provenientes do Orógeno Araçuaí-Congo Ocidental levando em conta as medidas de paleocorrente desta formação de

S-SW para N-NE. E no Grupo Almada, as principais fontes dos zircões são Paleoproterozóica e Arqueana, de proveniência direta do embasamento o que é consistente com o transporte dos sedimentos de oeste para leste definido pelas medidas sistemáticas de paleocorrente nas unidades estudadas. Por meio da análise dos dados dos isótopos de Lu-Hf, pode-se evidenciar que os zircões estudados do Grupo Brotas contêm componentes dominantes paleoproterozóicos e arqueanos. Mesmo os zircões de idade Neoproterozóica a Eo-Plaeozóica mostram idades modelo Hf e valores de  $\varepsilon_{\text{Hf}}(t)$  negativos em sua maior parte. Somente alguns grãos apresentaram componentes crustais juvenis para este grupo de zircões. Tal informação sugere que a evolução crustal do Craton São Francisco e mesmo do Orógeno Araçuaí tem como componentes principais de idade paleoproterozóica e arqueana.

Contudo, os artigos a serem apresentados no capítulo seguinte exemplificam de maneira clara que a combinação dos sistemas isotópicos de U-Pb e Lu-Hf, aplicada a diferentes áreas, diferentes tipos de zircões, é uma ferramenta confiável e importante para a geocronologia aplicada aos estudos de proveniência sedimentar, proveniência crustal e evolução tectônica da crosta ao longo do tempo do geológico. Em estudos de bacias sedimentares esta ferramenta torna-se imprescindível para avaliação precisa dos tipos de áreas fonte da bacia sedimentar e estabelecimento do sistema de paleodrenagem, onde não é possível determinar os dados de paleocorrentes e outras informações de cunho sedimentológico-estratigráfico com a resolução de análises de afloramentos. Em ambos os trabalhos, os dados obtidos forneceram informações complementares, mas precisas, em estudos de proveniência e de crescimento crustal das respectivas áreas.

## 1.4 Referências

- Blichert-Toft, J. & Albarède, F. 1997. The Lu-Hf isotope geochemistry of chondrites and the evolution of the mantle crust system. **Earth and Planetary Science Letters**, **148**: 243-258.
- Chemale Jr., F; Kawashita, K.; Dussin, I.A.; Ávila, J. N.; Justino, D. & Bertotti, A.L. 2009. **U-Pb zircon dating with MC-ICP-MS using mixed detector configuration.** Relatório Interno, Porto Alegre, UFRGS, 36 p.

- Faure, G. 1986. **Principles of Isotope Geology.** New York, John Wiley and Sons, Ed. 2, 589p.
- Gerdes, A. & Zeh, A. 2006. Combined U-Pb and Hf isotope LA-(MC)-ICP-MS analyses of detrital zircons: Comparison with SHRIMP and new constraints for the provenance and age of American metasediment in central Germany. **Earth and Planetary Science Letters**, **249**: 47-61.
- Gerdes, A. & Zeh, A. 2009. Zircon formation versus zircon alteration – New Insights from combined U-Pb and Lu-Hf in-situ LA-ICP-MS analyses, and consequences for the interpretation of archean zircon from the Central Zone of the Limpopo Belt. **Chemical Geology** **261**: 230-243.
- Griffin, W.L.; Pearson, N.J.; Belousova, E.; Jackson, S.E.; van Achterbergh, E.; O'Reilly, S.Y. & Shee, S.R. 2000. The Hf isotope composition of cratonic mantle: LAM-MC-ICPMS analysis of zircon megacrysts in Kimberlites. **Geochim. Cosmochim. Acta**, **64**: 133-147.
- Guillong, M.; Horn, I. & Günther, D. 2003. A comparison of 266 nm, 213 nm and 193 nm produced from a single solid state Nd:YAG laser for laser ablation ICP-MS. **J. Anal. At. Spectrom.**, **18**: 1224-1230.
- Iizuka, T. & Hirata, T. 2005. Improvements of precision and accuracy in situ Hf isotope microanalysis of zircon using the laser ablation-MC-ICPMS technique. **Chemical Geology**, **220**: 131-137.
- Kinny, P.D.; Compston, W. & Williams, I.S. 1991. A reconnaissance ion probe study of hafnium isotopes in zircons. **Geochim. Cosmochim. Acta**, **55**: 849-859.
- Kinny, P.D. & Maas, R. 2003. Lu-Hf and Sm-Nd Isotope systems in zircon. In: **Reviews in Mineralogy and Geochemistry**, **53**: 327-341.
- Košler, J.; Fonneland, H.; Sylvester, P.J.; Tubrett, M. & Pedersen, R.B. 2002. U-Pb dating of detrital zircons for sediment provenance studies – a comparison of laser ablation ICPMS and SIMS technique. **Chemical Geology**, **182**: 605-618.
- Košler, J. & Sylvester, P.J. 2003. Present Trends and the Future of Zircon in Geochronology: Laser Ablation ICPMS. In: **Reviews in Mineralogy and Geochemistry**, **53**: 243-275.
- Longerich, H. 2008. Laser Ablation – Inductively Coupled Plasma – Mass Spectrometry (LA-ICP-MS); an introduction. In: **Laser Ablation ICP-MS in the Earth Sciences: Current Practices and Outstanding Issues**. Short Course Series. Vancouver, BC, vol. 40, 348p.
- Louie, H. & Soo, S.Y.-P. 1992. Use of nitrogen and hydrogen in inductively plasma mass spectrometry. **Journal of Analytical Atomic Spectrometry**, **7**: 557-564.
- Ludwig, K.R. 1998. **Isoplot/Ex (v.1.00b): a geochronological toolkit for Microsoft Excel.** Berkeley Geochronological Center, 45 p. (Special Publication v.1).

- Morel, M.L.A.; Nebel, O.; Nebel-Jacobsen, Y.J.; Miller, J.S. & Vroon, P.Z. 2008. Hafnium isotope characterization of the GJ-1 zircon reference material by solution and laser-ablation MC-ICPMS. **Chemical Geology**, **255**: 231–235.
- Pachett, P.J. & Tatsumoto, M. 1980. Lu-Hf total rock isochron for the eucrite meteorites. **Nature**, **288**: 571-574.
- Patchett, P.J.; Kouvo, O.; Hedge, C.E. & Tatsumoto, M. 1981. Evolution of continental crust and mantle heterogeneity: evidence from Hf isotopes. **Contrib. Mineral. Petrol.**, **78**: 279-297.
- Slama, J., et al. 2008. Plešovice zircon — A new natural reference material for U–Pb and Hf isotopic microanalysis. **Chemical Geology**, **249**: 1-35.
- Stacey, J.S. & Kramers, J.D. 1975. Approximation of terrestrial lead isotope evolution by a two-stage model. **Earth and Planetary Science Letters**, **26**: 207–221.
- Thirwall, M.F. & Walder, A.J. 1995. In situ hafnium isotope ratio analyses of zircon by inductively coupled plasma mass spectrometry. **Chemical Geology**, **122**: 241-247.
- Williams, I.S. 1998. U–Th–Pb geochronology by ion microprobe. In: McKibben, M.A., Shanks III, W.C., Rydley, W.I. Applications of Microanalytical Techniques to Understanding Mineralizing Processes. **Rev. Econ. Geol.**, **7**: 1–35.
- Woodhead, J.; Herget, J.; Shelley, M.; Eggins, S. & Kemp, R. 2004. Zircon Hf-isotope analysis with an excimer laser, depthprofiling, ablation of complex geometries and concomitant age estimation. **Chemical Geology**, **209**: 121-135.
- Woodhead, J.D. & Herget, J.M. 2005. A preliminary appraisal of seven natural zircon reference materials for in situ hf isotope determination. **Geostandards and Geoanalytical Research**, **29**: 183-195.
- Wu, F.-Y.; Yang, Y.-H.; Xie, L.-W.; Yang, J.-H. & Xu, P. 2006. Hf isotopic compositions of the standard zircons and baddeleyites used in U-Pb geochronology. **Chemical Geology**, **234**: 105-126.
- Youden, W.J. 1951. **Statistical methods for chemists**. Journal of the Royal Statistical. New York, Wiley, 126 p.

## **Capítulo 2**

### **Corpo Principal - Artigos Submetidos**

## 2.1 Primeiro Artigo



UNIVERSIDADE FEDERAL DO RIO GRANDE DO SUL

INSTITUTO DE GEOCIÊNCIAS

*Pesquisas em Geociências*

---

Porto Alegre, 19 de setembro de 2011.

À

Anelise Losangela Bertotti

Venho comunicar o recebimento do manuscrito abaixo listado, submetido para publicação em *Pesquisas em Geociências*, órgão de divulgação científica editado pelo Instituto de Geociências da Universidade Federal do Rio Grande do Sul.

Agradeço a seleção de *Pesquisas em Geociências* para a publicação de sua contribuição. O manuscrito será analisado quanto ao conteúdo e enquadramento nas normas de preparação, para que seja iniciado o processo de análise por pares.

Título: *Lu-Hf em Zircão por LA-CIP-MS: Aplicação em Ofiolito de Aburrá, Colômbia.*

Autor(es): *Anelise Losangela Bertotti, Farid Chelae Jr. & Koji Kawashita.*

Atenciosamente,

Prof. Dr. Paulo Alves de Souza  
Editor Chefe

---

*Pesquisas em Geociências*

Instituto de Geociências – Departamento de Paleontologia e Estratigrafia  
Av. Bento Gonçalves, nº 9500 - Bloco 1 - Prédio 43127, Sala 209

CEP 91.540-000, Porto Alegre, RS, Brasil.

Tel.: +55.51.3308.7386

Email: paulo.alves.souza@ufrgs.br

Lu-Hf em Zircão por LA-ICP-MS: Aplicação em Ofiolito de Aburrá,

# Colômbia

## **Lu-Hf data in zircons by LA-ICPMS: Application in Aburrá Ophiolite,**

# Colombia

<sup>1</sup> Programa de Pós-Graduação em Geociências, Instituto de Geociências, Universidade Federal do Rio Grande do Sul, Cx Postal 15001, 91501-970, Porto Alegre, RS, Brasil. [anelise.bertotti@ufrgs.br](mailto:anelise.bertotti@ufrgs.br)

**2** Instituto de Geociências, Universidade de Brasília, Campus Darcy Ribeiro Asa Norte, 70910-900 Brasília, DF,  
Brasil. [fchemale@unb.br](mailto:fchemale@unb.br)

<sup>3</sup> Instituto de Geociências, Universidade de Brasília, Campus Darcy Ribeiro Asa Norte, 70910-900 Brasília, DF, Brasil. [koji@usp.br](mailto:koji@usp.br)

## Resumo

A metodologia Lu-Hf em zircão por LA-ICP-MS implantada no Laboratório de Geologia Isotópica da Universidade Federal do Rio Grande do Sul e aplicada em zircões ígneos do Ofiolito Aburrá, Colômbia, é sucintamente descrita. O interesse na aplicação desta metodologia, quando se dispõe de um sistema de análise de zircões *in situ* por LA-ICP-MS, deve ser consignado à relativa simplicidade, sensibilidade e rapidez de análise. A alta concentração de Hf no zircão, que pode alcançar milhares de ppm, propicia razões isotópicas e idades modelos bastante precisas, que podem subsidiar importantes inferências não só quanto à idade de extração mantélica, mas também quanto à sua possível história evolutiva, proveniência e estudos afins. A precisão da ordem de 20 ppm no erro do padrão nas razões  $^{176}\text{Hf}/^{177}\text{Hf}$  e de cerca de 10% nas razões  $^{176}\text{Lu}/^{177}\text{Hf}$  propiciada pelo Neptune (Thermo Finnigan) deve ser consignada à moderna tecnologia de medidas simultâneas dos isótopos envolvidos na metodologia. O laser de Nd:YAG (213 nm) da New Wave utilizado revelou-se muito apropriado ao usar os seguintes parâmetros: densidade de energia entre 5 a 6 J/cm<sup>2</sup>, freqüência de 10Hz, 50 s de ablação e diâmetro de 55 µm. Um fluxo de aproximadamente 4 mL/min de nitrogênio adicionado ao gás de arraste para inibir a formação de óxidos junto ao plasma mostrou-se eficaz na estabilização do sinal e trouxe um notável aumento na eficiência de ionização estimado até em 100% nos sinais, verificado nos padrões GJ-1 e Mud Tank. Estes padrões são de composições isotópicas ligeiramente diferentes para a razão  $^{176}\text{Hf}/^{177}\text{Hf}$  e forneceram valores de  $0,282004 \pm 0,000004$  e  $0,282466 \pm 0,000022$ , respectivamente. O procedimento analítico adotado seguiu um protocolo em que 3 zircões foram intercalados com padrão internacional GJ-1. Análises *in situ* de 12 grãos separados do Ofiolito de Aburrá revelaram  $\epsilon\text{Hf(t)}$  entre +2,01 e +5,35, enquanto as idades modelo TDM resultaram valores em um intervalo entre 1,15 e 1,44 Ga, revelando forte afinidade com as rochas da Província Rondoniana - San Ignacio.

## Abstract

The Lu-Hf methodology in zircon by LA-ICP-MS established at the Laboratory of Isotope Geology, Federal University of Rio Grande do Sul, and applied in the Aburrá Ophiolite igneous zircons, Colombia, is briefly described. The interest in the application of this methodology when it is available a system of *in situ* zircon analysis by LA-ICP-MS, should be consigned to relative simplicity, sensitivity and speed of analysis. The high concentration of Hf in zircon, which can reach thousands of ppm, provides highly accurate isotopic ratios and model ages that can support not only important inferences about the age of mantle extraction, but also as to its

possible evolutionary history, and provenance related studies. The accuracy in order of 20 ppm in standard error of the  $^{176}\text{Hf}/^{177}\text{Hf}$  ratios and about 10% in  $^{176}\text{Lu}/^{177}\text{Hf}$  ratios provided by the Neptune (Thermo Finnigan) should be consigned to the modern technology of simultaneous measurements of the isotopes involved in the methodology. The Nd: YAG (213 nm) laser from New Wave used proved to be very appropriate using the following parameters: energy density of 5-6 J/cm<sup>2</sup>, frequency of 10 Hz, 50 s of ablation and diameter of 55  $\mu\text{m}$ . A flow of approximately 4 mL/min of nitrogen added to the carrier gas to inhibit the oxide formation in plasma proved to be effective in stabilizing the sign and brought a remarkable increase in ionization efficiency estimated at up to 100% in the signs, seen in GJ-1 and Mud Tank standards. These standards are slightly different in isotopic compositions for the  $^{176}\text{Hf}/^{177}\text{Hf}$  ratio and provided values of  $0.282004 \pm 0.000004$  and  $0.282466 \pm 0.000022$ , respectively. The analytical procedure adopted followed a protocol in which three zircons were interspersed with the international standard GJ-1. *In situ* analyses of 12 grains from Aburrá Ophiolite, revealed  $\epsilon\text{Hf(t)}$  between +2.01 and +5.35, while the TDM model age values resulted in a range between 1.15 and 1.44 Ga, revealing strong affinity with rocks from Rondoniano - San Ignacio Province.

Palavras-Chave: Metodologia Lu-Hf, Zircão, LA-ICP-MS, Ofiolito de Aburrá.

Keywords: Lu-Hf Methodology, Zircon, LA-ICP-MS, Aburrá Ophiolite.

60

61

## 62 1. Introdução

63 Durante a última década, a eficiência de ionização dos espectrômetros de massa de fonte de  
 64 plasma indutivamente acoplado, fez do MC-ICP-MS o instrumento escolhido para análises de Lutécio-  
 65 Hafnio (Lu-Hf) no zircão. Embora a análise por ablação a laser apresente menor precisão comparada  
 66 às análises via solução no ICP-MS e ao TIMS, esta desvantagem pode ser superada pela rapidez e  
 67 praticidade em combinar medidas isotópicas *in situ* de Hf e U-Pb em um mesmo grão de zircão  
 68 fornecendo informações em alta resolução. O diâmetro do furo de laser para Hf pode ser até da ordem  
 69 de 60  $\mu\text{m}$ , sem se preocupar muito com a qualidade do alvo visado ou presença de Pb comum como  
 70 acontece na obtenção de dados U-Pb. Em termos analíticos, a intensidade do sinal com ICP chega a  
 71 ser até 100 vezes mais intensa do que a obtida com SHRIMP, sendo bem conhecida sua eficiência na  
 72 ionização de elementos refratários. No caso do Hf pode ser tão alta quanto 95% contra menos de 0,1%  
 73 no TIMS.

74 Desta forma, o sistema isotópico Lu-Hf se tornou uma das ferramentas mais inovadoras e  
 75 poderosas na geocronologia envolvendo zircões, e vem sendo vastamente utilizado como um traçador  
 76 para entender a evolução crustal e a diferenciação do manto da Terra (Patchett & Tatsumoto, 1980;  
 77 Thirwall & Walder, 1995; Blichert-Toft & Albarède, 1997; Vervoort & Blichert-Toft, 1999; Griffin *et*  
 78 *al.*, 2000; Gerdes & Zeh, 2006; Goodge & Vervoort, 2006; Nebel *et al.*, 2007; Zeh *et al.*, 2007). Cabe

79 destacar também que o zircão é um mineral com uma geoquímica de potencialidade inigualável,  
80 fornecendo dados do sistema U-Th-Pb de fácil interpretação (Woodhead et al., 2004; Wu et al., 2006).

81 Adicionalmente, o zircão possui alta concentração de Hf e preserva as razões isotópicas  
82 iniciais de Hf, características que podem ser úteis para datação e indicação petrogenética em estudos  
83 de proveniência de sedimentos. O estudo combinado envolvendo o método U-Pb, um dos métodos  
84 geocronológicos mais poderosos, à assinatura isotópica propiciada pelo Hf e idade modelo Lu-Hf  
85 permite inferir o magma primário dos quais os zircões derivaram e cristalizaram. A época de derivação  
86 é revelada pela idade conhecida como  $T_{DM}$ , com mesmo valor interpretativo propiciado originalmente  
87 pelo sistema Sm-Nd. Da mesma forma o parâmetro  $\epsilon$ ,  $\epsilon_{Hf}$  no presente caso, igualmente comparado  
88 com a curva de evolução de Hf para o reservatório condríctico (CHUR), serve para definir o possível  
89 campo ou ambiente de formação (manto ou crosta). Em uma única formação as diferentes assinaturas  
90 isotópicas de Hf encontradas em uma população de zircão ou mesmo em um único zircão permitem  
91 caracterizar diferentes eventos magmáticos ou metamórficos que aconteceram ao nível regional  
92 durante a evolução crustal das regiões de origem (Gerdes & Zeh, 2006; Gerdes & Zeh, 2009).

93 Neste trabalho será descrito em detalhes a metodologia Lu-Hf para LA-MC-ICP-MS em  
94 zircão, desenvolvido no Laboratório de Geologia Isotópica da Universidade Federal do Rio Grande do  
95 Sul. Ainda, serão apresentadas análises isotópicas de Hf obtidas por dois padrões de zircão, GJ-1e  
96 Mud Tank, e seus resultados com adição de nitrogênio durante suas análises. Por fim, será realizada a  
97 aplicação desta metodologia nos zircões de um gábro pegmatítico pertencente ao Ofiolito de Aburrá,  
98 Colômbia.

99

## 100 **2. Sistema Isotópico Lu-Hf**

101 Os primeiros estudos isotópicos envolvendo Hf foram feitos por Patchett & Tatsumoto (1980)  
102 utilizando o clássico procedimento para análises isotópicas de elementos sólidos conhecido  
103 abreviadamente por TIMS (*Thermal Ionization Mass Spectrometer*). A separação de Lu e Hf em  
104 colunas de troca catiônica (Patchett et al., 1981) foi necessária para evitar interferências isobáricas e  
105 melhorar a precisão nas medidas das razões isotópicas do Hf e consequentemente das idades do

106 sistema Lu-Hf. No entanto, a necessidade da ordem de 1 micrograma de Hf para obtenção de  
 107 resultados precisos em razão da baixa eficiência de ionização térmica (Blichert-Toft & Albarède,  
 108 1997) as análises isotópicas passaram gradualmente a ser executadas com ICP-MS, pois alguns mL da  
 109 solução de Hf com algumas dezenas de ppb são suficientes.

110 O elemento Hf é muito abundante chegando além de 10000 ppm (Hoskin & Schaltegger,  
 111 2003) em muitos zircões pelo fato dele substituir facilmente o Zr na sua estrutura. O Hf pertence ao  
 112 grupo IVB (valência +4), é um elemento de elevado potencial iônico (HFSE - *High Field Strength*  
 113 *Element*), possui raio iônico de 0,81 Å e propriedades químicas similares ao do zircônio ( $Zr^{+4}$ , 0,80 Å).  
 114 Além do zircão, o Hf pode ser também encontrado em alta concentração na badeleíta, em torno de  
 115 1,33 % (Faure, 2005).

116 O Lu é o último elemento na faixa dos Terras Raras Pesados (ETRP), trivalente, faz parte do  
 117 grupo dos lantanídeos e é o elemento que apresenta o menor raio atômico neste grupo (0,93 Å). O Lu  
 118 está presente em todos os tipos de rocha (Faure, 1986), mas em concentrações baixas e sempre junto  
 119 ao itérbio (Yb). O mineral que apresenta maior concentração de Lu é a badeleíta, cerca de 70 ppm. O  
 120 Lu também é encontrado em outros minerais como zircão, granada, monazita e o xenotímio (Kinny &  
 121 Maas, 2003; Faure, 2005).

122 O Hf possui seis isótopos naturais:  $^{174}\text{Hf}$  (0,16 %),  $^{176}\text{Hf}$  (5,2 %),  $^{177}\text{Hf}$  (18,6 %),  $^{178}\text{Hf}$  (27,1  
 123 %),  $^{179}\text{Hf}$  (13,63 %) e  $^{180}\text{Hf}$  (35,1 %). Já o Lutécio possui somente dois isótopos, o  $^{175}\text{Lu}$  (97,4 %) e o  
 124  $^{176}\text{Lu}$  (2,59 %). Sendo que o isótopo  $^{176}\text{Lu}$  é um radionuclídeo que decai espontaneamente para o  $^{176}\text{Hf}$   
 125 liberando uma partícula beta. Devido a este decaimento, o  $^{176}\text{Hf}$  aumenta com o tempo nas rochas e  
 126 nos minerais e a idade Lu-Hf de rochas e minerais pode ser calculada a partir da equação 1:  
 127

$$\frac{^{176}\text{Hf}}{^{177}\text{Hf}} = \left( \frac{^{176}\text{Hf}}{^{177}\text{Hf}} \right)_t + \frac{^{176}\text{Lu}}{^{177}\text{Hf}} (e^{\lambda t} - 1) \quad (1)$$

129  
 130 Onde o  $t$  é o tempo decorrido desde a formação da rocha ou do mineral e o  $\lambda$  é a constante de  
 131 decaimento de  $^{176}\text{Lu}$ . Hoje, ainda se tem incerteza referente ao melhor valor a ser assumido para a  
 132 constante de decaimento. Baseado em meteoritos (eucritos) Patchett & Tatsumoto (1980) propuseram

133 o valor de  $1.94 \times 10^{-11} \text{ a}^{-1}$ . Um trabalho mais recente de Söderlund et al. (2004) sugerem um valor mais  
 134 preciso e um pouco menor (3,8%) de  $1,867 \times 10^{-11} \text{ a}^{-1}$ . Para o nosso estudo foi assumido o valor de  
 135  $1,867 \times 10^{-11} \text{ a}^{-1}$  proposto por Söderlund e colaboradores que se basearam em resultados de Lu-Hf de  
 136 diferentes minerais de doleritos Sorkka e Karlshemn da Suécia e Finlândia.

137 O zircão também hospeda isótopos de vida longa tais como U e Th cujas concentrações podem  
 138 atingir 1% ou até mais, além dos produtos de decaimento e ETR's cujas concentrações são variáveis,  
 139 mas na faixa de ppm. A concentração de Lu é baixa, sendo a razão Lu/Hf normalmente menor que  
 140 0,002. Assim, a razão  $^{176}\text{Hf}/^{177}\text{Hf}$  do zircão pode ser considerada como sendo o valor inicial de quando  
 141 ele foi cristalizado. Outra característica que torna o zircão um mineral de interesse é sua alta  
 142 resistência para eventos termais posteriores, pois a temperatura de fechamento do Hf no zircão é de  
 143 200°C, mais alta do que a do Pb, mostrando que o Hf permanece isotopicamente fechado durante a  
 144 maioria dos eventos termais (Faure, 1986). O zircão é um mineral acessório comum em inúmeras  
 145 rochas e preserva uma complexa história de crescimento. Portanto, núcleos herdados e crescimentos  
 146 metamórficos no zircão podem ser usados para identificar e distinguir vários processos geológicos.

147 O Sm e o Nd são elementos geoquimicamente muito parecidos. Os raios iônicos são  
 148 semelhantes, da mesma forma que carga e eletronegatividade. Já o Lu e o Hf são diferentes em carga  
 149 e raio. Apesar destas diferenças, as propriedades geoquímicas de Lu-Hf são similares ao par Sm-Nd  
 150 quando se trata de seus comportamentos na fusão parcial do manto, pois Hf em relação ao Lu é mais  
 151 concentrado no líquido silicático assim como o Nd para o Sm. Desta forma, os magmas basálticos  
 152 derivados do manto têm razões Lu/Hf mais baixas que a da rocha fonte, e o sólido residual é  
 153 empobrecido em Hf e tem razão Lu/Hf mais alta que a rocha antes da diferenciação. O que vai  
 154 depender muito da presença ou não da granada no manto, pois a granada desempenha um papel  
 155 importantíssimo nesta parte por ter grande afinidade com Lu e inibir sua entrada no material fundido  
 156 (Faure, 2005).

157 Devido a estas características, a metodologia Lu-Hf nos possibilita, além da determinação da  
 158 idade de diferenciação, estabelecer um indicador petrogenético denominado de  $\varepsilon_{\text{Hf}}$ . O parâmetro  $\varepsilon_{\text{Hf}}$   
 159 consiste basicamente na comparação da razão  $^{176}\text{Hf}/^{177}\text{Hf}$  da amostra estudada para a época de sua  
 160 formação ou de seu valor atual, com um reservatório condritico uniforme padrão (CHUR). Este fator

161 auxilia na identificação das fontes de magmas e de processos de formação de rochas e mineralizações  
 162 e é expresso conforme a equação 2:

163

$$164 \quad \varepsilon^t(Hf) = \left[ \frac{\left( ^{176}Hf / ^{177}Hf \right)_{am}^t - 1}{\left( ^{176}Hf / ^{177}Hf \right)_{CHUR}^t} \right] \times 10^4 \quad (2)$$

165

166 Se na época de cristalização da rocha seu magma progenitor tiver uma razão  $^{176}\text{Hf}/^{177}\text{Hf}$  mais  
 167 elevada que o condrito, o  $\varepsilon_{Hf}$  será positivo, significando que a fonte deste magma possuía a razão  
 168 Lu/Hf mais elevada que o condrito, ou seja, a fonte seria o manto superior. Por outro lado, se quando  
 169 da formação da rocha, seu magma progenitor possuía uma razão  $^{176}\text{Hf}/^{177}\text{Hf}$  menor que a do condrito,  
 170 o valor de  $\varepsilon_{Hf}$  é negativo e, portanto, a fonte destas rochas tinha uma razão Lu/Hf menor que o  
 171 condrito, como é o caso dos magmas de origem crustal. Portanto, quando o parâmetro  $\varepsilon_{Hf}$  é positivo a  
 172 fonte é em geral de origem mantélica, e quanto maior for o seu valor mais empobrecido  
 173 geoquimicamente é este manto do qual se derivou.

174 Outra informação que pode ser obtida pela metodologia é a idade modelo do “manto  
 175 empobrecido” (DM - *Depleted Mantle*). Este modelo admite que o manto sofrera episódios de  
 176 fracionamento envolvendo a extração de magmas basálticos para a geração de crosta continental e  
 177 causou o empobrecimento em elementos leves (LILE – *Large Ion Lithophile Elements*) e também dos  
 178 elementos terras raras leves (ETRL) neste reservatório (Nebel et al., 2007). O resultado dessas  
 179 diferenciações é um manto residual enriquecido na razão Lu/Hf e empobrecido geoquimicamente em  
 180 elementos litófilos. A idade modelo do manto empobrecido pode ser calculada pela equação 3:

181

$$182 \quad T_{DM} = \frac{t_{(U/Pb)}}{1000} + \frac{1}{0.01867} \times \ln \left( 1 + \frac{\left( ^{176}Hf / ^{177}Hf \right)_{am}^t - \left( ^{176}Hf / ^{177}Hf \right)_{DM}^t}{\left( ^{176}Lu / ^{177}Hf \right)_{crosta}^t - \left( ^{176}Lu / ^{177}Hf \right)_{DM}^0} \right) \quad (3)$$

183

184 Onde os valores assumidos hoje do manto empobrecido para as razões  $^{176}\text{Hf}/^{177}\text{Hf}$  e  $^{176}\text{Lu}/^{177}\text{Hf}$  são  
185 iguais a 0,28325 e 0,0388, respectivamente (Andersen et al., 2009). A idade TDM é calculada a partir  
186 da composição isotópica inicial de Hf do momento que o zircão cristalizou e da razão Lu/Hf da crosta  
187 precursora, seja ela de composição máfica ou félscica (Pietranik et al., 2008). Portanto, é importante  
188 realizar as análises de U-Pb e Lu-Hf sobre a mesma porção de um grão de zircão, a fim de recalcular o  
189  $\epsilon\text{Hf}$  e a idade TDM do momento de sua cristalização.

190

### 191 **3. Procedimentos Analíticos**

#### 192 *3.1 ICP-MS*

193 As análises de Hf em zircão foram feitas utilizando o ICP-MS *Neptune da ThermoFinnigan*  
194 um espectrômetro de massa multicoletor de alta resolução para medidas de razões isotópicas com uma  
195 configuração especial para detectar simultaneamente uma ampla gama de nuclídeos de elementos  
196 como Hg até U. O Neptune é equipado com 9 coletores Faraday e 6 contadores de íons (MIC's), que  
197 podem ser combinados em diversas configurações. A configuração dos coletores utilizada para as  
198 análises de Lu-Hf acha-se ilustrada na tabela 1 e todas as análises foram realizadas no modo estático e  
199 em baixa resolução.

200

201 inserir tabela 1

202

#### 203 *3.2 Laser*

204 A microssonda a laser, modelo UP213 (Nd:YAG) de New Wave, utilizada para as análises por  
205 ablação em minerais pode emitir alta densidade de energia em vários tamanhos de crateras (4  $\mu\text{m}$  - 110  
206  $\mu\text{m}$ ). O gás hélio (He) é o responsável pelo transporte do material da ablação para o ICP com um fluxo  
207 de 0,35-0,45 l/min. Para as análises de Hf uma pequena quantidade de nitrogênio ( $\text{N}_2$ ) da ordem de 3,5  
208 a 4 mL/min foi adicionada ao gás Ar de arraste, conforme Louie e Soo aplicaram em 1992, para  
209 diminuir a formação de óxidos no plasma e aumentar a intensidade do sinal em mais de 100% em  
210 algumas análises, conforme detalhado mais adiante.

211 Durante as análises de Hf com laser foi utilizado uma taxa de repetição de 10 Hz. Dependendo  
212 do tipo de laser utilizado e parâmetros selecionados é uma prática corrente utilizar uma frequencia de  
213 10 a 20 pulsos por segundo. Com o laser UP213 de Nd:YAG, a taxa definida acima revelou-se  
214 totalmente satisfatória em termos de eficiência e estabilidade dos sinais. Diâmetro dos furos com laser  
215 foram de 55  $\mu\text{m}$  fornecendo um sinal intenso da ordem de 3 volts para  $^{178}\text{Hf}$  em todas as análises de  
216 Hf. De acordo com as quantidades de Hf dos padrões GJ-1 e Mud Tank, uma potência de 60% do laser  
217 mostrou-se adequada fornecendo uma densidade de energia de 5-6 J/cm<sup>2</sup>. A seqüência de análises foi a  
218 de intercalar três grãos com um dos padrões, preferencialmente GJ-1 em que a razão  $^{176}\text{Hf}/^{177}\text{Hf}$  é  
219 conhecida com mais precisão. Os grãos foram montados em uma pastilha de epoxi com pequena  
220 cavidade para inserção do pequeno cilindro com um dos padrões citados. Todos os parâmetros de  
221 instrumentação e operação usados para as análises de Lu-Hf em zircão no LA-ICPMS estão resumidos  
222 na tabela 2.

223

224 inserir tabela 2

225

### 226 3.3 Cálculos da Correção de Interferência Isobárica

227 Os isótopos de Lu, Hf e Yb são medidos simultaneamente durante as análises no MC-ICP-MS.  
228 As razões isotópicas medidas destes elementos durante os aproximadamente 50s de análise foram:  
229  $^{173}\text{Yb}/^{171}\text{Yb}$ ,  $^{179}\text{Hf}/^{177}\text{Hf}$ ,  $^{176}\text{Lu}/^{177}\text{Hf}$ ,  $^{176}\text{Hf}/^{177}\text{Hf}$ .

230 Para a correção do fracionamento isotópico do instrumento que ocorre durante as análises, as  
231 razões isotópicas de Yb foram normalizadas assumindo para  $^{173}\text{Yb}/^{171}\text{Yb}$  o valor de 1,1301 (Segal et  
232 al., 2003) e as razões isotópicas de Hf e Lu são normalizadas para a razão  $^{179}\text{Hf}/^{177}\text{Hf}$  com o valor de  
233 0,7325 (Patchett & Tatsumoto, 1980). Com o objetivo de testar as correções do Yb foram preparadas  
234 soluções do padrão JMC-475 (200 ppb) dopado com quantidades conhecidas de Yb ( $\text{Yb/Hf} = 0,05$  e  
235 0,1) fornecendo o valor de  $0,282149 \pm 0,000031$  ( $n=6$ , 2SD), em concordância com o valor aceito de  
236  $0,282159 \pm 0,000038$  (Chu et al., 2002).

237 Durante as análises *in situ* de Hf no zircão, os nuclídeos isóbaros interferentes,  $^{176}\text{Lu}$  e  $^{176}\text{Yb}$ ,  
238 são medidos juntamente com o  $^{176}\text{Hf}$ . Para se obter a razão  $^{176}\text{Hf}/^{177}\text{Hf}$  do zircão com acuracidade, as

239 interferências devidas a  $^{176}\text{Lu}$  e  $^{176}\text{Yb}$  foram cuidadosamente corrigidas com base nos sinais  
 240 observados do  $^{175}\text{Lu}$  e do  $^{173}\text{Yb}$ , ambos com as devidas normalizações. A intensidade ou sinal  
 241 correspondente ao  $^{176}\text{Hf}$  foi calculada através da equação 4:

242

$$243 \quad ^{176}\text{Hf} = ^{176}(\text{Hf} + \text{Lu} + \text{Yb})_m - \left[ ^{175}\text{Lu}_m \times \left( \frac{^{176}\text{Lu}}{^{175}\text{Lu}} \right)_N \times \left( \frac{M_{176(\text{Lu})}}{M_{175}} \right)^{\beta(\text{Lu})} \right. \\ \left. + ^{173}\text{Yb}_m \times \left( \frac{^{176}\text{Yb}}{^{173}\text{Yb}} \right)_N \times \left( \frac{M_{176(\text{Yb})}}{M_{173}} \right)^{\beta(\text{Yb})} \right] \quad (4)$$

244

245 Os fatores  $\beta_{(\text{Lu})}$  e o  $\beta_{(\text{Yb})}$  são os fatores de fracionamento para Lu e Yb. Estes dois fatores  
 246 variam durante o tempo da análise no grão de zircão (Iizuka & Hirata, 2005), isto indica que o fator  $\beta$   
 247 não pode ser assumido como uma constante durante as análises, devendo ser calculado para cada  
 248 medida feita.

249 Por fim, os dados são processados em planilhas Excel e específicas para Lu-Hf. Nestas  
 250 planilhas são selecionados aproximadamente 45 dados (de um total de 50 dados integrados de  
 251 1,049s/ponto) e calculada a idade modelo TDM e o parâmetro  $\epsilon_{\text{HF}}$  do ponto analisado.

252

#### 253 4. Resultados

##### 254 4.1 Análises dos Padrões de Hf

255 Em termos de estabilidade do sinal, as análises de solução com ICP-MS apresentam razões  
 256 isotópicas mais precisas do que por ablação a laser. Desta forma, antes de iniciar as sessões de ablação  
 257 a laser, o espectrômetro é rotineiramente focalizado e aferido com o padrão em solução após a  
 258 calibração de ganho dos amplificadores Faraday. Em um total de 24 análises da solução pura do  
 259 padrão de Hf JMC-475 (200 ppb) a razão média  $^{176}\text{Hf}/^{177}\text{Hf}$  normalizada foi de  $0,282156 \pm 0,000015$   
 260 ( $n=24, 2\text{SD}$ ).

261 Durante as análises *in situ* a laser dois padrões foram utilizados para verificar a  
 262 reproduzibilidade do aparelho. Um dos padrões conhecido por GJ-1 (Morel et al., 2008) e fornecido

263 pela GEMOC (Geochemical Evolution and Metallogeny of Continents, MacQuarie University,  
264 Sydney, Australia), foi extraído de um pegmatito Africano com idade de cristalização de  $608,5 \pm 0,4$   
265 Ma. As cores dos grãos deste padrão variam do vermelho ao amarelado e as imagens de CL (catodo  
266 luminescência) mostram boa homogeneidade em termos, por exemplo, de Pb radiogênico com  
267 respectivos pais. O segundo é o zircão conhecido como Mud Tank (Woodhead & Herdt, 2005),  
268 fornecido por Elena Belousova, trata-se de um padrão internacional para Lu/Hf separado de um  
269 carbonatito aflorante no Strangways Range situada a noroeste da Austrália e cuja idade U-Pb foi  
270 estabelecida como sendo de 732 Ma. Zircões e apatitas são encontrados em grande abundância e os  
271 tamanhos podem ser maiores que 10 cm.

272 O valor obtido para a razão  $^{176}\text{Hf}/^{177}\text{Hf}$  do GJ-1 durante as análises dos zircões do Ofiolito de  
273 Aburrá (ver seção 4.2) foi de  $0,282004 \pm 0,000004$  ( $n=3$ , 2SD), em perfeita concordância com o valor  
274 de  $0,282000 \pm 0,000004$  publicado (Morel et al., 2008). A respectiva razão para o Mud Tank foi de  
275  $0,282466 \pm 0,000022$  ( $n=3$ , 2SD) bastante concordante com a razão  $0,282504 \pm 0,000044$  publicada  
276 por Woodhead & Herdt (2005). Foram também obtidos valores destes padrões após diversos testes  
277 com diâmetros de 40 e 55  $\mu\text{m}$  e com nitrogênio, os resultados destes testes são apresentados na tabela  
278 3. Em geral as análises com 55  $\mu\text{m}$  e nitrogênio mostraram intensidades altas no  $^{178}\text{Hf}$  com valores em  
279 torno de 2,6 a 3,2 V no GJ-1 e de 3,13 a 3,27 V no Mud Tank, mostrando um aumento de mais de  
280 100% se compararmos com as demais análises que obtiveram intensidades em torno de 0,89 e 2,13 V.  
281 As medidas da razão  $^{176}\text{Hf}/^{177}\text{Hf}$  também foram mais precisas com 55  $\mu\text{m}$  e nitrogênio do que as  
282 demais análises com um valor de  $0,282010 \pm 0,000012$  ( $n=3$ , 2SD) para o GJ-1 e  $0,282472 \pm 0,000028$   
283 ( $n=3$ , 2SD) para o Mud Tank. A razão  $^{176}\text{Lu}/^{177}\text{Hf}$  apresentou erros baixos em todas as análises e  
284 manteve boa reproduzibilidade no GJ-1, enquanto no Mud Tank não se obteve a mesma  
285 reproduzibilidade devido ao baixo teor de  $^{176}\text{Lu}$  neste padrão.

286

287 inserir tabela 3

288

289           Na figura 1, a fim de discutir detalhes das análises de Hf são ilustrados os resultados no padrão  
290          GJ-1 com 55 µm, com e sem nitrogenio. Nas análises é possível verificar que as intensidades de Hf no  
291          decorrer das análises decrescem um pouco na medida em que o furo vai ficando com maior  
292          profundidade. O índice de fracionamento nas razões isotópicas de Hf é próximo a 1, o que indicaria  
293          leve fracionamento durante a ablação.

294

295          inserir figura 1

296

297          *4.2 Aplicação da Metodologia Lu-Hf*

298           Neste estudo usou-se zircões separados de um gábro pegmatítico pertencente ao Ofiolito de  
299          Aburrá (Correa et al., 2005), setor norte da Colômbia, Cordilheira Central. Este ofiolito consiste em  
300          duas unidades: o Dunito de Medellín composto por rochas ultramáficas do manto e os Metagabros de  
301          El Picacho, com rochas plutônicas máficas. O mesmo se encontra em contato tectônico sobre rochas  
302          metamórficas mais antigas do que o Triássico Médio e é intrudido por rochas do Jurássico e do  
303          Cretáceo (Martinez, 2007). O ofiolito comprehende um conjunto de rochas máficas e ultramáficas  
304          geradas nas cadeias meso oceânicas e que devido a tectônica foi alojado sobre bordas continentais  
305          ativas ou passivas. Assim, o estudo de Lu-Hf nos zircões do Ofiolito de Aburrá contribui para a  
306          história geológica da borda NW da América do Sul.

307           A preparação da amostra seguiu a sistemática descrita em Chemale Jr. et al. (*in press*). Os  
308          zircões separados foram montados sobre um cilindro epóxi e depois polidos até ficar exposta a  
309          superfície fresca dos grãos. Imagens dos cristais com o microscópio eletrônico de varredura (MEV),  
310          medindo em torno de 500 µm, mostram se bem formados e homogêneos. Alguns dos grãos apresentam  
311          um zoneamento atribuído ao processo magmático.

312           Primeiramente os zircões foram datados pelo método U/Pb fornecendo uma idade de 228 ±  
313          0,92 Ma (Restrepo et al., 2007). Esta foi a idade assumida para o cálculo da idade modelo TDM  
314          conforme equação 3 e também das razões  $^{176}\text{Hf}/^{177}\text{Hf}$  iniciais. Esta idade de 228 Ma é interpretada  
315          como sendo a idade de cristalização do magma gabróico hospedeiro e, consequentemente da seqüência  
316          ofiolítica, portanto no Triássico Superior.

317 inserir figura 2

318

319 As análises *in situ* de Hf foram feitas em doze zircões, seguindo a metodologia descrita na  
320 seção 3.2 deste trabalho. Os furos para as análises com laser foram feitos próximos dos alvos  
321 selecionados para as análises U-Pb (Fig. 2) para evitar eventuais dúvidas interpretativas. Na tabela 4  
322 são apresentados os valores para o  $\epsilon_{\text{Hf}}(t)$  que forneceram valores entre +2,01 a +5,35 e das idades  
323 modelos que se enquadram entre 1,15 a 1,44 Ga. Na figura 3, são ilustrados através de diagramas os  
324 valores de  $\epsilon_{\text{Hf}}(t)$  e da razão inicial  $^{176}\text{Hf}/^{177}\text{Hf}$  obtidos para a idade de cristalização de 228 Ma destes  
325 zircões.

326

327 inserir tabela 4

328

329 inserir figura 3

330

331 **5. Discussão dos resultados**

332 Durante as análises de Hf o nitrogênio foi injetado através de um fluxômetro e conexão T ao  
333 gás de arraste (Ar) com a finalidade de aumentar a sensibilidade para a obtenção das razões isotópicas  
334 do Hf. Nos testes efetuados com padrões comprovamos que o uso deste gás a uma vazão de  
335 aproximadamente 4 ml/min aumentava significativamente a intensidade dos sinais. Também foi  
336 observada a diferença de sinal entre um furo com 55  $\mu\text{m}$  de diâmetro contra um de 40  $\mu\text{m}$ . A diferença  
337 a favor de 55 microns é bem notória, de tal forma que, quando possível, é preferível usar diâmetros  
338 maiores. Na literatura constam diâmetros até da ordem de 100 microns.

339 Os valores de  $\epsilon_{\text{Hf}}(t)$  obtidos são positivo o que sugere a presença de um magma juvenil com  
340 uma possível contaminação crustal, o que explicaria a variabilidade nos valores se aproximando de  
341 zero. A idade U/Pb de aproximadamente 230 Ma é a idade de cristalização do magma gabróico  
342 hospedeiro e formação da sequência ofiolítica que reajustou o sistema U/Pb. Este evento assume-se  
343 que, preservou o sistema Lu-Hf.

344           A despeito de as razões Lu/Hf serem determinadas com baixa precisão devida ao baixo teor de  
345           Lu (cerca de 11 ppm, por exemplo, no padrão GJ-1) não afeta de forma significativa as idades modelos  
346           calculadas. Assim, as idades TDM obtidas de 1,15-1,44 Ga representariam a possível idade dos  
347           protólitos destes zircões. Esta faixa de idade coincide bem com os eventos magmáticos Grenvilianos  
348           (1,2-1,1 Ga) e contemporânea à formação das rochas da Província Rondoniana - San Ignacio (1,5-1,3  
349           Ga) conforme inúmeros trabalhos (e.g. Tohver et al., 2004).

350           Os dados de Hf aqui apresentados são semelhante aos dados já publicados de zircões desta  
351           área por Matteini et al. (2008). As diferenças maiores são verificadas nas idades modelo TDM.  
352           Matteini obteve valores entre 0,6-0,7 Ga, cerca de 50% mais baixos que os obtidos neste trabalho. A  
353           explicação para esta diferença é por ele ter utilizado no cálculo da idade o valor médio crustal igual a  
354           0,0113 para a razão  $^{176}\text{Lu}/^{177}\text{Hf}$ . No presente trabalho foi utilizado um valor de 0,022 para esta razão,  
355           que se refere a uma crosta precursora de composição máfica (Pietranik et al., 2008), sendo coerente  
356           com a área de estudo.

357

## 358       **6.      Conclusões**

359           A metodologia Lu-Hf descrita e aplicada no Laboratório de Geologia Isotópica da UFRGS  
360           para análises *in situ* de zircões por LA-MC-ICP-MS mostrou-se bastante confiável e expedita,  
361           conforme esperado. Os dois padrões GJ-1 e Mud Tank utilizados durante as análises reproduziram os  
362           valores da literatura dentro da margem de erro. Verificamos que o uso de nitrogênio durante as  
363           análises de Hf comprovou ser muito efetivo, não só em aumento na sensibilidade, mas também na  
364           estabilidade dos sinais, propiciando um ganho significativo na precisão dos resultados obtidos com  
365           análises *in situ* do sistema Lu-Hf em zircões.

366           A metodologia Lu-Hf aplicada aos zircões do Ofiolito de Aburrá forneceu novos dados  
367           isotópicos e idades modelos que aparentemente seriam mais coerentes com as recentes idéias da  
368           conexão da Província Amazônica e o Laurentia no contexto de amalgamação do Continente Rodinia.  
369           Os dados combinados U-Pb e Lu-Hf são ainda muito escassos para maiores interpretações, mas pode  
370           se antever como um potencial instrumento para robustecer melhor as idéias e novos conhecimentos  
371           sobre a evolução crustal, não só em nível regional mas a nível global.

372

373 **Agradecimentos**

374 O presente trabalho foi realizado com apoio do CNPq, Conselho Nacional de Desenvolvimento Científico e  
 375 Tecnológico através da bolsa de doutorado. Agradecemos ao Engenheiro Antonio Celso (Sens Representações  
 376 Ltda) pela cessão de um fluxômetro regulável para nitrogênio utilizado pioneiramente no país para as análises do  
 377 sistema Lu-Hf do presente trabalho. Agradecemos também aos pesquisadores J.J. Restrepo da Universidade  
 378 Nacional da Colômbia e ao J.C. Frantz da UFRGS pelo fornecimento dos zircões do Ofiolito de Aburrá,  
 379 Colômbia.

380

381 **Referências**

- 382 Andersen, T., Andersson, U.B., Graham, S., Åberg, G. & Simonsen, S.L. 2009. Granitic magmatism by melting  
 383 of juvenile continental crust: new constraints on the source of Palaeoproterozoic granitoids in Fennoscandia from  
 384 Hf isotopes in zircon. *Journal of Geological Society*, 166: 233-247.  
 385 Blichert-Toft, J. & Albarède, F. 1997. The Lu-Hf isotope geochemistry of chondrites and the evolution of the  
 386 mantle crust system. *Earth and Planetary Science Letters*, 148: 243-258.  
 387 Chemale Jr., F., Kawashita, K., Dussin, I.A., Justino, D. & Bertotti, A.L. U-Pb zircon in situ dating with LA-  
 388 MC-ICP-MS using mixed detector configuration. Anais da Academia Brasileira de Ciências, *in press*.  
 389 Chu, N.C., Taylor, R.N., Chavagnac, V., Nesbitt, R.W., Boella, M. & Milton, J.A. 2002. Hf isotope ratio  
 390 analysis using multi-collector inductively coupled plasma mass spectrometry: an evaluation of isobaric  
 391 interference corrections. *Journal of Analytical Atomic Spectrometry*, 17: 1567-1574.  
 392 Correa, A.M., Martens, U.C., Restrepo, J.J., Ordoñez-Carmona, O. & Pimentel, M. 2005. Subdivisión de lágs  
 393 metamorfitas básicas de los alrededores de Medellín, Cordillera Central de Colombia. Colombia. Revista  
 394 Academia Colombiana de Ciencias. 29 (112): 325-344.  
 395 Elhlou, S., Belousova, E., Griffin, W.L., Pearson, N.J. & O'Reilly, S.Y. 2006. Trace element and isotopic  
 396 composition of GJ-red zircon standard by laser ablation. *Geochimica Cosmochimica Acta*, 70 (18): 158.  
 397 Faure, G. 1986. *Principles of Isotope Geology*. New York, John Wiley & Sons, Ed. 2<sup>a</sup>, 589p.  
 398 Faure, G. 2005. *Isotopes: Principles and Applications*. New York, John Wiley & Sons, Ed. 3<sup>a</sup>, 897p.  
 399 Gerdes, A. & Zeh, A. 2006. Combined U-Pb and Hf isotope LA-(MC)-ICP-MS analyses of detrital zircons:  
 400 Comparison with SHRIMP and new constraints for the provenance and age of American metasediment in central  
 401 Germany. *Earth and Planetary Science Letters*, 249: 47-61.  
 402 Gerdes, A. & Zeh, A. 2009. Zircon formation versus zircon alteration – New Insights from combined U-Pb and  
 403 Lu-Hf in-situ LA-ICP-MS analyses, and consequences for the interpretation of archean zircon from the Central  
 404 Zone of the Limpopo Belt. *Chemical Geology*, 261: 230-243.  
 405 Goode, J.W. & Vervoort, J.D. 2006. Origin of Mesoproterozoic A-type granites in Laurentia: Hf isotope  
 406 evidence. *Earth and Planet Science Letters*, 243: 711-731.  
 407 Griffin, W.L., Pearson, N.J., Belousova, E., Jackson, S.E., van Achterbergh E., O'Reilly S.Y. & Shee, S.R. 2000.  
 408 The Hf isotope composition of cratonic mantle: LAM-MC-ICPMS analysis of zircon megacrysts in Kimberlites.  
 409 *Geochimica Cosmochimica Acta*, 64: 133-147.  
 410 Hoskin, P. & Schaltegger, U. 2003. The Composition of Zircon and Igneous and Metamorphic Petrogenesis. In:  
 411 Reviews in Mineralogy and Geochemistry, 53: 27-62.  
 412 Izuka, T. & Hirata, T. 2005. Improvements of precision and accuracy in situ Hf isotope microanalysis of zircon  
 413 using the laser ablation-MC-ICPMS technique. *Chemical Geology*, 220: 131-137.  
 414 Louie, H. & Soo, S.Y.-P. 1992. Use of nitrogen and hydrogen in inductively plasma mass spectrometry. *Journal*  
 415 *of Analytical Atomic Spectrometry*, 7: 557-564.  
 416 Kinny, P. & Maas, R. 2003. Lu-Hf and Sm-Nd Isotope systems in zircon. In: *Reviews in Mineralogy and*  
 417 *Geochemistry*, vol. 53, 327-341.  
 418 Martínez, A.M.C. 2007. Petrogênese e Evolução do Ofiolito de Aburrá, Cordilheira Central dos Andes  
 419 Colombianos. Brasília, 204p. Tese de Doutorado, Programa de Pós-Graduação em Geologia, Instituto de  
 420 Geociências, Universidade de Brasília.

- 421 Matteini, M., Restrepo, J.J., Correa, A. & Pimentel, M.M. 2008. Lu-Hf LA-MC-ICP-MS *In Situ* Analyses on  
 422 Petrographic Thin Section: Application on Zircon Macrocrysts from Aburrá Ophiolite, Central Cordillera of  
 423 Colombia. VI South American Symposium on Isotope Geology San Carlos de Bariloche, Argentina.
- 424 Morel, M.L.A., Nebel, O., Nebel-Jacobsen, Y.J., Miller, J.S. & Vroon, P.Z. 2008. Hafnium isotope  
 425 characterization of the GJ-1 zircon reference material by solution and laser-ablation MC-ICPMS. *Chemical*  
 426 *Geology*, 255: 231–235.
- 427 Nebel, O., Nebel-Jacobsen, Y., Mezger, K. & Berndt, J. 2007. Initial Hf isotope compositions in magmatic  
 428 zircon from early Proterozoic rocks from the Gawler Craton, Australia: A test for zircon model ages. *Chemical*  
 429 *Geology*, 241: 23–37.
- 430 Patchett, P.J. & Tatsumoto, M. 1980. Lu-Hf total rock isochron for the eucrite meteorites. *Nature*, 288: 571–574.
- 431 Patchett, P.J., Kouvo, O., Hedge, C.E. & Tatsumoto, M. 1981. Evolution of continental crust and mantle  
 432 heterogeneity: evidence from Hf isotopes. *Contribution to Mineralogy and Petrology*, 78: 279–297.
- 433 Pietranik, A.B., Hawkesworth, C.J., Storey, C.D., Kemp, A.I.S., Sircombe, K.N., Whitehouse, M.J. & Bleeker,  
 434 W. 2008. Episodic, mafic crust formation from 4.5 to 2.8 Ga: New evidence from detrital zircons, Slave craton,  
 435 Canada. *The Geological Society of America*, 36( 11): 875–878.
- 436 Restrepo, J.J., Frantz, J.C., Ordóñez-Carmona, O., Correa, A.M., Martens, U. & Chemale, F. 2007. Edad triásica  
 437 de formación de la Ofiolita de Aburrá, flanco occidental de la cordillera Central. *Memorias XI Congreso*  
 438 *Colombiano de Geología*, Bucaramanga.
- 439 Scherer, E.E., Münker, C. & Mezger, K. 2001. Calibration of the Lutetium-Hafnium Clock. *Science*, 293: 683–  
 440 686.
- 441 Scherer, E.E., Whitehouse, M.J. & Münker, C. 2007. Zircon as a monitor of crustal grown. *Elements*, 3: 19–24.
- 442 Segal, I., Halicz, L. & Platzner, I.T. 2003. Accurate isotope ratio measurements of ytterbium by multiple  
 443 collection inductively coupled plasma mass spectrometry applying erbium and hafnium in an improved double  
 444 external normalization procedure. *Journal of Analytical Atomic Spectrometry*, 18: 1217–1223.
- 445 Söderlund, U., Patchett, J.P., Vervoort, J.D. & Isachsen, C.E. 2004. The  $^{176}\text{Lu}$  decay constant determined by Lu–  
 446 Hf and U–Pb isotope systematics of Precambrian mafic intrusions. *Earth and Planetary Science Letters*, 219:  
 447 311–324.
- 448 Thirwall, M.F. & Walder, A. J. 1995. In situ hafnium isotope ratio analyses of zircon by inductively coupled  
 449 plasma mass spectrometry. *Chemical Geology*, 122: 241–247.
- 450 Tohver, E., Bettencourt, J.S., Tosdal, R., Mesger, K., Leite, W.B. & Payolla, B.L. 2004. Terrane transfer during  
 451 the Grenville orogeny: tracing the Amazonian ancestry of southern Appalachian basement through Pb and Nd  
 452 isotopes. *Earth and Planetary Science Letters*, 228: 161–176.
- 453 Vervoort, J. & Blichert-Toft, J. 1999. Evolution of the depleted mantle: Hf isotope evidence from juvenile rocks  
 454 through time. *Geochimica Cosmochimica Acta*, 63: 533–557.
- 455 Woodhead, J., Herdt, J., Shelley, M., Eggins, S. & Kemp, R. 2004. Zircon Hf-isotope analysis with an excimer  
 456 laser, depthprofiling, ablation of complex geometries and concomitant age stimation. *Chemical Geology*, 209:  
 457 121–135.
- 458 Woodhead, J.D. & Herdt, J. M. 2005. A preliminary appraisal of seven natural zircon reference materials for in  
 459 situ hf isotope determination. *Geostandards and Geoanalytical Research*, 29: 183–195.
- 460 Wu, F.-Y., Yang, Y.-H., Xie, L.-W., Yang, J.-H. & Xu, P. 2006. Hf isotopic compositions of the standard  
 461 zircons and baddeleyites used in U-Pb geochronology. *Chemical Geology*, 234: 105–126.
- 462 Zeh, A., Gerdes, A., Klemd, R. & Barton Jr., J.M. 2007. Archaean to Proterozoic Crustal Evolution in the  
 463 Central Zone of the Limpopo Belt (South Africa-Botswana): Constraints from Combined U-Pb and Lu-Hf  
 464 Isotope Analyses of Zircon. *Journal of Petrology*, 48: 1605–1639.
- 465
- 466
- 467
- 468
- 469
- 470
- 471
- 472
- 473

474 **Legendas Tabelas**

475

476 Tabela 1 – Configuração dos coletores Faraday adotada para as análises de Lu e Hf.

477 Tabela 2 – Parâmetros de instrumentação e operação para o Laser Ablation e o MC-ICPMS.

478 Tabela 3 - Resultados dos padrões GJ-1 e Mud Tank durante as análises e testes utilizando 40 e 55  $\mu\text{m}$   
479 e nitrogênio.

480 Tabela 4 – Resultados das análises de Hf nos zircões do Ofiolito de Aburrá.

481

482

483 **Legendas Figuras**

484

485 Figura 1 – Exemplo de comparação dos dados isotópicos de Hf, intensidade do sinal e índice de  
486 fracionamento no padrão GJ-1; a) 55 $\mu\text{m}$  e com nitrogênio e b) 55 $\mu\text{m}$  e sem nitrogênio.

487

488 Figura 2 - Imagem de MEV de alguns zircões do Ofiolito de Aburrá ilustrando os furos feitos nas  
489 análises de U-Pb (furo menor) e Lu-Hf.

490

491 Figura 3- Diagramas dos valores de  $\epsilon\text{Hf}$  (t) (a) e da evolução isotópica de Hf (b) dos zircões do  
492 Ofiolito de Aburrá. As áreas sombreadas indicam a tendência de evolução para o ophiolito.

493

494

495

496

497

498

499

500

501

502

503

504

505

506

507

508

509

510

511

512

513

514

515

516

517

518

519

520

521

522

523

524

525

526

527

528

529 **Tabela 1**

<b>Isótopos Interferentes</b>	<b>L4</b> $^{171}\text{Yb}$	<b>L3</b> $^{173}\text{Yb}$	<b>L2</b> $^{174}\text{Hf}$	<b>L1</b> $^{175}\text{Lu}$ $^{174}\text{Yb}$	<b>C</b> $^{176}\text{Hf}$	<b>H1</b> $^{177}\text{Hf}$	<b>H2</b> $^{178}\text{Hf}$	<b>H3</b> $^{179}\text{Hf}$ (Yb+Lu)
-------------------------------	--------------------------------	--------------------------------	--------------------------------	---	-------------------------------	--------------------------------	--------------------------------	---

531  
532  
533 **Tabela 2**  
534**MC-ICPMS**

Instrumento	Neptune (ThermoFinnigan)
<b>Fonte de íon</b>	
Potência	1200W
Fluxo de gás	Ar Resfriador: 15 L/min Ar Auxiliar: 0,7 L/min Ar Transporte: 0,72-0,76 L/min N <sub>2</sub> Transporte: 3,5-4,5 mL/min
Extração	-2000 V
Modo de Análise	Estático
Detecção	Coletores Faraday
<b>Aquisição de Dados</b>	
Tempo de integração	1,049s
Nº de integrações	1
<b>Laser Ablation</b>	
Instrumento	UP-213 (Nd:YAG) New Wave
Diâmetro do furo	55 μm
Energia	5-6 J/cm <sup>2</sup>
Freqüência	10 Hz
Total da ablação	50s
Fluxo de He	0,32 a 0,45 L/min

535  
536  
537 **Tabela 3**  
538

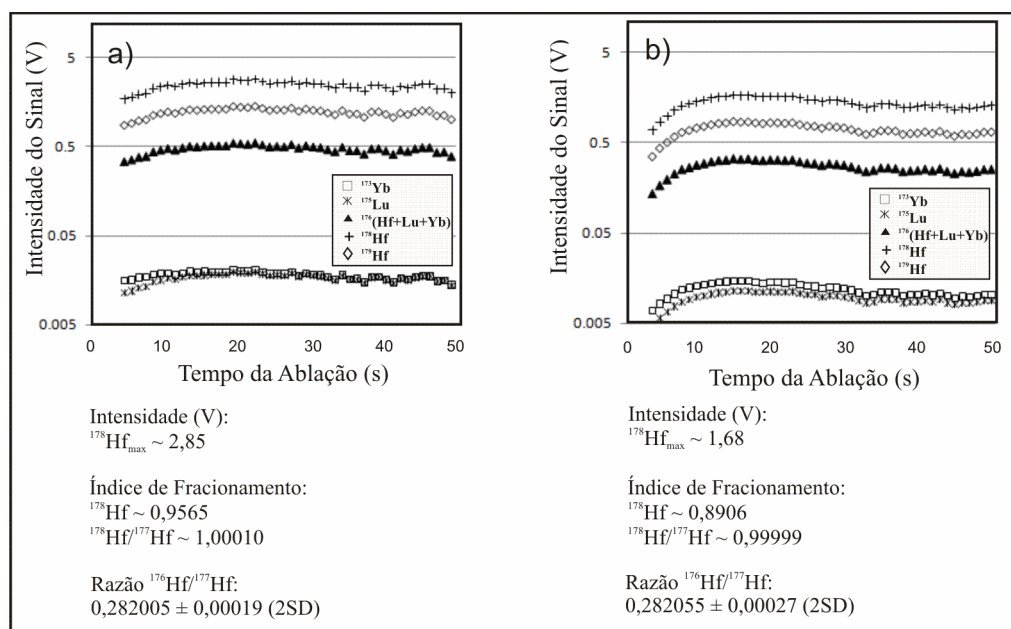
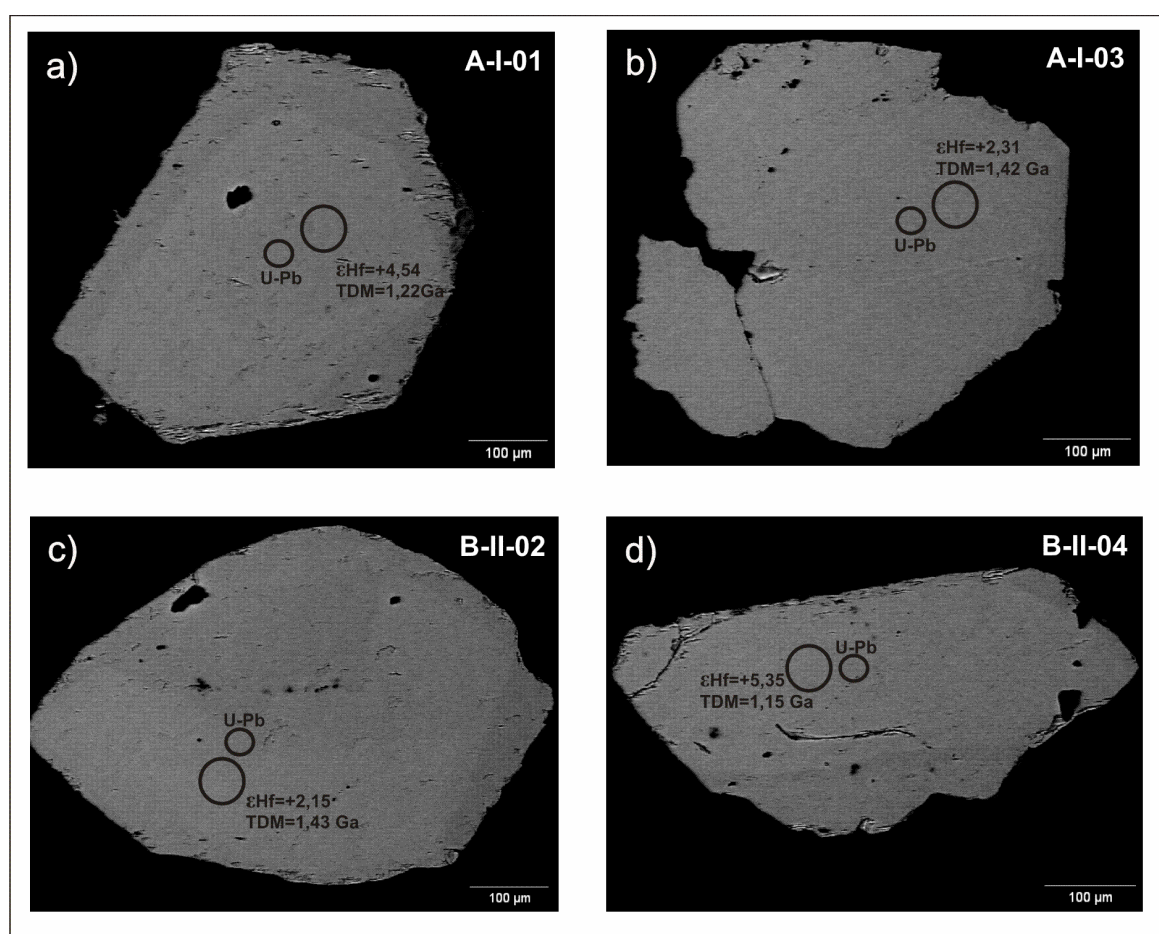
Padrão	$^{178}\text{Hf}_{\max}$ (V)	$^{176}\text{Hf}/^{177}\text{Hf}$	2DP	$^{176}\text{Lu}/^{177}\text{Hf}$	2DP	Observações
<b>Análises</b>						
<b>GJ-1</b>	2,34	0,282004	0,000004	0,000259	0,000008	n=3, 55μm e N <sub>2</sub>
<b>Testes</b>						
<b>GJ-1</b>	2,91	0,282010	0,000012	0,000283	0,000012	n=3,55μm e N <sub>2</sub>
<b>GJ-1</b>	1,72	0,282067	0,000022	0,000275	0,000012	n=3, 55 μm
<b>GJ-1</b>	1,40	0,282044	0,000062	0,000261	0,000012	n=3, 40 μm e N <sub>2</sub>
<b>GJ-1</b>	0,89	0,282040	0,000026	0,000258	0,000024	n=3 40 μm
<b>Análises</b>						
<b>Mud Tank</b>	3,19	0,282466	0,000022	0,000104	0,000012	n=3, 55μm e N <sub>2</sub>
<b>Testes</b>						
<b>Mud Tank</b>	3,20	0,282472	0,000028	0,000069	0,000020	n=3, 55 μm e N <sub>2</sub>
<b>Mud Tank</b>	2,13	0,282563	0,000046	0,000046	0,000004	n=3, 55 μm
<b>Mud Tank</b>	1,54	0,282455	0,000032	0,000074	0,000004	n=3, 40 μm e N <sub>2</sub>
<b>Mud Tank</b>	1,40	0,282452	0,000048	0,000058	0,000032	n=3, 40 μm

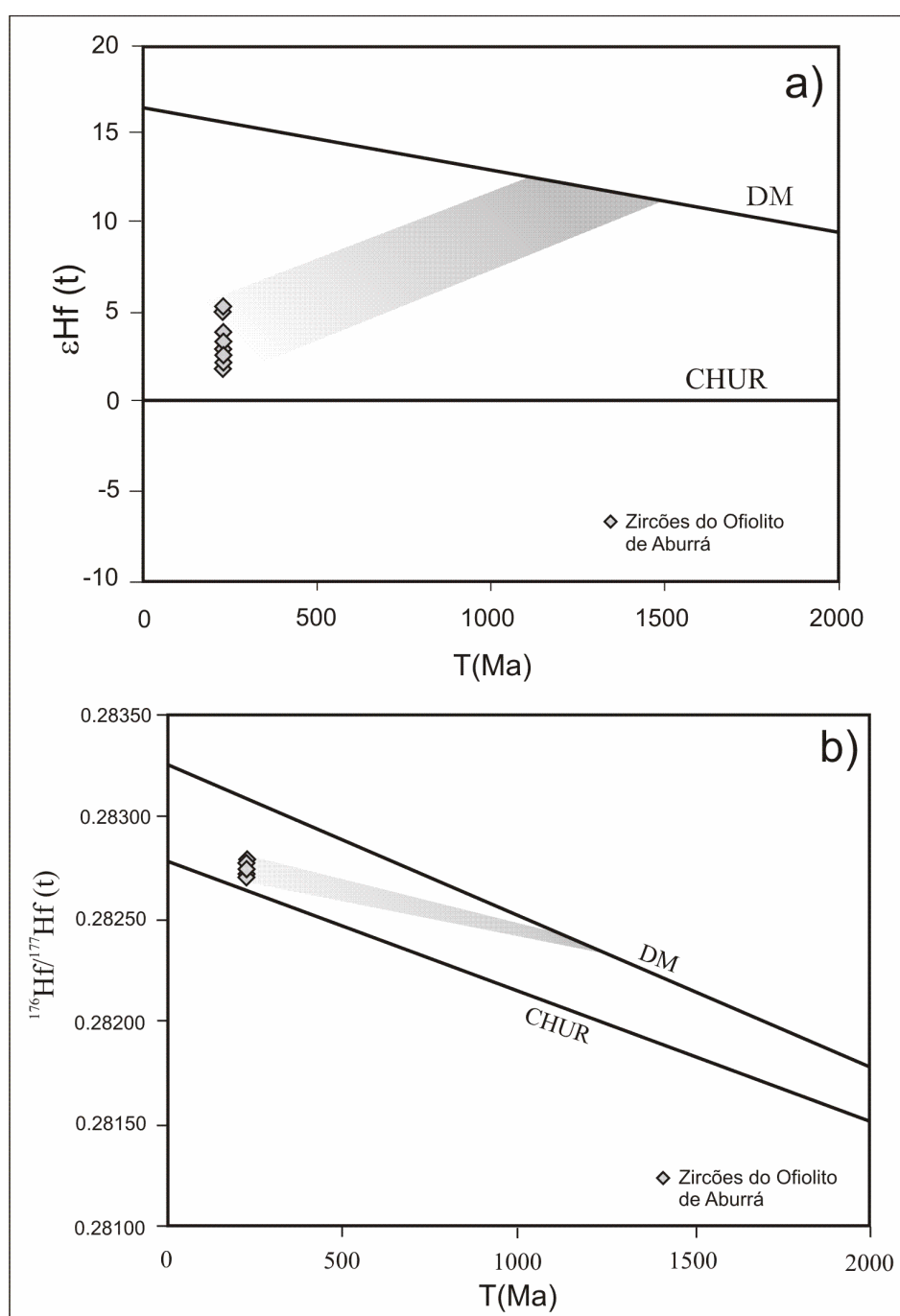
539

540  
541**Tabela 4**

Nome	$^{176}\text{Hf}/^{177}\text{Hf}$	$\pm 2\text{SE}$	$^{176}\text{Lu}/^{177}\text{Hf}$	$\pm 2\text{SE}$	$^{176}\text{Hf}/^{177}\text{Hf (t)}$	$\epsilon\text{Hf(t)}$	Idade TDM
<b>Zr-065-A-I-01</b>	0,282773	0,000033	0,000606	0,000008	0,282770	4,54	1,22
<b>Zr-065-A-I-03</b>	0,282708	0,000031	0,000219	0,000007	0,282707	2,31	1,42
<b>Zr-065-A-I-06</b>	0,282718	0,000033	0,000620	0,000011	0,282715	2,60	1,39
<b>Zr-065-B-II-01</b>	0,282700	0,000024	0,000325	0,000003	0,282698	2,01	1,44
<b>Zr-065-B-II-02</b>	0,282705	0,000029	0,000594	0,000011	0,282702	2,15	1,43
<b>Zr-065-B-II-03</b>	0,282766	0,000031	0,000224	0,000058	0,282765	4,37	1,24
<b>Zr-065-B-II-04</b>	0,282796	0,000022	0,000734	0,000007	0,282793	5,35	1,15
<b>Zr-065-B-II-05</b>	0,282784	0,000029	0,000372	0,000009	0,282783	5,00	1,18
<b>Zr-065-B-II-06</b>	0,282730	0,000029	0,000646	0,000056	0,282727	3,02	1,36
<b>Zr-065-B-II-07</b>	0,282734	0,000024	0,000127	0,000001	0,282734	3,26	1,33
<b>Zr-065-B-II-08</b>	0,282738	0,000032	0,000854	0,000011	0,282734	3,28	1,33
<b>Zr-065-C-III-01</b>	0,282716	0,000018	0,000595	0,000002	0,282713	2,53	1,40

542  
543  
544  
545  
546  
547  
548  
549  
550  
551  
552  
553  
554  
555  
556  
557  
558  
559  
560  
561  
562  
563  
564  
565  
566  
567  
568  
569  
570  
571  
572  
573  
574  
575  
576  
577  
578  
579  
580

581  
582**Figura 1**583  
584  
585  
586  
587**Figura 2**588  
589  
590  
591

592  
593**Figura 3**

594

## 2.2 Segundo Artigo

Correio :: Caixa de Entrada: [AABC] - Submission Completed - REF.: 768/11 Página 1 de 1

**Data:** Fri, 01 Jul 2011 10:29:24 -0300 [01-07-2011 10:29:24 BRST]  
**De:** aabc@abc.org.br  
**Para:** anelise.bertotti@ufrgs.br  
**Assunto:** [AABC] - Submission Completed - REF.: 768/11

REF.: 768/11  
Dr. Bertotti, Anelise  
Thank you for submitting your manuscript for publication in our journal "Anais da Academia Brasileira de Ciências" (AABC). Its reference code is . Please, use always this number in any correspondence regarding this manuscript. It will be evaluated and you will be contacted in due course. At any stage you may check the status of your manuscript logging into the AABC website <http://aabc.abc.org.br>. In case of any doubt, contact our Editorial Office at [aabc@abc.org.br](mailto:aabc@abc.org.br). For more information about AABC style, see latest papers published in [www.scielo.br/aabc](http://www.scielo.br/aabc). Thanks, once more, for your interest in the AABC.  
Cordially, "Lu-Hf Analysis by LA-ICP-MS: Methodology and Application in Capivarita Anorthosite Zircons"768/11

M.L.P. Maioli  
Editorial Assistant - AABC  
Rua Anfilofio de Carvalho, 29/3rd floor  
Rio de Janeiro, RJ  
20030-060 Brazil  
tel: +55.21.3907-8100 fax +55.21.3907-8101  
web: <http://aabc.abc.org.br>  
[aabc@abc.org.br](mailto:aabc@abc.org.br)

[https://webmail.ufrgs.br/horde/imp/message.php?actionID=print\\_message&mailbox=I...](https://webmail.ufrgs.br/horde/imp/message.php?actionID=print_message&mailbox=I...) 02/12/2011

# **Lu-Hf Analysis by LA-ICP-MS: Methodology and Application in Capivarita Anorthosite Zircons**

**ANELISE L. BERTOTTI<sup>1</sup>, FARID CHEMALE JR.<sup>2</sup>,**  
**PAUL J. SYLVESTER<sup>3</sup> AND MILTON L. L. FORMOSO<sup>1,4</sup>**

## **Address**

1. Programa de Pós-Graduação em Geociências, Instituto de Geociências, Universidade Federal do Rio Grande do Sul, Cx Postal 15001, 91501-970, Porto Alegre, RS, Brasil.
  2. Instituto de Geociências, Universidade de Brasília, Campus Darcy Ribeiro Asa Norte, 70910-900 Brasília, DF, Brasil.
  3. Department of Earth Sciences, Memorial University of Newfoundland, Alexander Murray Building / ER-45033, 300 Prince Philip Drive, St. John's, NL, A1B 3X5, Canada.
  4. Member of Brazilian Academy of Sciences.
- 

**Key words:** Capivarita Anorthosite, Hf Methodology, LA-ICP-MS, Zircon.

**Academy Section:** Earth Sciences

**Running Title:** Lu-Hf Analysis by LA-ICP-MS: Methodology and Application in  
Capivarita Anorthosite Zircons

## **Information of the corresponding author:**

Author: Anelise Losangela Bertotti

Phone Number: +55-51-8510-6355

E-mail: [anelise.bertotti@ufrgs.br](mailto:anelise.bertotti@ufrgs.br)

## ABSTRACT

The methodology of Lu-Hf in zircon is important for geochronology, as it complements studies of provenance and crustal growth. In recent decades become one of the most used methods in this field providing data with quality and speed supported by the efficiency of MC-ICP-MS. As a result, this paper presents a study of Lu-Hf methodology applied to magmatic and metamorphic zircons from Capivarita Anorthosite, located in southern Brazil. *In situ* analyses of Lu-Hf in zircons were first made in the Laboratório de Geologia Isotópica (LGI) at Universidade Federal do Rio Grande do Sul, Brazil, and later in the Microanalysis Facilities Inco Innovation Centre at Memorial University of Newfoundland, Canada, with the aim to test the reproducibility of the Hf method developed at LGI. Both laboratories used the same model of MC-ICP-MS, Thermo Finnigan Neptune, but different lasers and different methodologies. The main differences besides the use of different lasers, lies in its being used during analysis in the LGI a larger spot size for laser and nitrogen. Results from both laboratories show good reproducibility in Hf analyses. TDM ages and epsilon Hf values obtained are in agreement within experimental errors.

## INTRODUCTION

The isotopic system of Lutetium-Hafnium (Lu-Hf) has been widely used in geochronology as a tracer to understand the crustal evolution and differentiation of the Earth's mantle (Patchett and Tatsumoto 1980, Thirwall and Walder 1995, Blichert-Toft and Albarede 1997, Vervoort and Blichert-Toft 1999, Goode and Vervoort 2006). Numerous studies in the past three decades have shown that the combined use of different isotope systems can be effective in obtaining information on the crustal evolution, metamorphism and sediment provenance (Griffin et al. 2000, Gerdes and Zeh 2006, 2009, Nebel et al. 2007).

Zircon is a mineral with a geochemistry capability unmatched, easily datable by several radiometric methods (Woodhead et al. 2004, Wu et al. 2006). This mineral is important in Hf methodology due the fact the initial Hf isotope ratios are preserved in it, a characteristic that can be used in provenance studies and as petrogenetic indicator. Among the several issues to be addressed by the Hf in zircon, one stands out its applicability in the use combined with the age of zircon crystallization provided by the Uranium-Lead (U-Pb) method.

Furthermore, the high ionization efficiency in inductively coupled plasma instruments made the MC-ICP-MS the method for Hf analysis in zircon (Longerich et al. 2008). Although, analysis by laser ablation presents low accuracy comparative with TIMS and in solution analysis by ICP-MS, this disadvantage can be overcome by speed and convenience of combining U-Pb and Hf in-situ isotopic measurements in a single zircon grain, providing information in high resolution.

In this paper, are presented the Lu-Hf methodology and also its applications in zircons from Capivarita Anorthosite, performed in two distinct labs, LGI (Laboratório de Geologia Isotópica, Federal University of Rio Grande do Sul (UFRGS), Brazil) and

MAF-IIC (Microanalysis Facilities Inco Innovation Centre, Memorial University of Newfoundland (MUN), Canada) in order to determine the accuracy and precision of both labs.

## LU-HF GEOCHEMISTRY

The Lu-Hf isotopic system applies to minerals and rocks do not datable by conventional methodologies, like Rb-Sr and Sm-Nd, and proves to be very effective in complementing the other isotopic systems (Faure 1986). The most important factor is that the study of these radiogenic elements provide evidence regarding as the differentiation of the mantle and the growth of continental crust (Patchett et al. 1981).

Lu is a heavy rare earth elements (HREE), trivalent, part of the lanthanides group and the element that has the smallest atomic radius in this group (0.93 Å). Lu is present in all types of rocks (Faure 1986), but in low concentrations and always with the ytterbium (Yb). The mineral that has the highest concentration of Lu is monazite, approximately 0.003%. Lu is also found in other minerals such as zircon, garnet and xenotime (Kinny and Maas 2003, Faure 2005). The Hf element belongs to the IVB group (+4), has ionic radius of 0.81 Å and chemical properties similar to zirconium (Zr +4, 0.80 Å). This makes the zircon one of the minerals with the highest concentrations of Hf by the fact that it easily replaces Zr in its structure. Most zircons have concentrations of Hf around 0.5-2% (Hoskin and Schaltegger 2003), its distribution is uneven in other accessory minerals, causing heterogeneity in the rock, so the isochron for this methodology is not accurate (Faure 1986).

In addition to zircon, Hf can also be found in high concentration in baddeleyite, around 13,340 ppm (Faure 2005). Because Hf is an HFSE, High Field Strength Element, it differs chemically from the REE, including Lu, Sm and Nd. The HFSE's are

less soluble in aqueous fluids than LILE's, Large Ion Lithophile Elements, and REE's. Thus, the Lu-Hf pair is different from Sm-Nd isotopic systems in tectonic environments, being less mobile in convergent plates comparing to Sm-Nd during the dehydration in subducting oceanic crust (Faure 1986).

Sm and Nd are geochemically very similar elements; same radius, charge and electronegativity. Lu and Hf are different in charge and radius. Despite these differences, the geochemical properties of Lu-Hf are similar to the Sm-Nd pair when it takes into account to their behavior in the partial melting of the mantle, as Nd to Sm, Hf relative to Lu is more concentrated in the liquid silicate. Thus, mantle-derived basaltic magmas has low Lu/Hf ratio than the source rock, and the solid residue is depleted in Hf and higher Lu/Hf ratio than the rock before differentiation. Anyway, this depends on the presence or not of garnet in the mantle, because the garnet plays an important role in this chemical behavior since it has great affinity with Lu and inhibit its entry into the melted material (Faure 2005).

## DATING LU-HF

Hafnium has six naturally occurring isotopes,  $^{174}\text{Hf}$  (0.16%),  $^{176}\text{Hf}$  (5.2%),  $^{177}\text{Hf}$  (18.6%),  $^{178}\text{Hf}$  (27.1%),  $^{179}\text{Hf}$  (13.63%) and  $^{180}\text{Hf}$  (35.1%). Lutetium has only two isotopes,  $^{175}\text{Lu}$  (97.4%) and  $^{176}\text{Lu}$  (2.59%) (Faure 2005). Since the isotope  $^{176}\text{Hf}$  increases with time in rocks and minerals due to the beta decay of  $^{176}\text{Lu}$ . Because of this decay, the Lu-Hf age of rocks and minerals can be given by Equation 1:

$$\frac{^{176}\text{Hf}}{^{177}\text{Hf}} = \left( \frac{^{176}\text{Hf}}{^{177}\text{Hf}} \right)_I + \frac{^{176}\text{Lu}}{^{177}\text{Hf}} (e^{\lambda t} - 1) \quad \text{Equation (1)}$$

where  $t$  is the time elapsed since the formation of rock or mineral and  $\lambda$  is the decay constant of  $^{176}\text{Lu}$ . Different values for  $\lambda$  have been proposed in the past by several authors. Patchett and Tatsumoto (1980) proposed the value  $1.94 \times 10^{-11} \text{ y}^{-1}$ , calculated from the slope of a Lu-Hf isochron for eucrite meteorites of known age. The decay constant assumed in this work is the value of  $1.867 \times 10^{-11} \text{ y}^{-1}$  proposed recently by Söderlund et al. 2004.

## THE ISOTOPIC EVOLUTION OF Hf

Hf isotopic evolution in the BSE (Bulk Silicate Earth) reservoir is assumed to be equal to the chondritic meteorites (CHUR), according to Faure (2005). The initial ratio for  $^{176}\text{Hf}/^{177}\text{Hf}$  was determined by Patchett and Tatsumoto (1980) in an isochron of 13 chondrites with a value of  $0.27978 \pm 0.00009$  and 0.334 for Lu/Hf ratio. If the age of the chondrite patterns reservoir is  $4.55 \times 10^9$  years, then the present value for  $^{176}\text{Hf}/^{177}\text{Hf}$  is 0.28286. In Figure 1, is illustrated the Earth isotopic evolution from a primordial solar nebula in 4.55 Ga, with initial ratio of 0.279718 to the presumed current ratio 0.282772 (Faure 1986), such as in chondrites.

## Insert Figure 1

The most significant modification of the Lu/Hf ratio occurs in the mantle-crust differentiation event. The magma from the mantle arise in the crust and the Lu/Hf ratio is modified by radioactive decay or by events that crustal material undergoes during its geological history. This crust-mantle differentiation can occur through partial melting processes, fractional crystallization, or both (Dickin 2005).

The Lu/Hf methodology enables, beyond the age determination, to establish a petrogenetic parameter, the Epsilon Hf ( $\epsilon$ Hf), which support the identification of sources of magmas and processes of rock formation and mineralization. The parameter  $\epsilon$ Hf basically consists in comparing the ratio  $^{176}\text{Hf}/^{177}\text{Hf}$  of the sample at the time of its formation or its current value, with a standard uniform chondrite patterns reservoir (CHUR), which would be representative of the Bulk Earth and is expressed as Equation 2.

$$\epsilon'(\text{Hf}) = \left[ \frac{\left( ^{176}\text{Hf}/^{177}\text{Hf} \right)_{\text{sm}}^i}{\left( ^{176}\text{Hf}/^{177}\text{Hf} \right)_{\text{ch}}^t} - 1 \right] \times 10^4 \quad \text{Equation (2)}$$

Where the chondritic values used to calculate the  $(^{176}\text{Hf}/^{177}\text{Hf})_{\text{ch(t)}}$  ratio were 0.0336 to  $^{176}\text{Lu}/^{177}\text{Hf}$  and 0.282785 to  $^{176}\text{Hf}/^{177}\text{Hf}$  for present day (Bouvier et al. 2008). If at the time of the rock crystallization the parent magma has a  $^{176}\text{Hf}/^{177}\text{Hf}$  higher than the CHUR, the  $\epsilon$ Hf is positive, meaning that the source of this magma had Lu/Hf ratio higher than the chondrite, ie the source is the upper mantle (Faure 2005). Moreover, when the formation of the rock, its parent magma has  $^{176}\text{Hf}/^{177}\text{Hf}$  ratio lower than CHUR, the  $\epsilon$ Hf value is negative and therefore the source of these rocks have a Lu/Hf lower than the chondrite, this is the case of magmas of crustal origin. Therefore, when the  $\epsilon$ Hf is positive the source is the mantle and when the  $\epsilon$ Hf is negative value, the source is a crustal magma.

## DEPLETED MANTLE MODEL AGE

The Hf depleted mantle model age is the generation of continental crust from a mantle reservoir causing the depletion in the lighter elements (LILE - Large Ion

Lithophile Elements) and also the light rare earth elements (LREE) in this reservoir, resulting what is called as "depleted mantle" (DM) (Nebel et al. 2007). Therefore, this model assumes the mantle had suffered episodes of fractionation involving the extraction of basaltic magmas, remaining then a residual mantle enriched in the ratio Lu/Hf and geochemically depleted in LILE's. The Hf model age adopted to this work can be calculated by Equation 3, which is the possible evolution curve of Hf for the depleted mantle.

$$T_{DM} = \frac{t_{(U/Pb)}}{1000} + \frac{1}{0.01867} \times \ln \left( 1 + \frac{\left( ^{176}\text{Hf}/^{177}\text{Hf} \right)_{sm}^t - \left( ^{176}\text{Hf}/^{177}\text{Hf} \right)_{DM}^t}{\left( ^{176}\text{Lu}/^{177}\text{Hf} \right)_{sm}^t - \left( ^{176}\text{Lu}/^{177}\text{Hf} \right)_{DM}^0} \right) \quad \text{Equation (3)}$$

Where t is the U/Pb age. The depleted mantle values in present day are 0.28325 for  $^{176}\text{Hf}/^{177}\text{Hf}$  ratio and 0.0388 for  $^{176}\text{Lu}/^{177}\text{Hf}$  ratio (Griffin et al. 2000; updated by Andersen et al. 2009); and 0.015 to  $(^{176}\text{Lu}/^{177}\text{Hf})_{sm(t)}$  an assumed value for Bulk Silicate Earth (Goodge and Vervoort 2006).

## INSTRUMENTATION AND ANALYTICAL PROCEDURES

The MC-ICP-MS is a high-resolution mass spectrometer for isotopic ratio measurements with a special configuration for a wide range of nuclides simultaneously detecting. The sample in the ICP can be analyzed by solution or by analyzing in situ via laser ablation. In both forms, the sample is transported by air to the gas sector analyzer. The effects of fractionation in the processes of ablation and aspiration are monitored daily by internal and external standards, which in this study are GJ-1, Plešovice and 91500 zircon standards.

Analysis *in situ* of Hf in zircon from LGI and MAF-IIC were made using the ThermoFinnigan Neptune MC-ICP-MS, but different laser microprobe. A laser ablation system from New Wave Research UP213 (Nd:YAg) and GeoLas (ArF Excimer) were used, respectively. The zircons were firstly analyzed at LGI by U-Pb and Lu-Hf methods then after at MAF-IIC. Details of the instrumental operating conditions from both labs were as given in Table I and the methodologies from each lab are described separately below. In both labs, to minimize aerosol deposition around the ablation pit and improve transport efficiency, the helium gas was flushed into the ablation cell (Eggins et al. 1998).

### **Insert Table I**

#### **LGI METHODOLOGY**

The isotopic data of Lu-Hf are acquired by the static mode with spot size of 55  $\mu\text{m}$ , a repetition rate of 10 Hz and a density of energy of  $\sim$ 5-6 J/cm<sup>2</sup>. The laser ablation system used was a New Wave Research UP213 (Nd:YAg), which provides flats craters and high absorption or the analysis of opaque and transparent materials alike.

In this study, to obtain further improvements in precision of the Hf isotopic data from zircon material, a N<sub>2</sub> mixing technique was applied (Iizuka and Hirata 2005, Gerdes and Zeh 2006), with the purpose to reduce the oxide signals by an addition of small amounts of N<sub>2</sub> ( $\sim$  4 mL/min) into the carrier gas and an increase of 30% on Hf signals could be seen (Bertotti and Chemale Jr., in preparation).

Before proceeding with the Hf isotopic calculations, all raw signals are blank corrected using the mean of 50 points recorded as the gas blank baseline before ablation of the grains and standards. The analyses sequence was made by one standard, five

unknown and one standard again. A user-selected interval of ~45 data points (~45 seconds of data since the integration time is ~1 data point per second) covering the sample transient peak (~50 seconds of ablation) is used for calculation of the Hf ratio.

In order to calibrate the MC-ICP-MS, we analyzed the SRM reference material JMC-475 in solution and obtained a value of  $0.282156 \pm 0.000015$  (2SD), which reproduced the isotopic values of Hf reported in the literature (Wu et al. 2006, Chu et al. 2002). The standard used during Hf *in situ* analysis was the GJ-1, its reference value for  $^{176}\text{Hf}/^{177}\text{Hf}$  is  $0.282000 \pm 0.000005$  (2MSWD) (Morel et al. 2008). The obtained value for GJ-1 was  $0.282017 \pm 0.000009$  ( $n=5$ , 2SD) with an intensity of  $2.03 \pm 0.08$  V in  $^{178}\text{Hf}$ . The sequence used during the analysis was: one GJ-1, five grains of the sample and one GJ-1 again. The sample cell was not opened between the analyses.

## MAF-IIC METHODOLOGY

A GeoLas (ArF excimer laser) operating at a wavelength of 193nm and a pulse width of 20 ns laser ablation system linked to the MC-ICPMS was used for the in situ analyses at MAF-IIC. The wavelength from the laser of 193 nm produces a fine distribution of particles, which increases the efficiency in transporting the material resulting in better sensitivity and minimal deposition in the plasma, but also has a fractionation that must be corrected by standards.

A laser fluence of approximately  $5 \text{ J/cm}^2$ , repetition rate of 10 Hz and spot size of 49  $\mu\text{m}$  were used for all analyses. Here all raw signals are also blank corrected using the mean of ~20-25 points recorded as the gas blank baseline before each ablation. A user-selected interval of ~50 data points from the ~60 seconds of ablation is used for calculation of the Hf ratio in the Excel sheet.

The Plešovice (PL) and 91500 zircons were analyzed as quality control standards. The sequence of the analyses were one PL, one 91500, seven unknowns, one PL and one 91500 again. The reported value for Plešovice for  $^{176}\text{Hf}/^{177}\text{Hf}$  ratio is  $0.282482 \pm 0.000013$  (2SD) (Slama et al. 2008) and the obtained value during our analysis was  $0.282480 \pm 0.000049$  (2SD). The reference value for 91500 can be found in Blichert-Toft (2008) with  $^{176}\text{Hf}/^{177}\text{Hf} = 0.282308 \pm 0.000006$  (2SD) and the obtained value was  $0.282312 \pm 0.000061$  (2SD).

## ISOBARIC INTERFERENCE CORRECTIONS

Lu, Yb and Hf isotopes are measured simultaneously during the analysis *in situ* in MC- ICP-MS. The configuration used at LGI and MAF-IIC for Lu-Hf analysis is described in Table II. The isotopic ratios measured during the analyses of Lu-Hf were:  $^{173}\text{Yb}/^{171}\text{Yb}$ ,  $^{179}\text{Hf}/^{177}\text{Hf}$ ,  $^{178}\text{Hf}/^{177}\text{Hf}$ ,  $^{176}\text{Lu}/^{177}\text{Hf}$ ,  $^{176}\text{Yb}/^{177}\text{Hf}$  and  $^{176}\text{Hf}/^{177}\text{Hf}$ . Data were corrected and normalized following the procedure of the laser ablation analyses in the Excel sheet, both labs use the same equations and values to correct the isobaric interference as follow bellow.

## Insert Table II

During the *in situ* analysis of Hf in zircon, the isotope  $^{176}\text{Lu}$  and  $^{176}\text{Yb}$  were analyzed together with the  $^{176}\text{Hf}$ . Due this reason the ratio  $^{176}\text{Hf}/^{177}\text{Hf}$  was carefully corrected using a exponential law and the intensities of  $^{176}\text{Lu}$  and  $^{176}\text{Yb}$  monitored during the entire course of the analysis. A mass bias factor  $\beta$  is calculated for Yb and Hf. The measured (m) signals are the blank corrected signals from the instrument, while the corrected values (corr) are the expected natural values for these isotopic ratios.

$$\beta_{Hf} = \frac{\ln \left[ \left( \frac{^{179}Hf}{^{177}Hf} \right)_m \right]}{\ln \left[ \frac{M_{179(Hf)}}{M_{177(Hf)}} \right]}$$

$$\beta_{Yb} = \frac{\ln \left[ \left( \frac{^{173}Yb}{^{171}Yb} \right)_m \right]}{\ln \left[ \frac{M_{171(Yb)}}{M_{173(Yb)}} \right]}$$

Equations (6 and 7)

Where the corrected value for  $^{179}\text{Hf}/^{177}\text{Hf}$  is 0.7325 (Patchett and Tatsumoto 1980), and the corrected values for  $^{173}\text{Yb}/^{171}\text{Yb}$  and  $^{176}\text{Yb}/^{173}\text{Yb}$  are 1.1301 and 0.7938 (Segal et al. 2003), respectively.

The signal measured for the 176 mass is a combination of  $^{176}\text{Hf}$ ,  $^{176}\text{Yb}$  and  $^{176}\text{Lu}$ . In order to determine  $^{176}\text{Hf}$ , the interferences from Yb and Lu must be subtracted. The intensity of  $^{176}\text{Hf}$  can be calculated using Equation 8:

$$^{176}\text{Hf} = ^{176}(Hf + Lu + Yb)_m - \left[ ^{175}Lu_m \times \left( \frac{^{176}Lu}{^{175}Lu} \right)_N \times \left( \frac{M_{176(Lu)}}{M_{175}} \right)^{\beta(Lu)} \right. \\ \left. + ^{173}Yb_m \times \left( \frac{^{176}Yb}{^{173}Yb} \right)_N \times \left( \frac{M_{176(Yb)}}{M_{173}} \right)^{\beta(Yb)} \right]$$

Equation (8)

Where the corrected value assumed for  $^{176}\text{Lu}/^{175}\text{Lu}$  is 0.2656 (Chu et al. 2002).

For  $^{176}\text{Yb}/^{177}\text{Hf}$  and  $^{176}\text{Lu}/^{177}\text{Hf}$ , the mass bias correction is approximated using the mass bias factor for Hf,  $\beta(\text{Hf})$ :

$$\left( \frac{^{176}Yb}{^{177}Hf} \right)_{corr} = \left( \frac{^{176}Yb}{^{177}Hf} \right)_m \times \left( \frac{M_{176(Yb)}}{M_{177(Hf)}} \right)^{\beta(Hf)}$$

Equation (9)

$$\left( \frac{^{176}\text{Lu}}{^{177}\text{Hf}} \right)_{corr} = \left( \frac{^{176}\text{Lu}}{^{177}\text{Hf}} \right)_m \times \left( \frac{M_{^{176}\text{Lu}}}{M_{^{177}\text{Hf}}} \right)^{\beta(\text{Hf})} \quad \text{Equation (10)}$$

No outlier rejection is done for these ratios since Yb and Lu are not necessarily homogenous in a zircon.

## GEOLOGICAL SETTING OF CAPIVARITA ANORTHOSITE

The Capivarita Anorthosite is situated in the Pantano Grande locality in the NE portion of the Sul-Rio-Grandense Shield, Rio Grande do Sul State, Brazil (Figure 2). This anorthosite is part of the Dom Feliciano Belt (DFB), an orogenic belt formed during the Neoproterozoic (860-550 Ma). Many studies (Ribeiro et al. 1966, Tessari and Picada 1966, Formoso and Carraro 1968, Formoso 1973, Fernandes et al. 1992, Babinski et al. 1997, Philipp and Machado 2005, Chemale Jr. 2000, Chemale Jr. et al. 2011) were made on this anorthosite to define better the nature of this massif-type anorthosite.

### Insert Figure 2

Anorthosites are unique rocks, both in terms of occurrence, composition (> 90% of plagioclase) and genesis. The anorthosites are mainly found in Archean and Proterozoic terranes in all continents with significant occurrences in North America, Africa, Europe and Antarctica (Philipp and Machado 2005). Furthermore, they are also important in the reconstruction and evolution of ancient continents such as the Columbia and Rodinia, occurring in the final stages of continental consolidation or later, in the early stages of continental fragmentation.

According to Ashwal (1993), six types of anorthosites can occur: i) archean anorthosite plutons; ii) proterozoic “massif-type” anorthosite; iii) centimeter to 100 m thick layers in layered mafic intrusions; iv) thin cumulate layers in ophiolites/oceanic crust; v) small inclusions in other rock types and vi) Lunar Highland anorthosites. The Capivarita anorthosite is included in the second type. The Proterozoic “massif-type” anorthosite plutons are the most voluminous of terrestrial anorthosites. The emplacement of large anorthosite massifs in shield areas was one of the major processes of the growth of continental crust in the Proterozoic era.

In the Capivarita Anorthosite the major components are the anorthosite rocks with associated mafic rocks, metagabros and amphibolites tabular bodies, cogenetic related. The composition of plagioclase is homogeneous ( $\text{An}_{50}$ - $\text{An}_{64}$ ), one special occurrence displays  $\text{An}_{94}$  (Philipp and Machado 2005). Large crystals (7 to 20 centimeters) and a protoclastic texture are typical. The obtained ages for inherited zircons is  $2028 \pm 17$  Ma and for igneous zircons is  $1573 \pm 21$  Ma (Chemale et al. 2011). These ages agree with those of Proterozoic massif-type anorthosites.

## RESULTS

### LGI Lu-Hf Data

A detailed description of sample preparation for Capivarita Anorthosite’s samples is in Chemale et al. (2011). In this previous work, magmatic and metamorphic minerals were dated using the LA-MC-ICP-MS *in situ* method. The magmatic and metamorphic zircons, totalizing of 15 zircons, were first analyzed by U-Pb method which yielded an age of  $1573 \pm 21$  Ma and of  $606 \pm 6$  Ma, respectively. Some titanites were also analyzed, igneous titanites yielded an age of  $1530 \pm 33$  Ma and for metamorphic titanites yielded ages of  $651 \pm 9$  Ma and  $601 \pm 5$  Ma. To obtain information about the

provenance of the zircon, the authors carried out Lu-Hf in situ LA-ICP-MS analyses in the zircons that were chosen for U-Pb dating (see Table III). The Lu-Hf model ages showed two clusters from 1.81 to 2.03 Ga with  $\epsilon$ Hf values from +2.21 to +6.42 and 2.55 to 2.62 Ga with  $\epsilon$ Hf values from -4.59 to -5.64. All dated metamorphic zircons have TDM and  $\epsilon$ Hf similar to those of the crustal zircons with Hf model ages ranging from 2.47 to 2.54 and  $\epsilon$ Hf values from -15.34 to -16.58 for time of metamorphic recrystallization of 0.6 Ga. The baddeleyite grain (Zr-170-A-I-02) displays similar values as those of the metamorphic zircons, with Hf model age of 2.45 Ga and  $\epsilon$ Hf value of -15.4.

### **Insert Table III**

#### **MAF-IIC Lu-Hf Data**

The Hf analyses in the Capivarita Anorthosite at MAF-IIC were made in twelve zircons, seven magmatic and five metamorphic and one baddeleyite in the same sample as used in previous study described in Chemale et al. (2011). HF analyses were not performed in all dated zircons in LGI because since the small zircon size difficult this procedure. The hole of the laser was made on the top of the U-Pb analysis or close as possible to the U-Pb spot (see Figure 3).

### **Insert Figure 3**

In the magmatic zircons were founded two groups of zircons (see Figure 4 and Table IV). The first one yielded negative  $\epsilon$ Hf values of -5.9 to -4.4 and  $T_{DM}$  model ages between 2.54 to 2.63 Ga. The second group is reworked zircons from a Paleoproterozoic

source with positive  $\varepsilon$ Hf values of +2 to +3.5 and with younger  $T_{DM}$  model ages between 2.05 to 2.14 Ga. For metamorphic zircons the  $\varepsilon$ Hf values were very negative of -15.8 to -17.2 with  $T_{DM}$  model ages between 2.49 to 2.58 Ga. And the only one baddeleyite (Zr-170-A-I-02) yielded  $\varepsilon$ Hf value of -15.4 and  $T_{DM}$  model age of 2.47 Ga. The results obtained in this study supported the conclusion from previous study (Chemale et al. 2011) in the Capivarita zircons.

#### **Insert Figure 4**

#### **Insert Table IV**

### **DISCUSSION OF RESULTS**

In order to discuss details in Hf analyses, it is presented in Figure 5 an example of time-resolved Hf isotope spectra, intensity and fractionation index for Zr-A-I-01 grain from MAF-IIC and LGI, respectively. The obtained fractionation index is close to 1 for all Hf isotope ratios, which indicates that there is no fractionation during the ablation in both lasers (Fig. 5).

#### **Insert Figure 5**

The comparison of the Lu-Hf isotope results from both labs is presented in the Tables III and IV. The obtained intensity in Capivarita Anorthosite zircons at the LGI ranges from 1.7 to 3.5 V for  $^{178}\text{Hf}$  in igneous zircons and 2.38 to 3.16 V in metamorphic zircons, whereas in the MAF-IIC ranges from 1.6 to 2.0 V and 1.29 to 1.81 V, respectively. In general the intensities are approximately 30-50% higher at the LGI. The

main reason is related to the larger spot size used at LGI (55  $\mu\text{m}$ ) against the smaller spot size at MAF-IIC (49  $\mu\text{m}$ ). Other reason for this is because the spot was performed on the top of U/Pb analysis in the MAF-IIC and part of the material was already removed as well the use of nitrogen during the analyses which increases de signal at the LGI.

On other side, the measured  $^{176}\text{Hf}/^{177}\text{Hf}$  isotope ratios in both labs are almost the same (Table IV), usually differing in the in sixth position after point, whereas  $^{176}\text{Lu}/^{177}\text{Hf}$  values are somewhat different due to very low content of  $^{176}\text{Lu}$  compared to  $^{177}\text{Hf}$ . The errors (in 2SE) are in the expected values for this method, with better precision for those values obtained at the LGI (due to higher intensity and consequently stability of the signal).  $\varepsilon\text{Hf}$  values and  $T_{\text{DM}}$  ages are very consistent and similar for analytical results of both labs, even for igneous and metamorphic zircons as well for inherited zircons, with of Zr-170-B-II-06 zircon that presents substantial differences in the Model ages and  $\varepsilon\text{Hf}$  values.

## CONCLUSIONS

The Lu-Hf methodology in zircon presented in this work was very important, because it provided additional information for studies of provenance and crustal growth in the Capivarita Anorthosite. Furthermore, the high stability of Hf in zircon, really makes Hf as a good geochemistry tracer, this feature allowed the isotopes of Hf to contribute in understanding the discrepancy in age from U-Pb zircon and assist in the interpretation of zircon ages of high-grade metamorphic rocks as the case of Capivarita Anorthosite.

We had in our study not just different lasers (213 and 193nm) but many other differences as: different standards, different region for spots in the zircon, and just one

Hf analysis in each lab (the grains were very tiny) and differences during the analysis. Although it is necessary to determine more than 15 parameters interact mutually and the experiment needs to perform under identical laser ablation conditions, the obtained results and therefore interpretation are quite similar in both labs. Despite the differences between methodologies used in each lab we could see good reproducibility of the Hf analysis from LGI and MAF-IIC. All obtained Hf isotope ratios, TDM model ages and epsilon Hf values were in agreement within experimental errors.

#### **ACKNOWLEDGMENTS**

We thank the CNPq (Conselho Nacional de Desenvolvimento Científico e Tecnológico) for the PhD scholarship (140922/2008-3). We also thank the technicians from LGI/UFRGS and MAF-IIC/MUN for helping in the sample preparation and during the Hf analysis in the LA-MC-ICP-MS. We are very grateful to E. Koester and K. Kawashita for critical reading of the manuscript and helpful suggestions.

#### **RESUMO**

A metodologia de Lu-Hf em zircão é importante para a geocronologia, pois complementa estudos de proveniência e de crescimento crustal. Nas últimas décadas, tornou-se um dos métodos mais utilizados neste campo fornecendo dados com qualidade e rapidez devido à eficiência dos MC-ICP-MS. Em vista disso, o presente artigo apresenta um estudo da metodologia Lu-Hf aplicada a zircões magmáticos e metamórficos do Anortosito de Capivarita, localizado no sul do Brasil. As análises *in situ* de Lu-Hf nos zircões foram feitas primeiramente no Laboratório de Geologia Isotópica (LGI) da Universidade Federal do Rio Grande do Sul, Brasil, e depois no Microanalysis Facilities Inco Innovation Centre da Memorial University of

Newfoundland, Canada, com objetivo de testar a reproduzibilidade da metodologia desenvolvida no LGI. Ambos os laboratórios utilizaram o mesmo modelo de MC-ICP-MS, o Neptune da Thermo Finnigan, mas diferentes lasers assim como diferentes metodologias de trabalho. As principais diferenças além de diferentes lasers residem no fato de ter sido utilizado durante as análises no LGI um diâmetro maior para o furo do laser e nitrogênio. Os resultados dos dois laboratórios mostram boa reproduzibilidade nas análises de Hf. As idades TDM e os valores de epsilon Hf obtidos são concordantes dentro dos erros experimentais.

**Palavras-chave:** Anortosito de Capivarita, LA-ICP-MS, Metodologia Lu-Hf, Zircão.

## REFERENCES

- ANDERSEN T, ANDERSSON UB, GRAHAM S, ÅBERG G AND SIMONSEN SL. 2009. Granitic magmatism by melting of juvenile continental crust: new constraints on the source of Palaeoproterozoic granitoids in Fennoscandia from Hf isotopes in zircon. J. Geol. Soc. 166: 233-247.
- ASHWAL LD. 1993. Anorthosites. In: Minerals and rocks. Berlin: Springer-Verlag, xix, 422 p.
- BABINSKI M, CHEMALE JR F, VAN SCHMUS WR, HARTMANN LA AND SILVA LC. 1997. U-Pb and Sm-Nd Geochronology of the Neoproterozoic Granitic Gneissic Dom Feliciano Belt, Southern of Brazil. J. South Amer.Earth Sci. 10: 263-274.
- BLICHERT-TOFT J AND ALBARÈDE F. 1997. The Lu-Hf isotope geochemistry of chondrites and the evolution of the mantle crust system. Earth Planet. Sci. Lett. 148: 243-258.
- BLICHERT-TOFT J. 2008. The Hf isotopic composition of zircon reference material 91500. Chem. Geol. 253: 252-257.

BOUVIER A, VERVOORT JD AND PATCHETT PJ. 2008. The Lu–Hf and Sm–Nd isotopic composition of CHUR: Constraints from unequilibrated chondrites and implications for the bulk composition of terrestrial planets. *Earth Planet. Sci. Lett.* 273: 48–57.

CHEMALE JR F. 2000. Evolução Geológica do Escudo Sul-rio-grandense. In: HOLZ M AND DE ROS LF (eds.). *Geologia do Rio Grande do Sul*, Porto Alegre: CIGO, 13-52.

CHEMALLE JR F, PHILLIP RP, DUSSIN IA, FORMOSO MLL, KAWASHITA K AND BERTOTTI AL. 2011. Lu-Hf and U-Pb age determination of Capivarita Anorthosite in the Dom Feliciano Belt, Brazil. *Prec. Res.* 186: 117-126.

CHU NC, TAYLOR RN, CHAVAGNAC V, NESBITT RW, BOELLA M AND MILTON JA. 2002. Hf isotope ratio analysis using multi-collector inductively coupled plasma mass spectrometry: an evaluation of isobaric interference corrections. *J. Anal. At. Spectrom.* 17: 1567–1574.

DICKIN AP. 2005. *Radiogenic Isotope Geology*, 2nd ed., Cambridge University Press, 492p.

EGGINS SM, KINSLEY LPJ AND SHELLEY JMG. 1998. Deposition and element fractionation processes occurring during atmospheric pressure laser sampling for analysis by ICPMS. *Appl. Surf. Sci.* 127–129: 278–286.

FAURE G. 1986. *Principles of Isotope Geology*, 2nd ed., New York: John Wiley and Sons, 589p.

FAURE G. 2005. *Isotopes: Principles and Applications*, 3rd ed., New York: John Wiley & Sons, 897p.

FERNANDES LAD, TOMMASI AD, PORCHER CC. 1992. Deformation patterns in the southern Brazilian branch of the Dom Feliciano Belt: A reappraisal. *J. Sou. Am. Ear. Sci.* 5: 77-96.

FORMOSO MLL AND CARRARO CC. 1968. Anorthosito de Capivarita, Rio Pardo, RS. *An. Acad. Bras. Ciênc.* 40: 361-372.

FORMOSO MLL. 1973. Geologia da folha Capivarita – RS, Anortosito de Capivarita. Ph.D.Thesis, Instituto de Geociências, Universidade de São Paulo, São Paulo, 215p.

GERDES A AND ZEH A. 2006. Combined U-Pb and Hf isotope LA-(MC)-ICP-MS analyses of detrital zircons: Comparison with SHRIMP and new constraints for the provenance and age of American metasediment in central Germany. *Earth Planet. Sci. Lett.* 249: 47-61.

GERDES A AND ZEH A. 2009. Zircon formation versus zircon alteration – New Insights from combined U-Pb and Lu-Hf in-situ LA-ICP-MS analyses, and consequences for the interpretation of archean zircon from the Central Zone of the Limpopo Belt. *Chem. Geol.* 261: 230-243.

GOODGE JW AND VERVOORT JD. 2006. Origin of Mesoproterozoic A-type granites in Laurentia: Hf isotope evidence. *Earth Planet. Sci. Lett.* 243: 711-731.

GRIFFIN WL, PEARSON NJ, BELOUSOVA E, JACKSON SE, VAN ACHTERBERGH E, O'REILLY SY AND SHEE SR. 2000. The Hf isotope composition of cratonic mantle: LAM-MC-ICPMS analysis of zircon megacrysts in Kimberlites. *Geochim. Cosmochim. Acta* 64: 133-147.

HOSKIN P AND SCHALTEGGER U. 2003. The Composition of Zircon and Igneous and Metamorphic Petrogenesis. In: *Reviews in Mineralogy and Geochemistry* 53: 27-62.

- IIZUKA T AND HIRATA T. 2005. Improvements of precision and accuracy in situ Hf isotope microanalysis of zircon using the laser ablation-MC-ICPMS technique. *Chem. Geol.* 220: 131-137.
- KINNY P AND MAAS R. 2003. Lu-Hf and Sm-Nd Isotope systems in zircon. In: *Rev. Min. Geoc.* 53: 327-341.
- LONGERICH H. 2008. Laser Ablation – Inductively Coupled Plasma – Mass Spectrometry (LA-ICP-MS): an introduction. In: *Laser Ablation ICP-MS in the Earth Sciences: Current Practices and Outstanding Issues*. Short Course Series. Vancouver, BC, vol. 40, 348p.
- MOREL MLA, NEBEL O, NEBEL-JACOBSEN YJ, MILLER JS, VROON PZ. 2008. Hafnium isotope characterization of the GJ-1 zircon reference material by solution and laser-ablation MC-ICPMS. *Chem. Geol.* 255: 231–235.
- NEBEL O, NEBEL-JACOBSEN Y, MEZGER K AND BERNDT J. 2007. Initial Hf isotope compositions in magmatic zircon from early Proterozoic rocks from the Gawler Craton, Australia: A test for zircon model ages. *Chem. Geol.* 241: 23-37.
- PACHETT PJ AND TATSUMOTO M. 1980. Lu-Hf total rock isochron for the eucrite meteorites. *Nature* 288: 571-574.
- PATCHETT PJ, KOUVO O, HEDGE CE AND TATSUMOTO M. 1981. Evolution of continental crust and mantle heterogeneity: evidence from Hf isotopes. *Contrib. Mineral. Petrol.* 78: 279-297.
- PHILIPP RP AND MACHADO R. 2005. The Late Neoproterozoic 541 granitoid magmatism of the Pelotas Batholith, Southern Brazil. *J. Sou. Am. Ear. Sci.* 19: 461-478.
- PHILIPP RP, FORMOSO ML, DUSSIN I, CHEMALE Jr. F AND CAMPOS RS. 2010. Estruturas primárias e tectônicas do Anortosito Capivarita, Pântano Grande, RS:

significado e implicações para o entendimento da evolução petrológica. Rev. Bras. Geoc. 40: 99-110.

RIBEIRO M, BOCCHI PR, FIGUEIREDO F AND TESSARI RI. 1966. Geologia da Quadrícula de Caçapava do Sul, RGS. DNPM/DFPM, Rio de Janeiro, Boletim 127: 232 p.

SEGAL I, HALICZ L AND PLATZNER IT. 2003. Accurate isotope ratio measurements of ytterbium by multiple collection inductively coupled plasma mass spectrometry applying erbium and hafnium in an improved double external normalization procedure. J. Anal. At. Spectrom. 18: 1217–1223.

SLAMA J ET AL. 2008. Plešovice zircon — A new natural reference material for U–Pb and Hf isotopic microanalysis. Chem. Geol. 249: 1-35.

SÖDERLUND U, PATCHETT JP, VERVOORT JD AND ISACHSEN CE. 2004. The  $^{176}\text{Lu}$  decay constant determined by Lu–Hf and U–Pb isotope systematics of Precambrian mafic intrusions. Earth Planet. Sci. Lett. 219: 311–324.

TESSARI RI AND PICADA RS. 1966. Geologia da quadrícula de Encruzilhada do Sul, RS, Brasil. DNPM/DFPM, Rio de Janeiro, Boletim 124: 1-147.

THIRWALL MF AND WALDER AJ. 1995. In situ hafnium isotope ratio analyses of zircon by inductively coupled plasma mass spectrometry. Chem. Geol. 122: 241-247.

VERVOORT J AND BLICHERT-TOFT J. 1999. Evolution of the depleted mantle: Hf isotope evidence from juvenile rocks through time. Geochim. Cosmochim. Acta 63: 533-557.

WOODHEAD J, HERGT J, SHELLEY M, EGGINS S AND KEMP R. 2004. Zircon Hf-isotope analysis with an excimer laser, depthprofiling, ablation of complex geometries and concomitant age estimation. Chem. Geol. 209: 121-135.

WU F-Y, YANG Y-H, XIE L-W, YANG J-H AND XU P. 2006. Hf isotopic compositions of the standard zircons and baddeleyites used in U-Pb geochronology. Chem. Geol. 234: 105-126.

XIA X, SUN M, ZHAO G, LI H AND ZHOU M. 2004. Spot zircon U-Pb isotope analysis by ICP-MS coupled with a frequency quintupled (213 nm) Nd-YAG laser system. Geoch. J. 38:191-200.

Fig. 1 - Isotopic evolution of Hf in a chondritic reservoir (modified from Faure 1986).

Fig. 2 - Location of the Capivarita Anorthosite in the NE portion of the Sul-Rio-Grandense Shield, Rio Grande do Sul State, Brazil (Philipp et al. 2010).

Fig. 3 - Zircon backscattering images showing the spots from Hf (big hole) and U-Pb (small hole) analyses at LGI. Dotted circles are the Hf analyses at MAF-IIC. Mineral images: a) and b) are igneous zircons, c) is a metamorphic zircon and d) is a baddeleyite.

Fig. 4 –  $\varepsilon\text{Hf}(t)$  values (a) and Hf isotope (b) are evolution diagrams from Capivarita Anorthosite zircons. Shadowed areas indicate the evolution trend for this massif.

Fig. 5 – Example of time-resolved Hf isotope spectra, intensity and fractionation index for Zr-A-I-01 grain in (a) from MAF-IIC and in (b) from LGI.

Table I

Operating conditions used for LA-MC-ICPMS at LGI and MAF-IIC.

Table II

Cup configuration used during Lu-Hf measurements in both labs.

Table III

Results of Lu-Hf analyses from Capivarita Anorthosite zircons at LGI.

Table IV

Results of Lu-Hf analyses from Capivarita Anorthosite zircons at MAF-IIC.

**Figure 1**

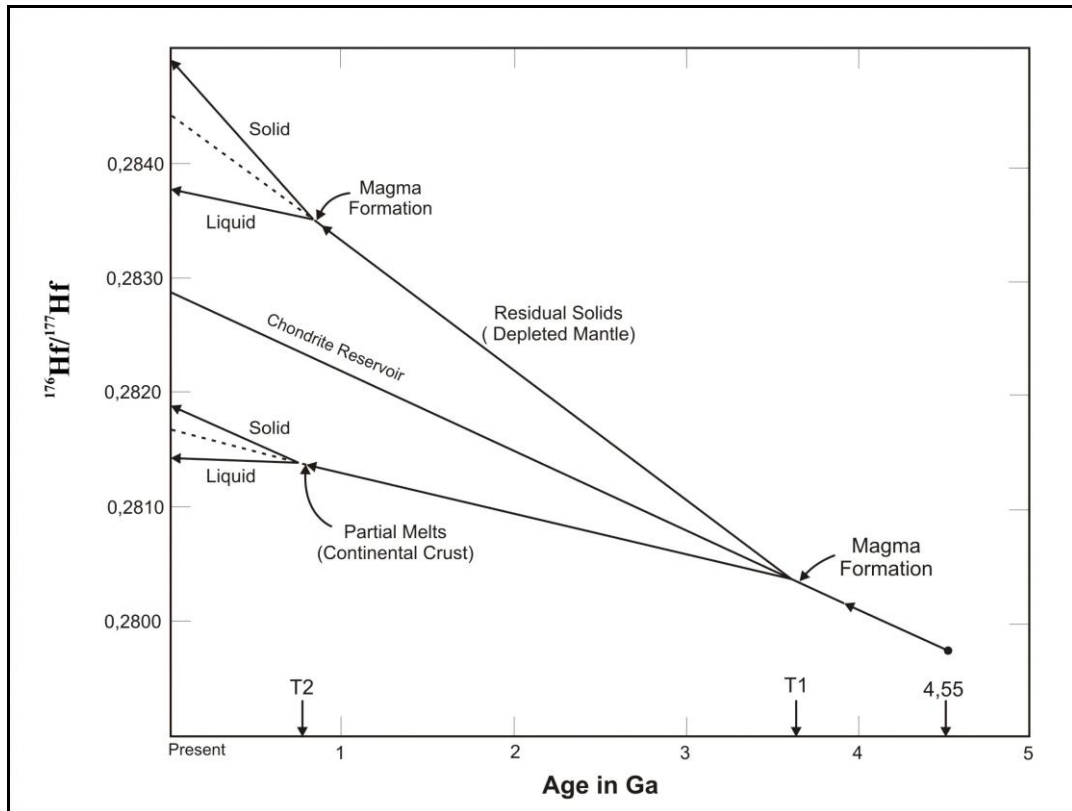


**Figure 2**

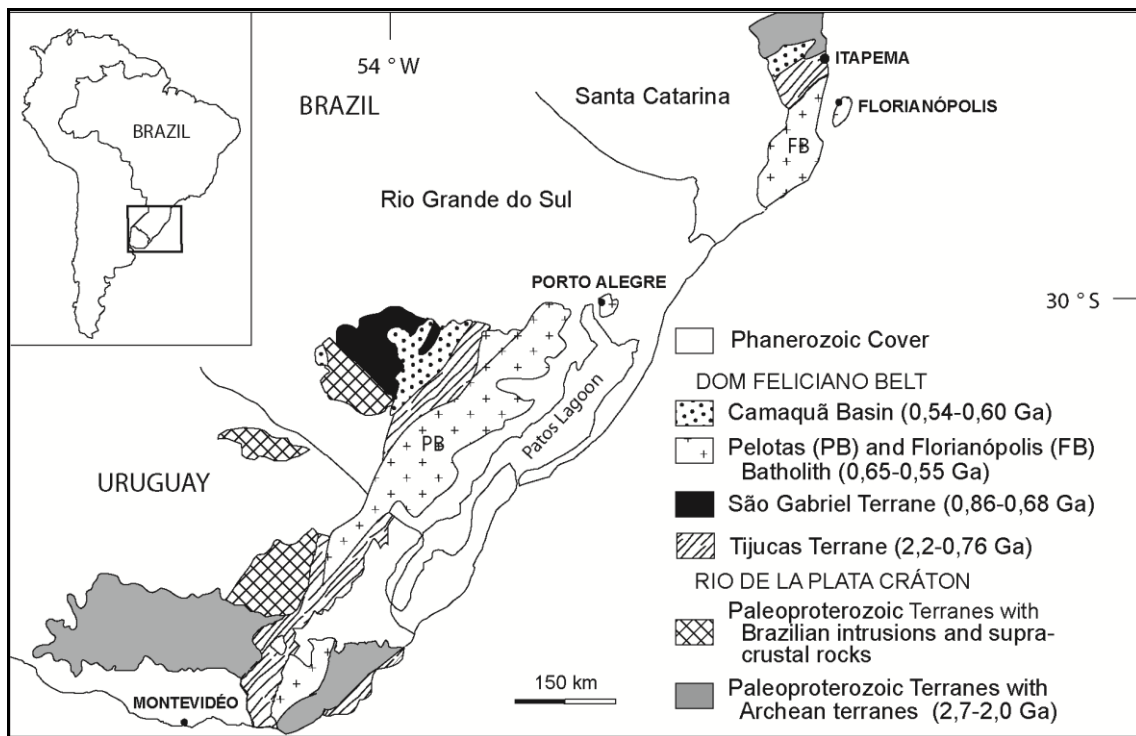


**Figure 3**

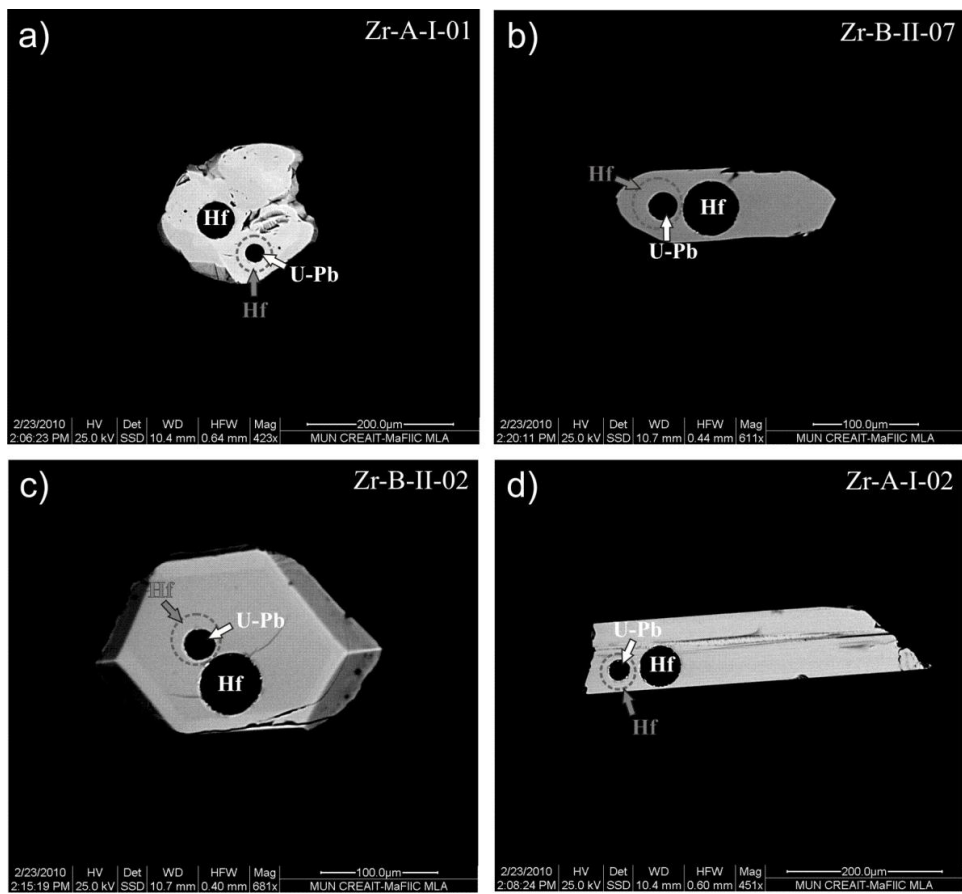


**Figure 4**

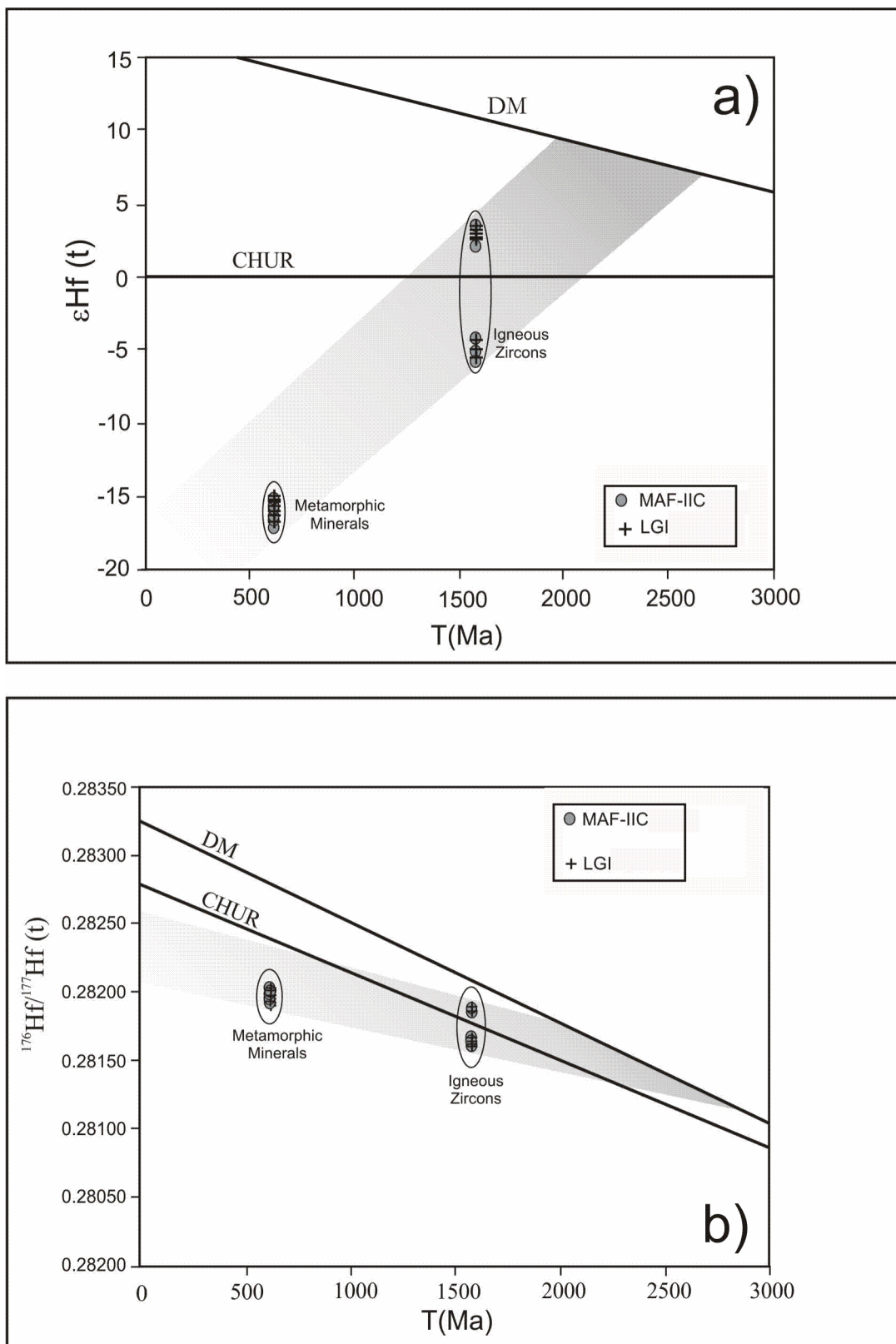


**Figure 5**

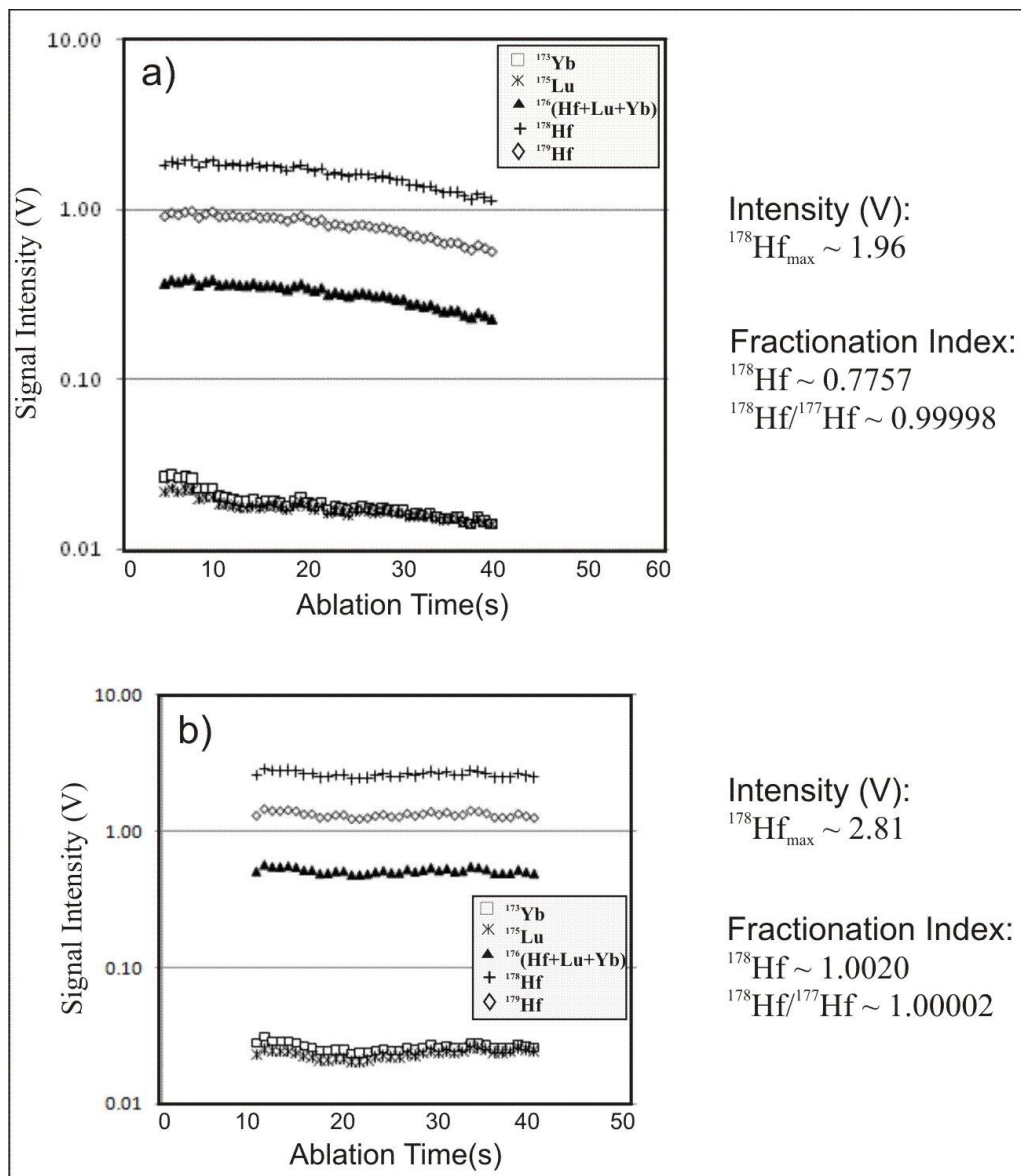


**Table I**

	<b>LGI</b>	<b>MAF-IIC</b>
MC-ICP-MS	Finnigan Neptune	Finnigan Neptune
<b>Ion Source</b>		
Power	1200W	1200W
Extraction	-2000 V	-2000 V
Ion Detection	Faraday	Faraday
Analysis Mode	Static	Static
<b>Gas flow rate</b>		
Cool (l/min)	15.0	16.0
Auxiliar (l/min)	0.73	0.75
Carrier Ar (l/min)	0.74	0.75
Carrier N <sub>2</sub> (ml/min)	4.0-5.0	-
<b>Data acquisition</b>		
Integration Time (s)	1,049	1,049
Integrations	1	1
<b>Laser Ablation</b>		
Instrument	UP-213 New Wave, Nd: YAG, 213 nm	GeoLas, Lambda Physik Compex Pro 110 ArF Excimer, 193nm
Spot Size ( $\mu\text{m}$ )	55	49
Energy Density (J/cm <sup>2</sup> )	5-6	5
Repetition rate (Hz)	10	10
Total ablation time (s)	50	60
He gas flow rate (l/min)	0.7	1.3

**Table II**

	<b>L4</b>	<b>L3</b>	<b>L2</b>	<b>L1</b>	<b>C</b>	<b>H1</b>	<b>H2</b>	<b>H3</b>
<b>Isotopes</b>	$^{171}\text{Yb}$	$^{173}\text{Yb}$	$^{174}\text{Hf}$	$^{175}\text{Lu}$	$^{176}\text{Hf}$	$^{177}\text{Hf}$	$^{178}\text{Hf}$	$^{179}\text{Hf}$
<b>Interferences</b>			$^{174}\text{Yb}$		$^{176}(\text{Yb+Lu})$			

**Table III**

Sample	U/Pb Age	$\pm 2s$	Mean $^{178}\text{Hf}$ (V)	$^{176}\text{Hf}/^{177}\text{Hf}$	$\pm 2\text{SE}$	$^{176}\text{Lu}/^{177}\text{Hf}$	$\pm 2\text{SE}$	$^{176}\text{Hf}/^{177}\text{Hf}$ (t)	$\epsilon\text{Hf(t)}$	T DM Age (Ga)
<b>Igneous Zircons</b>										
Zr-170-A-I-01	1573	21	2.61	0.281636	0.000029	0.000359	0.000006	0.281625	-5.64	2.62
Zr-170-B-II-11	1573	21	3.52	0.281643	0.000019	0.000298	0.000004	0.281635	-5.29	2.60
Zr-170-C-III-08	1573	21	1.69	0.281665	0.000039	0.000372	0.000004	0.281654	-4.59	2.55
Zr-170-B-II-06	1573	21	2.81	0.281899	0.000023	0.000028	0.000001	0.281898	4.05	2.01
Zr-170-B-II-07	1573	21	2.56	0.281885	0.000026	0.000060	0.000009	0.281884	3.55	2.04
Zr-170-C-III-02	1573	21	1.77	0.281894	0.000039	0.000773	0.000061	0.281871	3.10	2.07
Zr-170-C-III-05	1573	21	1.42	0.281849	0.000035	0.000093	0.000005	0.281846	2.21	2.13
Zr-170-C-III-10	1573	21	1.63	0.282003	0.000067	0.001288	0.000018	0.281965	6.42	1.86
Zr-170-C-III-16	1573	21	1.48	0.281903	0.000044	0.000083	0.000006	0.281901	4.15	2.01
<b>Metamorphic Zircons</b>										
Zr-170-B-II-01	611	4.8	2.41	0.281951	0.000022	0.000842	0.000012	0.281942	-16.21	2.52
Zr-170-B-II-02	611	4.8	2.59	0.281970	0.000027	0.000431	0.000004	0.281965	-15.39	2.47
Zr-170-B-II-03	611	4.8	2.81	0.281934	0.000027	0.000206	0.000003	0.281931	-16.58	2.54
Zr-170-B-II-04	611	4.8	2.38	0.281969	0.000022	0.000253	0.000002	0.281966	-15.34	2.47
Zr-170-B-II-08	611	4.8	3.16	0.281960	0.000026	0.000875	0.000032	0.281950	-15.90	2.50
<b>Baddeleyite</b>										
Zr-170-A-I-02	608	14	3.01	0.281978	0.000029	0.000315	0.000005	0.281975	-15.12	2.45

**Table IV**

Sample	U/Pb Age(Ma)	$\pm 2s$	Mean $^{178}\text{Hf}$ (V)	$^{176}\text{Hf}/^{177}\text{Hf}$	$\pm 2\text{SE}$	$^{176}\text{Lu}/^{177}\text{Hf}$	$\pm 2\text{SE}$	$^{176}\text{Hf}/^{177}\text{Hf}$ (t)	$\epsilon\text{Hf(t)}$	T DM Age (Ga)
<b>Igneous Zircons</b>										
Zr-170-A-I-01	1573	21	1.60	0.281630	0.000049	0.000435	0.000010	0.281617	-5.9	2.63
Zr-170-B-II-11	1573	21	1.78	0.281643	0.000064	0.000265	0.000006	0.281635	-5.3	2.60
Zr-170-C-III-08	1573	21	1.99	0.281671	0.000033	0.000340	0.000004	0.281661	-4.4	2.54
Zr-170-B-II-06	1573	21	1.92	0.281841	0.000035	0.000033	0.000001	0.281840	2.0	2.14
Zr-170-B-II-07	1573	21	1.67	0.281883	0.000043	0.000036	0.000001	0.281882	3.5	2.05
Zr-170-C-III-02	1573	21	2.01	0.281901	0.000034	0.000614	0.000013	0.281883	3.5	2.05
<b>Metamorphic Zircons</b>										
Zr-170-B-II-01	611	4.8	1.29	0.281952	0.000053	0.000823	0.000004	0.281943	-16.2	2.52
Zr-170-B-II-02	611	4.8	1.59	0.281918	0.000042	0.000440	0.000003	0.281913	-17.2	2.58
Zr-170-B-II-03	611	4.8	1.71	0.281940	0.000040	0.000216	0.000003	0.281937	-16.4	2.53
Zr-170-B-II-04	611	4.8	1.52	0.281941	0.000047	0.000175	0.000004	0.281939	-16.3	2.53
Zr-170-B-II-08	611	4.8	1.64	0.281966	0.000056	0.001117	0.000059	0.281953	-15.8	2.49
<b>Baddeleyite</b>										
Zr-170-A-I-02	608	14	1.81	0.281971	0.000047	0.000319	0.000003	0.281967	-15.4	2.47

## 2.3 Terceiro Artigo

From: epsl@elsevier.com  
To: anelise.bertotti@ufrgs.br  
Date: Mon, 13 Feb 2012 13:34:03 +0000  
Subject: Submission Confirmation

Dear Mrs. Bertotti,

Your submission entitled "Isotopic signature of sediments formed during the initial stage rifting, Camamu basin, Eastern Brazil" has been received by Earth and Planetary Science Letters

You may check on the progress of your paper by logging on to the Elsevier Editorial System as an author. The URL is  
<http://ees.elsevier.com/epsl/>.

Your manuscript will be given a reference number once an Editor has been assigned.

Thank you for submitting your work to this journal.

Kind regards,

Editorial Office  
Earth and Planetary Science Letters

1 Isotopic signature of sediments formed during the initial stage rifting,  
2 Camamu basin, Eastern Brazil  
3  
4

5 Bertotti, A.L.<sup>1\*</sup>, Chemale, F.<sup>2</sup>, Kayser, V.T.<sup>3</sup>, Sylvester, P. J.<sup>4</sup>, Gruber, L.<sup>1</sup>  
6  
7

- 8 1. Programa de Pós Graduação em Geociências, Universidade Federal do Rio Grande do Sul,  
9 Porto Alegre, RS, Brazil.  
10 2. Instituto de Geociências, Universidade de Brasília, Brasília, DF, Brazil.  
11 3. Programa de Pós Graduação em Engenharia de Minas, Metalúrgica e Materiais.  
12 Universidade Federal do Rio Grande do Sul, Porto Alegre, RS, Brazil.  
13 4. Department of Earth Sciences and Micro Analysis Facility - Inco Innovation Centre, Memorial  
14 University of Newfoundland, St. John's, NL, Canada.

15  
16  
17 ABSTRACT  
18

19 The Camamu basin is related to the breakup of Gondwana and belongs to the  
20 group of sedimentary basins that are part of the eastern Brazilian passive  
21 margin. To obtain information on the provenance of the original sediments,  
22 petrographic investigation of fluvial and eolian units from the pre-rift Brotas  
23 Group and the rift-associated Almada Group, as well as U-Pb and Hf isotopic  
24 analyses from detrital zircons, were performed. Detrital zircons from the Sergi  
25 Formation, Brotas Group, showed a main population with U-Pb ages of 480-600  
26 Ma and smaller populations with ages of 900-1000 Ma, 1900-2100 Ma, 2500-  
27 2800 Ma and 3000-3200 Ma. The Almada Group zircons are characterized by a  
28 distribution of ages predominantly in the Paleoproterozoic and Archean. The Hf  
29  $T_{DM}$  model ages of the Brotas Group zircons range from ca. 1.1 to 4.0 Ga, and  
30 the  $\epsilon_{Hf}(t)$  values vary from -31.4 to +9.6, providing evidence that some detrital  
31 zircon grains in the Camamu Basin contain a juvenile signature and that most  
32 zircons were formed during recycling or were contaminated with older crustal  
33 material. The integration of these data provided very important clues to the  
34 provenance history of the initial sedimentation on Camamu basin passive  
35 margin, where the pre-rift phase is marked by the input of a dominant  
36 Neoproterozoic to Eopaleozoic source (Brasiliano cycle), the Araçuaí-West  
37 Congo belt that is situated southern of the basin, whereas the rift sedimentation  
38 clearly received a contribution from the western terranes, the Paleoproterozoic  
39 (Transamazonian cycle) to Archean (Jequié cycle) São Francisco craton units.  
40  
41  
42  
43

44 Keywords: Provenance, Detrital zircon; U/Pb geochronology; Hf isotope; LA-  
45 MC-ICPMS; Camamu Basin.  
46  
47  
48  
49  
50  
51

## 52 1. Introduction

53

54 Continental passive margins are very important loci for the deposition of thick  
55 sedimentary packages, where the early stages are related to pre-rift and syn-rift  
56 sedimentation. The rift sequences are very well studied and demonstrate that  
57 the sedimentation infill is directly connected to mechanical subsidence and  
58 subsequent thermal subsidence, with the development of mega-sequences of  
59 rift-post-rift cycles, as presented by Lambiase and Bosworth (1995) and  
60 Prosser (1993). The pre-rift stage occurs on a stable platform, such as that of  
61 West Gondwana, recording the last depositional events of intraplate  
62 sedimentation.

63 With the recent advances in isotopic analytical techniques, especially those  
64 related to in situ zircon dating by ion microprobe or Multicollector - Inductively  
65 Coupled Plasma Mass Spectrometer with Laser Ablation Microprobe (LA-MC-  
66 ICPMS) (e.g., Košler et al., 2002), it has become possible to quickly obtain  
67 information on the paleodrainage and source areas of these sedimentary  
68 sequences.

69 The depositional locus of the pre-rift sedimentation of the South Atlantic  
70 margins is known as the Afro-Brazilian depression (Cesero and Ponte, 1972;  
71 Ponte and Asmus, 1978), and it extends from southern to northeastern Brazil.  
72 From the tectonic point of view, this depression can be defined as an  
73 intracratonic basin with dominant continental input or the early stages of a rifted  
74 passive margin, such as that of the Atlantic margin. The Afro-Brazilian  
75 depression is a large basin with dominant continental facies, including fluvial,  
76 eolian and lacustrine depositional systems (Ghignone, 1979), formed during the  
77 Late Jurassic, just before the main rifting of West Gondwana, whereas the  
78 overlying sequence (the so-called rift one) comprises similar depositional  
79 systems but is strongly controlled by mechanical subsidence. During the rifting  
80 of South America and Africa, large areas of these continents were eroded as a  
81 result of uplift and denudation associated with isostatic movements. Due to  
82 section preservation, one of the best places in the eastern Brazilian margin to  
83 study the initial stage of the sequences of an Atlantic-type rifted margin is the  
84 NE continental margin of Brazil because there are very well-exposed onshore

85 sections (Born et al., 2011) as well as abundant subsurface information from  
86 drill holes and seismic lines, such as those presented by Küchle et al. (2011).  
87 The sedimentary record of this section may provide very important information  
88 on the characterization of the main source areas of eolian and fluvial facies and  
89 the paleodrainage system involved in the early stages of the rifting of the  
90 Atlantic margin. To understand the depositional systems of the pre-rift and rift  
91 sequences and to identify the source areas, we performed integrated studies of  
92 the sedimentology, petrography and isotope geology on selected sections of the  
93 Camamu Basin. In this study, the combination of U-Pb and Lu-Hf zircon dating  
94 is a powerful tool for the identification of source areas, where we demonstrate a  
95 complex provenance history for the investigated section.

96

97

## 98 2. Geological Setting

99

100 The Camamu basin (Fig. 1) is located along the central coast of Bahia State,  
101 NE Brazil, and it formed as a result of continental rifting and the separation of  
102 South America and Africa, which began at ca. 140 Ma.

103

### 104 Insert Fig. 1

105

106 The Camamu basin presents a fairly complete geological record, where pre-rift,  
107 syn-rift and post-rift sequences are recognized (Ponte and Asmus, 1978). The  
108 main tectonic phases of the basin are described as follows:

109 i) Pre-rift section, consisting of the Brotas Group units (Fig. 2), which are  
110 interpreted as an intracontinental syncline formed between the  
111 Neojurassic and the Eocretaceous, as well as the first sedimentological  
112 infilling related to the pre-rift sequences of the South American and  
113 African plates.

114 ii) Rift section, consisting of the Almada Group units (Fig. 2) that formed in  
115 response to Gondwana breakup with the generation of asymmetric rift  
116 sequences similar to those of the East African rift. The rift section  
117 characterized by fluvial-deltaic-lacustrine sediments formed from  
118 extensional tectonism from the Neocomian to the Aptian.

119     iii) Transitional (drift) section, consisting of the basal portion of the Camamu  
120       Group (Fig. 2), represented by the first marine incursion into the basin.

121     iv) Post-rift or passive margin section, consisting of the intermediate and  
122       upper section of the Camamu Group and Espírito Santo Group (Fig. 2),  
123       formed from continental drift and characterized by passive margin  
124       sedimentation.

125     The crystalline basement rocks of the state of Bahia belong to the São  
126       Francisco craton (Fig. 1A). These rocks occupy approximately 50% of the total  
127       area of Bahia state and are composed almost exclusively of metamorphic rocks  
128       of high-to-medium grade (Barbosa and Sabaté, 2003), with small areas  
129       composed of greenschist facies rocks of greenstone belts. The rocks are  
130       represented by the following tectonic terranes: the Itabuna-Salvador Curuçá  
131       block, a Neoarchean to Paleoproterozoic block (2.6-2.1 Ga); the Jequié block,  
132       a well-constrained Archean block (2.9-2.6 Ga); the Serrinha block (3.1-2.0 Ga)  
133       and the Gavião block, an Archean block (2.7-3.4 Ga). The tectonic structures of  
134       the Camamu basin were controlled by the pre-existing basement (Netto et al.  
135       1994, Cupertino, 2000) and were constrained principally by an extensional  
136       stretching synchronous to rifting between Brazil and Africa in the Cretaceous.

137

138

## 139     2.1 Stratigraphy of the Camamu Basin

140

141     This basin covers an area of ca. 12,000 km<sup>2</sup>, including 2,000 km<sup>2</sup> onshore. The  
142       Camamu basin is bounded to the north with two basins: the Itapuã Fault with  
143       the Jacuípe basin marks one limit, and the other limit is defined by the Barra  
144       fault and the Jaguaribe accommodation zone along the Recôncavo basin. To  
145       the south, the Camamu basin is limited by the Itacaré structural high, which  
146       separates the Camamu and Almada basins, where a structural and stratigraphic  
147       continuation between both basins is observed (Caixeta et al., 2007). The  
148       basement units of the Camamu basin are composed of the Permian  
149       sedimentary rocks of the Afligidos Formation, interpreted to be part of an  
150       extensive intraplate Paleozoic basin, and the Precambrian rocks of the São  
151       Francisco craton. The chronostratigraphic chart is shown in Fig. 2.

152 The first depositional units of the Camamu basin comprising the pre-rift  
153 sequence (Upper Jurassic to Eocretaceous) is usually interpreted as part of the  
154 Afro-Brazilian depression (Ponte and Asmus, 1978), which consists of fluvial-  
155 eolic-lacustrine sediments of the Brotas Group. In this basin, the Aliança  
156 Formation and upper Sergi Formation are the main lithostratigraphic units. The  
157 Aliança Formation is represented by shales and sandstone deposited on fluvial-  
158 lacustrine environment with eolic reworking at the margin of the river and lakes.  
159 The Sergi Formation is composed of red-to-greenish gray sandstones and  
160 conglomeratic sandstones with trough cross lamination, shales and  
161 conglomerates, thought to be deposited by fluvial-eolian processes (Viana et  
162 al., 1971 and Netto et al., 1994). According to Caixeta et al. (2007), the pre-rift  
163 sediments are also composed of deltaic, fluvial-eolic and lacustrine deposits of  
164 the Santo Amaro Group (Itaparica, Candeias and Agua Grande Formations).  
165 The rift sequence formed during the Neoberriasian and Eoaptian stages is  
166 represented by the Almada Group units, which are divided into Morro do Barro  
167 and Rio de Contas Formations and the basal portion of the Taipus-Mirim  
168 Formation (Fig. 2). The deposits are associated mainly with alluvial fans and  
169 lacustrine environments, related to active extensional tectonism (Netto et al.,  
170 1994). Conglomeratic sequences of this stratigraphic unit were interpreted as a  
171 function of localized structural highs, and an increase in package thickness to  
172 the NW suggests a tectonic control on depositional settings, as rotation of  
173 cratonized areas could be responsible for normal faulting along the ridges of  
174 flux deposits (Born et al., 2011).

175

176 Insert Fig. 2

177

178 The evolution of the extensional processes resulted in the generation of a  
179 narrow gulf, which was progressively occupied by the proto-ocean (Souza-Lima  
180 et al., 2003), and the transitional stage (drift) was characterized by the first  
181 marine sedimentation. This transitional stage is represented by the upper  
182 portion of the Taipus-Mirim Formation with carbonate and evaporites, formed  
183 between the Eoaptian and the Albian.

184 The post-rift or passive margin sequence evolved from the Upper Cretaceous to  
185 the present and is composed of thick carbonate layers (Algódões Formation)

186 and the overlying carbonate-siliciclastic sedimentary units of the Espírito Santo  
187 Group (Urutuca, Cravelas and Rio Doce Formations), deposited in a typical  
188 shallow-to-deep-water passive margin environment.

189 Within the shale facies of Camamu basin, two types of conchostracan were  
190 found: *Cyzicus* and *Estheriina*. These organisms were described by Carvalho  
191 (1993) as common in Neocomian rocks in the sedimentary basins of  
192 northeastern Brazil and especially in those from the Aptian-Albian (Born et al.,  
193 2011).

194 The main hydrocarbon accumulations of the Camamu basin are associated with  
195 mixed or structural traps in the rift and pre-rift sections. The major  
196 accumulations occur in the Morro do Barro Formation, in the lacustrine turbiditic  
197 lobes, followed by the Neojurassic reservoir of the Sergi Formation, where they  
198 are associated with fluvial-eolian sandstones (Souza-Lima et al., 2003).

199

200

### 201 3. Analytical Procedures

202

203 Ten samples were collected from the sedimentary units of the Brotas and  
204 Almada groups on the onshore portion of the Camamu basin (Fig. 2). The  
205 samples were crushed and milled using a jaw crusher and pulverizer. The  
206 heavy minerals such as zircon, titanite and monazite were separated by  
207 conventional procedures using heavy liquids and a magnetic separator after  
208 concentration by hand panning.

209 The zircon grains were mounted in epoxy on circular grain mounts (2.5 cm in  
210 diameter) and polished until the central parts of the zircon grains were exposed.  
211 Images of zircons were obtained using a Leica MZ 125 microscope, and back-  
212 scattered electron images were acquired using a JEOL JSM 5800 electron  
213 microscope. The zircons were analyzed initially for their U-Pb ages and then for  
214 their Lu-Hf isotopic composition, on the same exact spot as where the laser had  
215 removed material for the U-Pb analysis. In general, the zircon grains presented  
216 round forms, although diverse populations presenting different sizes and  
217 shapes are recognized, suggesting that different types of erosion were active.

218

219

220 3.1 U-Pb Zircon Dating

221 U-Pb zircon dating of the samples was performed at the Isotope Geology  
222 Laboratory (LGI) of the Federal University of Rio Grande do Sul (UFRGS) by  
223 means of the in situ LA-MC-ICPMS technique (Guadagnin et al., 2010). In situ  
224 analyses were performed using a New Wave UP213 laser ablation microprobe  
225 coupled to a Neptune MC-ICPMS, with the collector configured for simultaneous  
226 measurements of Th, U, Pb and Hg isotopes. The isotope ratios and inter-  
227 element fractionation data were evaluated in comparison with the GJ-1 standard  
228 after every set of 10 zircon spots and were used to estimate the necessary  
229 corrections and internal instrumental fractionation. The laser spot size was 25  
230  $\mu\text{m}$ .

231 For every standard and sample set measurements were collected the blank  
232 values in same conditions as the standard and sample were run and its values  
233 were subtracted from all individual cycle measurements. The  $^{204}\text{Pb}$  value was  
234 corrected for  $^{204}\text{Hg}$ , assuming a  $^{202}\text{Hg}/^{204}\text{Hg}$  ratio of 4.355. The necessary  
235 correction for common  $^{204}\text{Pb}$ , after Hg correction based on the simultaneously  
236 measured  $^{202}\text{Hg}$ , was insignificant in most cases. Where the common Pb  
237 correction was necessary, the Pb isotopic composition was assumed to follow  
238 the isotopic evolution proposed by Stacey & Kramers (1975), using an  
239 estimated age. After the blank and common Pb corrections, the ratios and their  
240 absolute errors ( $1\sigma$ ) of  $^{206}\text{Pb}^*/^{238}\text{U}$ ,  $^{232}\text{Th}/^{238}\text{U}$  and  $^{206}\text{Pb}^*/^{207}\text{Pb}^*$  were calculated  
241 in an Excel spreadsheet, and the intercepts were determined as proposed by  
242 Youden (1951) and Sylvester & Ghaderi (1997).

243

244 Insert Table 1

245

246 3.2 Hafnium Isotope Analysis

247 A GeoLas (ArF excimer laser 193 nm) laser ablation system coupled to a  
248 Neptune MC-ICPMS at the Micro Analysis Facility Inco Innovation Centre (MAF-  
249 IIC) at the Memorial University of Newfoundland (MUN) was used in this study  
250 to measure Lu, Yb and Hf isotopic signatures in the zircons. The standards  
251 used during Hf analysis were Plešovice (Slama et al., 2008) and 91500  
252 (Blichert-Toft, 2008). The  $^{176}\text{Hf}/^{177}\text{Hf}$  values for the standards in three laser  
253 sessions were reproduced within the error margin, yielding results of 0.282482

254  $\pm 0.000043$  ( $n=50$ , 2SD) for Plešovice and  $0.282305 \pm 0.000061$  ( $n=25$ , 2SD)  
255 for 91500.

256 A laser energy of approximately  $5 \text{ J/cm}^2$  with a repetition rate of 10 Hz and a  
257 spot size of  $49 \mu\text{m}$  were used for all analyses. All raw signals are blank-  
258 corrected using the mean of approximately 20-25 points recorded as the gas  
259 blank baseline before ablation. A user-selected interval of approximately 50  
260 data points covering the sample transient peak is used for calculation of the Hf  
261 ratio with mass bias correction using the exponential law.

262 The isotopes  $^{175}\text{Lu}$ ,  $^{171}\text{Yb}$  and  $^{173}\text{Yb}$  were monitored during analysis and their  
263 relative abundances were used to calculate  $^{176}\text{Lu}$  and  $^{176}\text{Yb}$  interferences, which  
264 were subtracted from  $^{176}\text{Hf}$ . The data were corrected in an Excel spreadsheet  
265 offline using  $^{179}\text{Hf}/^{177}\text{Hf} = 0.7325$  (Patchett et al., 1981),  $^{176}\text{Lu}/^{175}\text{Lu} = 0.2656$   
266 (Chu et al., 2002),  $^{173}\text{Yb}/^{171}\text{Yb} = 1.1301$  and  $^{176}\text{Yb}/^{173}\text{Yb} = 0.7938$  (Segal et al.,  
267 2003). The Hf analyses were performed only on zircons with concordant U-Pb  
268 ages, and  $\varepsilon_{\text{Hf}}$  values were calculated where the U-Pb age had been measured  
269 for each single grain. The details of the instrumental operating conditions in  
270 both labs were as given in Table 1.

271

272

#### 273 4. Results

##### 274 4.1 Petrography

275 Due to the altered state of the minerals in the collected samples, only  
276 petrographic studies on the PCA 05, 07, 10 and 12 samples were performed.  
277 The petrographic analysis was performed with PetroLedge, which is a database  
278 system designed to standardize the petrographic description of sedimentary  
279 rocks. The Gazzi-Dickinson method (Dickinson et al., 1985) was employed in  
280 this study to determine the provenance category based on the sample  
281 composition.

282 Thus, medium arcosean and massive sandstones with very few lithic fragments  
283 characterize the units of the Brotas and Almada Groups. All samples possess  
284 high contents of organic matter. These results indicate that the sediments are  
285 derived from continental block (Fig. 3a). The observed diagenetic processes are  
286 feldspars dissolution and replacement by kaolinite, secondary growth of quartz,  
287 clay infiltration and hematite deposition. Some of these features are shown in

288 Fig. 3b, and all petrographic analyses and pictures of the samples can be found  
289 in the Data Repository (Supplementary Data).

290

291 Insert Fig. 3

292

### 293 4.2 U-Pb Zircon Ages

294 More than 500 zircon grains from ten samples of the Brotas and Almada groups  
295 were analyzed by the U-Pb in situ method (Fig. 4). The frequency diagrams do  
296 not include analyses with high common lead content and discordance greater  
297 than 15%. The analytical results are given in the Data Repository  
298 (Supplementary Data).

299

300 Insert Fig. 4

301

#### 302 4.2.1 Sergi Formation, Brotas Group

303 Samples were collected from four localities: PCA 08, PCA 10 and PCA 12 (Fig.  
304 2). Sample PCA 08 is from a section located in Tinhare, Morro de São Paulo  
305 and is characterized by fluvial sandstone at the base (PCA 08A) and eolian  
306 sediments at the top (PCA 08B). The fluvial sandstone is medium to coarse and  
307 moderately sorted with large cross-bedding and fluidization features. The eolian  
308 sandstone consists of fine sand that is well sorted, light-colored and that has  
309 oxidized layers. PCA 08A consists of large (150 to 300  $\mu\text{m}$ ), rounded, euhedral  
310 to subhedral zircon crystals, and out of the 82 grains analyzed, 79 yielded  
311 concordant data. The probability density plot (Fig. 5b) shows two main  
312 Neoproterozoic peaks at approximately 500 Ma and 1000 Ma, two minor peaks  
313 at 2000 Ma and 2500 Ma and just one Archean zircon at 3032 Ma. The  
314 youngest concordant grain yielded an age of  $427 \pm 13$  Ma. The grains from PCA  
315 08B are similar to those of PCA-08A. Out of all 80 dated zircons, just one was  
316 discordant. The age spectrum (Fig. 5d) shows six groups of U-Pb ages, two  
317 main peaks at 498 Ma and 590 Ma, three minor peaks at 928 Ma, 2004 Ma and  
318 2649 Ma and just one zircon with 3059 Ma. The youngest concordant grain  
319 yielded the age of  $452 \pm 9$  Ma.

320 Sample PCA 10, located at the beach of Arraial D'Ajuda, is from a small outcrop  
321 of fine-to-coarse grained, brown-gray, poorly sorted sandstone. The zircon

322 grains are rounded, euhedral and subhedral. A total of 61 zircons from the 63  
323 dated samples are concordant. Five groups were recognized in the sample; one  
324 main peak at 500 Ma and four minor peaks at 260, 1000, 2000, 2500 and 3193  
325 Ma (Fig. 5c).

326 Sample PCA 12 represents fluvial sandstone. It is coarse grained, yellowish,  
327 poorly sorted and intercalated with purple siltstone. The zircon grains are  
328 rounded, euhedral, subhedral and their sizes vary from 75 to 200 µm. A total of  
329 104 grains were analyzed, and 101 are concordant. The probability density plot  
330 (Fig. 5a) shows a broad distribution, with five minor peaks, but with a main  
331 concentration of ages at 518 Ma. The youngest concordant grain yielded an age  
332 of  $146 \pm 7$  Ma.

333

334 Insert Fig. 5

335

336 4.2.2 Almada Group

337 Samples PCA 05, 06, 07 and PCA 9 of the Almada Group were collected (Fig.  
338 2) for zircon dating. The PCA 05A/B section consists of fluvial sandstone with  
339 channel cross-bedding. Paleocurrent data indicate sediment transport to the E-  
340 SE, which is similar to the eastward sediment flow reported by Born et al.  
341 (2011). The sets are characterized by medium-to-coarse sandstone, which  
342 yielded 38 zircons. These grains are rounded, colorless or reddish crystals. All  
343 of them were analyzed, and 32 produced concordant data. The relative  
344 probability distribution plot of the  $^{207}\text{Pb}/^{206}\text{Pb}$  dates (Fig. 6a) shows two main  
345 groups with Paleoproterozoic and Archean ages. Four zircons grains have  
346 Neoproterozoic and Brasiliano ages, and the youngest concordant grain has the  
347 age of  $543 \pm 24$  Ma.

348 The PCA 06 section is located near the town of Camamu. The outcrop  
349 comprises red fluvial sandstones at the base (sample PCA 06B), with  
350 conglomeratic layers and large cross-bedding stratification, and eolian  
351 sandstones at the top (PCA 06A), which are predominantly quartzose in  
352 composition, medium-to-coarse grained and moderately sorted.

353 PCA 06A zircons are rounded, broken and euhedral crystals. From the 53  
354 analyzed zircons, only one yielded discordant data. Two main peaks at 2084  
355 Ma (dominant) and 997 Ma are recognized. Mesoproterozoic, Neoarchean, and

356 Mesoarchean ages are represented by minor populations (Fig. 6b). The  
357 youngest concordant grain yielded an age of  $950 \pm 17$  Ma. PCA 06B zircons are  
358 dark rounded, subhedral and euhedral. Of the 59 grains, only two produced  
359 discordant analyses. The majority of the analyzed grains indicate two main  
360 Paleoproterozoic age peaks at approximately 2050 Ma and 2450 Ma. The  
361 youngest grain has an age of  $560 \pm 31$  Ma (Fig. 6c).

362 Sample PCA 07 is medium-to-fine grained, dark brown, well-sorted eolian  
363 sandstone, with cross-bedding. Most zircon grains are colorless or reddish.  
364 From all of the 37 zircons, only one produced data with discordance >15%,  
365 indicating two main age peaks at ~2050 Ma (Paleoproterozoic) and ~2600 Ma  
366 (Archean) (Fig. 6d). The youngest grain has an age of  $492 \pm 26$  Ma.

367 The PCA 09 sample is from a 6 m thick layer of a polymitic, matrix-supported  
368 reddish conglomerate. It contains poorly sorted round clasts of quartz,  
369 sandstone and basement rocks. The zircons are rounded, broken, long  
370 euhedral and subhedral crystals. Out of the 27 grains analyzed, 24 are  
371 concordant. Two main groups are recognized at approximately 2100 Ma and  
372 2600 Ma (Fig. 6e). The youngest concordant grain yielded the age of  $635 \pm 10$   
373 Ma.

374

375 Insert Fig. 6

376

#### 377 4.2.3 Lu-Hf Data

378 Two samples (PCA 08B and PCA 12) were analyzed for their Hf isotopic  
379 compositions, out of a total of 113 grains with U-Pb concordant ages from the  
380 eolian and fluvial Sergi sediments of the Brotas Group. All of the Lu-Hf  
381 analytical results are listed in the Data Repository (Table 12).  $T_{DM}$  model ages  
382 were calculated assuming a  $^{176}\text{Lu}/^{177}\text{Hf}$  ratio of 0.015 as the crustal average  
383 (Goodge and Vervoort, 2006). Backscattered electron images of dated detrital  
384 zircon grains with their U-Pb zircon ages and respective  $\epsilon_{\text{Hf}}(t)$  values are shown  
385 in Figure 7. The diagram of  $\epsilon_{\text{Hf}}(t)$  values versus U-Pb zircon age for PCA 08B  
386 and PCA 12 samples is presented in Fig. 8.

387

388 Insert figures 7 and 8

389

390 Paleozoic zircons from sample PCA 08B have  $\varepsilon_{\text{Hf}}(t)$  values between -10.9 to -  
391 6.4 with  $T_{\text{DM}}$  ages of 2.1 to 1.8 Ga. The Neoproterozoic zircons (U-Pb ages  
392 between 554 and 1001 Ma) show a wider range of  $\varepsilon_{\text{Hf}}(t)$  values, which vary from  
393 -14.1 to -0.6, with  $T_{\text{DM}}$  model ages between 2.6 and 1.6 Ga. Two zircons,  
394 however, display positive  $\varepsilon_{\text{Hf}}(t)$  values and younger  $T_{\text{DM}}$  ages. Paleoproterozoic  
395 zircons grains (with U-Pb ages between 1898 and 2147 Ma) gave  $\varepsilon_{\text{Hf}}(t)$  between  
396 -17.3 to +0.2 and  $T_{\text{DM}}$  model ages between 3.8 to 2.5 Ga. Neoarchean zircons  
397 (with U-Pb ages between 2554 and 2703 Ma) gave  $\varepsilon_{\text{Hf}}(t)$  values between -6.6  
398 and -1.8 and  $T_{\text{DM}}$  between 3.4 and 3.2 Ga. The Mesoarchean zircon (with a U-  
399 Pb age of 3095 Ma) showed an  $\varepsilon_{\text{Hf}}(t)$  value of -8.9 and a  $T_{\text{DM}}$  model age of 4.0  
400 Ga.

401 In sample PCA-12, Paleozoic zircons (with U-Pb ages between 454 and 541  
402 Ma) include only two zircons with very negative  $\varepsilon_{\text{Hf}}(t)$  values of -31.4 and -18.1  
403 and one with a positive value of +1.45; most of the zircons have values between  
404 -12.8 to -4.2 and  $T_{\text{DM}}$  ages between 2.2 and 1.7 Ga. Neoproterozoic zircons  
405 (with U-Pb ages between 547 and 999 Ma) form two groups; one yielded  
406 negative  $\varepsilon_{\text{Hf}}(t)$  values from -17.8 to -1.25 and  $T_{\text{DM}}$  ages from 2.90 to 1.6 Ga, and  
407 the other yielded positive values from +1.0 to +9.2 with  $T_{\text{DM}}$  values varying from  
408 1.5 to 1.1 Ga. In the group of Mesoproterozoic zircons (with U-Pb ages between  
409 1001 to 1386 Ma), two zircons yielded negative  $\varepsilon_{\text{Hf}}(t)$  values between -15.5 and  
410 -5.6 and  $T_{\text{DM}}$  ages of 2.8 to 2.5 Ga, and one zircon yielded a positive value of  
411 +5.5 and  $T_{\text{DM}}$  of 1.6 Ga. The Paleoproterozoic zircons (with U-Pb ages between  
412 1744 to 2433 Ma) display  $\varepsilon_{\text{Hf}}(t)$  between -13.6 to -0.8 with  $T_{\text{DM}}$  ages between  
413 3.5 to 2.4 Ga and one zircon with a positive  $\varepsilon_{\text{Hf}}(t)$  value. In the group of  
414 Neoarchean zircons (with U-Pb ages between 2529 to 2729 Ma), the  $\varepsilon_{\text{Hf}}(t)$   
415 values are between -6.1 to -0.6 with  $T_{\text{DM}}$  ages between 3.4 to 3.2 Ga.

416

417

## 418 5. Discussion

419

420 The present study combining geologic, petrographic and isotopic analyses  
421 provides very important information on the provenance and maximum

422 depositional age of the early stages of rifting of the Atlantic margin in the  
423 Eastern Brazil and Western Africa.

424 The paleocurrent measurements from the Sergi Formation unit, Brotas Group,  
425 in the onshore Camamu basin are dominantly northwards (Küchle et al., 2011),  
426 whereas paleocurrent measurements from the Almada Group units in the  
427 onshore Camamu basin (this work and Born et al., 2011) indicate that the main  
428 channel system flowed eastwards. This information suggests a change in the  
429 source areas for the pre-rift and the rift sediments.

430 Age constraints on the pre-rift units of the eastern Atlantic margin are based on  
431 paleontological records from the Dom João section. Viana et al. (1971) and  
432 Schaller (1969) proposed a Late Jurassic age for the Brotas Group in the  
433 Reconcavo and Sergipe-Alagoas basin, whereas Caixeta et al. (1994) assumed  
434 a Tithonian age (Late Jurassic) due to the presence of non-marine ostracods in  
435 the Aliança Formation (the basal section of the Brotas Group in the Tucano and  
436 Jatobá basins). In contrast, Silva et al. (2006) dated the Bananeiras Formation  
437 of the Sergipe-Alagoas basin using the Rb-Sr isotope method at  $227.1 \pm 2.2$   
438 Ma. Because this unit is chronocorrelated with the Aliança Fm., the age of the  
439 pre-rift sequence should be Triassic, which is not supported by the fossil  
440 content. Indeed, the zircon at age  $146 \pm 7$  Ma that was obtained from sample  
441 PCA-12 (Sergi Fm., Brotas Group) suggests that pre-rifting processes affected  
442 South America and Africa several million years before the rifting stage, as  
443 already has been suggested by the paleontological studies with estimated ages  
444 of approximately Late Jurassic. The Rb-Sr age obtained by Silva et al. (2006)  
445 probably corresponds to the age of the dated clay minerals, i.e., the  
446 provenance, rather than the depositional age.

447 Provenance information is well constrained in both stratigraphic groups based  
448 on the whole rock Sm-Nd and Pb isotope analyses of samples PCA 05, 06, 07,  
449 08, 09, 10, 11 and 12 (Fig. 2) performed by Kayser (2006), which also confirm  
450 the distribution of the two groups that are related to the pre-rift and the rift  
451 sequences. From the  $f_{\text{Sm}/\text{Nd}}$  versus  $\epsilon_{\text{Nd}}(0)$  plot, it is apparent that the Almada  
452 Group samples display a signature typical of the Archean to Paleoproterozoic  
453 cratonic area of South America (Fig. 9a). The samples from the Brotas Group  
454 yield an Nd  $T_{\text{DM}}$  model ages between 1.45 and 1.59 Ga, while the Almada  
455 Group samples have model ages between 2.07 and 3.2 Ga (Fig. 9b). The Pb

456 isotope data of Almada Group samples are also very distinct compared with  
457 those data from the Brotas Group samples (Figs. 9c and 9d).

458 The age pattern for the dated Brotas Group samples (Fig. 5) shows a strong  
459 signal of Neoproterozoic ages, with main peaks at 500 Ma to 600 Ma, related to  
460 the timing of the agglutination of Araçuaí orogen and its post-orogenic phase  
461 (Pedrosa-Soares et al., 2008). Peaks at 900Ma to 1000 Ma, 1900Ma to 2100  
462 Ma, 2500 Ma to 2800 Ma and 3000 Ma to 3200 Ma are subordinate and related  
463 to Neoproterozoic rifting, the Transamazonian cycle (Paleoproterozoic), the  
464 Jequié cycle (Neoarchean) and the Mesoarchean cycle, which are very well  
465 represented in the São Francisco craton. Additionally, there is an important  
466 population of zircons aged  $262.8 \pm 7.6$  Ma (95% conf., MSWD 0.51) that was  
467 collected from samples PCA 12 and PCA 10 and that is interpreted as having  
468 been formed during the Gondwanides magmatism, when the Pangea  
469 supercontinent formed.

470 The detrital zircon age distribution of those samples (PCA 05, 06, 07 and 09)  
471 from Almada Group, the first-described rifting cycle of the Camamu Basin, is  
472 quite different from that of the underlying Brotas Group samples. Strong signals  
473 at the 2000 Ma to 2200 Ma and 2500 Ma 2800 Ma peaks are recognized (Fig.  
474 6), and these ages are related to the Transamazonian and Jequié cycles and  
475 directly related to the crystalline basement rocks adjacent to the Camamu  
476 basin. A subsidiary peaks at 900 Ma to 1000 Ma and smaller peaks at 500 Ma  
477 to 600 Ma are also recognized in the Almada Group samples (Fig. 6), recording  
478 the rifting of the São Francisco craton and the collisional to post-collisional  
479 events the Brasiliano orogeny (e.g., Alkmin et al., 2006; Pedrosa-Soares et al.,  
480 respectively.

481 There are three major source areas of the Paleoproterozoic and Archean  
482 zircons; one is from the Jequié Block (JB), a second one is from Ítabuna  
483 Salvador Curuçá (BISC) and a third is from Serrinha Block (SB). The analyzed  
484 samples from the Almada Group have had major contributions from these  
485 sources, a finding that is consistent with the eastwards paleocurrent data  
486 measured by Kayser (2006) and Born et al. (2011). This result indicates that the  
487 depositional systems of this Camamu rifting phase are directly controlled by the  
488 N-S trending fault system (e.g., the Maragogipe fault system, Born et al., 2011),  
489 with a strong contribution of crystalline basement of the São Francisco units, as

490 shown in figure 10 (see Phase II). The minor contribution at 900 Ma to 1000 Ma  
491 is associated with rocks formed during the rifting phase in the early  
492 Neoproterozoic of the São Francisco-Congo craton (Pedrosa-Soares et al.,  
493 2008).

494 The Neoproterozoic period between 700 Ma and 540 Ma is related to the  
495 Araçuaí-West Congo belt that is situated in the southern part of the Camamu  
496 basin, which is indicated in Fig. 10 as Phase I (pre-rift phase). This finding is  
497 strongly supported by the large number of detrital zircons with Eopaleozoic  
498 ages in the samples PCA 8, 10 and 12. These Eopaleozoic zircons were  
499 derived from the post-orogenic magmatism that occurred from 0.53 Ga to 0.48  
500 Ga in the Araçuaí-West Congo belt, as defined by Pedrosa-Soares et al. (2008).  
501 The main drainage at the time of the Sergi Fm. deposition was from S-SW to N-  
502 NE, based on the paleocurrent measurement and new U-Pb detrital zircon data.  
503 The distributions of  $\varepsilon_{\text{Hf}}(t)$  values in the PCA 08B and PCA 12 samples in  
504 Eopaleozoic zircons were very similar and clearly suggest that this population  
505 resulted from crustal melting. The  $\varepsilon_{\text{Hf}}(t)$  values from the Neoproterozoic zircons  
506 suggest two distinct populations, one formed in a juvenile magma with positive  
507 values and the other formed from older or mixed crust with negative  $\varepsilon_{\text{Hf}}(t)$   
508 values. Most likely, these zircons were formed primarily during the Rhyacian  
509 (Transamazonian cycle) and Statherian (Paleoproterozoic rifting) ages. Those  
510 Neoproterozoic zircons with positive  $\varepsilon_{\text{Hf}}(t)$  values are from the Araçuaí belt,  
511 which is a classic orogen formed by the collision of the São Francisco-Congo  
512 craton in the Neoproterozoic to Eopaleozoic (Pedrosa-Soares et al., 2008). In  
513 the PCA-8b and PCA-12 samples, most of the Mesoproterozoic and  
514 Paleoproterozoic zircons were formed by crustal melting of Archean crust,  
515 whereas the Archean zircons have slightly negative  $\varepsilon_{\text{Hf}}(t)$  values.

516 The Hf isotopic data indicate more complex source areas for the studied  
517 material but are complementary to the petrographic, whole rock Nd-Sm-Pb  
518 isotopes, and U-Pb in situ zircon dating. In contrast, Hf isotopes obtained from  
519 the detrital zircons of the Camamu basin provide important clues to the crustal  
520 growth of Brazilian shield in the São Francisco craton region and adjacent  
521 mobile belts. A period of major crustal growth during the Paleoproterozoic and

522 Archean, even by those magmatic zircons that crystallized during the Brasiliano  
523 cycle (Neoproterozoic to Eopaleozoic) is indicated.

524

525 Insert Fig. 9  
526 Insert Fig. 10

527

528

529

530 6. Conclusions

531 (i) Integrated studies of sedimentology, petrography and isotope geology of  
532 the Brotas and Almada Groups aid in the understanding of the  
533 depositional systems of the pre-rift and syn-rift sequences and help to  
534 identify the source areas. The combination of U-Pb ages with Hf isotopic  
535 information indicated that some detrital zircons in the Camamu basin  
536 crystallized from juvenile magmas, whereas most zircons crystallized from  
537 magmas formed during crustal recycling or contaminated by older crust of  
538 Paleoproterozoic and Archean age.

539 (ii) The analyzed fluvial and eolian samples of the Brotas Group show four  
540 main U/Pb age groups, approximately 480 Ma to 600 Ma (Cambrian-  
541 Vendian), 900 Ma to 1000 Ma (Neoproterozoic), 1900 Ma to 2100 Ma  
542 (Paleoproterozoic) and 2500 Ma to 2800 Ma (Neoarchean), suggesting a  
543 similar source for the analyzed stratigraphic intervals. However, the  
544 dominant population was formed in the interval of 480 Ma to 600 Ma.

545 (iii) In the Almada Group, detrital zircons exhibit major contribution from  
546 Paleoproterozoic and Archean sources, while the U/Pb ages in the range  
547 of 480 Ma to 600 Ma (Cambrian-Vendian) represent a small contribution.

548 (iv) The Paleoproterozoic and Archean sources are well constrained directly  
549 adjacent to the basement and include the Itabuna-Salvador Curuçá block  
550 (2.6-2.1 Ga) and the Jequié block (2.9-2.6 Ga) in both groups. Zircons  
551 that crystallized at approximately 1.0-0.9 Ga came from dykes in the São  
552 Francisco craton that are related to the rifting of the adjacent Araçuaí-  
553 West-Congo belt.

554 (v) The Cambrian-Vendian zircons, 60 to 70 % of analyzed zircons from the  
555 Brotas Group, were most likely sourced from the southern portion of the  
556 Bahia and the northern portion of Espírito Santo and Minas Gerais, where

557 the syn to post-orogenic granites of the Araçuaí-West Congo belt are  
558 exposed.

559 (vi) In the Almada Group, the main source of the Camamu basin sediments is  
560 Paleoproterozoic and Archean, and approximately 80% to 90% of the  
561 zircons come directly from the basement. All of the samples have a strong  
562 crustal component. Most likely, the Paleoproterozoic zircons were  
563 remelted during the Brasiliano cycle.

564 (vii) The sedimentological-stratigraphic profiles, petrographic studies, U-Pb  
565 zircon dating and Lu-Hf isotopic analysis, demonstrate the following: (I)  
566 the main source of the pre-rift phase (Brotas Group) is the southern  
567 portion of the Camamu basin, i.e., the Neoproterozoic to Eopaleozoic  
568 Araçuaí belt, and (II) the main source of the rift phase (Almada Group) is  
569 the adjacent Archean-to-Paleoproterozoic São Francisco craton.

570 (viii) Paleogeographic reconstructions and understanding the provenance of  
571 depositional systems is possible by the use of these combined  
572 methodologies in an area of subsurface sampling (drill core or cutting).  
573 The isotopic data obtained from sedimentary rocks can define, with high  
574 precision, not only the source area(s) but also the mechanisms of  
575 sediment transport and the tectonic evolution of the studied sedimentary  
576 basin.

577

578

579

## 580 Acknowledgements

581 We thank the CNPq (Conselho Nacional de Desenvolvimento Científico e  
582 Tecnológico) for a PhD scholarship (140922/2008-3). We also thank the  
583 technicians from LGI/UFRGS and MAF-IIC/MUN (Rebecca Lam and Michael  
584 Shaffer) for their assistance with sample preparation and during the U-Pb and  
585 Hf analyses using the LA-MC-ICP-MS.

586

587

## 588 References

- 589 Alkmim, F.F., Marshak, S., Pedrosa-Soares, A.C., Peres, G.G., Cruz, S., and  
590 Whittington, A., 2006. Kinematic evolution of the Araçuaí-West Congo  
591 orogen in Brazil and Africa: Nutcracker tectonics during the  
592 Neoproterozoic assembly of Gondwana. *Precambrian Research* 149, 43-  
593 64.  
594 Blichert-Toft, J., 2008. The Hf isotopic composition of zircon reference material  
595 91500. *Chemical Geology* 253, 252-257.

- 596 Cesero, P., Ponte, F.C., 1972. Análise comparativa da paleogeologia dos  
 597 litorais atlânticos brasileiro e africano. Boletim de Geociências da  
 598 PETROBRAS 11 (1), 1-18.
- 599 Chu, N.C., Taylor, R.N., Chavagnac, V., Nesbitt, R.W., Boella, M., Milton, J.A.,  
 600 2002. Hf isotope ratio analysis using multi-collector inductively coupled  
 601 plasma mass spectrometry: an evaluation of isobaric interference  
 602 corrections. *Journal of Analytical Atomic Spectrometry* 17, 1567–1574.
- 603 Cupertino, J.A., 2000. Evolução tectono-climática na fase rift das bacias de  
 604 Camamu, parte norte e sul do Recôncavo com ênfase na utilização de  
 605 isótopos estáveis e traços de fissão. Tese de doutorado, 2 volumes.  
 606 Instituto de Geociências, Curso de Geologia, Universidade Federal do Rio  
 607 Grande do Sul.
- 608 Dickinson, W.R., 1985. Interpreting provenance relation from detrital modes of  
 609 sandstones, in: ZUFFA, G.G. ed., *Provenance of arenites*. D. Reidel  
 610 Publishing Company, Boston, pp. 333-361.
- 611 Guadagnin, F., Chemale Jr., F., Dussin, I.A., Jelinek, A.R., Santos, M.N., Borba,  
 612 M.L., Justino, D., Bertotti, A.L., Alessandretti, L., 2010. Depositional age  
 613 and provenance of the Itajaí Basin, Santa Catarina State, Brazil:  
 614 Implications for SW Gondwana correlation. *Precambrian Research* 180,  
 615 156-182.
- 616 Ghignone, J.I., 1979. Geologia dos sedimentos fanerozóicos do estado da  
 617 Bahia, in: Inda, H.A.V. (Ed.), *Geologia e recursos minerais do estado da*  
 618 *Bahia. Textos Básicos*, Vol. 1. SME/CPM, Salvador, pp. 24-117.
- 619 Goode, J.W., Vervoort J.D., 2006. Origin of Mesoproterozoic A-type granites in  
 620 Laurentia: Hf isotope evidence. *Earth Planetary Science Letters* 243, 711-  
 621 731.
- 622 Kayser, V. 2006. Proveniencia por Estudos Isotópicos de Sm-Nd e Pb-Pb em  
 623 Rocha Total e U-Pb em Zircão Detritico das Secões Pre-Rifte e Pos-Rifte  
 624 das Bacias de Almada e Camamu, Bahia. Trabalho de Conclusão do Curso  
 625 de Geologia. Instituto de Geociências, Universidade Federal do Rio Grande  
 626 do Sul. Porto Alegre, 115 p.
- 627 Košler J., Fonneland, H., Sylvester, P., Tubrett, M., Pedersen, R.B., 2002. U-Pb  
 628 dating of detrital zircons for sediment provenance studies – a comparison of  
 629 laser ablation ICPMS and SIMS technique. *Chemical Geology* 182, 605-  
 630 618.
- 631 Küchle, J., 2005. Análise estratigráfica da seção rift da Bacia de Camamu-  
 632 Almada, Bahia. Dissertação de Mestrado em Geociências. Instituto de  
 633 Geociências, Universidade Federal do Rio Grande do Sul. Porto Alegre,  
 634 157 p.
- 635 Küchle, J., Scherer, C.M.S., Born, C.C., Alvarenga, R.S., Adegas, F., 2011. A  
 636 contribution to regional stratigraphic correlations of the Afro-Brazilian  
 637 depression - The Dom João Stage (Brotas Group and equivalent units –  
 638 Late Jurassic) in North eastern Brazilian sedimentary basins. *Journal of*  
 639 *South American Earth Sciences* 31, 358-371.
- 640 Lambiase, J.J., Bosworth, W., 1995. Structural controls on sedimentation in  
 641 continental rifts, in: Lambiase, J.J., ed., *Hydrocarbon habitat in rift basins*.  
 642 Geological Society Special Publication 80, pp.117-144.
- 643 McDaniel, D.K., McLennan, S.M., Hanson, G.N., 1997. Provenance of Amazon  
 644 fan muds: Constraints from Nd and Pb isotopes, in: Flood, R.D., et al.,

- 645 Proceedings of the Ocean Drilling Program, Scientific Results, Volume 155.  
646 College Station, Texas, Ocean Drilling Program, pp. 169–176.

647 Netto, A.S.T., Wanderley Filho, J.R., Feijó, F.J., 1994. Bacias de Jacuípe,  
648 Camamu e Almada. Boletim de Geociências da Petrobrás 8, 173–184.

649 Patchett, P.J., Kuovo, O., Hedge, C.E., Tatsumoto, M., 1981. Evolution of  
650 continental crust and mantle heterogeneity: evidence from Hf isotopes.  
651 Contributions to Mineralogy and Petrology 78, 279– 297.

652 Pedrosa-Soares, A.C., Alkmim, F.F., Tack, L., Noce, C.M., Babinski, M., Silva,  
653 L.C., Martins Neto, M., 2008. Similarities and differences between the  
654 Brazilian and African counterparts of the Neoproterozoic Araçuaí West  
655 Congo Orogen. Geological Society Special Publication 294, 153–172.

656 Ponte, F.C., Asmus, H.E., 1978. Geological framework of the Brazilian  
657 continental margin. Geologische Rundschau 67(1), 201–235.

658 Prosser, S., 1993. Rift-related linked depositional systems and their seismic  
659 expression. Geological Society London Special Publications 71, 35–66.

660 Segal, I., Halicz, L., Platzner, I., 2003. Accurate isotope ratio measurements of  
661 ytterbium by multiple collection inductively coupled plasma mass  
662 spectrometry applying erbium and hafnium in an improved double external  
663 normalization procedure. Journal of Analytical Atomic Spectrometry 18,  
664 1217–1223.

665 Schaller, H., 1969. Revisão Estratigráfica da bacia de Sergipe/Alagoas. Boletim  
666 técnico da PETROBRAS 12 (1), 21–86.

667 Silva, D.R.A., Mizusaki, A.M.P., Milani, E.J., Tassinari, C.C.G., 2006. Idade  
668 deposicional da Formação Bananeiras (Bacia Sergipe-Alagoas), uma  
669 aplicação do método radiométrico Rb-Sr em rochas sedimentares. Boletim  
670 de Geociências 14(2), 235–245.

671 Slama, J., et al., 2008. Plešovice zircon — A new natural reference material for  
672 U-Pb and Hf isotopic microanalysis. Chemical Geology 249, 1–35.

673 Souza-Lima, W., Manso, C.L.C., Andrade, W.E.J., Grillo, S., 2003. Bacias  
674 Sedimentares Brasileiras – Bacia de Camamu. Fundação Paleontológica  
675 Phoenix 54, 1–6.

676 Stacey, J.S., Kramers, J.D., 1975. Approximation of terrestrial lead isotope  
677 evolutionby a two-stage model. Earth and Planetary Science Letters 26,  
678 207–221.

679 Sylvester, P.J., Ghaderi, M., 1997. Trace element analysis of scheelite by  
680 excimer laser ablation inductively coupled plasma mass spectrometry (ELA-  
681 ICP-MS) using a synthetic silicate glass standard. Chemical Geology 141,  
682 49–65.

683 Viana, C.F., Gama Jr., E.G., Simões, E.A., Moura, J.A., Fonseca, J.R., Alves,  
684 R.J., 1971. Revisão estratigráfica da Bacia do Recôncavo/Tucano. Boletim  
685 Técnico da PETROBRAS 14 (3/4), 157–192.

686 Youden, W.J., 1951. Statistical methods for chemists. Journal of the Royal  
687 Stastitical. New York, Wiley, 126 p.

688

689

690

691

692

693

694

695

696 **Figure Captions**

697

698 Fig. 1. (A) Outline of the São Francisco craton and the adjacent Brasiliiano belts  
 699 (simplified after Alkmim et al., 2006) with the studied area; (B) Geological map  
 700 of the onshore area of the Camamu basin (after Scherer et al., 2011) with  
 701 sample locations.

702

703 Fig. 2. Chronostratigraphic chart of the Camamu basin, onshore and offshore  
 704 areas (modified after Caixeta et al., 2007). Age constraints on the pre-rift  
 705 depositional units are based on detrital zircon ages from the Brotas Group at  
 706  $146 \pm 7$  Ma (this work).

707

708 Fig. 3. A) Provenance of samples PCA 05, PCA 07, PCA 10 and PCA 12. PCA  
 709 05 and PCA 12 are derived from basement uplift source rocks, while PCA 07  
 710 and PCA 10 are derived from transitional continental source rocks. b)  
 711 Petrographic photographs of PCA 10 in crossed polarized light (left) and plane  
 712 polarized light (right), showing bimodal quartz feldspar sandstone with grain  
 713 size varying from 0.15-0.30 mm. C) Petrographic photographs of PCA 5 in  
 714 crossed polarized light (left) and plane polarized light (right), showing bimodal  
 715 quartz feldspar sandstone with a grain size varying from 0.15-0.30 mm, with  
 716 high organic matter content.

717

718 Fig. 4. Backscattered electron images of zircon crystals that are representative  
 719 of the grains analyzed with LA-MC-ICP-MS. The spots (white circles) and the  
 720 measured U-Pb concordia ages are indicated by the sample number.

721

722 Fig. 5. Histogram of the detrital zircon ages from samples of the Sergi Fm.,  
 723 Brotas Group (pre-rift sequence). The color fields represent the duration of the  
 724 main orogenic cycles that affected the São Francisco craton and the Araçuaí  
 725 belt, where MArC = Mesoarchean cycle, JC = Jequié cycle (2.9-2.6 Ga), TC =  
 726 Transamazonian cycle (2.26–1.9 Ga), CSFag = the Araçuaí cycle, including  
 727 rifting to agglutination at the São Francisco craton (0.93-0.48 Ga). The yellow  
 728 field represents zircons formed during the Gondwanides cycle (G).

729

730 Fig. 6. Histogram of detrital zircon ages from the Almada Group samples (rift  
 731 sequence). The color fields represent the duration of the main orogenic cycles  
 732 that affected the São Francisco craton and Araçuaí belt, where MArC =  
 733 Mesoarchean cycle, JC = Jequié cycle (2.9-2.6 Ga), TC = Transamazonian  
 734 cycle (2.26–1.9 Ga), CSFag = the Araçuaí cycle, including rifting (Rf) to  
 735 agglutination (A=agglutination and P= post-orogenic magmatism) at the São  
 736 Francisco craton (0.93-0.48 Ga).

737

738 Fig. 7. Zircon images showing the laser ablation craters formed during U-Pb  
 739 (ca. 25  $\mu\text{m}$  – black circle) and Lu-Hf analysis (49  $\mu\text{m}$  – dotted circles), with their  
 740 respective data.

741

742 Fig. 8.  $\varepsilon_{\text{Hf}}(t)$  evolution diagram showing the results for zircons from samples  
 743 PCA-08B and PCA-12.

744 Fig. 9. (a) Plot of  $f\text{Sm}/\text{Nd}$  versus  $\varepsilon\text{Nd}$  ( $t$ ) in the sedimentary rocks of the  
745 Camamu basin. Also shown for comparison are the fields of South American  
746 cratonic rocks, Andean foreland sediments, and Andean igneous (arc) rocks  
747 (McDaniel et al., 1997); (b)  $T_{\text{DM}}$  versus  $\varepsilon\text{Nd}_{(0)}$ ; (c) and (d) Pb-Pb isotope  
748 diagrams for the same samples (see text for explanation) (analytical data from  
749 Kayser, 2006).

750

751 Fig. 10. Geologic map of the potential basement source rocks for the Camamu  
752 basin, grouping the lithological associations after the main periods of obtained  
753 zircon ages. Arrow (I) indicates the direction of sediment flow in the Brotas  
754 Group, whereas the arrows (II) indicate that of the Almada Group (see text for  
755 explanation).

756

757

758 **Table caption**

759

760 **Table 1** - Operating conditions used for U-Pb and Lu-Hf analysis at LGI and  
761 MAF-IIC, respectively.

Figure 1

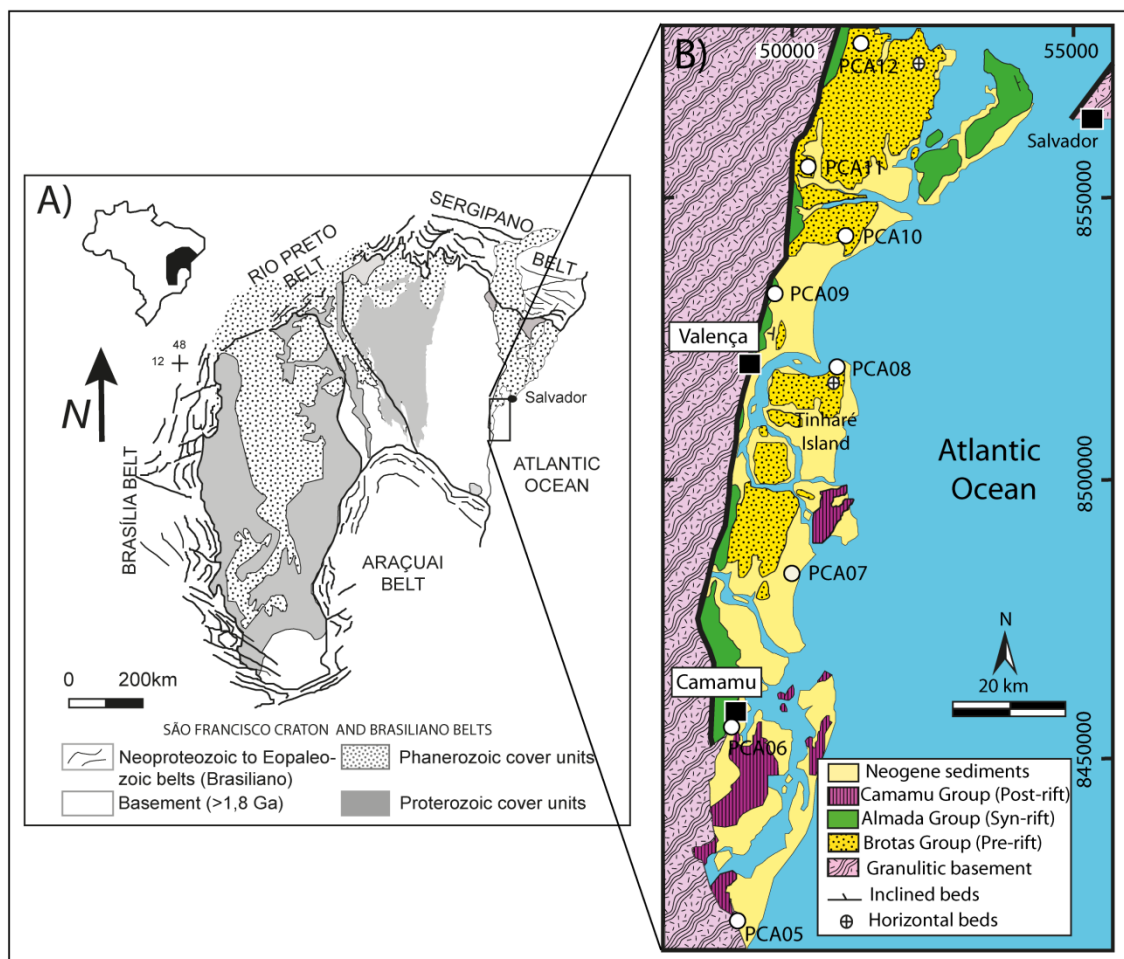


Figure 2

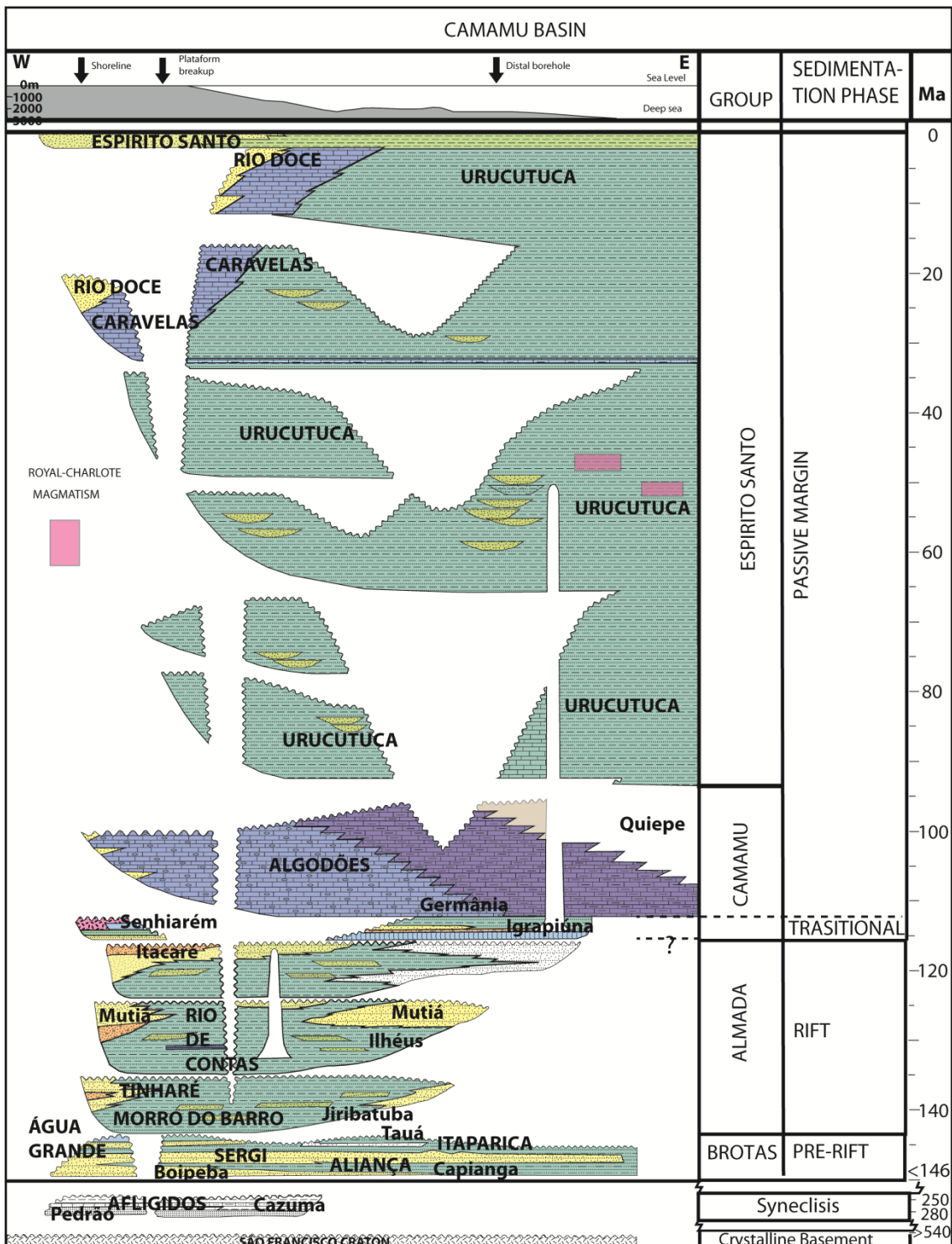


Figure 3

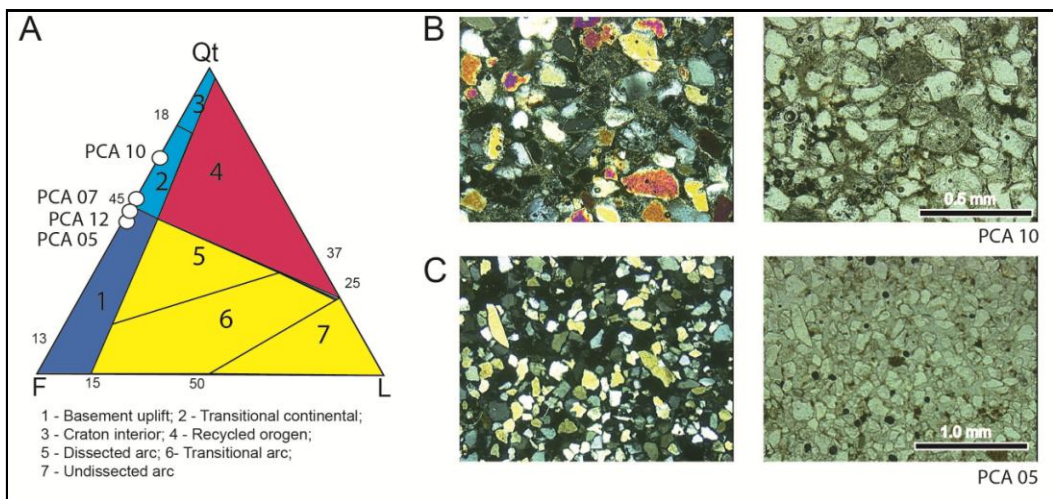


Figure 4

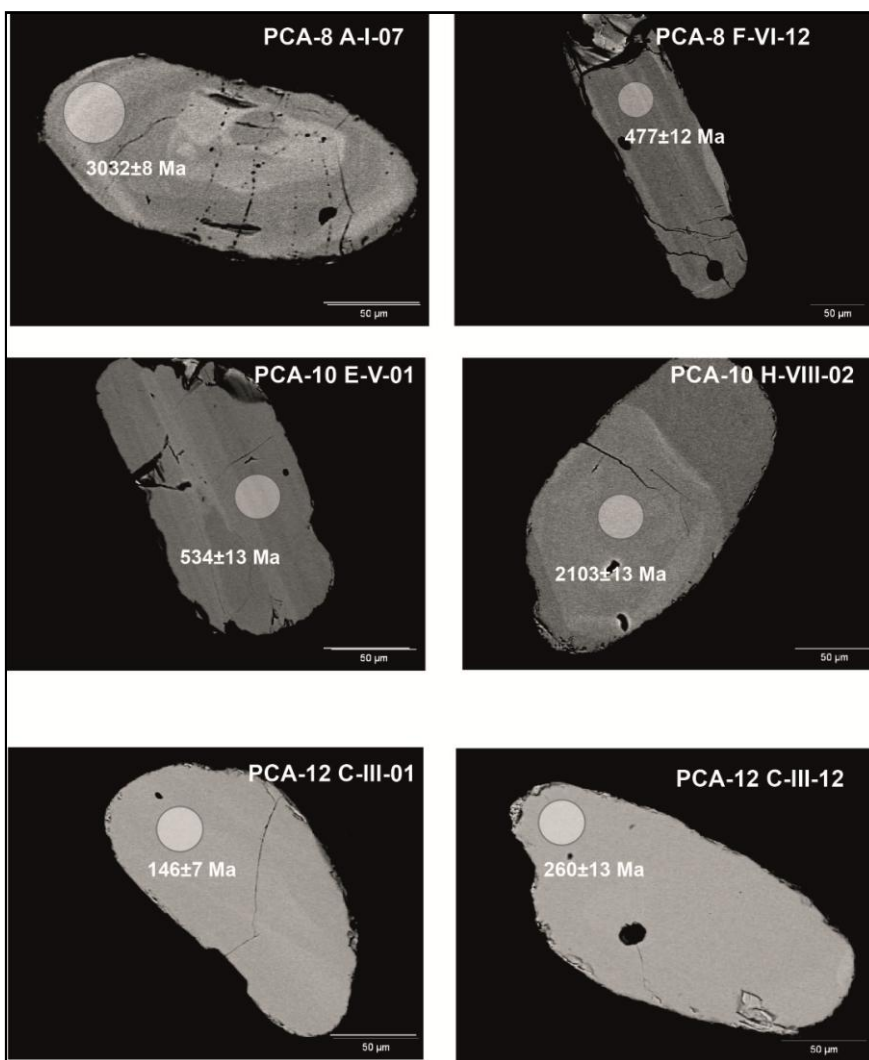


Figure 5

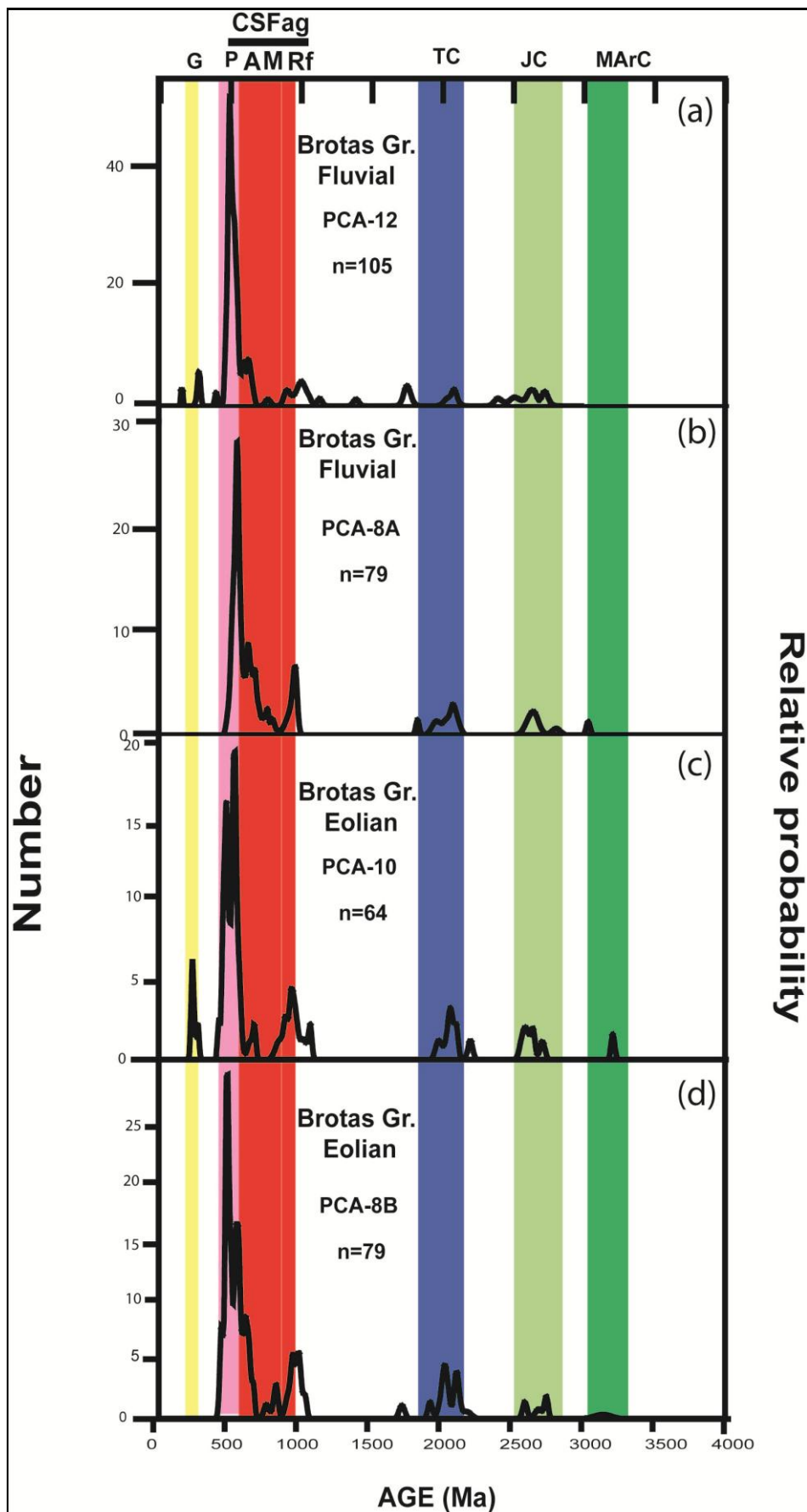
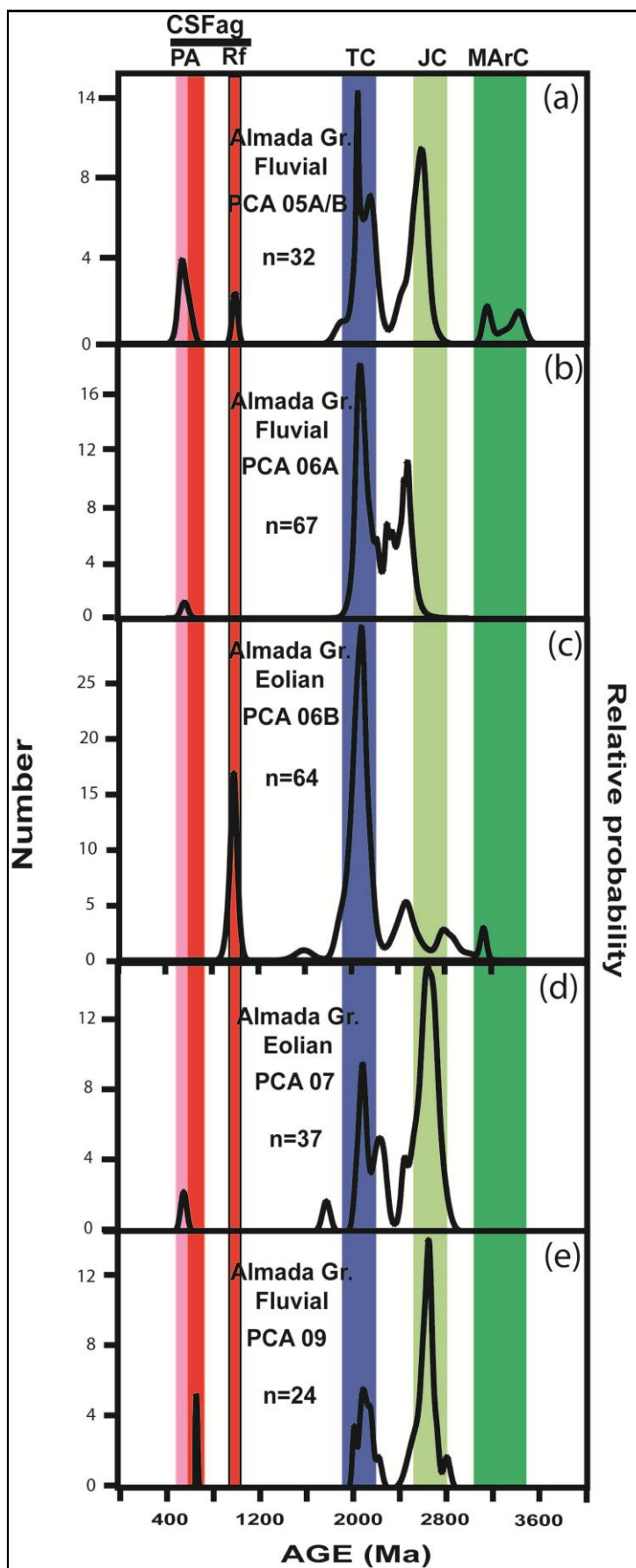


Figure 6



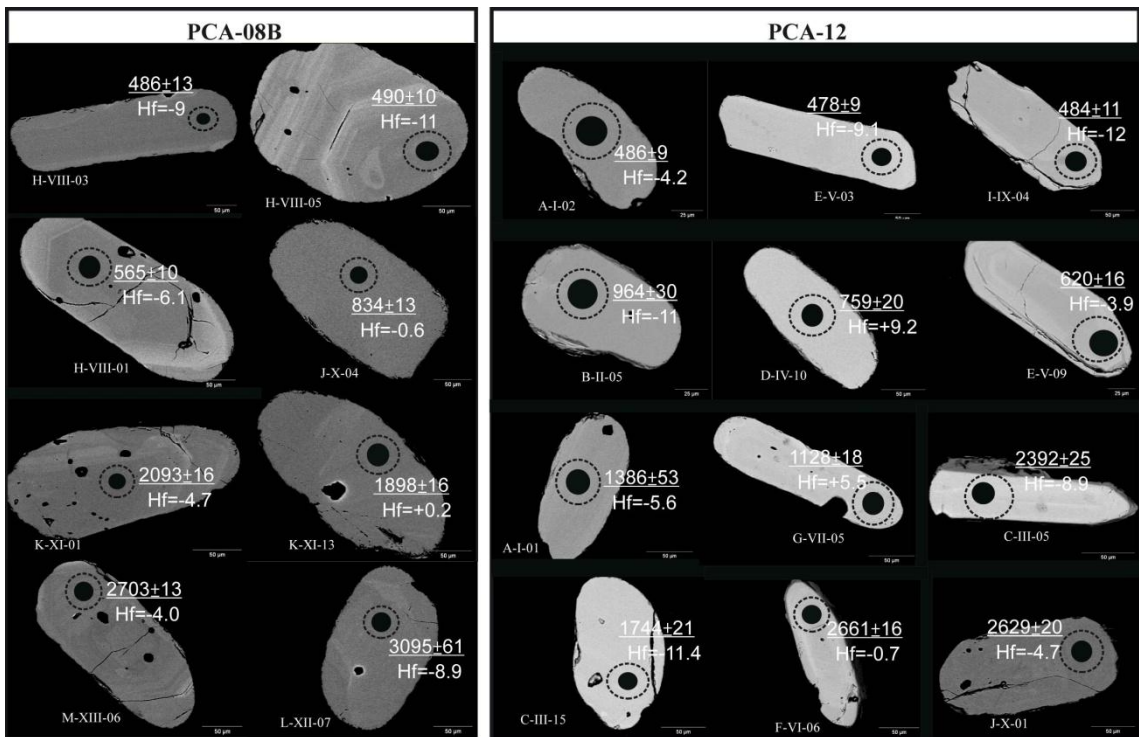
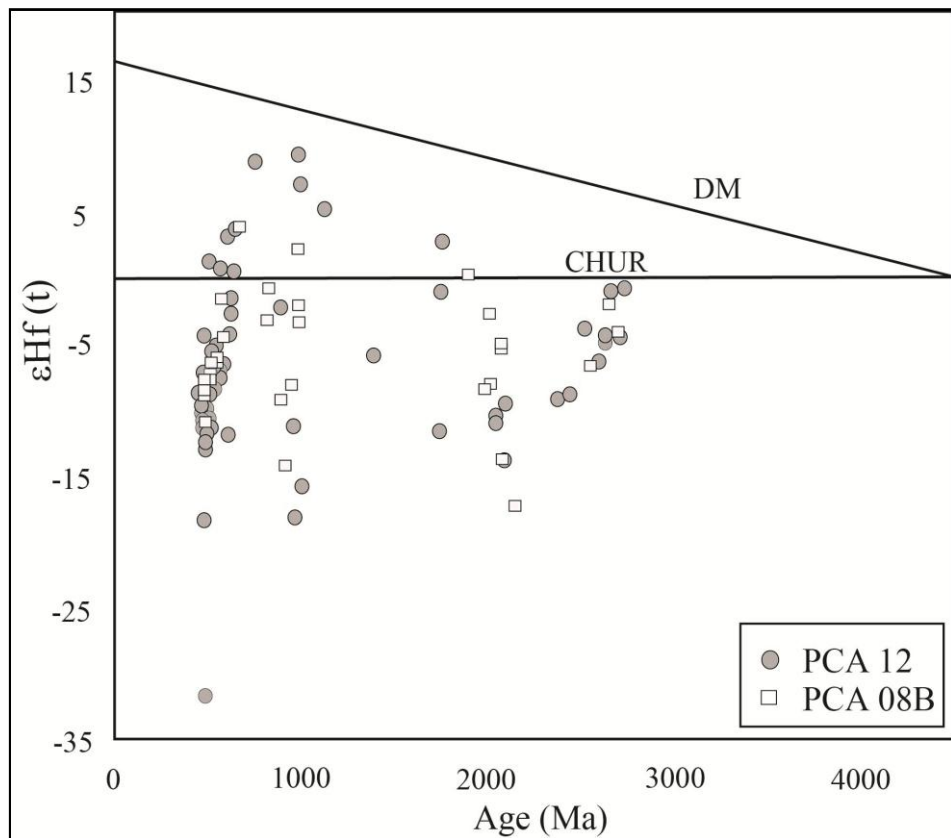
**Figure 7****Figure 8**

Figure 9

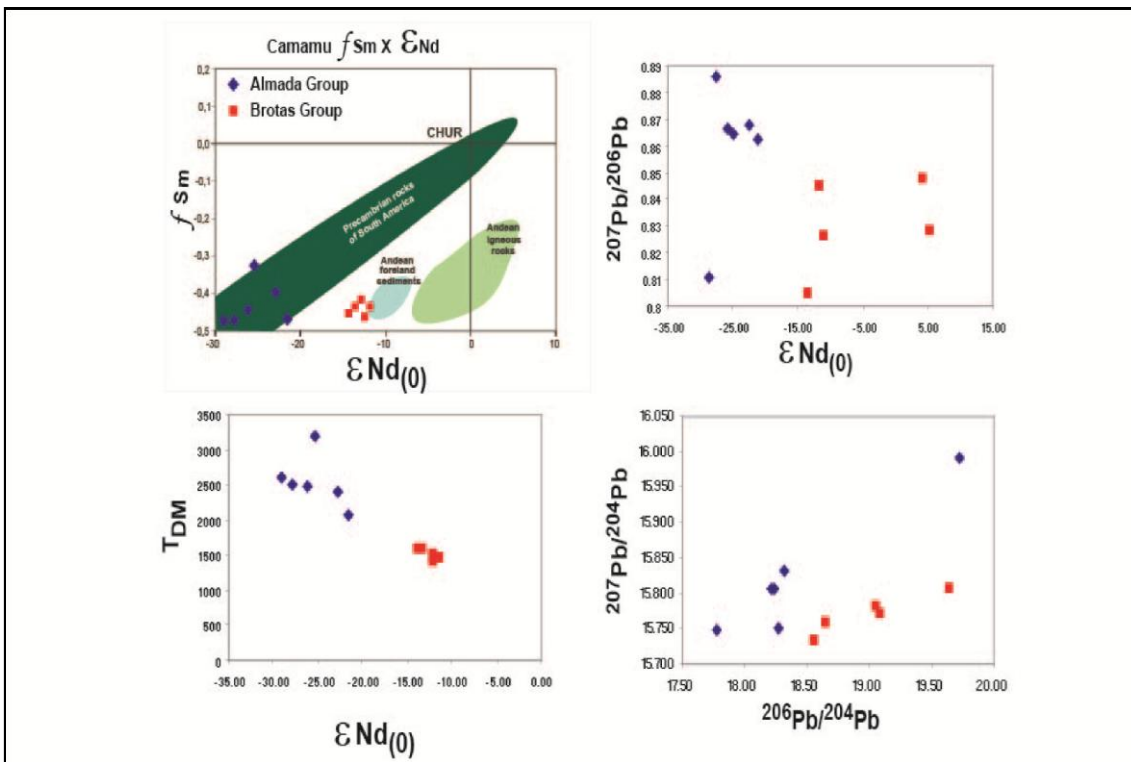
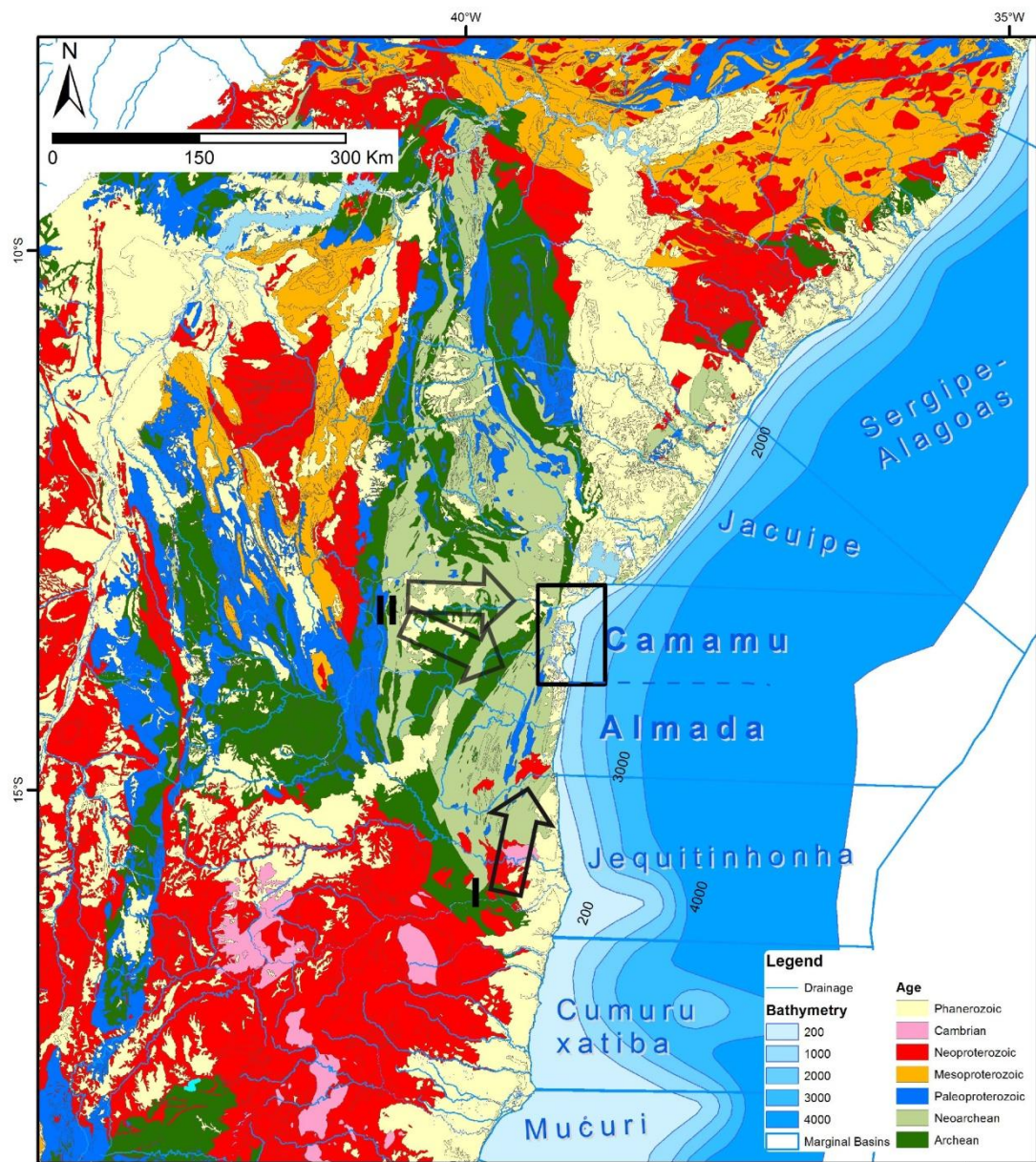


Figure 10



**Table 1**

	U-Pb Analysis	Lu-Hf Analysis
Instrument	Neptune (Finnigan)	Neptune (Finnigan)
Operation power	1200 W	1200 W
Carrier Ar	0.85 l min <sup>-1</sup>	0.75 l min <sup>-1</sup>
Cool gas	15 l min <sup>-1</sup>	16 l min <sup>-1</sup>
Auxiliary gas	0.72 l min <sup>-1</sup>	0.75 l min <sup>-1</sup>
Analysis Mode	Static	Static
Detection	Faraday and MIC's	Faraday
Laser	New Wave UP213 (Nd:YAG)	GeoLas (ArF excimer 193nm)
Spot Size	25 μm	49 μm
Energy Density	4 J cm <sup>-2</sup>	5 J cm <sup>-2</sup>
Repetition rate	10 Hz	10 Hz
Integration Time	1.049s	1.049s
Ablation time	50s	60s
He gas flow	0.9 l min <sup>-1</sup>	1.3 l min <sup>-1</sup>

## Supplementary Data – Analytical Results

### 1. Petrography Data

**Fig. 1. Petrography of PCA 05.**

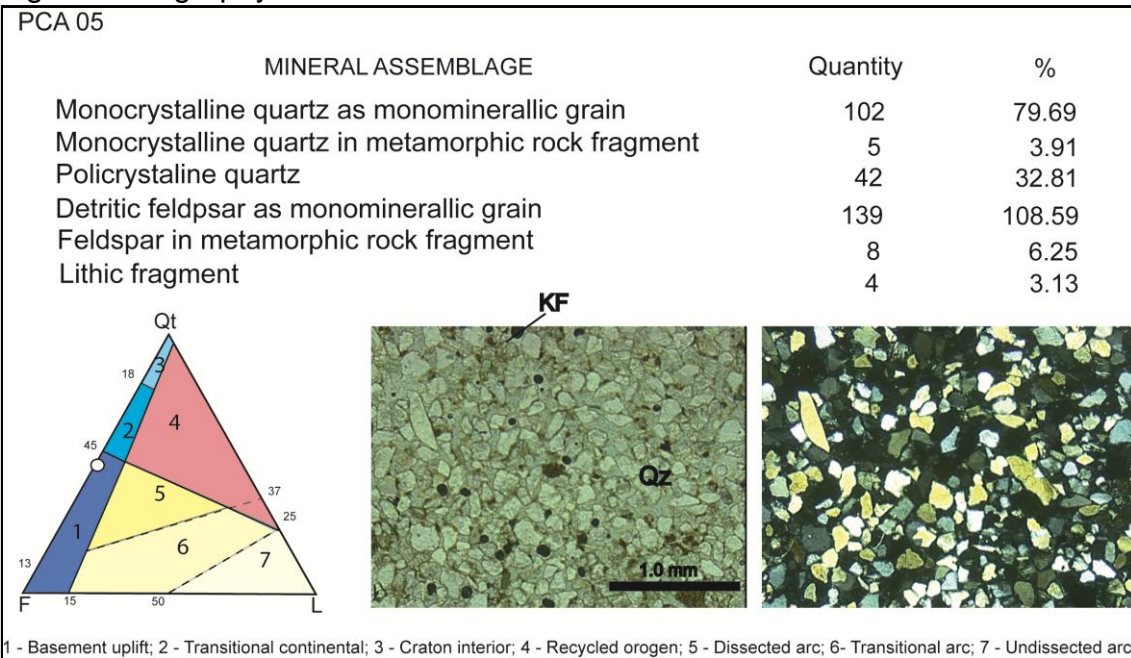


**Fig. 2. Petrography of PCA 07.**

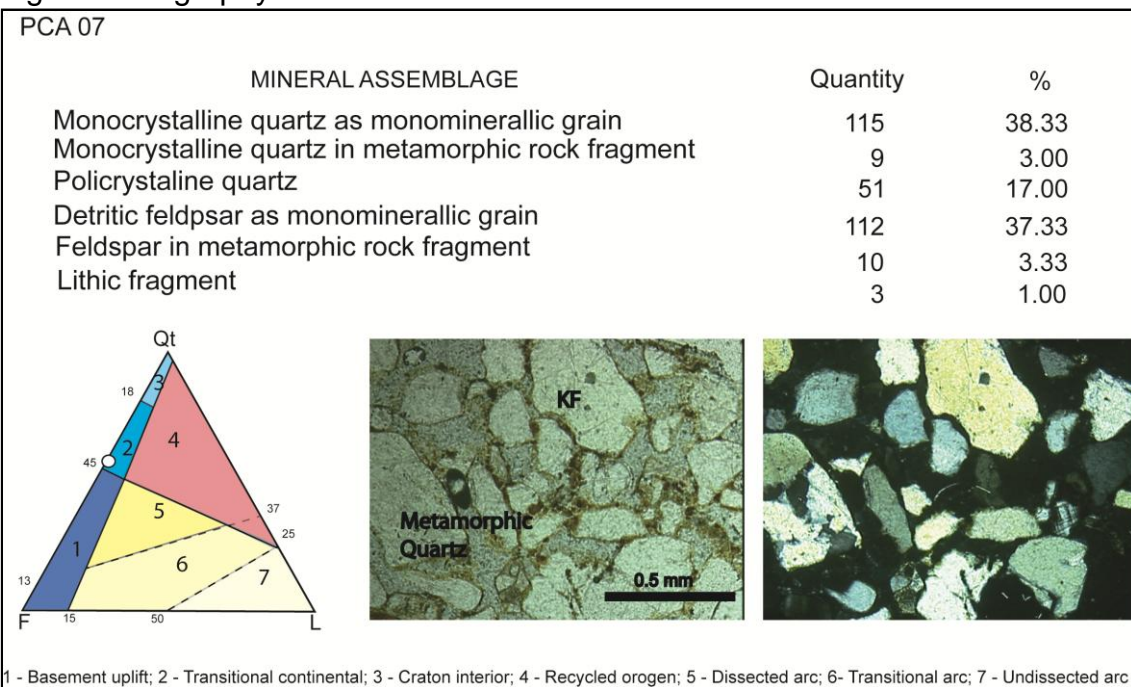


Fig. 3. Petrography of PCA 10.

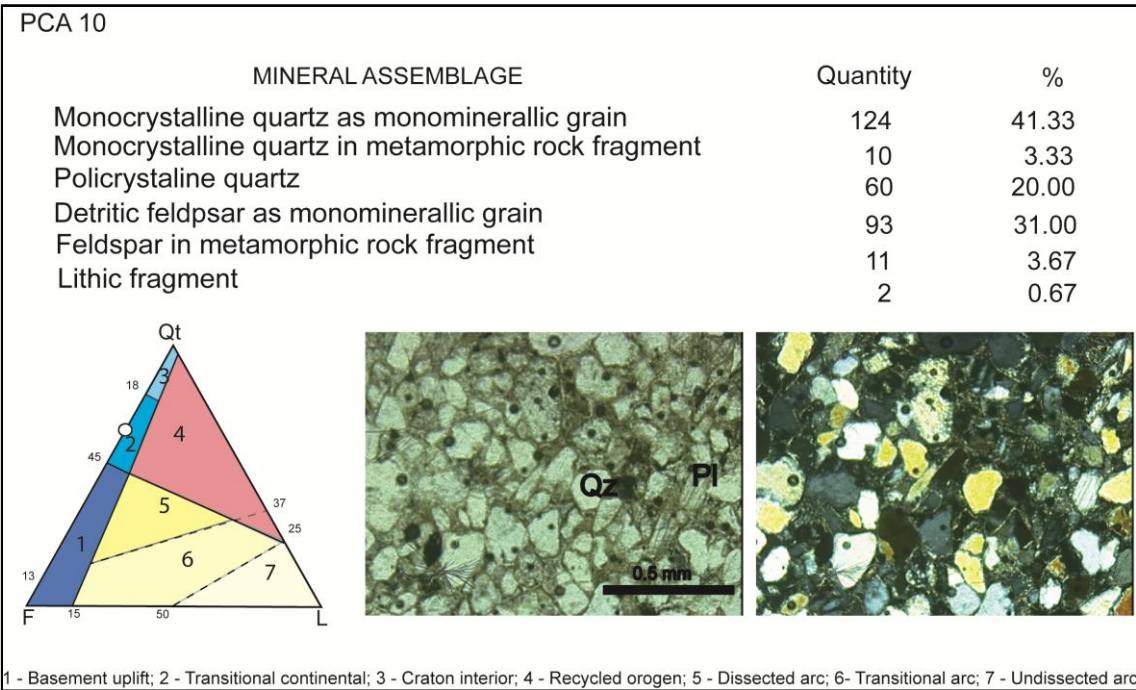
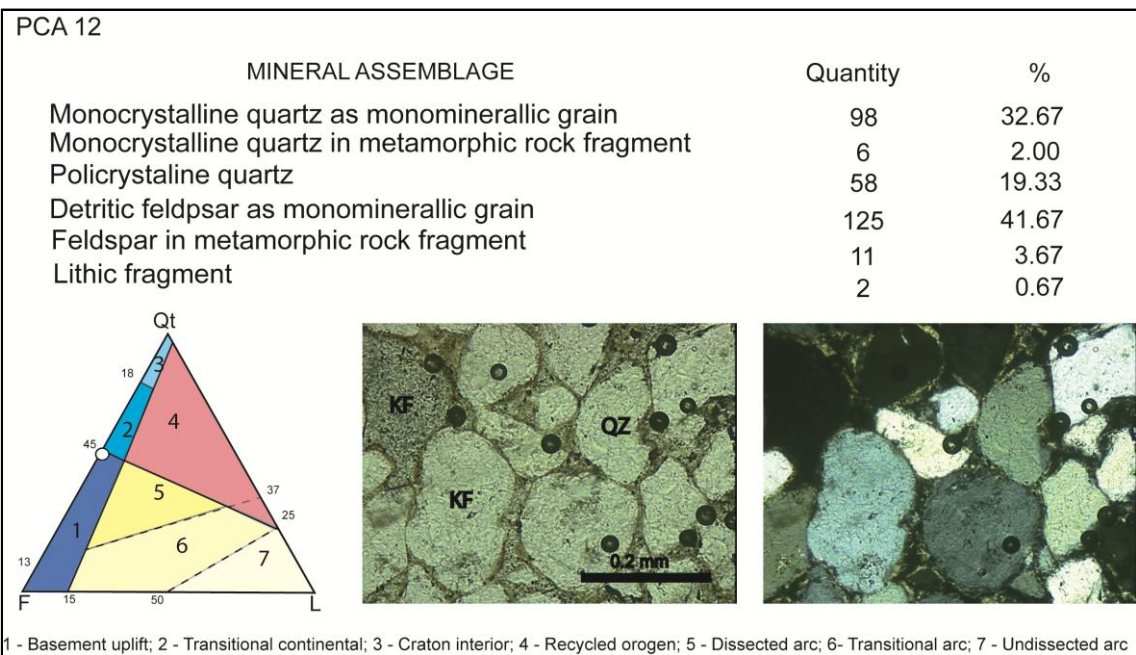


Fig. 4. Petrography of PCA 12.



## 2. U-Pb Results of the Camamu Basin Zircons

Table 1. Sample PCA 5A – Fluvial sandstone of Almada Group.

Spot number	f206	Th/U <sup>a</sup>	<sup>207</sup> Pb/ 1 s		<sup>206</sup> Pb/ 1 s		Rho <sup>c</sup>	<sup>207</sup> Pb/ 1 s		<sup>206</sup> Pb/ 1 s		<sup>207</sup> Pb/ 1 s		% Conc <sup>e</sup>
			<sup>235</sup> U	[%]	<sup>238</sup> U	[%]		<sup>206</sup> Pb <sup>d</sup>	[%]	<sup>238</sup> U	abs	<sup>206</sup> Pb	abs	
Zr-010-A-I-01	0.0008	0.05	5.73663	1.70	0.31744	0.41	0.24	0.13107	1.65	1777	7	2112	35	84
Zr-010-A-I-03	0.0004	0.69	1.47009	1.29	0.14745	0.32	0.25	0.07231	1.25	887	3	995	12	89
Zr-010-A-I-10	0.0002	0.65	8.98765	0.77	0.39190	0.47	0.61	0.16633	0.61	2132	10	2521	15	85
Zr-010-A-I-12A	0.0043	0.19	0.85532	3.72	0.10368	1.84	0.50	0.05983	3.23	636	12	598	19	106
Zr-010-A-I-12	0.0012	0.03	6.78131	1.12	0.36284	0.43	0.39	0.13555	1.03	1996	9	2171	22	92
Zr-010-B-II-04	0.0014	0.57	12.20754	1.08	0.50179	0.84	0.78	0.17644	0.67	2621	22	2620	18	100
Zr-010-B-II-04-II	0.0014	0.71	10.84051	0.97	0.45633	0.63	0.65	0.17229	0.73	2423	15	2580	19	94
Zr-010-C-III-01	0.0017	0.63	6.22856	1.81	0.33928	0.92	0.51	0.13315	1.56	1883	17	2140	33	88
Zr-010-C-III-02	0.0006	0.03	7.22877	1.26	0.39428	0.51	0.41	0.13297	1.15	2143	11	2138	25	100
Zr-010-C-III-03	0.0007	0.40	8.66343	1.81	0.39753	0.98	0.54	0.15806	1.53	2158	21	2435	37	89
Zr-010-C-III-03b	0.0003	0.41	7.43759	1.19	0.40151	0.84	0.70	0.13435	0.84	2176	18	2156	18	101
Zr-010-C-III-06b	0.0006	0.27	6.62645	1.26	0.37785	0.77	0.61	0.12719	1.00	2066	16	2060	21	100
Zr-010-C-III-06a	0.0043	0.29	8.95013	1.96	0.41410	1.62	0.83	0.15675	1.10	2234	36	2421	27	92
Zr-010-C-III-07a	0.0010	0.53	11.84199	1.99	0.48590	1.38	0.69	0.17676	1.43	2553	35	2623	37	97
Zr-010-C-III-07b	0.0007	0.20	11.77750	2.09	0.49653	1.55	0.74	0.17203	1.41	2599	40	2578	36	101
Zr-010-C-III-08	0.0010	0.97	11.56719	2.59	0.48392	1.30	0.50	0.17336	2.24	2544	33	2590	58	98
Zr-010-C-III-09	0.0059	0.19	27.16215	1.26	0.67397	1.05	0.83	0.29230	0.70	3321	35	3430	24	97
Zr-010-C-III-09b	0.0038	0.31	16.68243	1.47	0.44499	0.44	0.30	0.27190	1.41	2373	10	3317	47	72
Zr-010-D-IV-01a	0.0002	0.36	10.50780	1.17	0.44918	0.42	0.35	0.16967	1.10	2392	10	2554	28	94
Zr-010-D-IV-01b	0.0001	0.11	12.13945	2.03	0.51251	1.93	0.95	0.17179	0.64	2667	51	2575	17	104
Zr-010-D-IV-05	0.0000	1.22	0.59990	3.15	0.07472	1.92	0.61	0.05823	2.49	465	9	538	13	86
Zr-010-D-IV-05 b	0.0004	0.67	0.69043	4.46	0.08581	0.91	0.20	0.05835	4.37	531	5	543	24	98

Table 2. Sample PCA 5B – Fluvial sandstone of Almada Group.

Spot number	f206	Th/U <sup>a</sup>	<sup>207</sup> Pb/ <sup>235</sup> U	1 s [%]	<sup>206</sup> Pb/ <sup>238</sup> U	1 s [%]	Rho <sup>c</sup>	<sup>207</sup> Pb/ <sup>206</sup> Pb <sup>d</sup>	1 s [%]	<sup>206</sup> Pb/ <sup>238</sup> U	1 s abs	<sup>207</sup> Pb/ <sup>206</sup> Pb	1 s abs	% Conc <sup>e</sup>
Zr-010-E-V-01	0.0200	0.67	4.47230	4.69	0.21507	2.46	0.53	0.15082	3.99	1256	31	2355	94	53
Zr-010-E-V-02 met	0.0025	0.08	10.78683	1.36	0.44410	1.20	0.88	0.17616	0.65	2369	28	2617	17	91
Zr-010-E-V-04	0.0013	0.09	6.41238	1.48	0.36816	1.26	0.85	0.12632	0.77	2021	26	2047	16	99
Zr-010-F-VI-03	0.0001	0.26	5.61533	0.99	0.32318	0.97	0.98	0.12602	0.22	1805	17	2043	4	88
Zr-010-E-V-02 met	0.0125	0.06	6.71858	4.98	0.35561	4.75	0.95	0.13702	1.52	1961	93	2190	33	90
Zr-010-F-VI-05	0.0001	0.26	6.07171	2.06	0.35088	1.74	0.84	0.12550	1.10	1939	34	2036	22	95
Zr-010-G-VII-03	0.0003	0.41	19.04265	2.29	0.56475	2.22	0.97	0.24455	0.57	2886	64	3150	18	92
Zr-010-I-IX-06	0.0125	0.21	4.96661	2.53	0.30835	1.99	0.79	0.11682	1.56	1733	34	1908	30	91
Zr-010-J-X-09	0.0399	0.12	0.95204	8.92	0.09733	2.38	0.27	0.07094	8.59	599	14	956	82	63
Zr-010-K-XI-01	0.0724	0.05	1.92850	14.53	0.14713	1.84	0.13	0.09507	14.41	885	16	1529	220	58
Zr-010-K-XI-01	0.0708	0.04	1.84142	4.66	0.13495	3.84	0.82	0.09897	2.64	816	31	1605	42	51
Zr-010-I-IX-07	0.0022	0.44	6.74310	9.93	0.36662	1.55	0.16	0.13339	9.81	2013	31	2143	210	94
Zr-010-I-IX-10	0.2642	0.14	1.15595	27.11	0.10590	1.09	0.04	0.07917	27.08	649	7	1176	319	55
Zr-010-I-IX-12a	0.0006	0.41	11.38124	2.17	0.49237	1.24	0.57	0.16765	1.78	2581	32	2534	45	102
Zr-010-I-IX-12b	0.0014	0.06	4.31448	3.09	0.23097	2.91	0.94	0.13548	1.05	1340	39	2170	23	62
Zr-010-J-X-03	0.0212	0.08	1.05826	3.22	0.09975	0.98	0.30	0.07695	3.07	613	6	1120	34	55

Table 3. Sample PCA 6A – Eolian sandstone of Almada Group.

Spot number	f206	Th/U <sup>a</sup>	<sup>207</sup> Pb/ <sup>235</sup> U	1 s [%]	<sup>206</sup> Pb/ <sup>238</sup> U	1 s [%]	Rho <sup>c</sup>	<sup>207</sup> Pb/ <sup>206</sup> Pb <sup>d</sup>	1 s [%]	<sup>206</sup> Pb/ <sup>238</sup> U	1 s abs	<sup>207</sup> Pb/ <sup>206</sup> Pb	1 s abs	% Conc <sup>e</sup>
Zr-010-L-XII-02	0.0005	0.53	15.65953	3.21	0.56056	3.10	0.97	0.20261	0.82	2869	89	2847	23	101
Zr-010-L-XII-02 b	0.0014	0.33	8.33384	1.97	0.34184	0.95	0.48	0.17682	1.72	1896	18	2623	45	72
Zr-010-L-XII-02 b met	0.0098	0.13	5.78662	2.90	0.34267	1.17	0.40	0.12247	2.65	1900	22	1993	53	95
Zr-010-L-XII-03	0.0004	0.74	7.07246	1.22	0.40491	0.56	0.46	0.12668	1.08	2192	12	2052	22	107
Zr-010-L-XII-04	0.0008	0.72	6.54482	2.65	0.37293	1.75	0.66	0.12728	1.98	2043	36	2061	41	99

Zr-010-L-XII-05	0.0008	0.78	6.26409	1.45	0.36312	0.47	0.32	0.12512	1.37	1997	9	2030	28	98
Zr-010-L-XII-6a	0.0009	0.34	6.60228	1.83	0.37708	1.12	0.61	0.12699	1.45	2063	23	2057	30	100
Zr-010-L-XII-06b	0.0002	0.48	6.13018	1.40	0.35228	0.64	0.46	0.12621	1.24	1945	12	2046	25	95
Zr-010-L-XII-07	0.0003	0.32	10.31386	1.56	0.46556	1.07	0.68	0.16067	1.14	2464	26	2463	28	100
Zr-010-L-XII-08	0.0034	0.03	3.72082	3.05	0.27497	1.88	0.62	0.09814	2.40	1566	30	1589	38	99
Zr-010-L-XII-09	0.0006	0.56	6.69921	1.75	0.38971	1.00	0.57	0.12467	1.44	2121	21	2024	29	105
Zr-010-L-XII-6a	0.0010	0.34	6.58473	1.69	0.37665	0.73	0.43	0.12679	1.52	2061	15	2054	31	100
Zr-010-M-XIII-01a	0.0021	0.94	7.04669	2.10	0.38543	1.67	0.80	0.13260	1.26	2102	35	2133	27	99
Zr-010-M-XIII-01b	0.0003	0.78	6.61956	2.23	0.37498	1.77	0.80	0.12803	1.35	2053	36	2071	28	99
Zr-010-M-XIII-02	0.0038	0.51	19.91408	0.45	0.60203	0.21	0.46	0.23991	0.40	3038	6	3119	13	97
Zr-010-M-XIII-03a	0.0582	0.57	1.59746	6.38	0.14928	1.80	0.28	0.07761	6.12	897	16	1137	70	79
Zr-010-M-XIII-03b	0.0007	0.57	1.63343	3.44	0.16505	2.37	0.69	0.07178	2.49	985	23	980	24	101
Zr-010-M-XIII-04	0.0003	0.96	6.70807	1.99	0.37986	1.49	0.75	0.12808	1.31	2076	31	2072	27	100
Zr-010-M-XIII-05	0.0015	0.27	10.50129	1.89	0.45240	1.53	0.81	0.16835	1.11	2406	37	2541	28	95
Zr-010-M-XIII-06	0.0013	0.68	6.70707	1.52	0.38342	0.32	0.21	0.12687	1.49	2092	7	2055	31	102
Zr-010-M-XIII-06b	0.0015	0.50	6.75277	1.86	0.36579	1.74	0.93	0.13389	0.66	2010	35	2150	14	93
Zr-010-N-XIV-01	0.0063	0.46	5.38655	7.46	0.31068	0.48	0.06	0.12575	7.45	1744	8	2039	152	86
Zr-010-N-XIV-03	0.0001	0.37	1.56718	2.23	0.16067	1.29	0.58	0.07074	1.83	961	12	950	17	101
Zr-010-N-XIV-04	0.0002	0.34	6.17596	1.47	0.36707	1.06	0.73	0.12203	1.01	2016	21	1986	20	101
Zr-010-N-XIV-05	0.0009	0.77	6.37456	2.83	0.36393	2.28	0.80	0.12704	1.68	2001	46	2057	35	97
Zr-010-N-XIV-06	0.0012	1.02	6.45972	2.42	0.36693	1.52	0.63	0.12768	1.88	2015	31	2066	39	98
Zr-010-N-XIV-07	0.0002	0.56	6.53528	2.80	0.36611	2.42	0.86	0.12947	1.41	2011	49	2091	29	96
Zr-010-N-XIV-09	0.0001	0.49	10.52844	1.61	0.47498	1.39	0.86	0.16076	0.81	2505	35	2464	20	102
Zr-010-N-XIV-10	0.0001	0.34	1.61510	2.46	0.16426	2.13	0.86	0.07131	1.25	980	21	966	12	101
Zr-010-N-XIV-11	0.0003	1.58	14.36450	1.39	0.53981	1.20	0.86	0.19300	0.71	2783	33	2768	20	101
Zr-010-N-XIV-13	0.0019	0.43	6.48399	1.72	0.36569	1.32	0.77	0.12860	1.09	2009	27	2079	23	97
Zr-010-N-XIV-14	0.0005	1.92	5.72632	1.93	0.35568	1.42	0.74	0.11676	1.31	1962	28	1907	25	103
Zr-010-O-XV-01	0.0003	0.49	13.40391	2.34	0.53088	1.47	0.63	0.18312	1.82	2745	40	2681	49	102
Zr-010-O-XV-02	0.0015	0.44	15.55092	2.09	0.51947	0.48	0.23	0.21712	2.03	2697	13	2959	60	91
Zr-010-O-XV-04	0.0015	1.06	6.27589	3.21	0.35321	2.12	0.66	0.12887	2.41	1950	41	2083	50	94
Zr-010-O-XV-05	0.0004	0.37	1.61129	2.36	0.16132	1.67	0.71	0.07244	1.67	964	16	998	17	97
Zr-010-O-XV-06a	0.0002	0.42	10.53308	2.74	0.47377	1.02	0.37	0.16125	2.55	2500	25	2469	63	101
Zr-010-O-XV-06b	0.0020	0.82	7.15408	2.71	0.39264	0.86	0.32	0.13215	2.57	2135	18	2127	55	100

Zr-010-O-XV-07	0.0008	1.13	5.95415	2.31	0.33461	1.41	0.61	0.12906	1.83	1861	26	2085	38	89
Zr-010-P-XVI-01	0.0057	0.60	7.57065	3.71	0.41601	1.35	0.36	0.13198	3.46	2242	30	2125	73	106
Zr-010-P-XVI-02	0.0017	0.61	8.29824	4.03	0.38869	3.82	0.95	0.15484	1.30	2117	81	2400	31	88
Zr-010-P-XVI-03	0.0001	0.57	8.30673	1.69	0.39377	1.06	0.63	0.15300	1.32	2140	23	2380	31	90
Zr-010-P-XVI-04	0.0002	0.49	4.95124	1.48	0.30895	0.94	0.64	0.11623	1.14	1736	16	1899	22	91
Zr-010-P-XVI-05a	0.0011	1.01	1.65393	1.58	0.16548	0.96	0.61	0.07249	1.26	987	10	1000	13	99
Zr-010-P-XVI-05b	0.0004	0.26	1.56871	2.20	0.15545	1.63	0.74	0.07319	1.48	931	15	1019	15	91
Zr-010-Q-XVII-02	0.0021	0.57	6.17527	1.43	0.35467	0.54	0.38	0.12628	1.32	1957	11	2047	27	96
Zr-010-Q-XVII-03	0.0004	1.71	5.99795	1.67	0.33899	0.51	0.30	0.12832	1.60	1882	10	2075	33	91
Zr-010-Q-XVII-05	0.0001	0.72	6.79143	0.92	0.38415	0.55	0.60	0.12822	0.74	2096	11	2074	15	101
Zr-010-Q-XVII-06	0.0002	0.70	6.50018	0.75	0.37410	0.39	0.52	0.12602	0.64	2049	8	2043	13	100
Zr-010-Q-XVII-07	0.0001	0.44	7.09119	1.33	0.39742	1.25	0.94	0.12941	0.44	2157	27	2090	9	103
Zr-010-Q-XVII-08	0.0001	0.51	6.92023	0.80	0.38853	0.57	0.71	0.12918	0.57	2116	12	2087	12	101
Zr-010-Q-XVII-09	0.0003	0.54	1.91513	1.66	0.19273	1.34	0.81	0.07207	0.98	1136	15	988	10	115
Zr-010-Q-XVII-11	0.0002	0.32	1.61416	1.25	0.16180	0.79	0.63	0.07236	0.97	967	8	996	10	97

Table 4. Sample PCA 6B – Fluvial sandstone of Almada Group.

Spot number	f <sup>206</sup>	Th/U <sup>a</sup>	<sup>207</sup> Pb/		1 s		<sup>206</sup> Pb/		1 s		<sup>207</sup> Pb/		1 s		% Conc <sup>e</sup>
			<sup>235</sup> U	[%]	<sup>238</sup> U	[%]	Rho <sup>c</sup>	<sup>206</sup> Pb <sup>d</sup>	[%]	<sup>238</sup> U	abs	<sup>206</sup> Pb	abs	<sup>207</sup> Pb/	1 s
Zr-011 A-I-1	0.0002	0.99	7.47927	2.46	0.41670	2.21	0.90	0.13018	1.09	2245	50	2100	23	107	
Zr-011 A-I-2	0.0013	0.41	6.06344	2.02	0.34059	0.79	0.39	0.12912	1.85	1890	15	2086	39	91	
Zr-011 A-I-3a	0.0024	0.41	6.52922	1.92	0.36173	1.40	0.73	0.13091	1.31	1990	28	2110	28	94	
Zr-011 A-I-3b	0.0032	0.38	6.20334	1.60	0.34388	1.17	0.74	0.13083	1.08	1905	22	2109	23	90	
Zr-011 A-I-4	0.0006	0.69	6.69560	2.57	0.36137	0.85	0.33	0.13438	2.43	1989	17	2156	52	92	
Zr-011 A-I-5a	0.0006	0.75	7.00940	0.85	0.36367	0.40	0.47	0.13979	0.75	2000	8	2225	17	90	
Zr-011-A-I-06	0.0002	0.41	10.63596	1.27	0.46949	1.10	0.87	0.16430	0.63	2481	27	2500	16	99	
Zr-011-A-I-08	0.0002	0.48	10.38943	1.44	0.46181	1.37	0.95	0.16316	0.44	2448	34	2489	11	98	
Zr-011-A-I-10	0.0001	0.62	11.00436	2.28	0.47701	2.08	0.91	0.16732	0.95	2514	52	2531	24	99	
Zr-011-A-I-11	0.0002	0.22	7.02301	1.98	0.38858	1.43	0.72	0.13108	1.37	2116	30	2112	29	100	
Zr-011-A-I-12	0.0005	0.31	9.68078	1.56	0.44401	0.98	0.63	0.15813	1.22	2369	23	2436	30	97	

Zr-011-B-II-01	0.0001	1.51	10.54735	1.95	0.45713	0.85	0.44	0.16734	1.75	2427	21	2531	44	96
Zr-011-B-II-02	0.0073	0.65	10.78503	2.85	0.46817	1.45	0.51	0.16708	2.45	2476	36	2529	62	98
Zr-011-B-II-05	0.0195	0.36	5.84128	4.50	0.34121	3.80	0.84	0.12416	2.42	1893	72	2017	49	94
Zr-011-B-II-06	0.0001	0.43	9.62125	1.89	0.43506	1.83	0.97	0.16039	0.46	2328	43	2460	11	95
Zr-011-B-II-08	0.0006	0.74	8.87404	4.18	0.42933	1.85	0.44	0.14991	3.74	2303	43	2345	88	98
Zr-011-B-II-09	0.0003	0.67	7.47672	3.55	0.40196	3.29	0.92	0.13491	1.35	2178	72	2163	29	101
Zr-011-B-II-11	0.0027	2.14	7.21774	3.77	0.37868	2.40	0.64	0.13824	2.91	2070	50	2205	64	94
Zr-011-B-II-13	0.0004	0.50	9.53892	3.56	0.43137	3.11	0.87	0.16038	1.74	2312	72	2460	43	94
Zr-011-C-III-01	0.0002	0.97	6.18605	3.44	0.35092	3.31	0.96	0.12785	0.94	1939	64	2069	20	94
Zr-011-C-III-03	0.0002	0.48	7.06366	5.97	0.38016	5.86	0.98	0.13476	1.17	2077	122	2161	25	96
Zr-011-C-III-04	0.0002	0.65	6.29543	4.19	0.34804	3.94	0.94	0.13119	1.43	1925	76	2114	30	91
Zr-011-C-III-05	0.0004	0.42	6.50467	5.24	0.36242	5.12	0.98	0.13017	1.08	1994	102	2100	23	95
Zr-011-C-III-07	0.0021	1.57	9.27427	3.89	0.42321	3.50	0.90	0.15894	1.69	2275	80	2444	41	93
Zr-011-C-III-08	0.0002	0.45	6.85150	2.86	0.39290	2.76	0.96	0.12647	0.77	2136	59	2050	16	104
Zr-011-C-III-09	0.0011	0.13	6.59739	5.75	0.37652	5.56	0.97	0.12708	1.47	2060	115	2058	30	100
Zr-011-C-III-10	0.0011	0.62	6.24924	5.55	0.35581	4.87	0.88	0.12738	2.67	1962	96	2062	55	95
Zr-011-C-III-11	0.0005	0.37	8.99523	6.61	0.42753	6.05	0.92	0.15260	2.67	2295	139	2375	63	97
Zr-011-C-III-12	0.0031	0.56	7.63192	5.18	0.34734	4.85	0.94	0.15936	1.82	1922	93	2449	45	78
Zr-011-C-III-14	0.0001	0.67	6.55543	4.67	0.36816	4.48	0.96	0.12914	1.33	2021	90	2086	28	97
Zr-011-D-IV-01	0.0001	0.28	7.04463	2.91	0.37588	2.61	0.90	0.13593	1.28	2057	54	2176	28	95
Zr-011-D-IV-03	0.0004	0.73	9.36224	2.13	0.40686	0.27	0.13	0.16689	2.11	2201	6	2527	53	87
Zr-011-D-IV-04	0.0001	0.51	6.71005	1.91	0.38078	1.20	0.63	0.12781	1.48	2080	25	2068	31	101
Zr-011-E-V-01	0.0028	0.37	4.70987	4.63	0.27020	4.43	0.96	0.12642	1.36	1542	68	2049	28	75
Zr-011-E-V-02	0.0003	0.53	10.62604	3.34	0.47935	2.51	0.75	0.16078	2.20	2524	63	2464	54	102
Zr-011-E-V-04	0.0015	0.08	6.78236	7.27	0.38167	6.82	0.94	0.12888	2.54	2084	142	2083	53	100
Zr-011-E-V-06	0.0006	0.46	9.51107	3.12	0.45809	2.53	0.81	0.15058	1.82	2431	62	2353	43	103
Zr-011-E-V-09	0.0043	0.16	7.55452	2.59	0.39786	1.51	0.58	0.13771	2.10	2159	33	2199	46	98
Zr-011-E-V-10	0.0054	0.23	6.37192	2.49	0.35167	1.85	0.74	0.13141	1.68	1943	36	2117	35	92
Zr-011-E-V-11	0.0003	0.44	11.33913	3.70	0.52137	3.33	0.90	0.15774	1.60	2705	90	2432	39	111
Zr-011-E-V-14	0.0019	0.37	8.22887	2.63	0.39625	2.51	0.95	0.15062	0.79	2152	54	2353	19	91
Zr-011-F-VI-01	0.0001	0.68	7.11061	3.52	0.40936	1.99	0.57	0.12598	2.90	2212	44	2043	59	108
Zr-011-F-VI-04	0.0002	0.60	6.85935	1.61	0.39282	0.28	0.17	0.12665	1.58	2136	6	2052	33	104
Zr-011-F-VI-06	0.0005	0.41	9.81428	4.88	0.49089	3.74	0.77	0.14500	3.14	2575	96	2288	72	113

Zr-011-F-VI-13	0.0214	0.34	2.78621	70.05	0.17287	0.63	0.04	0.11689	70.05	4028	7	1909	1337	54
Zr-011-G-VII-01	0.0038	0.53	6.44235	1.82	0.33039	0.33	0.18	0.14142	1.79	1840	6	2245	40	82
Zr-011-G-VII-02	0.0003	1.34	6.67530	2.96	0.37823	2.84	0.96	0.12800	0.82	2068	59	2071	17	100
Zr-011-G-VII-07	0.0040	0.43	0.73001	6.17	0.09067	5.62	0.91	0.05839	2.54	560	31	544	14	103
Zr-011-G-VII-09a	0.0021	0.72	6.70457	4.84	0.38199	3.89	0.80	0.12730	2.88	2086	81	2061	59	101
Zr-011-G-VII-09b	0.0009	0.78	8.05249	1.73	0.39410	0.81	0.47	0.14819	1.52	2142	17	2325	35	92
Zr-011-G-VII-10	0.0005	0.70	9.73622	4.51	0.46470	3.74	0.83	0.15196	2.52	2460	92	2368	60	104
Zr-011-G-VII-12	0.0002	0.31	6.69259	3.82	0.38154	3.57	0.93	0.12722	1.36	2083	74	2060	28	101
Zr-011-G-VII-13	0.0006	0.86	8.27530	0.69	0.40886	0.41	0.60	0.14680	0.55	2210	9	2309	13	96
Zr-011-G-VII-14	0.0003	0.73	10.04377	1.14	0.44319	0.25	0.22	0.16436	1.12	2365	6	2501	28	95
Zr-011-G-VII-15	0.0001	0.27	6.59753	3.04	0.37555	2.60	0.86	0.12741	1.58	2055	53	2063	33	100
Zr-011-H-VIII-01	0.0006	0.50	11.66265	5.42	0.49898	2.31	0.43	0.16952	4.90	2609	60	2553	125	102
Zr-011-H-VIII-02	0.0035	0.11	9.12419	4.78	0.43420	3.60	0.75	0.15240	3.14	2325	84	2373	75	98
Zr-011-H-VIII-03a	0.0010	0.62	10.69035	3.18	0.48262	2.60	0.82	0.16065	1.84	2539	66	2463	45	103
Zr-011-H-VIII-03b	0.0029	1.10	7.96952	7.46	0.40263	6.21	0.83	0.14356	4.14	2181	135	2271	94	96

Table 5. Sample PCA 07 – Eolian sandstone of Almada Group.

Spot number	f206	Th/U <sup>a</sup>	<sup>207</sup> Pb/ <sup>235</sup> U		1 s [%]	<sup>206</sup> Pb/ <sup>238</sup> U		1 s [%]	Rho <sup>c</sup>	<sup>207</sup> Pb/ <sup>206</sup> Pb <sup>d</sup>		1 s [%]	<sup>206</sup> Pb/ <sup>238</sup> U		1 s abs	<sup>207</sup> Pb/ <sup>206</sup> Pb		1 s abs	%	Conc <sup>e</sup>
Zr-011-I-IX-03	0.0013	0.69	11.65090	4.31	0.48554	2.73	0.63	0.17403	3.34	2551	70	2597	87	98						
Zr-011-I-IX-04	0.0008	0.27	11.13748	3.91	0.45725	3.46	0.89	0.17666	1.81	2427	84	2622	47	93						
Zr-011-I-IX-05	0.0021	0.40	8.47861	4.44	0.38884	2.75	0.62	0.15814	3.48	2117	58	2436	85	87						
Zr-011-I-IX-06	0.0001	0.43	10.81407	3.79	0.47551	2.69	0.71	0.16494	2.68	2508	67	2507	67	100						
Zr-011-I-IX-07	0.0003	0.39	11.57612	3.79	0.49587	3.63	0.96	0.16931	1.07	2596	94	2551	27	102						
Zr-011-I-IX-08	0.0020	1.18	0.61674	6.02	0.07934	5.25	0.87	0.05638	2.95	492	26	467	14	105						
Zr-011-I-IX-0X	0.0009	0.48	11.70517	4.08	0.49624	3.10	0.76	0.17107	2.65	2598	81	2568	68	101						
Zr-011-I-IX-09	0.0002	0.51	11.52780	7.35	0.49054	5.46	0.74	0.17044	4.91	2573	141	2562	126	100						

Zr-011-I-IX-10	0.0003	0.54	11.93695	3.01	0.50037	2.26	0.75	0.17302	2.00	2615	59	2587	52	101
Zr-011-I-IX-11	0.0003	0.42	11.37927	4.15	0.47962	3.69	0.89	0.17207	1.89	2526	93	2578	49	98
Zr-011-I-IX-12	0.0003	0.33	9.16611	2.48	0.43910	2.28	0.92	0.15140	0.97	2347	53	2362	23	99
Zr-011-J-X-01	0.0029	0.64	4.22562	2.21	0.29369	0.95	0.43	0.10435	2.00	1660	16	1703	34	97
Zr-011-J-X-02	0.0001	0.46	9.35832	11.26	0.41486	10.19	0.91	0.16360	4.77	2237	228	2493	119	90
Zr-011-J-X-04	0.0003	0.64	5.85003	4.56	0.35253	4.38	0.96	0.12035	1.29	1947	85	1961	25	99
Zr-011-J-X-05	0.0003	0.43	6.63859	4.04	0.36902	3.53	0.87	0.13047	1.97	2025	71	2104	42	96
Zr-011-J-X-06	0.0001	0.46	12.73255	2.53	0.52694	2.32	0.92	0.17525	1.02	2729	63	2608	27	105
Zr-011-K-XI-02	0.0001	0.22	6.75817	3.47	0.39718	3.30	0.95	0.12341	1.08	2156	71	2006	22	107
Zr-011-K-XI-06	0.0001	0.20	12.33433	3.02	0.49955	2.61	0.87	0.17908	1.51	2612	68	2644	40	99
Zr-011-K-XI-07	0.0002	0.70	6.20144	2.04	0.35870	1.33	0.65	0.12539	1.55	1976	26	2034	31	97
Zr-011-K-XI-09	0.0010	0.14	5.91869	3.01	0.34887	2.40	0.80	0.12305	1.83	1929	46	2001	37	96
Zr-011-K-XI-10	0.0004	0.06	6.05636	3.32	0.35328	2.71	0.82	0.12433	1.92	1950	53	2019	39	97
Zr-011-K-XI-12	0.0001	0.42	7.52963	3.39	0.40447	2.83	0.83	0.13502	1.87	2190	62	2164	41	101
Zr-011-K-XI-15	0.0012	0.42	9.79397	4.02	0.44766	2.50	0.62	0.15867	3.15	2385	60	2442	77	98
Zr-011-L-XII-03	0.0005	0.53	11.60449	2.38	0.48602	0.64	0.27	0.17317	2.29	2553	16	2588	59	99
Zr-011-M-XIII-01	0.0001	0.39	10.09632	3.07	0.43581	2.72	0.89	0.16802	1.43	2332	63	2538	36	92
Zr-011-M-XIII-02	0.0011	0.38	7.00536	3.15	0.36997	2.83	0.90	0.13733	1.39	2029	57	2194	30	93
Zr-011-M-XIII-03	0.0011	0.38	6.13922	2.44	0.32912	0.33	0.14	0.13529	2.41	1834	6	2168	52	85
Zr-011-M-XIII-04	0.0002	0.47	11.76832	3.03	0.47970	2.42	0.80	0.17793	1.82	2526	61	2634	48	96
Zr-011-M-XIII-05	0.0032	0.59	10.29359	3.59	0.46829	3.22	0.90	0.15942	1.59	2476	80	2450	39	101
Zr-011-M-XIII-06	0.0004	0.43	7.12861	3.13	0.39006	2.72	0.87	0.13255	1.55	2123	58	2132	33	100
Zr-011-M-XIII-07	0.0003	0.31	12.94766	2.18	0.50451	1.41	0.65	0.18613	1.66	2633	37	2708	45	97
Zr-011-M-XIII-08	0.0001	0.60	11.38903	2.18	0.49210	1.75	0.80	0.16785	1.31	2580	45	2536	33	102
Zr-011-M-XIII-09	0.0001	0.23	6.32166	2.61	0.37000	2.28	0.87	0.12392	1.29	2029	46	2013	26	101
Zr-011-M-XIII-12	0.0002	0.12	18.28412	11.45	0.52039	9.67	0.84	0.25482	6.13	2704	264	3215	497	84
Zr-011-M-XIII-13	0.0001	0.38	12.23762	2.54	0.50447	2.25	0.88	0.17594	1.19	2633	59	2615	31	101
Zr-011-M-XIII-15	0.0001	0.61	10.16412	5.33	0.45311	4.69	0.88	0.16269	2.54	2409	113	2484	63	97
Zr-011-N-IX-01	0.0002	0.62	10.94302	2.85	0.46757	2.44	0.86	0.16974	1.48	2473	60	2555	38	97

Table 6. Sample PCA 8A – Fluvial sandstone of Sergi Formation, Brotas Group.

Spot number	f206	Th/U <sup>a</sup>	<sup>207</sup> Pb/ <sup>235</sup> U	1 s [%]	<sup>206</sup> Pb/ <sup>238</sup> U	1 s [%]	Rho <sup>c</sup>	<sup>207</sup> Pb/ <sup>206</sup> Pb <sup>d</sup>	1 s [%]	<sup>206</sup> Pb/ <sup>238</sup> U	1 s abs	<sup>207</sup> Pb/ <sup>206</sup> Pb	1 s abs	% Conc <sup>e</sup>
Zr-012-A-I-01	0.0013	0.67	1.31308	3.15	0.14112	1.95	0.62	0.06748	2.47	851	17	853	21	100
Zr-012-A-I-02	0.0009	0.27	0.74838	2.49	0.09150	2.10	0.84	0.05932	1.33	564	12	579	8	98
Zr-012-A-I-03	0.0009	0.52	9.42395	1.49	0.39167	0.77	0.52	0.17450	1.28	2131	16	2601	33	82
Zr-012-A-I-04	0.0005	0.53	1.28187	2.55	0.13486	1.30	0.51	0.06894	2.20	816	11	897	20	91
Zr-012-A-I-05	0.0006	2.83	0.78626	6.11	0.09668	3.36	0.55	0.05899	5.10	595	20	567	29	105
Zr-012-A-I-06	0.0007	0.89	5.32987	1.26	0.30594	0.94	0.75	0.12635	0.83	1721	16	2048	17	84
Zr-012-A-I-07	0.0012	0.32	14.43574	1.08	0.46086	0.97	0.89	0.22718	0.48	2443	24	3032	15	81
Zr-012-A-I-08	0.0004	0.71	0.57110	3.19	0.07269	2.34	0.73	0.05698	2.17	452	11	491	11	92
Zr-012-A-I-09	0.0010	0.26	0.76531	3.30	0.09306	2.18	0.66	0.05965	2.48	574	13	591	15	97
Zr-012-A-I-10	0.0008	1.42	0.62987	3.56	0.08002	3.22	0.90	0.05709	1.52	496	16	495	8	100
Zr-012-A-I-11	0.0012	1.76	0.62229	3.42	0.07916	2.88	0.84	0.05701	1.84	491	14	492	9	100
Zr-012-A-I-12	0.0006	0.51	11.13255	4.71	0.46051	4.45	0.94	0.17533	1.56	2442	109	2609	41	94
Zr-012-A-I-13	0.0038	2.03	0.60432	4.38	0.07816	3.13	0.71	0.05608	3.07	485	15	455	14	107
Zr-012-A-I-14	0.0009	0.52	11.62687	1.98	0.47140	1.54	0.78	0.17888	1.25	2490	38	2643	33	94
Zr-012-A-I-15	0.0025	0.34	5.99973	1.20	0.33531	0.59	0.49	0.12977	1.05	1864	11	2095	22	89
Zr-012-B-II-01	0.0012	0.09	0.64996	2.97	0.08123	2.17	0.73	0.05803	2.03	503	11	531	11	95
Zr-012-B-II-02	0.0048	0.66	0.61507	4.75	0.07939	2.41	0.51	0.05619	4.09	492	12	460	19	107
Zr-012-B-II-03	0.0014	0.34	0.71575	3.91	0.08813	2.08	0.53	0.05890	3.32	544	11	564	19	97
Zr-012-B-II-04	0.0025	0.65	0.62389	3.58	0.08042	2.47	0.69	0.05627	2.59	499	12	463	12	108
Zr-012-B-II-05	0.0021	1.21	0.90424	3.10	0.10513	2.09	0.67	0.06238	2.29	644	13	687	16	94
Zr-012-B-II-06	0.0005	0.63	1.01846	2.22	0.11702	1.67	0.75	0.06312	1.46	713	12	712	10	100
Zr-012-B-II-07	0.0007	1.28	5.43217	1.85	0.33598	1.02	0.55	0.11726	1.55	1867	19	1915	30	98
Zr-012-B-II-08	0.0000	0.40	1.40793	2.36	0.14671	1.93	0.82	0.06960	1.36	882	17	917	12	96
Zr-012-B-II-09	0.0007	0.17	0.87164	2.22	0.10452	1.59	0.72	0.06048	1.55	641	10	621	10	103
Zr-012-C-III-01	0.0005	1.93	15.05935	1.79	0.55447	1.41	0.79	0.19698	1.09	2844	40	2801	31	102
Zr-012-C-III-02	0.0004	0.82	0.60898	2.85	0.07875	1.81	0.63	0.05609	2.21	489	9	456	10	107
Zr-012-C-III-03	0.0008	1.51	0.52295	4.50	0.06852	3.11	0.69	0.05536	3.25	427	13	427	14	100
Zr-012-C-III-04	0.0003	0.42	11.70440	1.67	0.47326	1.30	0.78	0.17937	1.05	2498	32	2647	28	94
Zr-012-C-III-05	0.0010	0.96	5.71078	2.22	0.33426	1.99	0.89	0.12391	1.00	1859	37	2013	20	92

Zr-012-C-III-06	0.0076	1.26	0.54863	5.07	0.07174	3.85	0.76	0.05546	3.30	447	17	431	14		104
Zr-012-C-III-08	0.0025	0.79	0.61208	2.94	0.07809	1.99	0.68	0.05685	2.16	485	10	486	11		100
Zr-012-C-III-09	0.0011	0.73	0.52172	5.25	0.06556	2.61	0.50	0.05772	4.56	409	11	519	24		79
Zr-012-C-III-10	0.0053	1.24	0.58049	6.32	0.07643	3.46	0.55	0.05509	5.29	475	16	416	22		114
Zr-012-C-III-11	0.0024	1.05	0.61528	7.47	0.07820	2.94	0.39	0.05706	6.87	485	14	494	34		98
Zr-012-C-III-12	0.0018	0.58	0.63337	4.72	0.08029	2.04	0.43	0.05721	4.25	498	10	500	21		100
Zr-012-C-III-13	0.0003	1.02	0.71583	2.65	0.08660	1.58	0.60	0.05995	2.12	535	8	602	13		89
Zr-012-C-III-14	0.0007	1.17	0.61706	4.84	0.07854	2.94	0.61	0.05698	3.85	487	14	491	19		99
Zr-012-D-IV-01	0.0018	0.24	0.70932	3.77	0.08737	1.96	0.52	0.05888	3.22	540	11	563	18		96
Zr-012-D-IV-02	0.0002	0.55	5.76808	1.51	0.33023	1.07	0.71	0.12668	1.07	1839	20	2052	22		90
Zr-012-D-IV-04	0.0014	1.64	0.63771	4.26	0.08031	2.00	0.47	0.05759	3.77	498	10	514	19		97
Zr-012-E-V-01	0.0005	0.54	5.17133	1.84	0.30760	1.31	0.71	0.12193	1.30	1729	23	1985	26		87
Zr-012-E-V-02	0.0028	0.63	0.55448	6.46	0.07204	1.80	0.28	0.05582	6.20	448	8	445	28		101
Zr-012-E-V-03	0.0009	0.17	0.75401	2.60	0.09279	2.12	0.82	0.05894	1.50	572	12	565	8		101
Zr-012-E-V-04	0.0010	0.38	0.78348	4.98	0.09503	1.97	0.39	0.05979	4.57	585	12	596	27		98
Zr-012-E-V-05	0.0014	0.54	0.67089	2.24	0.08371	1.62	0.72	0.05813	1.56	518	8	535	8		97
Zr-012-E-V-06	0.0002	0.22	0.66564	2.28	0.07995	1.51	0.66	0.06039	1.72	496	7	617	11		80
Zr-012-E-V-07	0.0011	0.29	0.58088	2.52	0.07369	1.85	0.73	0.05717	1.72	458	8	498	9		92
Zr-012-E-V-08	0.0030	1.22	0.62377	3.22	0.07920	2.58	0.80	0.05712	1.93	491	13	496	10		99
Zr-012-E-V-09	0.0026	0.44	1.19504	10.78	0.13247	9.31	0.86	0.06543	5.44	802	75	788	43		102
Zr-012-E-V-10	0.0047	2.39	0.59201	3.89	0.07729	3.34	0.86	0.05555	2.01	480	16	435	9		110
Zr-012-E-V-11	0.0011	0.65	0.90558	4.05	0.10665	1.88	0.46	0.06158	3.59	653	12	660	24		99
Zr-012-E-V-12	0.0078	0.60	0.57447	9.96	0.07162	4.71	0.47	0.05817	8.78	446	21	536	47		83
Zr-012-E-V-13	0.0070	0.48	11.34963	5.27	0.46000	4.90	0.93	0.17895	1.93	2440	120	2643	51		92
Zr-012-E-V-14	0.0010	0.13	0.81486	4.26	0.09977	2.24	0.53	0.05924	3.62	613	14	576	21		106
Zr-012-E-V-15	0.0008	0.30	1.37228	2.92	0.14506	1.66	0.57	0.06861	2.41	873	14	887	21		98
Zr-012-F-VI-01	0.0011	0.54	1.32741	2.43	0.13829	1.77	0.73	0.06962	1.67	835	15	917	15		91
Zr-012-F-VI-02	0.0006	0.28	4.85344	2.06	0.29616	1.56	0.76	0.11885	1.34	1672	26	1939	26		86
Zr-012-F-VI-04	0.0018	0.86	0.59445	3.15	0.07691	2.48	0.79	0.05606	1.95	478	12	455	9		105
Zr-012-F-VI-05	0.0002	0.83	0.58522	3.09	0.07539	2.16	0.70	0.05630	2.21	469	10	464	10		101
Zr-012-F-VI-06	0.0003	1.64	0.63190	3.76	0.08111	2.17	0.58	0.05650	3.07	503	11	472	14		106
Zr-012-F-VI-07	0.0026	0.19	0.77026	2.03	0.09346	1.42	0.70	0.05978	1.45	576	8	595	9		97
Zr-012-F-VI-08	0.0002	0.97	1.40648	2.48	0.14717	1.33	0.54	0.06931	2.09	885	12	908	19		97

Zr-012-F-VI-09	0.0161	0.08	7.97340	1.91	0.28124	1.76	0.92	0.20562	0.75	1598	28	2871	21		56
Zr-012-F-VI-10	0.0021	0.48	0.88375	2.31	0.10464	1.33	0.58	0.06125	1.89	642	9	648	12		99
Zr-012-F-VI-11	0.0018	2.32	0.58123	3.43	0.07462	1.64	0.48	0.05649	3.01	464	8	472	14		98
Zr-012-F-VI-12	0.0016	1.14	0.59509	4.64	0.07674	2.42	0.52	0.05624	3.95	477	12	462	18		103
Zr-012-F-VI-13	0.0048	0.97	0.72459	2.07	0.08873	1.40	0.68	0.05922	1.52	548	8	575	9		95
Zr-012-F-VI-14	0.0041	0.28	5.25710	3.80	0.24410	3.68	0.97	0.15620	0.98	1408	52	2415	24		58
Zr-012-F-VI-15	0.0025	1.10	0.60786	7.29	0.07841	1.86	0.26	0.05622	7.05	487	9	461	32		106
Zr-012-G-VII-01	0.0017	0.73	1.35884	3.88	0.14331	1.32	0.34	0.06877	3.65	863	11	892	33		97
Zr-012-G-VII-02	0.0005	0.89	6.48623	1.57	0.36815	1.26	0.80	0.12778	0.93	2021	26	2068	19		98
Zr-012-G-VII-03	0.0005	1.30	0.64706	2.94	0.08071	1.88	0.64	0.05814	2.27	500	9	535	12		94
Zr-012-G-VII-04	0.0003	0.34	4.95484	1.32	0.32700	1.08	0.82	0.10990	0.75	1824	20	1798	13		101
Zr-012-G-VII-05	0.0004	0.37	2.24278	2.66	0.16850	1.97	0.74	0.09653	1.78	1004	20	1558	28		64
Zr-012-G-VII-06	0.0009	0.99	0.66689	2.35	0.08480	1.81	0.77	0.05704	1.50	525	10	493	7		106
Zr-012-G-VII-07	0.0015	2.18	0.62315	5.25	0.07909	2.91	0.55	0.05714	4.37	491	14	497	22		99
Zr-012-G-VII-08	0.0004	0.48	1.01355	2.35	0.11454	1.24	0.53	0.06418	2.00	699	9	747	15		94
Zr-012-G-VII-09	0.0006	2.57	0.66000	4.39	0.08322	2.63	0.60	0.05752	3.51	515	14	511	18		101
Zr-012-G-VII-10	0.0002	0.80	1.47689	1.93	0.15439	1.33	0.69	0.06938	1.40	926	12	910	13		102
Zr-012-G-VII-11	0.0007	0.71	0.63124	3.40	0.07943	1.82	0.54	0.05764	2.87	493	9	516	15		95
Zr-012-G-VII-12	0.0015	0.17	0.83029	2.61	0.09922	1.75	0.67	0.06069	1.93	610	11	628	12		97
Zr-012-G-VII-14	0.0009	0.47	0.66066	4.12	0.08353	1.97	0.48	0.05737	3.61	517	10	506	18		102

Table 7. Sample PCA 8B – Eolian sandstone of Sergi Formation, Brotas Group.

Spot number	f206	Th/U <sup>a</sup>	207Pb/ 235U		1 s [%]		206Pb/ 238U		1 s [%]		207Pb/ 206Pb <sup>d</sup>		1 s abs		206Pb/ 238U		1 s abs		207Pb/ 206Pb		1 s abs		% Conc <sup>e</sup>
			Rho <sup>c</sup>	Rho <sup>c</sup>	Rho <sup>c</sup>	Rho <sup>c</sup>	Rho <sup>c</sup>	Rho <sup>c</sup>	Rho <sup>c</sup>	Rho <sup>c</sup>	Rho <sup>c</sup>	Rho <sup>c</sup>	Rho <sup>c</sup>										
Zr-012-H-VIII-01	0.0008	0.65	0.73654	3.74	0.09158	1.70	0.46	0.05833	3.33	565	10	542	18		104								
Zr-012-H-VIII-02	0.0004	0.19	0.73310	2.93	0.08973	1.54	0.53	0.05926	2.49	554	9	577	14		96								
Zr-012-H-VIII-03	0.0037	1.65	0.62588	3.91	0.07825	2.60	0.67	0.05801	2.91	486	13	530	15		92								
Zr-012-H-VIII-04	0.0002	0.21	0.66042	2.51	0.08338	1.59	0.63	0.05744	1.95	516	8	509	10		102								
Zr-012-H-VIII-05	0.0006	1.26	0.61516	2.70	0.07903	2.04	0.75	0.05646	1.78	490	10	470	8		104								
Zr-012-H-VIII-06	0.0010	0.71	0.63172	2.33	0.07946	1.64	0.71	0.05766	1.65	493	8	517	9		95								

Zr-012-H-VIII-07	0.0004	0.44	10.04337	1.26	0.42951	1.09	0.86	0.16959	0.64	2304	25	2554	16	90
Zr-012-H-VIII-08	0.0009	1.39	0.61984	5.76	0.07918	2.69	0.47	0.05678	5.09	491	13	483	25	102
Zr-012-H-VIII-09	0.0016	1.36	3.86896	1.61	0.26892	1.12	0.70	0.10434	1.15	1535	17	1703	20	90
Zr-012-H-VIII-10	0.0029	1.27	0.56938	7.31	0.07356	2.70	0.37	0.05614	6.79	458	12	458	31	100
Zr-012-H-VIII-11	0.0072	0.72	5.50848	1.09	0.32525	0.75	0.69	0.12283	0.79	1815	14	1998	16	91
Zr-012-H-VIII-12	0.0008	1.16	0.56846	3.69	0.07256	1.93	0.52	0.05682	3.15	452	9	484	15	93
Zr-012-H-VIII-13	0.0003	0.64	6.50392	1.31	0.36750	1.06	0.81	0.12836	0.76	2018	21	2076	16	97
Zr-012-H-VIII-14	0.0015	1.67	0.77167	2.40	0.09297	1.58	0.66	0.06020	1.81	573	9	611	11	94
Zr-012-H-VIII-15	0.0012	0.45	0.68256	3.25	0.08493	1.52	0.47	0.05829	2.87	525	8	541	16	97
Zr-012-I-IX-01	0.0012	1.13	0.79396	4.08	0.09595	1.71	0.42	0.06002	3.70	591	10	604	22	98
Zr-012-I-IX-02	0.0010	0.75	1.46331	1.95	0.15017	0.96	0.49	0.07067	1.70	902	9	948	16	95
Zr-012-I-IX-03	0.0012	0.10	0.71351	2.37	0.08972	1.46	0.61	0.05768	1.87	554	8	518	10	107
Zr-012-I-IX-04	0.0008	0.82	1.45608	2.94	0.15198	1.59	0.54	0.06949	2.47	912	15	913	23	100
Zr-012-I-IX-05	0.0007	0.58	0.62003	3.86	0.07865	1.93	0.50	0.05718	3.34	488	9	498	17	98
Zr-012-I-IX-06	0.0006	0.62	0.62629	3.29	0.07979	1.99	0.61	0.05693	2.62	495	10	489	13	101
Zr-012-I-IX-07	0.0177	4.83	13.17783	3.31	0.53144	3.14	0.95	0.17984	1.05	2748	86	2651	28	104
Zr-012-I-IX-08	0.0012	0.72	0.61903	3.99	0.07844	2.03	0.51	0.05723	3.44	487	10	501	17	97
Zr-012-J-X-01	0.0015	1.48	0.62065	4.70	0.07923	2.01	0.43	0.05681	4.25	492	10	484	21	102
Zr-012-J-X-02	0.0011	1.07	5.61475	2.10	0.33394	1.44	0.68	0.12194	1.53	1857	27	1985	30	94
Zr-012-J-X-03	0.0005	1.62	0.60981	3.04	0.07881	2.51	0.83	0.05612	1.72	489	12	457	8	107
Zr-012-J-X-04	0.0023	0.80	1.36730	2.22	0.14826	1.63	0.74	0.06689	1.50	891	15	834	13	107
Zr-012-J-X-05	0.0005	0.58	1.59068	1.66	0.15654	1.07	0.64	0.07370	1.27	938	10	1033	13	91
Zr-012-J-X-06	0.0015	1.64	0.80648	2.64	0.09668	2.08	0.79	0.06050	1.63	595	12	621	10	96
Zr-012-J-X-07	0.0042	0.93	0.64364	13.82	0.07641	5.96	0.43	0.06109	12.47	475	28	642	80	74
Zr-012-J-X-08	0.0002	1.65	0.58093	5.71	0.07289	3.37	0.59	0.05780	4.61	454	15	522	24	87
Zr-012-J-X-09	0.0015	1.10	0.61552	2.95	0.07837	2.41	0.82	0.05697	1.71	486	12	490	8	99
Zr-012-J-X-10	0.0022	0.57	1.51692	2.44	0.15253	1.85	0.76	0.07213	1.58	915	17	990	16	92
Zr-012-J-X-11	0.0012	0.37	6.87553	1.95	0.37290	0.98	0.50	0.13372	1.68	2043	20	2147	36	95
Zr-012-J-X-13	0.0018	1.76	0.57012	3.87	0.07255	2.63	0.68	0.05699	2.84	452	12	491	14	92
Zr-012-J-X-14	0.0007	0.11	0.83333	2.90	0.10046	1.81	0.62	0.06016	2.27	617	11	609	14	101
Zr-012-J-X-15	0.0009	0.52	0.75448	4.27	0.09276	2.37	0.56	0.05899	3.55	572	14	567	20	101
Zr-012-K-XI-01	0.0004	0.35	5.95201	1.92	0.33293	1.76	0.92	0.12966	0.77	1853	33	2093	16	88
Zr-012-K-XI-02	0.0021	1.11	5.52900	1.78	0.32344	1.50	0.84	0.12398	0.96	1807	27	2014	19	90

Zr-012-K-XI-03	0.0010	0.53	0.85589	2.56	0.10157	1.96	0.76	0.06111	1.65	624	12	643	11	97
Zr-012-K-XI-04	0.0066	0.54	1.29391	2.84	0.13447	1.89	0.66	0.06979	2.12	813	15	922	20	88
Zr-012-K-XI-05	0.0004	0.14	0.73595	2.79	0.09070	1.78	0.64	0.05885	2.14	560	10	561	12	100
Zr-012-K-XI-06	0.0012	1.22	0.74948	3.71	0.09188	1.95	0.52	0.05916	3.17	567	11	573	18	99
Zr-012-K-XI-08	0.0095	0.55	1.46739	2.72	0.14091	1.63	0.60	0.07553	2.18	850	14	1083	24	78
Zr-012-K-XI-09	0.0010	0.52	1.38884	3.27	0.14110	2.90	0.89	0.07139	1.50	851	25	969	15	88
Zr-012-K-XI-10	0.0020	0.85	0.81072	2.78	0.09649	1.87	0.67	0.06094	2.05	594	11	637	13	93
Zr-012-K-XI-11	0.0004	0.21	0.85066	2.10	0.09944	1.47	0.70	0.06204	1.50	611	9	676	10	90
Zr-012-K-XI-13	0.0019	1.07	5.08687	1.64	0.31767	1.39	0.85	0.11614	0.87	1778	25	1898	16	94
Zr-012-L-XII-01	0.0003	1.46	0.60267	2.68	0.07825	1.81	0.68	0.05586	1.97	486	9	447	9	109
Zr-012-L-XII-02	0.0011	0.94	1.16100	2.73	0.13010	1.15	0.42	0.06472	2.47	788	9	765	19	103
Zr-012-L-XII-03	0.0117	1.74	0.65104	5.82	0.08197	3.49	0.60	0.05761	4.66	508	18	515	24	99
Zr-012-L-XII-04	0.0037	0.95	1.34982	2.52	0.14704	1.28	0.51	0.06658	2.17	884	11	825	18	107
Zr-012-L-XII-05	0.0000	1.10	0.62948	3.93	0.07958	2.34	0.60	0.05737	3.16	494	12	506	16	98
Zr-012-L-XII-06	0.0004	0.93	6.94074	1.28	0.39159	1.07	0.84	0.12855	0.70	2130	23	2078	15	102
Zr-012-L-XII-07	0.0009	1.25	19.64967	2.16	0.60329	0.88	0.41	0.23622	1.98	3043	27	3095	61	98
Zr-012-L-XII-08	0.0007	0.19	0.67515	2.85	0.08443	1.51	0.53	0.05800	2.42	523	8	530	13	99
Zr-012-L-XII-09	0.0013	0.26	0.82437	3.48	0.09856	1.34	0.38	0.06066	3.22	606	8	627	20	97
Zr-012-M-XIII-01	0.0010	0.93	0.64337	3.45	0.08160	1.75	0.51	0.05718	2.98	506	9	498	15	101
Zr-012-M-XIII-02	0.0002	1.02	6.07035	1.65	0.36079	1.10	0.67	0.12203	1.22	1986	22	1986	24	100
Zr-012-M-XIII-03	0.0004	0.51	1.65399	2.30	0.16539	1.55	0.67	0.07253	1.70	987	15	1001	17	99
Zr-012-M-XIII-04	0.0002	0.11	0.78790	2.54	0.09578	1.65	0.65	0.05966	1.93	590	10	591	11	100
Zr-012-M-XIII-05	0.0008	0.86	0.62958	4.53	0.07980	2.19	0.48	0.05722	3.97	495	11	500	20	99
Zr-012-M-XIII-06	0.0002	0.50	13.01504	1.19	0.50882	1.09	0.91	0.18552	0.48	2652	29	2703	13	98
Zr-012-M-XIII-08	0.0170	1.76	0.68559	4.33	0.08208	1.61	0.37	0.06058	4.02	509	8	624	25	81
Zr-012-M-XIII-09	0.0002	0.10	0.75420	2.32	0.09307	1.47	0.63	0.05877	1.79	574	8	559	10	103
Zr-012-M-XIII-10	0.0000	1.32	0.77404	2.58	0.09401	1.81	0.70	0.05972	1.84	579	10	593	11	98
Zr-012-M-XIII-11	0.0007	0.13	0.72368	2.52	0.08852	1.53	0.60	0.05930	2.01	547	8	578	12	95
Zr-012-M-XIII-12	0.0016	0.13	5.89447	2.69	0.34587	2.39	0.89	0.12360	1.24	1915	46	2009	25	95
Zr-012-M-XIII-13	0.0003	0.64	1.67458	1.72	0.16838	1.18	0.69	0.07213	1.25	1003	12	990	12	101
Zr-012-M-XIII-14	0.0013	1.63	0.67974	3.67	0.08496	1.82	0.49	0.05803	3.19	526	10	531	17	99
Zr-012-N-XIV-01	0.0007	0.14	0.73990	2.98	0.09042	2.27	0.76	0.05935	1.93	558	13	580	11	96
Zr-012-N-XIV-02	0.0011	1.43	0.65241	4.17	0.08242	1.87	0.45	0.05741	3.73	511	10	507	19	101

Zr-012-J-X-07 (40 micra)	0.0011	0.98	0.63408	3.60	0.08019	1.43	0.40	0.05735	3.30	497	7	505	17	98
Zr-012-J-X-08 (40 micra)	0.0004	0.96	0.64425	2.57	0.08193	1.27	0.50	0.05703	2.23	508	6	493	11	103
Zr-012-J-X-10 (40 micra)	0.0007	0.51	1.59763	2.55	0.16222	0.87	0.34	0.07143	2.40	969	8	970	23	100
Zr-012-J-X-13 (40 micra)	0.0052	1.77	0.58010	7.04	0.07170	1.59	0.23	0.05868	6.86	446	7	555	38	80
Zr-012-K-XI-08 (40 micra)	0.0018	0.68	1.59138	1.39	0.16340	0.71	0.52	0.07064	1.19	976	7	947	11	103
Zr-012-K-XI-10 (40 micra)	0.0005	0.89	0.90983	2.30	0.10745	1.00	0.43	0.06141	2.07	658	7	654	14	101
Zr-012-L-XII-03 (40 micra)	0.0012	1.82	0.69770	2.20	0.08759	1.50	0.68	0.05777	1.61	541	8	521	8	104
Zr-012-M-XIII-10 (40 micra)	0.0003	1.18	0.81972	2.66	0.09879	1.07	0.40	0.06018	2.44	607	6	610	15	100

Table 8. Sample PCA 9 – Conglomerate of Almada Group.

Spot number	f206	Th/U <sup>a</sup>	<sup>207</sup> Pb/ <sup>235</sup> U			<sup>206</sup> Pb/ <sup>238</sup> U			<sup>207</sup> Pb/ <sup>206</sup> Pb <sup>d</sup>			% Conc <sup>e</sup>		
			1 s	[%]	1 s	[%]	Rho <sup>c</sup>	1 s	[%]	1 s	abs	<sup>207</sup> Pb/ <sup>206</sup> Pb	abs	
Zr-014-A-I-01	0.0007	0.45	13.01376	0.93	0.52481	0.66	0.71	0.17985	0.66	2720	18	2651	17	103
Zr-014-A-I-03	0.0058	0.40	1.06491	3.58	0.11308	2.37	0.66	0.06830	2.68	691	16	878	24	79
Zr-014-A-I-04	0.0002	0.44	13.42330	1.07	0.51990	0.75	0.70	0.18726	0.77	2699	20	2718	21	99
Zr-014-A-I-05	0.0004	0.55	0.84674	2.35	0.10089	1.77	0.75	0.06087	1.54	620	11	635	10	98
Zr-014-A-I-07	0.0020	0.48	11.13277	2.93	0.45473	2.19	0.75	0.17756	1.94	2416	53	2630	51	92
Zr-014-A-I-09	0.0059	0.50	9.89778	2.68	0.43489	1.92	0.72	0.16507	1.87	2328	45	2508	47	93
Zr-014-A-I-10	0.0005	0.90	7.10119	2.12	0.39644	1.61	0.76	0.12991	1.38	2153	35	2097	29	103
Zr-014-A-I-11	0.0008	0.51	12.95962	1.60	0.52204	1.25	0.78	0.18005	0.99	2708	34	2653	26	102
Zr-014-A-I-13	0.0011	1.03	7.04141	1.76	0.38145	1.51	0.86	0.13388	0.91	2083	31	2150	19	97
Zr-014-A-I-14	0.0027	0.89	6.42498	3.02	0.37835	2.91	0.96	0.12316	0.82	2069	60	2003	16	103
Zr-014-B-II-02	0.0004	0.63	6.92878	1.66	0.38270	0.97	0.59	0.13131	1.34	2089	20	2116	28	99
Zr-014-B-II-03	0.0005	0.47	14.99597	1.78	0.55060	1.43	0.80	0.19753	1.06	2828	40	2806	30	101

Zr-014-B-II-05	0.0022	0.22	3.31968	9.21	0.18830	0.79	0.09	0.12786	9.17	1112	9	2069	190	54
Zr-014-B-II-05 a	0.0023	0.39	11.64509	16.52	0.56587	0.26	0.02	0.14925	16.52	2891	8	2337	386	124
Zr-014-B-II-07	0.0006	0.37	11.57645	1.73	0.47976	1.22	0.70	0.17500	1.23	2526	31	2606	32	97
Zr-014-B-II-09	0.0007	0.60	12.08072	1.95	0.48943	1.50	0.77	0.17902	1.24	2568	38	2644	33	97
Zr-014-B-II-08	0.0114	0.29	7.49073	1.44	0.39130	0.47	0.33	0.13884	1.36	2129	10	2213	30	96
Zr-014-C-III-01	0.0012	0.38	6.11678	1.92	0.34529	1.05	0.55	0.12848	1.61	1912	20	2077	34	92
Zr-014-C-III-03	0.0071	0.57	8.75221	2.73	0.38927	1.53	0.56	0.16307	2.26	2119	33	2488	56	85
Zr-014-C-III-05	0.0034	0.57	11.38973	2.36	0.48795	1.88	0.80	0.16929	1.43	2562	48	2551	37	100
Zr-014-C-III-07	0.0005	0.57	6.80848	1.42	0.38752	0.89	0.63	0.12742	1.10	2111	19	2063	23	102
Zr-014-C-III-08	0.0002	0.50	11.32964	1.50	0.46640	0.70	0.47	0.17618	1.32	2468	17	2617	35	94
Zr-014-C-III-09	0.0280	0.83	4.37607	1.59	0.24252	1.28	0.80	0.13087	0.95	1400	18	2110	20	66
Zr-014-C-III-10	0.0004	0.44	12.03191	1.73	0.49756	1.44	0.83	0.17538	0.96	2603	37	2610	25	100
Zr-014-C-III-11	0.0046	0.46	12.31117	4.01	0.50259	3.52	0.88	0.17766	1.92	2625	92	2631	50	100
Zr-014-C-III-13	0.0009	0.40	12.99833	2.10	0.52182	1.80	0.86	0.18066	1.07	2707	49	2659	29	102
Zr-014-C-III-14	0.0005	0.43	13.02196	1.85	0.51917	1.65	0.89	0.18191	0.84	2696	45	2670	22	101

Table 9. Sample PCA 10 – Eolian sandstone of Sergi Formation, Brotas Group.

Spot number	f206	Th/U <sup>a</sup>	<sup>207</sup> Pb/ <sup>235</sup> U		1 s [%]		<sup>206</sup> Pb/ <sup>238</sup> U		1 s [%]		<sup>207</sup> Pb/ <sup>206</sup> Pb <sup>d</sup>		1 s [%]		<sup>206</sup> Pb/ <sup>238</sup> U		1 s abs		<sup>207</sup> Pb/ <sup>206</sup> Pb		1 s abs		% Conc <sup>e</sup>	
			Rho <sup>c</sup>	Rho <sup>c</sup>	<sup>206</sup> Pb <sup>d</sup>	<sup>206</sup> Pb <sup>d</sup>	Rho <sup>c</sup>	Rho <sup>c</sup>	<sup>206</sup> Pb <sup>d</sup>	<sup>206</sup> Pb <sup>d</sup>	<sup>206</sup> Pb <sup>d</sup>	<sup>206</sup> Pb <sup>d</sup>	<sup>206</sup> Pb <sup>d</sup>	<sup>206</sup> Pb <sup>d</sup>	<sup>206</sup> Pb <sup>d</sup>	<sup>206</sup> Pb <sup>d</sup>	<sup>206</sup> Pb <sup>d</sup>	<sup>206</sup> Pb <sup>d</sup>	<sup>206</sup> Pb <sup>d</sup>	<sup>206</sup> Pb <sup>d</sup>	<sup>206</sup> Pb <sup>d</sup>	<sup>206</sup> Pb <sup>d</sup>	<sup>206</sup> Pb <sup>d</sup>	<sup>206</sup> Pb <sup>d</sup>
Zr-014-D-IV-01	0.0164	0.46	10.40778	1.98	0.42368	1.91	0.96	0.17816	0.53	2277	44	2636	14	86										
Zr-014-D-IV-02	0.0004	0.42	9.57525	2.44	0.40749	2.29	0.94	0.17042	0.85	2203	50	2562	22	86										
Zr-014-D-IV-03	0.0003	0.30	0.73553	2.88	0.08897	1.58	0.55	0.05996	2.41	549	9	602	15	91										
Zr-014-D-IV-04 b	0.0008	0.87	0.63507	3.45	0.07955	1.89	0.55	0.05790	2.89	493	9	526	15	94										
Zr-014-D-IV-04 a	0.0010	1.68	0.61359	2.84	0.07726	2.42	0.85	0.05760	1.49	480	12	514	8	93										
Zr-014-D-IV-05	0.0058	0.66	1.28471	4.07	0.13750	2.17	0.53	0.06777	3.44	831	18	861	30	96										
Zr-014-D-IV-06	0.0016	0.49	0.65579	4.47	0.08239	2.23	0.50	0.05773	3.87	510	11	519	20	98										
Zr-014-D-IV-07	0.0010	0.53	1.35106	3.43	0.14007	2.48	0.72	0.06996	2.37	845	21	927	22	91										

Zr-014-D-IV-08	0.0045	1.31	0.77327	8.67	0.09580	3.84	0.44	0.05854	7.77	590	23	550	43	107
Zr-014-D-IV-09	0.0009	0.93	0.63814	4.55	0.07988	2.13	0.47	0.05794	4.02	495	11	528	21	94
Zr-014-D-IV-10	0.0010	0.42	0.63013	3.19	0.07966	2.07	0.65	0.05737	2.43	494	10	506	12	98
Zr-014-D-IV-11	0.0008	0.43	13.34784	1.37	0.52237	1.19	0.87	0.18532	0.68	2709	32	2701	18	100
Zr-014-D-IV-12	0.0009	0.43	0.78047	3.31	0.09616	1.69	0.51	0.05887	2.85	592	10	562	16	105
Zr-014-E-V-10	0.0005	1.44	0.60431	4.67	0.07630	2.68	0.57	0.05744	3.82	474	13	509	19	93
Zr-014-E-V-13	0.0004	0.41	1.46172	2.03	0.14805	1.10	0.55	0.07161	1.70	890	10	975	17	91
Zr-014-E-V-14	0.0007	0.82	0.63792	3.48	0.08038	2.57	0.74	0.05756	2.35	498	13	513	12	97
Zr-014-D-IV-13	0.0007	0.18	0.73508	2.85	0.09017	1.87	0.66	0.05913	2.15	557	10	572	12	97
Zr-014-E-V-01	0.0015	0.64	0.69259	3.42	0.08634	2.41	0.71	0.05818	2.43	534	13	536	13	100
Zr-014-E-V-02	0.0003	0.14	0.65809	2.75	0.08242	2.22	0.81	0.05791	1.62	511	11	526	9	97
Zr-014-E-V-03	0.0007	0.30	0.69994	3.06	0.08571	1.75	0.57	0.05923	2.50	530	9	575	14	92
Zr-014-E-V-04	0.0003	0.74	20.94848	1.08	0.60452	1.00	0.93	0.25133	0.41	3048	30	3193	13	95
Zr-014-E-V-05	0.0003	0.21	6.52627	2.71	0.37730	1.49	0.55	0.12545	2.26	2064	31	2035	46	101
Zr-014-E-V-06	0.0007	0.45	1.48343	2.02	0.15505	1.37	0.68	0.06939	1.49	929	13	910	14	102
Zr-014-E-V-07	0.0025	0.49	6.87996	1.65	0.36256	1.45	0.88	0.13763	0.79	1994	29	2198	17	91
Zr-014-E-V-08	0.0010	0.98	0.56019	3.20	0.07098	2.05	0.64	0.05724	2.46	442	9	501	12	88
Zr-014-E-V-09	0.0018	0.87	0.34204	3.89	0.04681	3.03	0.78	0.05300	2.44	295	9	329	8	90
Zr-014-E-V-10	0.0005	1.44	0.60431	4.67	0.07630	2.68	0.57	0.05744	3.82	474	13	509	19	93
Zr-014-E-V-13	0.0004	0.41	1.46172	2.03	0.14805	1.10	0.55	0.07161	1.70	890	10	975	17	91
Zr-014-E-V-14	0.0007	0.82	0.63792	3.48	0.08038	2.57	0.74	0.05756	2.35	498	13	513	12	97
Zr-014-F-VI-01	0.0007	0.53	1.42984	2.15	0.14693	1.81	0.84	0.07058	1.17	884	16	945	11	93
Zr-014-F-VI-02	0.0003	0.86	5.58490	1.52	0.33421	1.09	0.72	0.12120	1.06	1859	20	1974	21	94
Zr-014-F-VI-05	0.0002	0.21	0.72177	2.58	0.08918	1.84	0.71	0.05870	1.81	551	10	556	10	99
Zr-014-F-VI-06	0.0013	1.10	0.29831	7.05	0.04210	4.31	0.61	0.05139	5.58	266	11	258	14	103
Zr-014-F-VI-07	0.0008	0.96	0.70563	3.71	0.08876	3.27	0.88	0.05766	1.75	548	18	517	9	106
Zr-014-F-VI-08	0.0003	0.32	0.61300	3.09	0.07752	2.36	0.76	0.05736	1.99	481	11	505	10	95
Zr-014-F-VI-09	0.0013	0.66	0.62686	3.10	0.08050	2.50	0.81	0.05648	1.83	499	12	471	9	106
Zr-014-F-VI-10	0.0002	0.13	0.69604	2.50	0.08673	1.85	0.74	0.05821	1.69	536	10	538	9	100
Zr-014-F-VI-11	0.0001	0.64	1.92415	1.41	0.18491	0.94	0.67	0.07547	1.04	1094	10	1081	11	101
Zr-014-F-VI-12	0.0002	0.84	0.71776	4.19	0.08951	3.04	0.73	0.05816	2.88	553	17	536	15	103
Zr-014-F-VI-13	0.0002	0.43	13.01071	2.16	0.53942	1.89	0.88	0.17493	1.03	2781	53	2605	27	107
Zr-014-F-VI-15	0.0009	0.52	0.91738	3.26	0.10798	1.81	0.56	0.06162	2.70	661	12	661	18	100

Zr-014-G-VII-01	0.0011	0.19	0.70747	3.52	0.08767	1.92	0.54	0.05853	2.95	542	10	550	16	99
Zr-014-G-VII-02	0.0056	1.74	0.76629	2.95	0.09304	2.59	0.88	0.05973	1.40	573	15	594	8	97
Zr-014-G-VII-03	0.0009	0.80	1.78732	3.10	0.17523	1.45	0.47	0.07398	2.74	1041	15	1041	28	100
Zr-014-G-VII-04	0.0016	0.57	0.72610	3.05	0.08931	2.13	0.70	0.05897	2.19	551	12	566	12	97
Zr-014-G-VII-05	0.0003	0.09	1.00783	2.40	0.11696	1.84	0.77	0.06250	1.54	713	13	691	11	103
Zr-014-G-VII-06	0.0014	0.52	1.70884	3.97	0.16940	2.51	0.63	0.07316	3.08	1009	25	1018	31	99
Zr-014-G-VII-09	0.0014	0.55	1.61810	3.40	0.16538	3.05	0.90	0.07096	1.50	987	30	956	14	103
Zr-014-G-VII-10	0.0004	0.18	6.74020	1.43	0.38455	1.19	0.83	0.12712	0.79	2097	25	2059	16	102
Zr-014-G-VII-11	0.0002	0.37	6.42142	1.92	0.36533	1.61	0.84	0.12748	1.05	2007	32	2063	22	97
Zr-014-G-VII-12	0.0005	0.14	0.73254	2.87	0.08949	2.08	0.73	0.05937	1.97	553	12	581	11	95
Zr-014-G-VII-14	0.0007	0.55	0.73898	2.85	0.08992	1.76	0.62	0.05960	2.24	555	10	589	13	94
Zr-014-G-VII-15	0.0011	1.23	0.77310	2.15	0.09368	1.49	0.69	0.05985	1.55	577	9	598	9	97
Zr-014-H-VIII-01	0.0001	0.38	10.86511	1.30	0.45583	0.94	0.72	0.17287	0.90	2421	23	2586	23	94
Zr-014-H-VIII-02	0.0004	1.32	6.86047	0.95	0.38213	0.74	0.78	0.13021	0.60	2086	15	2101	13	99
Zr-014-H-VIII-03	0.0002	0.23	0.71674	2.06	0.08951	1.62	0.79	0.05807	1.27	553	9	533	7	104
Zr-014-I-IX-07	0.0014	0.56	0.28114	4.57	0.04036	3.65	0.80	0.05052	2.75	255	9	219	6	116
Zr-014-I-IX-09	0.0007	0.59	0.63082	4.91	0.08054	3.05	0.62	0.05680	3.84	499	15	484	19	103
Zr-014-I-IX-10	0.0005	0.84	6.11442	2.56	0.34982	2.07	0.81	0.12677	1.52	1934	40	2054	31	94
Zr-014-I-IX-12	0.0011	0.62	0.74436	3.05	0.09120	2.23	0.73	0.05919	2.08	563	13	574	12	98
Zr-014-I-IX-13	0.0009	0.49	0.28657	4.80	0.04078	3.28	0.68	0.05096	3.50	258	8	239	8	108
Zr-014-I-IX-14	0.0013	1.17	1.33747	3.97	0.14179	1.46	0.37	0.06841	3.69	855	13	881	32	97
Zr-014-I-IX-15	0.0004	0.02	0.60456	2.37	0.07568	1.56	0.66	0.05794	1.78	470	7	527	9	89

Table 11. Sample PCA 12 – Fluvial sandstone of Sergi Formation, Brotas Group.

Spot number	f206	Th/U <sup>a</sup>	<sup>207</sup> Pb/	1 s	<sup>206</sup> Pb/	1 s	Rho <sup>c</sup>	<sup>207</sup> Pb/	1 s	<sup>206</sup> Pb/	1 s	<sup>207</sup> Pb/	1 s	%
			<sup>235</sup> U	[%]	<sup>238</sup> U	[%]		<sup>206</sup> Pb <sup>d</sup>	[%]	<sup>238</sup> U	abs	<sup>206</sup> Pb	abs	Conc <sup>e</sup>
Zr-015-A-I-02	0.0013	0.99	0.6227	3.87	0.0782	1.82	0.47	0.0578	3.41	485	9	521	18	93
Zr-015-A-I-04	0.0010	0.13	0.7768	2.82	0.0947	2.03	0.72	0.0595	1.96	583	12	586	11	100
Zr-015-A-I-05	0.0020	1.08	1.6065	3.08	0.1626	1.35	0.44	0.0717	2.77	971	13	976	27	99

Zr-015-A-I-06	0.0021	0.29	1.7032	2.36	0.1665	1.22	0.52	0.0742	2.02	993	12	1047	21	95
Zr-015-A-I-07	0.0005	0.27	0.7071	3.07	0.0876	1.47	0.48	0.0585	2.70	541	8	550	15	98
Zr-015-A-I-08	0.0076	0.43	0.6724	2.84	0.0842	1.57	0.55	0.0579	2.37	521	8	528	13	99
Zr-015-A-I-09	0.0039	0.45	1.2116	3.98	0.1262	3.09	0.78	0.0696	2.50	766	24	918	23	83
Zr-015-A-I-11	0.0009	0.59	0.8205	2.89	0.0982	1.30	0.45	0.0606	2.57	604	8	624	16	97
Zr-015-A-I-14	0.0017	1.12	0.2927	4.37	0.0422	3.22	0.74	0.0503	2.96	266	9	211	6	126
Zr-015-A-I-15	0.0046	0.78	0.5638	3.27	0.0730	1.62	0.49	0.0560	2.84	454	7	453	13	100
Zr-015-B-II-01	0.0011	0.88	0.8185	3.27	0.0986	1.20	0.37	0.0602	3.04	606	7	611	19	99
Zr-015-B-II-02	0.0004	1.18	6.2537	1.59	0.3490	0.96	0.61	0.1300	1.26	1930	19	2097	26	92
Zr-015-B-II-03	0.0009	0.44	0.6163	3.08	0.0777	1.52	0.49	0.0575	2.69	483	7	511	14	95
Zr-015-B-II-04	0.0004	0.81	0.3142	7.40	0.0433	3.49	0.47	0.0527	6.53	273	10	315	21	87
Zr-015-B-II-05	0.0014	0.84	1.4392	3.99	0.1465	2.46	0.62	0.0712	3.14	882	22	964	30	91
Zr-015-B-II-06	0.0084	1.13	0.8509	2.45	0.1006	1.50	0.61	0.0614	1.93	618	9	652	13	95
Zr-015-B-II-07	0.0000	1.32	0.6216	3.93	0.0802	2.98	0.76	0.0562	2.56	497	15	461	12	108
Zr-015-B-II-08	0.0005	0.40	0.6680	3.36	0.0845	1.40	0.42	0.0573	3.05	523	7	504	15	104
Zr-015-B-II-09	0.0012	0.33	0.8247	3.13	0.0985	1.37	0.44	0.0608	2.81	605	8	630	18	96
Zr-015-B-II-10	0.0011	0.55	0.7238	5.62	0.0883	3.35	0.60	0.0594	4.52	546	18	583	26	94
Zr-015-B-II-12	0.0037	0.67	1.5707	3.16	0.1572	1.26	0.40	0.0725	2.90	941	12	999	29	94
Zr-015-B-II-13	0.0009	0.82	1.5066	2.13	0.1501	0.80	0.38	0.0728	1.98	901	7	1008	20	89
Zr-015-C-III-01	0.0019	1.34	0.151766	5.18	0.02283	4.57	0.89	0.0482	2.45	146	7	110	3	132
Zr-015-C-III-02	0.0010	0.30	0.7753	2.90	0.0932	1.26	0.43	0.0603	2.62	575	7	615	16	93
Zr-015-C-III-03	0.0012	0.98	0.6199	2.46	0.0789	1.55	0.63	0.0570	1.90	489	8	491	9	100
Zr-015-C-III-04	0.0004	0.06	0.7215	2.39	0.0893	1.64	0.69	0.0586	1.74	551	9	552	10	100
Zr-015-C-III-05	0.0005	0.46	9.2989	1.50	0.4375	1.09	0.72	0.1541	1.04	2340	25	2392	25	98
Zr-015-C-III-06	0.0004	0.22	0.6729	2.76	0.0850	1.39	0.50	0.0574	2.38	526	7	508	12	104
Zr-015-C-III-07	0.0021	1.30	0.8608	3.20	0.1031	1.74	0.54	0.0605	2.68	633	11	623	17	102
Zr-015-C-III-08	0.0201	0.28	0.6783	5.71	0.0836	3.36	0.59	0.0588	4.62	518	17	561	26	92
Zr-015-C-III-09	0.0205	0.29	12.5231	1.54	0.4789	1.21	0.79	0.1896	0.95	2523	31	2739	26	92
Zr-015-C-III-10	0.0009	0.63	6.5509	1.78	0.3771	1.08	0.60	0.1260	1.42	2063	22	2043	29	101
Zr-015-C-III-12	0.0001	0.98	0.2910	8.73	0.0411	5.16	0.59	0.0513	7.04	260	13	256	18	101
Zr-015-C-III-13	0.0000	0.63	0.4784	5.56	0.0624	2.54	0.46	0.0556	4.95	390	10	436	22	90
Zr-015-C-III-15	0.0010	0.46	4.7526	1.77	0.3230	1.29	0.73	0.1067	1.22	1804	23	1744	21	103
Zr-015-D-IV-01	0.0116	0.37	11.2159	1.46	0.4688	0.70	0.48	0.1735	1.28	2478	17	2592	33	96

Zr-015-D-IV-02	0.0611	1.90	0.6084	4.08	0.0760	2.91	0.71	0.0581	2.87	472	14	533	15	89
Zr-015-D-IV-03	0.0016	0.14	0.7581	2.84	0.0926	1.30	0.46	0.0594	2.52	571	7	581	15	98
Zr-015-D-IV-04	0.0009	0.41	0.6476	3.89	0.0831	1.81	0.47	0.0565	3.44	515	9	473	16	109
Zr-015-D-IV-05	0.0001	0.27	1.3766	3.03	0.1385	1.86	0.61	0.0721	2.39	836	16	989	24	85
Zr-015-D-IV-06	0.0010	0.23	0.6672	3.02	0.0826	1.72	0.57	0.0586	2.49	512	9	552	14	93
Zr-015-D-IV-07	0.0008	0.53	11.3850	2.93	0.4424	2.49	0.85	0.1866	1.55	2362	59	2713	42	87
Zr-015-D-IV-08	0.0006	0.06	0.6297	3.22	0.0795	1.70	0.53	0.0574	2.74	493	8	508	14	97
Zr-015-D-IV-09	0.0064	0.79	0.6413	3.90	0.0790	2.95	0.76	0.0589	2.56	490	14	563	14	87
Zr-015-D-IV-10	0.0009	0.20	1.1000	2.94	0.1237	1.24	0.42	0.0645	2.66	752	9	759	20	99
Zr-015-D-IV-12	0.0024	0.40	4.5847	1.95	0.3091	1.15	0.59	0.1076	1.57	1736	20	1759	28	99
Zr-015-D-IV-13	0.0011	1.48	1.4525	4.65	0.1435	3.17	0.68	0.0734	3.40	865	27	1025	35	84
Zr-015-D-IV-14	0.0003	0.41	9.7676	1.93	0.4488	0.90	0.47	0.1579	1.70	2390	22	2433	41	98
Zr-015-D-IV-15	0.0013	0.21	0.6878	2.90	0.0841	1.91	0.66	0.0593	2.19	520	10	579	13	90
Zr-015-E-V-01	0.0006	0.38	0.6974	3.13	0.0849	1.97	0.63	0.0596	2.44	525	10	588	14	89
Zr-015-E-V-02	0.0014	0.54	0.6911	2.65	0.0845	2.17	0.82	0.0593	1.53	523	11	579	9	90
Zr-015-E-V-03	0.0006	0.89	0.6137	2.75	0.0770	1.80	0.66	0.0578	2.08	478	9	521	11	92
Zr-015-E-V-04	0.0011	0.61	0.6446	2.53	0.0808	1.84	0.73	0.0579	1.74	501	9	526	9	95
Zr-015-E-V-05	0.0010	1.00	0.6264	3.22	0.0789	1.97	0.61	0.0576	2.55	489	10	515	13	95
Zr-015-E-V-06	0.0022	0.66	0.5860	5.45	0.0791	3.69	0.68	0.0537	4.01	491	18	359	14	137
Zr-015-E-V-07	0.0033	0.61	0.6319	4.02	0.0786	1.79	0.45	0.0583	3.59	487	9	543	19	90
Zr-015-E-V-08	0.0006	0.99	0.6090	3.74	0.0763	2.44	0.65	0.0579	2.84	474	12	527	15	90
Zr-015-E-V-09	0.0005	0.45	0.8161	3.32	0.0979	2.09	0.63	0.0605	2.58	602	13	620	16	97
Zr-015-E-V-11	0.0004	0.34	0.5864	2.81	0.0737	1.62	0.58	0.0577	2.29	459	7	517	12	89
Zr-015-E-V-12	0.0004	0.55	6.4321	1.48	0.3612	1.28	0.86	0.1292	0.75	1988	25	2087	16	95
Zr-015-E-V-13	0.0005	0.36	12.6835	1.78	0.4881	1.63	0.91	0.1885	0.72	2563	42	2729	20	94
Zr-015-E-V-14	0.0012	1.74	0.7179	2.33	0.0886	1.66	0.71	0.0588	1.64	547	9	559	9	98
Zr-015-F-VI-01	0.0074	0.65	12.6866	1.44	0.5193	1.08	0.75	0.1772	0.96	2696	29	2627	25	103
Zr-015-F-VI-02	0.0017	0.66	1.4501	3.42	0.1529	1.60	0.47	0.0688	3.02	917	15	893	27	103
Zr-015-F-VI-03	0.0006	0.27	0.6458	2.63	0.0817	1.72	0.65	0.0573	1.99	506	9	504	10	101
Zr-015-F-VI-04	0.0008	0.44	6.6250	2.47	0.3796	1.64	0.66	0.1266	1.85	2074	34	2051	38	101
Zr-015-F-VI-05	0.0051	0.40	0.6803	3.14	0.0842	1.82	0.58	0.0586	2.56	521	10	551	14	95
Zr-015-F-VI-06	0.0008	0.53	12.5645	1.79	0.5038	1.68	0.94	0.1809	0.60	2630	44	2661	16	99

Zr-015-F-VI-07	0.0011	0.44	0.6233	3.64	0.0778	2.14	0.59	0.0581	2.95	483	10	534	16	90
Zr-015-F-VI-08	0.0003	0.23	1.3890	2.24	0.1468	1.12	0.50	0.0686	1.94	883	10	887	17	100
Zr-015-F-VI-09	0.0059	0.49	0.6586	2.55	0.0830	1.50	0.59	0.0576	2.06	514	8	514	11	100
Zr-015-G-VII-01	0.0010	0.61	0.6357	3.39	0.0807	1.93	0.57	0.0572	2.79	500	10	498	14	100
Zr-015-G-VII-02	0.0015	1.11	0.6241	2.92	0.0794	2.16	0.74	0.0570	1.97	492	11	492	10	100
Zr-015-G-VII-03	0.0007	0.14	0.7076	3.20	0.0868	1.64	0.51	0.0591	2.75	536	9	572	16	94
Zr-015-G-VII-04	0.0030	0.43	0.6032	4.65	0.0777	1.99	0.43	0.0563	4.21	483	10	463	19	104
Zr-015-G-VII-05	0.0099	0.36	1.8431	2.68	0.1730	2.13	0.79	0.0773	1.63	1029	22	1128	18	91
Zr-015-G-VII-06	0.0009	0.45	0.7008	3.72	0.0864	2.87	0.77	0.0588	2.36	534	15	560	13	95
Zr-015-G-VII-07	0.0008	0.38	9.5751	3.03	0.4156	2.71	0.89	0.1671	1.36	2240	61	2529	34	89
Zr-015-G-VII-08	0.0009	0.57	4.6257	2.22	0.3125	1.17	0.53	0.1074	1.88	1753	21	1755	33	100
Zr-015-H-VIII-01	0.0005	0.40	8.2498	1.72	0.3621	1.23	0.72	0.1653	1.19	1992	25	2510	30	79
Zr-015-H-VIII-02	0.0063	0.83	0.6298	3.58	0.0788	2.67	0.75	0.0580	2.38	489	13	529	13	92
Zr-015-H-VIII-03	0.0027	0.96	0.6011	4.93	0.0753	2.00	0.40	0.0579	4.51	468	9	525	24	89
Zr-015-H-VIII-04	0.0008	0.43	4.5068	1.60	0.3053	0.94	0.59	0.1071	1.30	1717	16	1750	23	98
Zr-015-H-VIII-05	0.0263	0.58	0.6386	2.97	0.0791	1.95	0.66	0.0585	2.25	491	10	549	12	89
Zr-015-H-VIII-06	0.0007	0.86	0.6176	3.05	0.0784	1.72	0.56	0.0571	2.53	487	8	495	13	98
Zr-015-H-VIII-09	0.0022	0.87	0.6475	3.02	0.0821	2.05	0.68	0.0572	2.21	508	10	500	11	102
Zr-015-H-VIII-10	0.0003	0.38	0.6195	2.47	0.0782	1.38	0.56	0.0575	2.05	485	7	509	10	95
Zr-015-H-VIII-11	0.0011	1.26	0.5911	4.88	0.0759	2.27	0.46	0.0565	4.33	472	11	471	20	100
Zr-015-H-VIII-12	0.0055	0.86	0.5887	4.40	0.0781	3.10	0.70	0.0547	3.13	485	15	399	12	122
Zr-015-H-VIII-13	0.0023	0.93	0.6970	4.62	0.0863	2.09	0.45	0.0585	4.12	534	11	550	23	97
Zr-015-I-IX-01	0.0012	0.90	0.6160	3.85	0.0775	1.94	0.50	0.0577	3.32	481	9	517	17	93
Zr-015-I-IX-02	0.0008	0.48	0.8220	3.85	0.1000	1.95	0.51	0.0596	3.32	614	12	591	20	104
Zr-015-I-IX-04	0.0010	0.56	0.6166	3.27	0.0779	2.20	0.67	0.0574	2.42	484	11	507	12	95
Zr-015-I-IX-05	0.0010	0.87	0.6486	2.26	0.0810	1.58	0.70	0.0581	1.63	502	8	534	9	94
Zr-015-I-IX-06	0.0020	0.80	0.6973	2.93	0.0869	1.84	0.63	0.0582	2.28	537	10	536	12	100
Zr-015-I-IX-08	0.0011	0.84	0.6667	3.84	0.0831	1.78	0.46	0.0582	3.41	515	9	536	18	96
Zr-015-I-IX-10	0.0005	1.95	0.6564	3.40	0.0808	1.68	0.49	0.0589	2.96	501	8	564	17	89
Zr-015-I-IX-11	0.0008	0.87	0.7141	3.30	0.0873	1.57	0.48	0.0594	2.90	539	8	580	17	93
Zr-015-I-IX-13	0.0003	0.43	0.6464	2.52	0.0813	1.25	0.49	0.0577	2.19	504	6	517	11	98
Zr-015-I-IX-14	0.0008	0.27	0.7787	2.66	0.0949	1.38	0.52	0.0595	2.28	584	8	586	13	100
Zr-015-J-X-01	0.0016	0.47	12.5111	1.29	0.5113	1.05	0.81	0.1775	0.76	2662	28	2629	20	101

Zr-015-J-X-02	0.0018	0.71	0.5975	4.48	0.0768	3.05	0.68	0.0564	3.28	477	15	468	15	102
Zr-015-J-X-03	0.0013	1.86	0.5969	5.72	0.0760	2.75	0.48	0.0570	5.01	472	13	490	25	96
Zr-015-J-X-04	0.0013	0.42	0.6331	2.43	0.0785	1.58	0.65	0.0585	1.85	487	8	550	10	89

a.Th/U ratios are calculated relative to GJ-1 reference zircon. b.Corrected for background and within-run Pb/U fractionation and normalised to reference zircon GJ-1 (ID-TIMS values/measured value);  $^{207}\text{Pb}/^{235}\text{U}$  calculated using  $(^{207}\text{Pb}/^{206}\text{Pb})/(^{238}\text{U}/^{206}\text{Pb} * 1/137.88)$ . c.Rho is the error correlation defined as the quotient of the propagated errors of the  $^{206}\text{Pb}/^{238}\text{U}$  and the  $^{207}/^{235}\text{U}$  ratio. d.Corrected for mass-bias by normalising to GJ-1 reference zircon and common Pb using the model Pb composition of Stacey and Kramers (1975). e.Degree of concordance =  $(^{206}\text{Pb}/^{238}\text{U}$  age \*  $100/^{207}\text{Pb}/^{206}\text{U}$  age).

### 3. Lu-Hf Data

Table 12. Results of Lu-Hf analyses from Camamu Basin zircons in PCA 08B and PCA 12 samples.  
 $*^{176}\text{Lu}/^{177}\text{Hf}$  assumed ratio for  $T_{\text{DM}}$  age was the crustal average of 0.015.

Grain	U-Pb (Ma)	$\pm 2s$	$^{176}\text{Hf}/^{177}\text{Hf}$	$\pm 2\text{SE}$	$^{176}\text{Lu}/^{177}\text{Hf}$	$\pm 2\text{SE}$	$^{176}\text{Hf}/^{177}\text{Hf}$ (t)	eHf (t)	$\pm 2\text{SE}$	TDM (Ga)
<b>PCA 08B</b>										
Zr-012-H-VIII-03	486	13	0.282234	0.000079	0.000481	0.000017	0.282230	-8.81	0.55	1.97
Zr-012-H-VIII-05	490	10	0.282172	0.000065	0.000321	0.000006	0.282169	-10.87	0.44	2.10
Zr-012-H-VIII-15	525	8	0.282264	0.000036	0.001082	0.000070	0.282254	-7.09	0.57	1.89
Zr-012-I-IX-05	488	9	0.282262	0.000051	0.000737	0.000013	0.282256	-7.85	0.28	1.91
Zr-012-I-IX-06	495	10	0.282241	0.000062	0.000326	0.000003	0.282238	-8.32	0.24	1.94
Zr-012-M-XIII-01	506	9	0.282291	0.000050	0.000660	0.000030	0.282285	-6.41	0.41	1.83
Zr-012-N-XIV-02	511	10	0.282250	0.000028	0.000425	0.000002	0.282246	-7.69	0.18	1.92
Zr-012-H-VIII-01	565	10	0.282265	0.000039	0.000910	0.000020	0.282256	-6.12	0.25	1.86
Zr-012-H-VIII-02	554	9	0.282290	0.000048	0.002524	0.000237	0.282264	-6.08	0.67	1.85
Zr-012-I-IX-02	948	16	0.281970	0.000058	0.000535	0.000031	0.281961	-7.95	0.60	2.27
Zr-012-I-IX-03	554	8	0.282281	0.000054	0.000698	0.000110	0.282274	-5.73	0.98	1.83
Zr-012-I-IX-04	913	23	0.281822	0.000050	0.000832	0.000003	0.281808	-14.16	0.42	2.63
Zr-012-I-IX-09	904	8	0.281973	0.000033	0.000672	0.000006	0.281961	-8.92	0.16	2.30

<b>Zr-012-J-X-04</b>	834	13	0.282258	0.000053	0.001149	0.000017	0.282240	-0.63	0.02	1.73
<b>Zr-012-J-X-10</b>	990	16	0.282230	0.000035	0.000397	0.000003	0.282222	2.27	0.05	1.67
<b>Zr-012-K-XI-11</b>	676	10	0.282474	0.000068	0.000137	0.000003	0.282472	4.02	0.15	1.31
<b>Zr-012-L-XII-04</b>	825	18	0.282196	0.000048	0.001215	0.000020	0.282177	-3.06	0.12	1.87
<b>Zr-012-M-XIII-03</b>	1001	17	0.282110	0.000030	0.000749	0.000008	0.282095	-1.98	0.05	1.94
<b>Zr-012-M-XIII-04</b>	591	11	0.282304	0.000048	0.001419	0.000062	0.282288	-4.40	0.28	1.77
<b>Zr-012-M-XIII-10</b>	579	10	0.282382	0.000043	0.000367	0.000022	0.282378	-1.49	0.11	1.58
<b>Zr-012-M-XIII-13</b>	990	12	0.282080	0.000023	0.000544	0.000042	0.282070	-3.14	0.28	2.01
<b>Zr-012-H-VIII-11</b>	1998	16	0.281297	0.000028	0.000467	0.000009	0.281279	-8.13	0.21	3.10
<b>Zr-012-H-VIII-13</b>	2076	16	0.281317	0.000034	0.000252	0.000001	0.281307	-5.33	0.07	2.99
<b>Zr-012-J-X-11</b>	2147	36	0.280939	0.000029	0.000335	0.000001	0.280925	-17.26	0.36	3.78
<b>Zr-012-K-XI-01</b>	2093	16	0.281337	0.000045	0.000619	0.000007	0.281312	-4.75	0.09	2.97
<b>Zr-012-K-XI-02</b>	2014	19	0.281289	0.000036	0.000436	0.000006	0.281273	-7.99	0.19	3.11
<b>Zr-012-K-XI-13</b>	1898	16	0.281588	0.000037	0.000238	0.000005	0.281579	0.22	0.01	2.51
<b>Zr-012-L-XII-06</b>	2078	15	0.281085	0.000032	0.000290	0.000007	0.281073	-13.60	0.41	3.50
<b>Zr-012-M-XIII-02</b>	1986	24	0.281293	0.000054	0.000366	0.000006	0.281279	-8.40	0.23	3.11
<b>Zr-012-M-XIII-12</b>	2009	25	0.281461	0.000033	0.000959	0.000071	0.281424	-2.71	0.23	2.77
<b>Zr-012-H-VIII-07</b>	2554	16	0.280995	0.000031	0.000754	0.000018	0.280958	-6.61	0.20	3.44
<b>Zr-012-I-IX-07</b>	2651	28	0.281081	0.000065	0.001061	0.000059	0.281027	-1.87	0.12	3.22
<b>Zr-012-M-XIII-06</b>	2703	13	0.280977	0.000051	0.000811	0.000011	0.280935	-3.96	0.08	3.39
<b>Zr-012-L-XII-07</b>	3095	61	0.280574	0.000038	0.000632	0.000009	0.280537	-8.89	0.30	4.00
<b>PCA 12</b>										
<b>Zr-015-A-I-02</b>	486	9	0.282368	0.000048	0.001005	0.000032	0.282359	-4.23	0.21	1.68
<b>Zr-015-A-I-07</b>	541	8	0.282268	0.000029	0.000567	0.000095	0.282263	-6.42	1.17	1.86
<b>Zr-015-A-I-15</b>	454	7	0.282266	0.000047	0.000343	0.000005	0.282263	-8.36	0.25	1.91
<b>Zr-015-B-II-03</b>	483	7	0.282209	0.000050	0.000594	0.000008	0.282204	-9.80	0.27	2.02
<b>Zr-015-B-II-07</b>	497	15	0.282239	0.000042	0.000572	0.000024	0.282234	-8.42	0.60	1.95
<b>Zr-015-B-II-08</b>	523	7	0.282166	0.000028	0.000389	0.000027	0.282162	-10.38	0.85	2.09

Zr-015-C-III-06	526	7	0.282229	0.000039	0.000290	0.000013	0.282226	-8.04	0.48	1.95
Zr-015-D-IV-02	472	14	0.282244	0.000054	0.000552	0.000023	0.282239	-8.79	0.63	1.95
Zr-015-D-IV-04	515	9	0.282312	0.000040	0.000493	0.000021	0.282307	-5.44	0.33	1.78
Zr-015-D-IV-06	512	9	0.282505	0.000045	0.000132	0.000002	0.282503	1.45	0.05	1.35
Zr-015-D-IV-08	493	8	0.281590	0.000044	0.000290	0.000012	0.281587	-31.42	1.78	3.35
Zr-015-D-IV-09	490	14	0.282216	0.000050	0.000594	0.000013	0.282211	-9.40	0.47	2.00
Zr-015-D-IV-15	520	10	0.282279	0.000031	0.000872	0.000168	0.282271	-6.59	1.40	1.85
Zr-015-E-V-01	525	10	0.282266	0.000042	0.001472	0.000093	0.282251	-7.18	0.59	1.89
Zr-015-E-V-02	523	11	0.282140	0.000043	0.000251	0.000004	0.282138	-11.24	0.41	2.14
Zr-015-E-V-03	478	9	0.282228	0.000048	0.000318	0.000002	0.282225	-9.15	0.22	1.98
Zr-015-E-V-04	501	9	0.282205	0.000052	0.000407	0.000004	0.282201	-9.49	0.27	2.02
Zr-015-E-V-05	489	10	0.282264	0.000050	0.000407	0.000008	0.282260	-7.66	0.31	1.90
Zr-015-E-V-08	474	12	0.282173	0.000051	0.000301	0.000006	0.282170	-11.19	0.52	2.10
Zr-015-E-V-11	459	7	0.282221	0.000039	0.000577	0.000013	0.282216	-9.92	0.38	2.01
Zr-015-F-VI-03	506	9	0.282216	0.000057	0.000247	0.000013	0.282214	-8.94	0.62	1.99
Zr-015-F-VI-07	483	10	0.282223	0.000044	0.000582	0.000039	0.282218	-9.31	0.82	1.99
Zr-015-F-VI-09	514	11	0.282216	0.000045	0.000541	0.000030	0.282211	-8.86	0.69	1.99
Zr-015-G-VII-01	498	14	0.282262	0.000037	0.001034	0.000028	0.282253	-7.73	0.43	1.91
Zr-015-G-VII-02	492	10	0.281969	0.000037	0.000668	0.000037	0.281963	-18.13	1.39	2.54
Zr-015-G-VII-06	534	15	0.282227	0.000039	0.001066	0.000096	0.282216	-8.21	0.97	1.97
Zr-015-H-VIII-02	489	13	0.282250	0.000041	0.000519	0.000020	0.282245	-8.21	0.54	1.93
Zr-015-H-VIII-05	491	10	0.282181	0.000039	0.000406	0.000016	0.282177	-10.56	0.63	2.08
Zr-015-H-VIII-06	487	8	0.282280	0.000030	0.000530	0.000005	0.282275	-7.18	0.19	1.87
Zr-015-H-VIII-09	508	10	0.282255	0.000027	0.000316	0.000003	0.282252	-7.52	0.21	1.90
Zr-015-H-VIII-10	485	7	0.282123	0.000037	0.000502	0.000002	0.282119	-12.77	0.24	2.21
Zr-015-I-IX-01	481	9	0.282217	0.000040	0.000440	0.000017	0.282213	-9.50	0.55	2.00
Zr-015-I-IX-04	484	11	0.282140	0.000036	0.000460	0.000019	0.282136	-12.18	0.77	2.17
Zr-015-I-IX-05	502	8	0.282269	0.000040	0.000215	0.000007	0.282267	-7.13	0.35	1.87

<b>Zr-015-I-IX-06</b>	537	10	0.282280	0.000034	0.000640	0.000022	0.282274	-6.12	0.33	1.84
<b>Zr-015-I-IX-08</b>	515	9	0.282266	0.000034	0.000374	0.000004	0.282262	-7.03	0.20	1.88
<b>Zr-015-I-IX-10</b>	501	8	0.282143	0.000036	0.000425	0.000033	0.282139	-11.68	1.10	2.15
<b>Zr-015-I-IX-11</b>	539	8	0.282279	0.000042	0.001425	0.000208	0.282264	-6.40	1.03	1.86
<b>Zr-015-I-IX-13</b>	504	6	0.282246	0.000030	0.000451	0.000002	0.282241	-8.00	0.12	1.93
<b>Zr-015-J-X-04</b>	487	8	0.282140	0.000038	0.000864	0.000029	0.282132	-12.23	0.61	2.18
<b>Zr-015-A-I-04</b>	583	12	0.282254	0.000039	0.001470	0.000118	0.282238	-6.34	0.64	1.89
<b>Zr-015-A-I-05</b>	971	13	0.281678	0.000052	0.000519	0.000030	0.281668	-17.79	1.28	2.90
<b>Zr-015-A-I-11</b>	624	16	0.282361	0.000046	0.000418	0.000009	0.282356	-1.25	0.06	1.60
<b>Zr-015-B-II-05</b>	964	30	0.281882	0.000038	0.000789	0.000020	0.281867	-10.89	0.62	2.47
<b>Zr-015-C-III-04</b>	551	9	0.282307	0.000037	0.000520	0.000048	0.282302	-4.82	0.52	1.77
<b>Zr-015-C-III-07</b>	623	17	0.282340	0.000050	0.001158	0.000099	0.282326	-2.33	0.26	1.67
<b>Zr-015-D-IV-03</b>	571	7	0.282234	0.000053	0.001150	0.000060	0.282221	-7.21	0.46	1.93
<b>Zr-015-E-V-09</b>	620	16	0.282284	0.000033	0.000159	0.000008	0.282283	-3.94	0.31	1.77
<b>Zr-015-E-V-14</b>	547	9	0.282278	0.000034	0.001348	0.000047	0.282264	-6.24	0.32	1.85
<b>Zr-015-F-VI-02</b>	893	27	0.282186	0.000049	0.001080	0.000039	0.282167	-1.87	0.12	1.85
<b>Zr-015-G-VII-03</b>	572	16	0.282257	0.000032	0.001487	0.000049	0.282241	-6.50	0.40	1.89
<b>Zr-015-I-IX-02</b>	614	11	0.282077	0.000040	0.000773	0.000020	0.282069	-11.65	0.51	2.24
<b>Zr-015-I-IX-14</b>	584	8	0.282255	0.000043	0.001139	0.000022	0.282242	-6.18	0.20	1.88
<b>Zr-015-B-II-01</b>	611	19	0.282527	0.000058	0.002604	0.000110	0.282497	3.44	0.25	1.30
<b>Zr-015-B-II-06</b>	652	13	0.282501	0.000044	0.000976	0.000025	0.282489	4.10	0.19	1.29
<b>Zr-015-B-II-09</b>	630	18	0.282422	0.000043	0.000620	0.000013	0.282414	0.96	0.05	1.47
<b>Zr-015-B-II-12</b>	999	29	0.282369	0.000036	0.000366	0.000010	0.282362	7.44	0.42	1.35
<b>Zr-015-C-III-02</b>	575	7	0.282458	0.000042	0.000426	0.000011	0.282454	1.11	0.04	1.42
<b>Zr-015-D-IV-05</b>	989	24	0.282438	0.000063	0.000383	0.000102	0.282431	9.65	2.82	1.20
<b>Zr-015-D-IV-10</b>	759	20	0.282568	0.000028	0.000293	0.000001	0.282564	9.16	0.26	1.06
<b>Zr-015-A-I-01</b>	1386	53	0.281804	0.000030	0.002197	0.000121	0.281747	-5.59	0.52	2.47
<b>Zr-015-B-II-13</b>	1008	20	0.281734	0.000044	0.001369	0.000088	0.281708	-15.53	2.20	2.79

<b>Zr-015-G-VII-05</b>	1128	18	0.282243	0.000037	0.000795	0.000090	0.282226	5.52	0.95	1.57
<b>Zr-015-B-II-02</b>	2097	26	0.281188	0.000038	0.000190	0.000011	0.281180	-9.35	0.67	3.26
<b>Zr-015-C-III-05</b>	2392	25	0.281048	0.000046	0.001040	0.000055	0.281001	-8.88	0.56	3.46
<b>Zr-015-C-III-10</b>	2043	29	0.281218	0.000037	0.000761	0.000019	0.281188	-10.31	0.40	3.27
<b>Zr-015-C-III-15</b>	1744	21	0.281370	0.000045	0.000522	0.000006	0.281352	-11.39	0.27	3.11
<b>Zr-015-D-IV-12</b>	1759	28	0.281779	0.000041	0.000963	0.000017	0.281747	2.99	0.10	2.22
<b>Zr-015-D-IV-14</b>	2433	41	0.281018	0.000047	0.000782	0.000007	0.280982	-8.60	0.22	3.47
<b>Zr-015-E-V-12</b>	2087	16	0.281089	0.000044	0.000541	0.000007	0.281068	-13.58	0.28	3.51
<b>Zr-015-F-VI-04</b>	2051	38	0.281190	0.000063	0.000437	0.000006	0.281173	-10.66	0.34	3.30
<b>Zr-015-H-VIII-04</b>	1750	23	0.281681	0.000037	0.001026	0.000016	0.281647	-0.80	0.02	2.45
<b>Zr-015-D-IV-01</b>	2592	33	0.280973	0.000048	0.000496	0.000010	0.280949	-6.06	0.20	3.43
<b>Zr-015-D-IV-07</b>	2713	42	0.280946	0.000040	0.000521	0.000007	0.280919	-4.27	0.13	3.42
<b>Zr-015-E-V-13</b>	2729	20	0.281043	0.000035	0.000585	0.000007	0.281013	-0.57	0.01	3.20
<b>Zr-015-F-VI-01</b>	2627	25	0.281043	0.000061	0.001388	0.000077	0.280973	-4.37	0.29	3.36
<b>Zr-015-F-VI-06</b>	2661	16	0.281105	0.000045	0.001020	0.000020	0.281053	-0.74	0.02	3.16
<b>Zr-015-G-VII-07</b>	2529	34	0.281090	0.000038	0.000674	0.000015	0.281058	-3.66	0.13	3.24
<b>Zr-015-J-X-01</b>	2629	20	0.281007	0.000041	0.000881	0.000012	0.280963	-4.69	0.10	3.38

## Anexo A. Resumo Publicado no 45º Congresso Brasileiro de Geologia



### APLICAÇÃO DA METODOLOGIA Lu-Hf EM ZIRCÃO POR LA-ICP-MS

Anelise Losangela Bertotti<sup>1</sup>; Farid Chemale Jr.<sup>2</sup>; Paul J. Sylvester<sup>3</sup>

<sup>1</sup> UNIVERSIDADE FEDERAL DO RIO GRANDE DO SUL; <sup>2</sup> UNIVERSIDADE FEDERAL DE SERGIPE; <sup>3</sup> MEMORIAL UNIVERSITY OF NEWFOUNDLAND

**RESUMO:** Nas duas últimas décadas devido ao grande avanço na espectrometria de massa de fonte de plasma, o sistema isotópico de Lu-Hf tem sido vastamente utilizado na Geologia. Com uma meia vida longa de 35,9 Ga, este sistema mostra-se adequado para traçar a história do sistema solar e a evolução do manto-crosta da Terra. A metodologia Lu-Hf em zircão pode ser usada em estudos de proveniência como um indicador petrogenético, pois nele são preservadas as razões isotópicas iniciais de Hf. Além do mais, o zircão é um mineral com uma geoquímica de grande potencialidade, resistente aos processos de erosão, transporte e até mesmo eventos de metamorfismo de alto grau, preservando idades de cristalização magnética e metamórfica obtidas pelo sistema U-Pb. Dessa forma, Lu-Hf e U-Pb combinados num mesmo grão de zircão formam uma ferramenta importante para a Geocronologia, pois permitem a diferenciação de episódios magnéticos de acreção de material do manto juvenil daqueles que simplesmente reciclam a crosta existente (Gérides & Zeh, 2006). As análises in-situ de Lu-Hf deste trabalho foram feitas utilizando o ICP-MS Neptune (ThermoFinnigan) e o laser Excimer 193 nm Geolas (Lambda Physik), ambos equipamentos do MAF-IIC da Memorial University of Newfoundland. Os dados isotópicos de Lu-Hf foram adquiridos pelo modo estático numa duração de 150 s, freqüência de 10 Hz, energia de 5 J/cm<sup>2</sup> e com furo de 49 µm. A cada sete análises de grãos, os padrões de zircão Plesovice e 91150 foram analisados para avaliar estabilidade e reproduzibilidade do equipamento. Durante as análises, as intensidades do 176Lu e do 176Yb foram monitoradas e corrigidas para não interferirem no 176Hf. As razões isotópicas de Yb, Lu e Hf foram corrigidas exponencialmente para fracionamento utilizando as razões 173Yb/171Yb = 1,1301 (Segal et al., 2003) e 179Hf/177Hf = 0,7325 (Patchett & Tatsumoto, 1980) via Excel. Para exemplificar a metodologia de Lu-Hf em zircão por LA-ICP-MS foram selecionadas amostras da Bacia de Ischigualasto - Villa Unión (Argentina), da Bacia de Camamu-Almada (Brasil) e da Bacia de Quebrada Seca (Colômbia), já previamente datadas pela metodologia U-Pb. As idades modelo (TDM) destas amostras foram calculadas baseadas na fonte do manto empobrecido com 176Hf/177Hf = 0,28325 e 176Lu/177Hf = 0,0388 (Andersen et al., 2009). E para cada zircão foram calculadas idades modelo TDM máfica e felsítica que assumem uma composição para o magma parental máfica (Lu/Hf=0,022) ou felsítica (Lu/Hf=0,010) (Pietranik et al., 2008). Os valores de épsilon Hf(t) foram calculados usando a razão 176Hf/177Hf = 0.282785 para CHUR (Bouvier et al., 2008) e a constante de decaimento para 176Lu = 1,867 × 10–11/a proposta por Söderland et al. (2004).

**PALAVRAS-CHAVE:** METODOLOGIA LU-HF; ZIRCÃO; MC-ICP-MS.

## Anexo B. Resumos Publicados no VII SSAGI



### Lu/Hf ANALYSIS IN ZIRCONS FROM ARGENTINEAN TRIASSIC BASINS

Anelise L. Bertotti<sup>1</sup>, Farid Chemale Junior<sup>2</sup>, Paul J. Sylvester<sup>3</sup>

<sup>-1</sup> Programa de Pós-Graduação em Geociências, UFRGS, Porto Alegre, RS, Brazil, <sup>2</sup>Núcleo de Geologia, Universidade Federal de Sergipe, Campus Universitário, CEP 49100-000, São Cristovão-SE  
[farid.chemale@efs.br](mailto:farid.chemale@efs.br), <sup>3</sup>MAF-IIC, MUN, St. John's, NL, Canada [psylvester@mun.ca](mailto:psylvester@mun.ca)

#### INTRODUCTION

The Argentinean Triassic Basins, the Ischigualasto and Cuyo basins, are directly related to the Cuyana Terrane, an allocthonous terrane of Laurentia Supercontinent that it has been accreted to the Gondwana Terrane at 465 Ma and now is exposed in the Argentinean Precordilleran. For this study we dated seven samples from Cerro Morada (Ischigualasto Basin), Rio Blanco and Cerro Pontudo Sub-basins (Cuyo Basin). These samples are represented by volcanic tuffs and lavas in the rift-related Triassic sequence from the mentioned basins. Therefore, the aim of this study is to obtain precise and accurate Hf isotopic data for zircons from Ischigualasto Basin and Cuyo Basin. In situ analysis of U/Pb and Hf isotopes in zircon by laser ablation MC-ICP-MS (LA-MC-ICP-MS) was expanded in the geological community in the last three decades. Furthermore, various studies confirm the importance of U-Pb and Lu-Hf methodologies in geochemistry and demonstrated the potential of the laser ablation-MC-ICPMS (Woodhead et al. (2004), Nebel et al. (2007), Sylvester (2008), Gerdes and Zeh (2006, 2009)). We thus combine U-Pb age and Lu-Hf isotopes in order to understand the tectonic environment of these basins.

#### GEOLOGICAL SETTING

Triassic sedimentary basins in Argentina are distributed along the east of the Andean arc and formed during the final stages of the Gondwanides orogenesis in a dominantly extensional-transstensional tectonic setting (Ramos and Kay, 1991, Spallati, 2001, Zerfass et al., 2004). During Cenozoic time, most of these basins were tectonically affected by the east-vergent Andean thrusts. The Ischigualasto Basin (see Figure 1) is located between the provinces of La Rioja and San Juan in northeastern Argentina, whereas the Triassic-Cretaceous Cuyo Basin is located in the southern portion of the Argentine Precordillera. These basin can be regarded as a Triassic rift, filled with clastic sediments and volcanogenic reversed by compressive deformation of the Andean orogeny (Cenozoic-Recent), and were controlled by inherited Paleozoic sutures (Ramos and Kay, 1991). These basins record at least three main tectono- separated by erosional/angular unconformities, all of them associated with different rift stages (Barredo et al. in prep.).

BERTOTTI ET AL.; Lu/Hf ANALYSIS IN ZIRCONS FROM ARGENTINEAN TRIASSIC BASINS

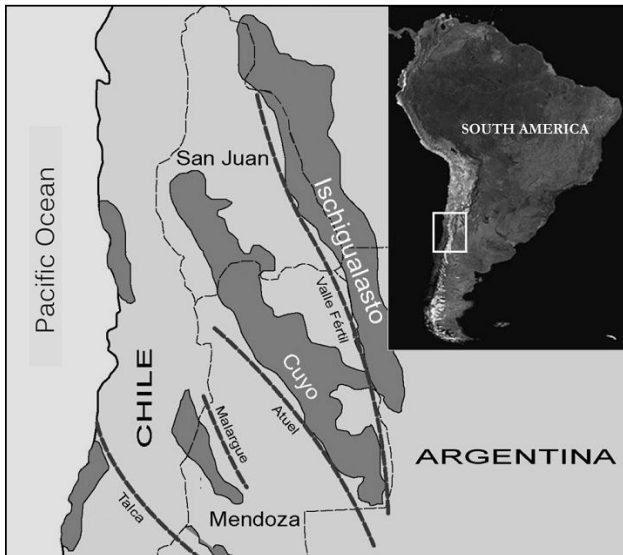


Figure 1 - Geological map of the Ischigualasto and Cuyo Basins (modified after Spalletti, 2001)).

U-Pb zircon dating of volcanic lavas and tuffs interlayered in the sedimentary beds of the Ischigualasto and Cuyo Basin yielded ages from 246 to 227 Ma (Ávila et al. 2006, Mancuso et al. in press, Spalletti 2008, Barredo et al. in prep), while the Sm-Nd WR data suggest as the main source for these basin a Grenvillian material (Ávila et al., 2006, Guadagnin et al., in press).

#### METHOD AND RESULTS

Two mounts of different samples were made for this study and all zircons were mounted in epoxy in 2.5 cm diameter circular grain mounts and polished until the zircons were just revealed. The zircons were analyzed first for U-Pb (Mancuso et al. in press, Barredo et al. in press, Guadagnin et al. in press) and then for Lu-Hf in the same zircon phase (this work). A GeoLas (Laser Excimer 193 nm) coupled to a Neptune MC-ICP-MS at Micro Analysis Facility Inco Innovation Centre (MUN) was used in this study to measure Lu, Yb and Hf isotopic signals. The standard used during Hf analysis was Plešovice. The  $^{176}\text{Lu}$  and  $^{176}\text{Yb}$  were monitored during analysis and subtracted from  $^{176}\text{Hf}$ . Data were corrected in the Excel spreadsheet where the exponential law was used, as well as  $^{179}\text{Hf}/^{177}\text{Hf} = 0.7325$  (Patchett et al., 1981) and  $^{173}\text{Yb}/^{171}\text{Yb} = 1.123456$  (Segal et al, 2003) values.

The Lu-Hf analyses were carried out in all zircons dated for U-Pb, either on the same pit of the U-Pb analysis or closer as possible to the U-Pb pit. Analysis in the samples of Rincon Blanco and Cerro Pontudos sub-basins (Cuyo Basin) samples yielded TDM model



ages between 0.88 to 1.29 Ga and  $\epsilon$ Hf values between -5.6 to -2.47. Tuffs of the basal rift I of the Ischigualasto Basin (249 and 245 Ma old tuffs) yielded Hf model ages between 1.39 to 1.51 Ga and  $\epsilon$ Hf values between -5.89 and -8.68 (Fig. 2).

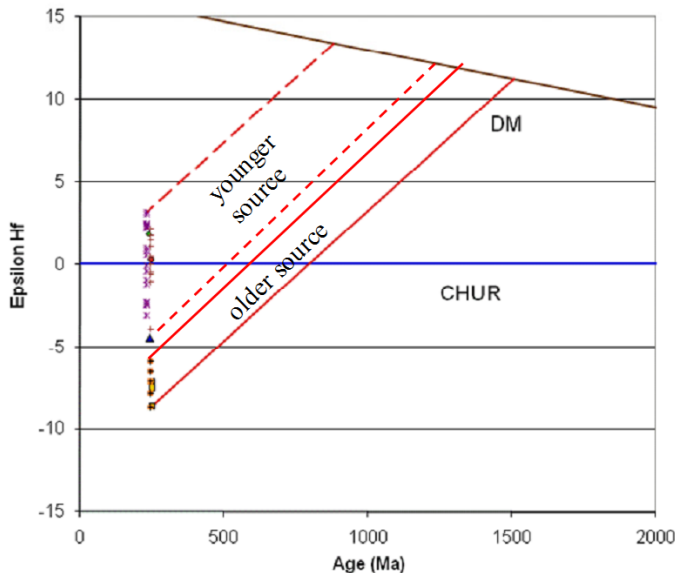


Figure 2 –  $\epsilon$ Hf versus age (Ma) Diagram for the zircon from volcanic rocks and tuffs of the Ischigualasto and Cuyo basins (see text for explanation).

## CONCLUSIONS

Hf isotopes from Rio Blanco and Cerro Pontudo are in agreement with Sm-Nd data from previous studies in Cacheuta sub-basin (Ávila et al. 2006) and provided a Grenvillian age, supporting that source of these sedimentary rocks was a Grenvillian basement (as the Laurentian Margin). Hf model ages allow us to characterize the Cuyo Basin like a source dominantly Grenvillian, supporting the work hypotheses that the Cuyania Terrane was attached to the Laurentia. The Sub-basin Caucheta (in the Cuyo Basin), where Avila et al. (2006) have Sm-Nd, shows a legacy of Grenvillian material. This is confirmed by our new Hf data from the adjacent sub-basins and indicates that the source material was almost exclusively Grenvilliano, which sustains the hypothesis that this crustal fragment is part of Laurentia. While Hf data from Cerro Morada indicates an older source, which implies that we dated the basal units of the Ischigualasto Basin. A previous study in Guadagnin (2005) show Sm-Nd model ages of the basal portion of Cerro Morado region (Rifte I), in the Ischigualasto Basin, fall between 1.33 to 1.60 Ga, that is in perfect agreement the obtained Lu-Hf data.



## REFERENCES

- Ávila, J.N. Chemale Jr., F., Mallmann, G., Kawashita, K., Armstrong, R.A., 2006. Combined stratigraphic and isotopic studies of Triassic strata, Cuyo Basin, Argentine Precordillera. *Bulletin of the Geological Society of America* 118, 1088-1098.
- Barredo, S., Chemale, F., Ávila, J. N., Marsicano, C., Ottone, G. and Ramos V. A. U-Pb SHRIMP ages of the Rincón Blanco northern Cuyo rift, Argentina (submitted to Gondwana Research)
- Chu, N.C., Taylor, R.N., Chavagnac, V., Nesbitt, R.W., Boella, M., Milton, J.A., 2002. Hf isotope ratio analysis using multi-collector inductively coupled plasma mass spectrometry: an evaluation of isobaric interference corrections. *J. Anal. At. Spectrom.* 17, 1567-1574.
- Gerdes, A., Zeh, A. (2006). Combined U-Pb and Hf isotope LA-(MC)-ICP-MS analyses of detrital zircons: Comparison with SHRIMP and new constraints for the provenance and age of American metasediment in central Germany. *Earth and Planetary Science Letters* 249, 47-61.
- Gerdes, A., Zeh, A. 2009. Zircon formation versus zircon alteration – New Insights from combined U-Pb and Lu-Hf in-situ LA-ICP-MS analyses, and consequences for the interpretation of archean zircon from the Central Zone of the Limpopo Belt. *Chemical Geology* 261, 230-243.
- Guadagnin, E., Chemale Jr., F., Dussin, I. A., Shroeder, G. S., Born, C. C. & Guadagnin, F. (2005). Comparação estratigráfica e isotópica (Sm/Nd) das regiões do cerro Morado e la Torre, Bacia do Ischigualasto – Villa Unión, Noroeste Argentino. *Revista de Geociências, Petrobras* (in press).
- Mancuso, A.C., Chemale, F., Barredo, S.P., Ávila, J., Ottone, E.G. and Marsicano, C., 2010. Age constraints for the northernmost outcrops of the Triassic Cuyana Basin, Argentina. *Journal of Southamerican Earth Sciences* (in press).
- Nebel, O., Nebel-Jacobsen, Y., Mezger, K., Berndt, J. 2007. Initial Hf isotope compositions in magmatic zircon from early Proterozoic rocks from the Gawler Craton, Australia: A test for zircon model ages. *Chemical Geology* 241, 23-37.
- Patchett, P.J., Kuovo, O., Hedge, C.E., Tatsumoto, M., 1981. Evolution of continental crust and mantle heterogeneity: evidence from Hf isotopes. *Contrib. Mineral. Petrol.* 78, 279–297.
- Ramos, V.A. and S.M. Kay, 1991. Triassic rifting and associated basalts in the Cuyo basin, central Argentina. In R.S. Harmon y C. W. Rapela (eds.) Andean Magmatism and its Tectonic Setting, Geological Society of America, Special Paper 265: 79-91.
- Spallètti, L.A., Fanning, C.N. y Rapela, C.W., 2008. Dating the Triassic continental rift in the southern Andes, The Potrerillos Formation, Cuyo Basin, Argentina. *Geologica Acta*, V6 (3): 267-283.
- Sylvester, P., 2008. Laser Ablation ICPMS in the Earth Sciences: Current Practices and Outstanding Issues. Vancouver, vol. 40, 348 p.
- Woodhead, J., Herget, J., Shelley, M., Eggins, S., Kemp, R., 2004. Zircon Hf-isotope analysis with an excimer laser, depthprofiling, ablation of complex geometries and concomitant age stimation. *Chemical geology* 209, 121-135.
- Zerfass, H., Chemale, F., Jr., Schultz, C.L., and Lavina, E.L., 2004, Tectonics and sedimentation in southern South America during Triassic: *Sedimentary Geology*, v. 166, p. 265–292.



## U/Pb AND Lu/Hf ANALYSIS IN DETRITAL ZIRCONS FROM CAMAMU-ALMADA BASIN, EAST COAST OF BRAZIL

Anelise L. Bertotti<sup>1</sup>, Farid Chemale Junior<sup>2</sup>, Paul J. Sylvester<sup>3</sup>, Vivian Kayser<sup>1</sup>

<sup>1</sup> Instituto de Geociências, UFRGS, Porto Alegre, RS, Brazil; <sup>2</sup>Núcleo de Geologia, Universidade Federal de Sergipe, Campus Universitário, CEP 49100-000, São Cristovão-SE , <sup>3</sup> MAF-IIC, MUN, St. John's, NL, Canada,

### INTRODUCTION

The Camamu-Almada is a passive-margin basin located at the eastern Brazilian margin and formed due to the rifting and drifting of South America and Africa (Ponte & Asmus, 1978). This basin was deposited on the Paleoproterozoic to Archean basement of the São Francisco-Congo during the Mesocenozoic. Besides the conventional petrographic analyses, detailed study in detrital zircons from the sedimentary rocks of the basin can bring very important information on the source areas and the paleodrainage dispersion, that can be applied to the tectono-sedimentary basin evolution and also to the prediction of hydrocarbon reservoirs. A number of studies (e.g.: Woodhead *et al.* 2004, Gerdes & Zeh 2006) have attempted the measurement of Hf-isotope ratios combined with U-Pb, as well as improvements in situ analytical techniques by ICP-MS, with the potential to unlock the detailed isotopic record preserved in zircons. Therefore, the mineral zircon has a high resistance to erosion and/or secondary metamorphic events through geological time, preserving a high-quality record of near-initial Hf-isotope ratios, which can be used both in provenance studies and as a petrogenetic indicator. In this paper we present U-Pb LA-ICP-MS ages of detrital zircon combined with Hf isotope data to constrain the provenance of the sediment in the Sergi Formation, which forms an important constituent of the Camamu-Almada Basin.

### GEOLOGICAL SETTING

The area of interest in this study is in the Camamu-Almada Basin (see Figure 1). The Camamu-Almada basins are located to the south of the Salvador, in the Bahia state, NE Brazil, formed due to continental rifting and drifting of the South America and Africa continents, lasting from ca. 140 Ma to the present. These basins have similar geological evolution and are characterized by four main tectonic phases (Ponte & Asmus, 1978), as follow: pre-rift, rift, transitional and post-rift tectonic.



The emerse and adjacent basement is represented by the following tectonic terranes: (i) the Itabuna-Salvador Curuçá Block, a Neoproterozoic to Paleoproterozoic block (2.6-2.0 Ga); (ii) Jequié Block, a well constrained Archean Block (2.7-3.4 Ga); (iii) Gavião Block, a Archean Block (2.7-3.4 Ga); (iv) Serrinha Block (2.7-2.9 Ga) and (v) Rio Itapicuru Greenstone Belts (2.0-2.1 Ga). The tectonic structures of the Camamu-Almada Basins were controlled by the pre-existing basement (Netto et al. 1994, Cupertino 2000). The oldest sedimentary units of the Camamu-Almada Basin are the Permian sedimentary rocks of the Afligidos Formation, interpreted to be part of the larger intraplate Paleozoic Basin. On these units are exposed the first depositional units of the Camamu Basin, the pre-rift sequence (Tithonian-Valanginian) associated to the Afro-Brazilian Depression (Ponte & Asmus, 1978). In this basin, the basal Aliança Formation and upper Sergi Formation are the main lithostratigraphic units (Netto et al., 1994). The evolution of the extensional processes resulted in generation of widely and narrow gulf, which were progressively occupied by the protoocean, characterizing the transitional stage (drift) with the first marine sedimentation. It is represented by the upper portion of the Taipus-Mirim Formation with carbonate and evaporites sediments, formed between Eoaptian to Albian. The post-rift sequence is a typical shallow to deep-water passive margin environment.

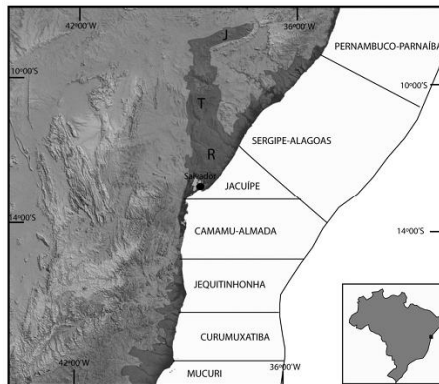


**Figure 1.** SRTM 90 images with the main Mesocenozoic passive margin basins of NE Brazil. The shadow areas correspond to the emerse (on shore) sedimentary units of the basins.

#### METHODS AND RESULTS

We sampled a sedimentary unit of the Sergi Formation on the emerse portion of the Camamu and Almada Basin. The most clear and inclusion-free zircon grains were handpicked and mounted in two epoxy circular grain mounts (2.5 cm diameter) and polished until the zircons were just revealed. The zircons were analyzed first for U-Pb with a Laser Microprobe New Wave 213 nm (UFRGS) and then for Lu-Hf with Laser



Microprobe GeoLas (Laser Excimer 193 nm) (MUN, Canada), both coupled to a Neptune (MC-ICP-MS). The Lu-Hf analysis were exactly in the top of U-Pb analysis. 72 and 102 zircons from PCA-08B and PCA-12 samples were analyzed by the U-Pb in situ method, respectively. The age spectrum for the sample PCA-08B shows six groups of U/Pb ages, two main peaks at 498 Ma (37%) and 590 Ma (29%), three minor peaks at 928 (15%), 2004 (14%) and 2649 (4%) Ma and just one zircon with 3059 Ma (Figure 2). Six groups were recognized in the sample PCA-12, but just one main peak at 518 Ma (69%) and five minor peaks at 890 (11%), 1730 (5%), 2065 (4%), 2390 (3%) and 2651 (8%) Ma.

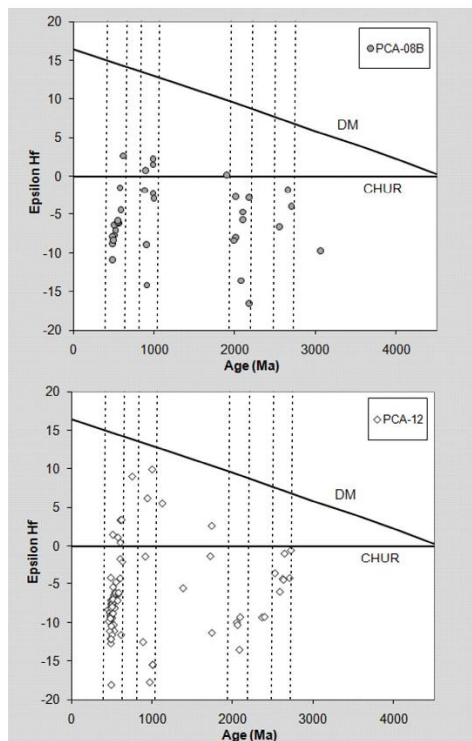


**Figure 2.**  $\epsilon$ Hf evolution diagram showing the results for PCA-08B and PCA-12 zircons. Dotted bars emphasize the four groups of U/Pb age: 500 Ma, 900 Ma, 2000 Ma and 2600 Ma (see text for explanation).



For Hf isotope data from the samples PCA-08B and PCA-12 we analyzed 35 and 78 grains with U/Pb concordant ages, respectively (Fig. 2). In general, the TDM crustal model ages ( $\text{Lu/Hf} = 0.015$ , Goodge & Vervoort, 2006) are between 1.06 to 3.51 Ga and  $\epsilon\text{Hf}$  values varying from -18.1 to +9.0. This distribution of  $\epsilon\text{Hf}$  values suggests that some zircons from Neoproterozoic group were formed in a juvenile magma, but the major population were formed from older or mixed crust (see Figure 2). They are mostly formed during the Rhyacian (Transamazonian Cycle) and Statherian (Paleoproterozoic rifting) ages. In both samples, the Mesoproterozoic zircons have two clear population, one with positive and another with negative values. Most of the Paleoproterozoic zircons were formed by crustal melting of Archean crust, whereas the Archean zircons have slightly negative  $\epsilon\text{Hf}$  values.

### CONCLUSIONS

Both samples show four groups of U/Pb ages, approximately 500-600 Ma (Cambrian-Vendian), 900 Ma (Neoproterozoic), 2000 Ma (Paleoproterozoic) and 2600 Ma (Neoarchean), suggesting a similar source for the analyzed stratigraphic intervals. The Paleoproterozoic and Archean sources are well constrained directly of the adjacent basement. Zircons crystallized around 900 Ma came from those dykes related to the rifting of adjacent Brasiliano Belt. The Cambrian-Vendian zircons are from the southern portion of the Bahia and northern portion of Espírito Santo and Minas Gerais, where are exposed the syn to post-orogenic granites of the Araçuaí Belt. Combining the zircon ages with the zircon  $\epsilon\text{Hf}(t)$  results provides evidence that some detrital zircon grains in the Camamu-Almada Basin crystallized in a juvenile magma, whereas most zircon grains were formed during recycling or contaminated with older crust. Furthermore, we could characterize the main source of the Camamu –Almada Basin in both samples 60 to 70% of the analyzed zircons are with Cambrian-Vendian U/Pb age formed during the Araçuaí Belt with a strong crustal component (Paleoproterozoic zircons remelted during the Brasiliano Cycle).

### REFERENCES

- Gerdes, A., Zeh, A. (2006). Combined U-Pb and Hf isotope LA-(MC)-ICP-MS analyses of detrital zircons: Comparison with SHRIMP and new constraints for the provenance and age of American metasediment in central Germany. *Earth and Planetary Science Letters* 249, 47-61.
- Goodge, J. W., Vervoort, J. D. 2006 Origin of Mesoproterozoic A-type granites in Laurentia: Hf isotope evidence. *Earth and Planetary Science Letters*, 243: 711-731.
- Netto, A. S. T., Wanderley Filho, J. R., Feijó, 1994. Bacias de Jacuípe, Camamu e Almada. Boletim de Geociências da Petrobrás, 8, 173-184.
- Ponte, F. C. & Asmus, H. E. 1978. Geological framework of the Brazilian continental margin. *Geologische Rundschau*, 67: 201-235.
- Woodhead, J., Hergt, J., Shelley, M., Eggins, S., Kemp, R. (2004). Zircon Hf-isotope analysis with an excimer laser, depthprofiling, ablation of complex geometries and concomitant age stimation. *Chemical geology* 209, 121-135.

**Anexo C. Artigo publicado na Revista Precambrian Research**



## Lu–Hf and U–Pb age determination of Capivarita Anorthosite in the Dom Feliciano Belt, Brazil

Farid Chemale <sup>a,\*</sup>, Ruy Paulo Philipp <sup>b</sup>, Ivo Antonio Dussin <sup>c</sup>, Milton Luiz Liquintinie Formoso <sup>b</sup>, Koji Kawashita <sup>c</sup>, Anelise Losangela Berttotti <sup>b</sup>

<sup>a</sup> Laboratório de Geocronologia, Instituto de Geociências, Universidade de Brasília, 70.904-970, Brasília, DF, Brazil

<sup>b</sup> PPGGEO, Instituto de Geociências, Universidade Federal do Rio Grande do Sul, Cx. Postal 15001, 91501-970, Porto Alegre, RS, Brazil

<sup>c</sup> CPGEO, Instituto de Geociências, Universidade de São Paulo, Brazil

### ARTICLE INFO

#### Article history:

Received 10 February 2010

Received in revised form 3 January 2011

Accepted 4 January 2011

Available online 13 January 2011

#### Keywords:

Capivarita Anorthosite

Lu–Hf and U–Pb in situ dating

Mesoproterozoic supercontinent

Brasiliano Cycle

Dom Feliciano Belt

### ABSTRACT

The Capivarita Anorthosite, formed in an intraplate environment and later metamorphosed under amphibolites facies conditions, is exposed in the Dom Feliciano Belt as part of the Brasiliano magmatic arc and occurs as a roof-pedant in, or is even intruded by, 0.6 Ga post-collisional granites. In this work, magmatic and metamorphic minerals were dated using the LA-MC-ICP-MS *in situ* method. U–Pb magmatic and metamorphic zircon dating yielded an age of  $1573 \pm 21$  Ma and of  $606 \pm 6$  Ma, respectively, whereas the igneous titanite dating yielded an age of  $1530 \pm 33$  Ma and the metamorphic ages were  $651 \pm 9$  Ma and  $601 \pm 5$  Ma. The Lu–Hf model ages showed two clusters from 1.81 to 2.03 Ga ( $\epsilon_{\text{Hf}}$  from +2.21 to +6.42) and 2.55–2.62 Ga ( $\epsilon_{\text{Hf}}$  from –4.59 to –5.64). This intraplate magmatism can be connected to a very important episode of continental accretion in an extensional setting from the fragmentation of the supercontinent during the Early Mesoproterozoic.

© 2011 Elsevier B.V. All rights reserved.

### 1. Introduction

Anorthosites are unique rocks in the geological cycle and are mainly exposed in the Archean to Mesoproterozoic terranes widespread in North America, Africa, Europe and Antarctica. These magmatic rocks were also very important at the beginning of the solar system and can be found in the Moon's crust (Heather and Dunkin, 2003; Takeda et al., 2006).

Worldwide anorthosite occurrences can be grouped mainly into two genetic types namelybodies caused by mantle magma differentiation (e.g., Mayer et al., 2004; Wilson and Overgaard, 2005; Morse, 2006; Drüppel et al., 2007) and those derived from crustal rock melting (e.g. Kruger et al., 2000; Geringer et al., 1998; Bogdanova et al., 2004; Duschene et al., 2007). It is noteworthy that the period when most larger anorthosite bodies were generated in the Earth's crust was from 2.1 to 0.9 Ga (e.g. Morse, 2006). Consequently, anorthosites were very important rocks in the reconstruction and evolution of older continents, especially the Columbia and Rodinia, during the earlier stages of continental fragmentation and the final stages of the continental consolidation or post-collisional period (Rogers and Santosh, 2002; Zhao et al., 2004; Zhai and Liu, 2003; Mukherjee and Das, 2002).

The Capivarita Anorthosite is an earlier crustal unit in the Dom Feliciano Belt (DFB), an orogenic belt formed during the assembly of West Gondwana in the Brasiliano-Pan-African cycle (Neoproterozoic to Eopaleozoic). It was first described by Tessari and Picada (1966) and Ribeiro et al. (1966). Later, Formoso and Carraro (1968) characterized the main petrographic and mineralogical characteristics as well as the kaolin alteration product for industrial uses. Fernandes et al. (1988) recognized the tectono-metamorphic processes that acted on the anorthosite and adjacent ortho and para-derived gneissic complexes. A more comprehensive work was presented by Philipp et al. (in press), who defined this body as a typical intraplate igneous complex affected by the Brasiliano orogeny. To date, however, there is no reliable or direct dating of the metamorphosed anorthosite complex. The only available isotopic data are K–Ar age of  $568 \pm 28$  Ma (Formoso, 1973) and  $610 \pm 18$  Ma (Teixeira, 1982) and an Nd Model age of 2.02 Ga, which is interpreted as the maximum age of this complex (Babinski et al., 1997). Although the Capivarita Anorthosite is situated in the orogenic Brasiliano-Pan-African Belt as basement sept, the precise age of the magmatism and deformation can reveal very important clues to the reconstruction of Rio de Plata, Kahalari and São-Francisco-Congo Paleoplates or earlier continents before the fragmentation, dispersion and agglutination of the syn-Brasiliano-Pan-African cratons associated with the West Gondwana assembly.

In this work, we dated the Capivarita Anorthosite by *in situ* LA-MC-ICP-MS on zircon and titanite grains in order to determine the

\* Corresponding author. Tel.: +55 79 21056305.

E-mail addresses: faridchemale@gmail.com, fchemale@unb.br (F. Chemale).

range of the igneous and metamorphic ages of the body situated in the Dom Feliciano Belt, an orogenic belt formed during the Neo-proterozoic (860–540 Ma). A discussion of the significance of the obtained ages with respect to the West Gondwana evolution is also presented herein.

## 2. Sampling and analytical methods

After field mapping and petrographic studies, we collected four samples for isotope analyses: two anorthosite samples, one amphibolite sample and one metagabbro sample. Because we found few

zircons in the 100 kg anorthositic samples from the Porteirinha and Santo Antonio farms, we resampled the outcrops twice, and brought around 500 kg of each sample to the lab for new mineral separation. The selected samples were crushed and milled using a jaw crusher and pulverizer. The heavy minerals zircon, titanite and baddeleyite were separated by conventional procedures using heavy liquids and a magnetic separator after concentration by hand panning. The most clear and inclusion-free minerals were handpicked for U-Th-Pb and Lu-Hf laser ablation MC-ICP-MS analyses. A detailed description of analytical procedures is in Appendix I.

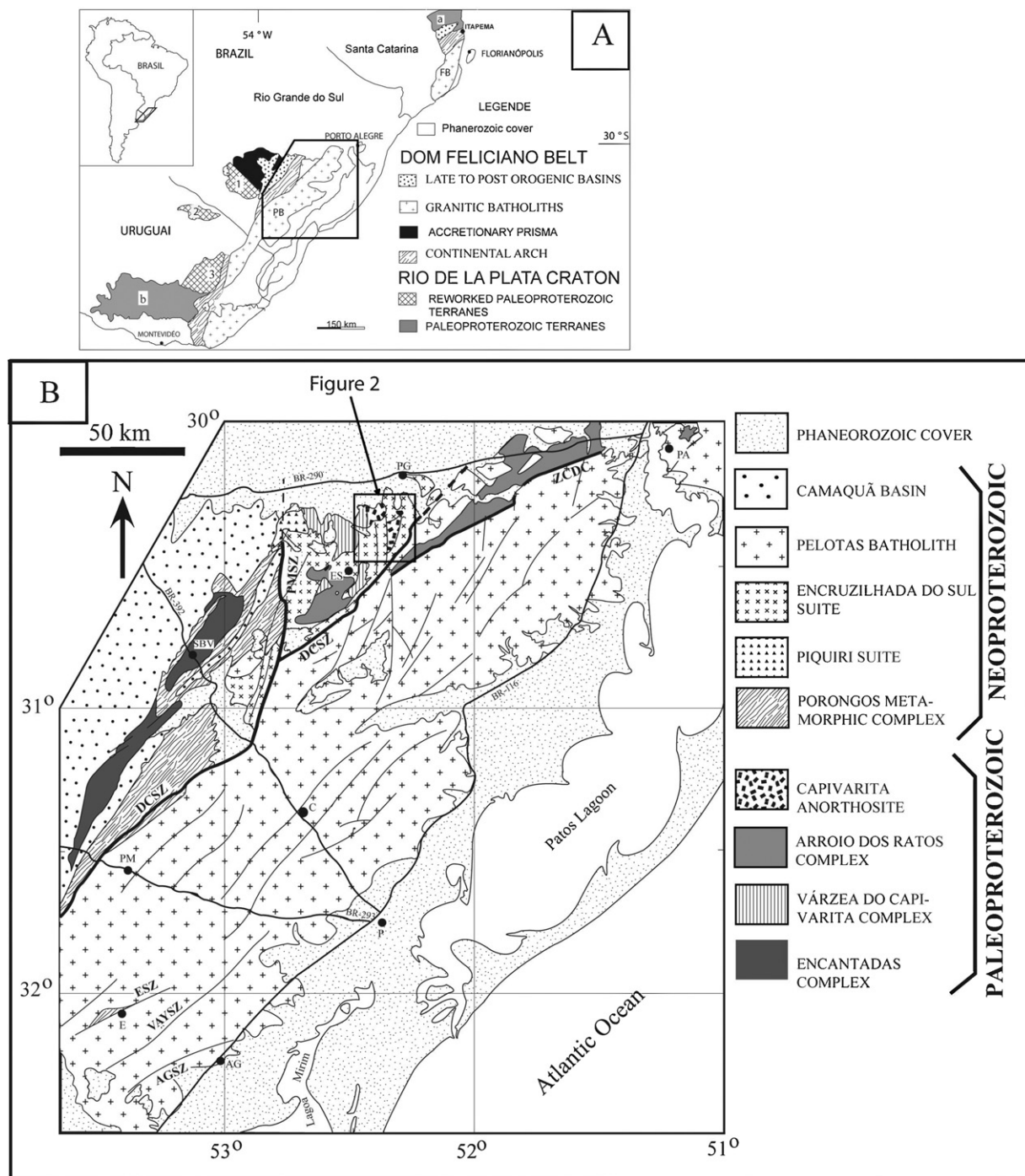


**Fig. 1.** (A) Main tectonic units of southern Brazil and Uruguay. a = Luis Alves Terrane, b = Piedras Altas Terrane, 1 = Taquarembó Terrane, 2 = Rivera Terrane, 3 = Valentines Terrane (modified after Chemale, 2000). (B) Geologic map of central part of the Dom Feliciano Belt with insert of Fig. 2 (after Philipp et al., 2005).

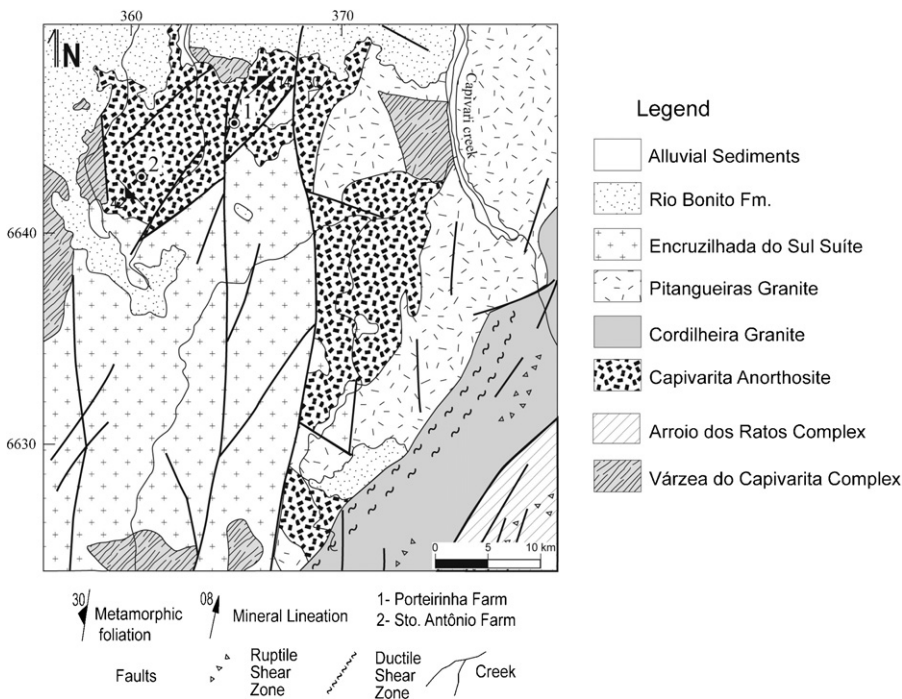


**Fig. 2.** Geological map of the Encruzilhada do Sul region (modified from Ramgrab et al., 1993).

### 3. Geological setting

The Capivarita Anorthosite occurs in the Capivarita region, Pântano Grande municipality, in the NE portion of the Sul-Rio-Grandense Shield, Rio Grande do Sul state, Brazil. It is believed to belong to the basement rocks of the Neoproterozoic granitic suites of Pelotas Batholith (Babinski et al., 1997; Chemale, 2000; Silva et al., 2005), as part of the Dom Feliciano Belt (Fig. 1).

The Dom Feliciano Belt formed during the Neoproterozoic to Eopaleozoic due to the agglutination of the Kahalari, Congo and Rio de La Plata Paleoplates (e.g.: Fernandes et al., 1992; Chemale et al., 1995). It consists of four major associations: (i) the juvenile accreted terrane, the São Gabriel or Vila Nova Terrane, situated in the west portion of the Dom Feliciano Belt (Babinski et al., 1996), which is represented mainly by ophiolites, calc-alkaline arc-related rocks, passive margin or back-arc sedimentation slices formed from 0.9 to 0.7 Ga (Leite et al., 1998; Hartmann et al., 2000). It is interpreted by Chemale (2000) as a Neoproterozoic accretionary prisma (Fig. 1A), (ii) the NE-SW trending volcano-sedimentary association with crustal blocks of Archean and Paleoproterozoic granite-gneisses (Hartmann et al., 2000, 2001; Silva et al., 2005), Mesoproterozoic (e.g. Gaucher et al., 2010) and Neoproterozoic metavolcanosedimentary sequences (Mallmann et al., 2007) as part of Brasiliano continental arch with septa of Archean to Mesoproterozoic basement rocks, (iii) granite-gneissic magmatic arch formed from 650 Ma to 540 Ma pre-, syn and post-collisional granite, gneisses and migmatites, 780–750 Ma tonalitic xenoliths and septa of Paeloproterozoic basement rocks in the eastern portion of the DFB (Babinski et al., 1997; Leite et al., 2000; Silva et al., 2005; Passarelli et al., 2010). This magmatic arch is ca. 800 km long and 150 km wide, represented by the Florianópolis (Silva et al., 2005) and Pelotas (Philipp and Machado, 2005) batholiths and Cutilllo Dionísio Terrane (Bossi et al., 1998), exposed from Uruguay to southern Brazil (Rio Grande do Sul and Santa Catarina states) (Fig. 1A).

In the Pelotas Batholith, which is the eastern granitic batholith of the Dom Feliciano Belt in the Rio Grande do Sul state, Brazil

(Fig. 1B), the exposed Capivarita Anorthosite consists of two main bodies, oriented W-E and N-S (Fig. 2). The anorthosite bodies are part of a triangle-shaped block, known as Encruzilhada do Sul Block, that is bordered to the SE by the Dorsal do Cangaçu Shear Zone (denoted DCSZ in Fig. 1A), to the west by the Passo do Marinheiro Shear Zone (denoted PMSZ in Fig. 1A) and to the north by the Phanerozoic sediments. In this block are the exposed Capivarita Anorthosite and Paleoproterozoic basement rocks (Fig. 2) that metamorphosed under medium amphibolite to granulite facies. The Paleoproterozoic basement units are represented by the Al-rich, calc-silicate and quartz-feldspar paragneisses of the Várzea Capivarita and orthogneisses of the Arroio dos Ratos Complexes (Fernandes et al., 1990). The magmatic ages of the orthogneisses of the Arroio dos Ratos Complex are Paleoproterozoic (ca. 2.0–2.1 Ga) (Leite et al., 2000; Silva et al., 2005) with juvenile signature. Silva et al. (2005) determined the metamorphism of this complex to be  $631 \pm 13$  Ma (U-Pb SHRIMP zircon data). These units are intruded by calc-alkaline and K-rich calc-alkaline to alkaline granites (Fig. 2) formed between 650 and 550 Ma (Babinski et al., 1997; Philipp and Machado, 2005), and are related to orogenic and post-orogenic processes in the Brasiliano Dom Feliciano Belt.

The main body of the Capivarita Anorthosite is situated to the NW and is structured as a roof pendant in the 595 Ma old post-collisional Encruzilhada do Sul Granite (Babinski et al., 1997), which is covered to the north by the Paleozoic sediments of the Paraná Basin. A close relationship with the Capivarita Anorthosite is shown by smaller occurrences of paragneisses of the Varzea da Capivarita Complex. Although both units have the same metamorphic grade, i.e., medium to upper amphibolite facies, the contact between these units is tectonic. The second body, an N-S elongated one, is a roof pendant in Pitangueiras Granite, which is coeval to the Encruzilhada do Sul Granite (Fig. 2). The Capivarita Anorthosite is in tectonic contact with the Brazilian (Neoproterozoic) granites, or is intruded by these granites. Besides K-Ar ages, the only isotope data for the anorthosite are a Sm-Nd data set with  $T_{DM} = 2.04$  Ga (Babinski et al., 1997).

#### 4. Field relationships

Two areas of the main body of the Capivarita Anorthosite outcropping are situated in the Porteirinha and Santo Antonio farms (denoted locations 1 and 2, respectively, in Fig. 2). They are large outcrops containing boulders with lengths of ten to one hundred meters. Anorthosite is the dominant lithotype, but there are subordinate occurrences of garnet anorthosites, metagabbros, amphibolites and thin layers of Fe-Ti oxide-rich rocks.

These units were affected by an orogenic metamorphic event, a display partial obliteration of igneous structures and magmatic texture replacement by metamorphic processes. However, the preserved primary structures have been described often in the literature (Philipp et al., in press).

The Capivarita Anorthosite is of a homogeneous type with light gray color; it is medium- to coarse-grained and has an equigranular texture and mafic content ranging from 2 to 5%. The main structure is irregular and has discontinuous mm-thick banding defined by the hornblende aggregate plus some titanite and Fe-Ti oxide (ilmenite and magnetite), grossular and rare diopside (Fig. 3A). The hornblende is oriented with the regional tectonic which generated a mineral lineation. This tectonic fabric is correlated with the main regional deformational phase of the Várzea Capivarita Complex defined by Gross et al. (2006).

In the Porteirinha Farm, an anorthositic tabular body between 7 and 20 m thick with pegmatoid texture and plagioclase crystals can be found. The large pegmatoid layers are from 2 to 4 cm-thick and exhibit a preserved early igneous texture. Zircon crystals are often included in the large plagioclase and titanite crystals of the pegmatoid layers.

It is very common to find mafic bodies, such as metagabbro or amphibolite, in the anorthosite. The metagabbro layers are 1–5 m thick, tabular and concordant with primary banding. Their boundaries are defined by curvilinear to interlobbed shapes with some reentrance and apophyses (Fig. 3B and C). Exposed in the main anorthositic outcrop in the Santo Antonio Farm is one deformed, 2-m thick, black amphibolite body with metamorphic foliation concordant with anorthosite banding and marked by the orientation of the hornblende crystals. The hornblende grains are in a nematic-blastic texture arrangement that also defines the regional mineral lineation.

#### 5. Petrography and geochemistry

##### 5.1. Anorthosite

The Capivarita Anorthosite is characterized by the presence of plagioclase and low amphibole, titanite, ilmenite and magnetite contents. In the Porteirinha farm outcrop, a garnet aggregate, which is related to metamorphic processes, is also found (up to 1%). The primary textual aspect of the anorthosite is medium- to coarse-grained blastoequigranular to blastoinequigranular with megacrystals or porphyroclasts of plagioclase in tabular shapes from 5 to 30 mm.

The igneous textures can be recognized by the relict plagioclase grains, which constitute 20–55% and are surrounded by metamorphic plagioclase aggregates in an equigranular polygonal granoblastic arrangement (Fig. 4A). The textural variations have a layered structure composed of 2–7-m thick layers of alternating equigranular (grain size between 5 and 10 mm) and inequigranular anorthosite. The latter contains megacrysts between 2 and 5 cm in size contained in the equigranular matrix. The interstitial spaces are occupied by aggregates of hornblende, titanite, ilmenite and magnetite and by isolated crystals of grossular, titanite, hornblende and diopside. Under the microscope, the plagioclase crystals exhibit

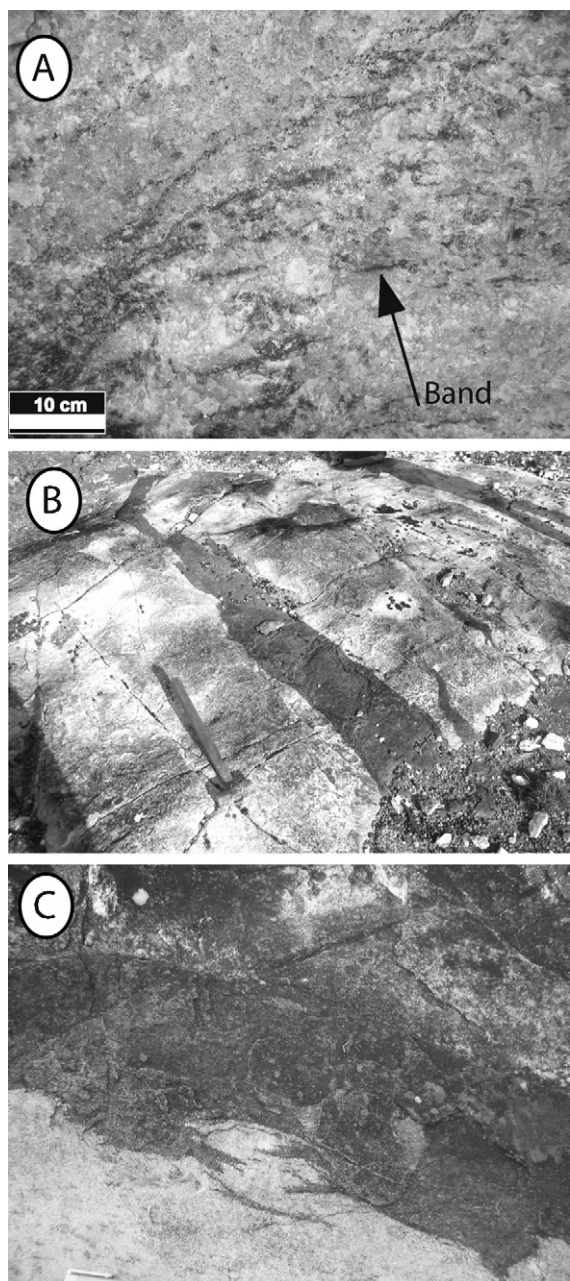


**Fig. 3.** (A) Typical weak-developed banding marked by mafic minerals in the anorthosite. (B) Contact relationship of mafic rocks and anorthosite. Tabular metagabbro bodies with interlobbed boundaries and apophyses suggesting contemporaneous magmatism in ductile conditions; (C) detail of intrusive (comagmatic) relationships with small apophyses of the metagabbro.

interpenetrating contacts, polysynthetic twinning, and complex normal zonation and euhedral inclusions of titanite, zircon and rare grossular (Fig. 4B). There is a secondary cumulitic texture marked by interstitial plagioclase grains in the intercumulus portion with ameboid shapes, interlobbed boundaries and interpenetrative contacts. A protoclastic texture is revealed by the deformed plagioclase porphyroclasts with subgrain formation, lamellae deformation of the polysynthetic twins and ondulose extinction. This evidence can be interpreted as a deformation process in the ductile conditions associated with later cooling and/or late movement of the anorthosite massif-like crystal mush.

The dominant metamorphic texture is a polygonal, equigranular to inequigranular, medium to coarse (0.4–1 mm) granoblastic

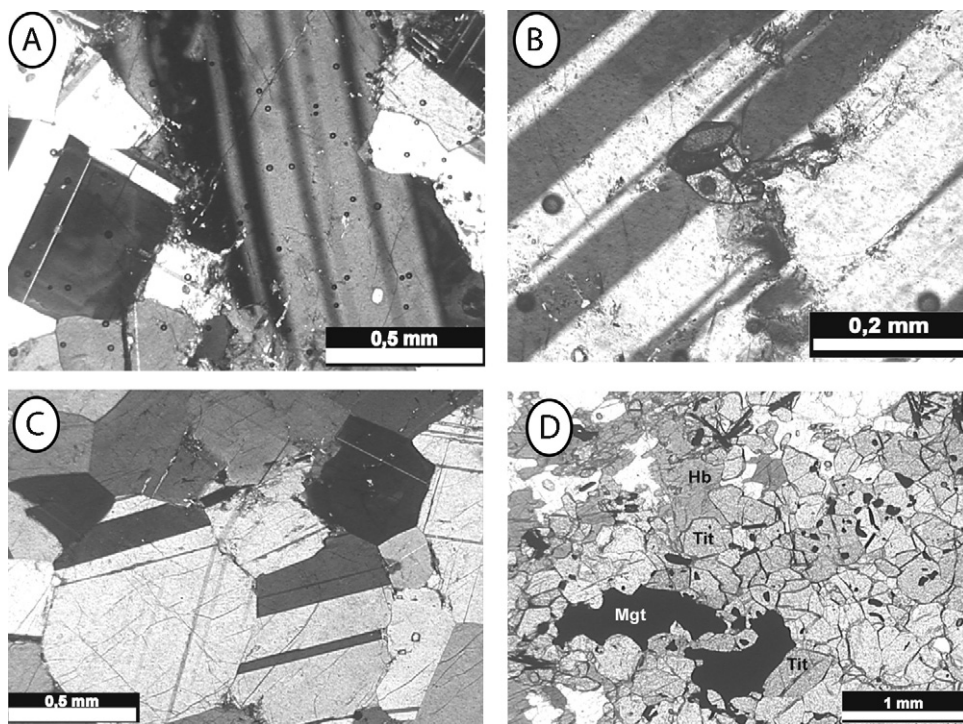


**Fig. 4.** Main petrographic features of Capivari Anorthosite. (A) Primastic-shaped, relict plagioclase grain surrounding by smaller recovered grains, (B) euhedral sphenite titanite inclusions in relict plagioclase, (C) inequigranular, polygonal granoblastic texture and (D) interrupted mafic string as an aggregate of hornblende (Hb), titanite (Tit) and magnetite (Mgt) producing a polygonal granoblastic texture.

texture with a polygonal-shaped plagioclase and polysynthetic twinning (Fig. 4C). An arrangement of titanite, magnetite and ilmenite with polygonal granoblastic texture was also found (Fig. 4D). Recovery plagioclase grains occur with internal zonation and boundaries well-defined by two or three straight faces or interlobbed to curvilinear shapes also occur. The metamorphic mineral paragenesis is plagioclase, hornblende, diopside, grossular, titanite and Fe-Ti oxides that indicate conditions with a minimum temperature equivalent to the medium amphibolite facies of the regional orogenic metamorphism (Butcher and Frey, 1994). The presence of orthopyroxene in the country rocks suggests that the entire package achieved granulite facies conditions.

In the external limits of the anorthositic bodies and in the xenoliths, there is a hydrothermal alteration related to the intrusion of Encruzilhada do Sul ( $594 \pm 5$  Ma, Babinski et al., 1997) and Pitangueiras granites that resulted in the generation of low temperatures and hydrated mineralogy (Fig. 2). This alteration is represented by an irregular cm-thick band in which the composition of the original plagioclase changes to white mica, chlorite, pistacite; the hornblende changes to chlorite, pistacite and opaque minerals and the grossular changes to chlorite and clinozoizite.

Chemical analyses of the plagioclase reveal the dominant presence of labradorite and limited occurrence of anorthite. The latter is only seen in anorthosite with garnet (Formoso, 1973; Philipp et al., in press).

## 5.2. Metagabbros and amphibolites

The metagabbros possess a medium (1–3 mm) grained, blasto-inequigranular texture defined by a crystal fabric of hornblende and biotite with interstitial labradorite, titanite, apatite and magnetite. A medium to coarse grained (0.3–1.2 mm) nematoblastic texture with a dimensional orientation of subidioblastic hornblende, and, to a lesser extent, diopside, are the main textural aspects of the amphibolites. A polygonal arrangement of plago-

clase, diopside, titanite, ilmenite and magnetite as a symplectic texture was also observed in the amphibolitic layers. The latter texture was interpreted to be a modified igneous texture due to metamorphism. However, the diopside growths at the hornblende rims point to progressively increasing metamorphism. Indeed, the metamorphic assemblage of hornblende + labradorite + diopside for mafic lithotypes indicates conditions with a minimum temperature equivalent to medium amphibolite facies and low pressure conditions (Butcher and Frey, 1994). The plagioclases of amphibolites are also labradorite (Formoso, 1973).

## 6. Isotope results

The minerals that were analyzed from samples CAP-010-08 (coarse-grained anorthosite), CAP-009-08 (amphibolite) and CAP-008-08 (metagabbro). We dated zircon, titanite and baddeleyite grains from sample CAP-010-08 and titanite from samples CAP-009-08 and CAP-008-08 using the U-Pb and Lu-Hf methods. The analytical data are presented in Appendices A–C.

### 6.1. Sample CAP-010-08—coarse anorthosite

We separated zircon, baddeleyite and titanite using optical and electronic microscopes. We separated 37 zircon, 2 baddeleyite and 15 titanite grains and analyzed them by MEV.

Based on U-Pb isotope data, zircon grains were divided into three main groups: (i) inherited zircons ( $2028 \pm 17$  Ma), (ii) igneous zircons ( $1573 \pm 21$  Ma), and (iii) metamorphic zircons ( $606.4 \pm 5.9$  Ma) (Fig. 5). The igneous zircons have Th/U ratios from 0.3 to 0.77, whereas the ratios of the metamorphic grains range from 0.07 to 0.17. The baddeleyite yielded a  $^{207}\text{Pb}/^{206}\text{Pb}$  age of  $608 \pm 14$  Ma, which is herein also interpreted as the metamorphic age. It is noteworthy that the metamorphic zircons occur as individual crystals and as overgrowth on 1.57 Ga igneous zircon (Fig. 6). The titanites comprise two groups, one darker and the

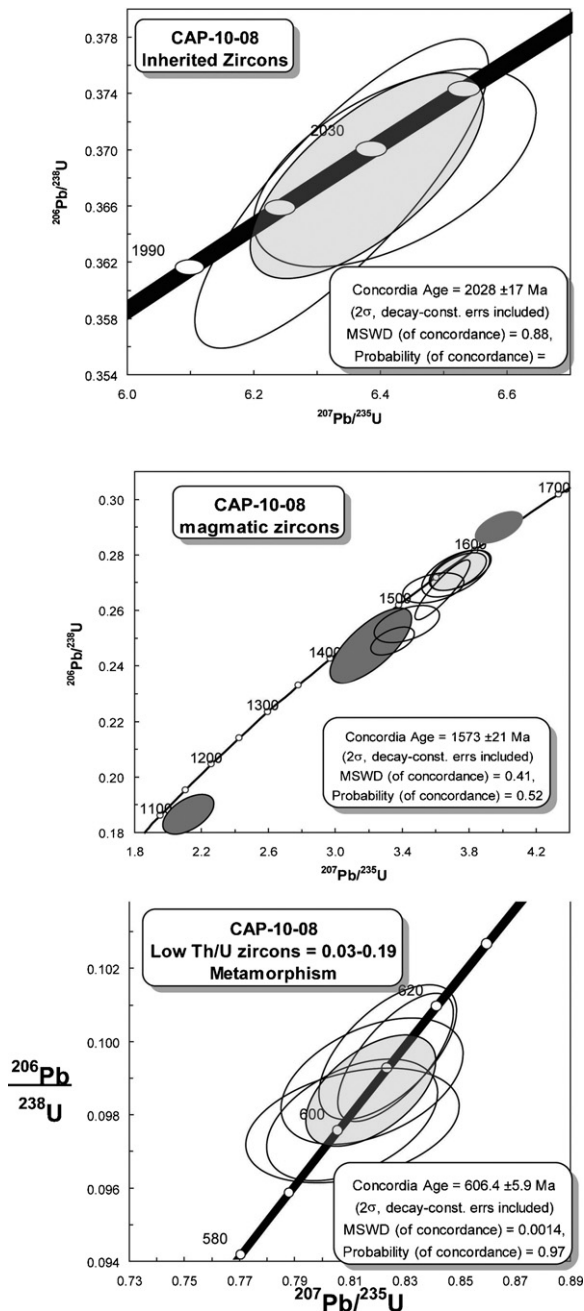


**Fig. 5.** Concordia diagram for Capivarita Anorthosite (sample CAP-10-08) with inherited, magmatic and metamorphic zircons.

other lighter, but all analyzed grains contain large amounts of common Pb. The measured ages were  $599.1 \pm 5.2$  Ma and  $651.5 \pm 8.8$  Ma (Fig. 7). These were interpreted to be metamorphic ages based on regional relationships and the measured metamorphic ages for metamorphic rocks and amphibolite facies minerals of the surrounding Várzea da Capivarita Complex (see Fig. 2) as presented by Gross et al. (2006). In Figs. 5 and 7, we show the concordia diagrams for the igneous and metamorphic ages obtained by U-Pb zircon and titanite dating.

To obtain information about the provenance of the zircon, we carried out Lu-Hf in situ LAM-ICP-MS analyses in the zircons that were chosen for U-Pb dating. The igneous zircon grains present two groups of  $T_{DM}$  and Epsilon Hf (for  $t = 1.57$  Ga) values (Appendix C). The juvenile zircons had Hf model ages ranging from 1.81 to 2.03 Ga and  $\epsilon$ Hf from +2.21 to +6.42. The second group are reworked zir-

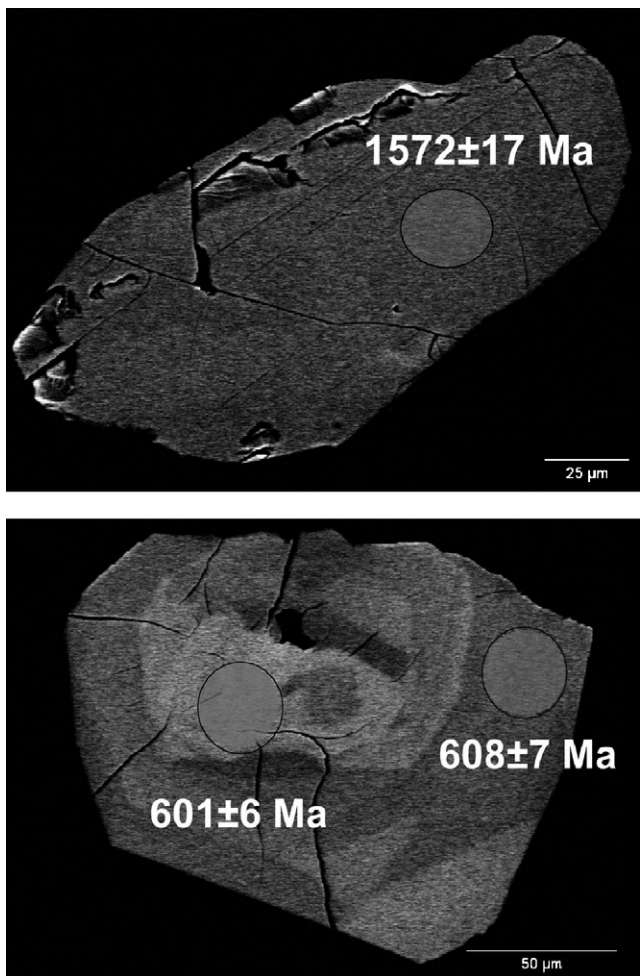


**Fig. 6.** BSE images of the magmatic and metamorphic zircons (sample CAP-10-08) analyzed by LA-MC-ICP-MS with indication of spots and obtained U-Pb ages.

cons from a Paleoproterozoic source with Hf model ages between 2.55 and 2.62 Ga and  $\epsilon$ Hf from -4.59 to -5.64 (Fig. 8). All dated metamorphic zircons have  $T_{DM}$  and similar to those of the crustal zircons with Hf model ages ranging from 2.47 to 2.54 and  $\epsilon$ Hf values from -15.34 to -16.58 for time of metamorphic recrystallization (0.6 Ga). The baddeleyite grain (Zr-170-A-I-02) displays similar values as those of the metamorphic zircons with Hf model age of 2.45 Ga (see Appendix C).

## 6.2. Sample CAP-009-08—Metagabbro

The next sampled rock we will discuss corresponds to the metagabbro, from which titanite grains were separated. Based on microscopic and MEV analyses, it was possible to distinguish two main groups of titanite (Fig. 9). The first was made up of lighter titanite grains and yielded an age of  $1530 \pm 33$  Ma, which means it was formed during the igneous event of the anorthosite generation and emplacement (Fig. 10). The second group corresponded to darker titanites and yielded an age of  $601.2 \pm 5.2$  Ma, which we interpreted as the metamorphic age of the titanite. While the metamorphic titanite grains have large amounts of common Pb, the igneous titanite grains are almost free of common Pb.

## 6.3. Sample CAP-008-08—Amphibolite

This rock sample is an amphibolite with a large amount of titanite. The separated titanite grains were dated using the LA-MC-

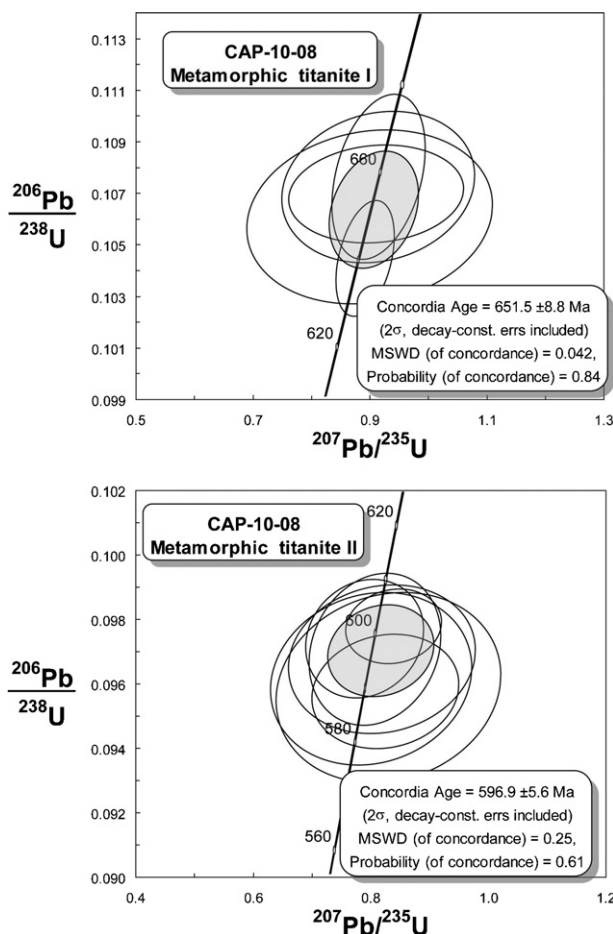


**Fig. 7.** U-Pb LA-MC-ICP-MS titanite results. Concordia diagram of two first metamorphic titanite phases (titanite I and titanite II) for Capivari Anorthosite (sample CAP-10-08).

ICP-MS in situ method. We recognized two main titanite growth phases for this sample (Fig. 11). One of these growth phases formed at  $596.8 \pm 5.6 \text{ Ma}$  and the other at  $564.0 \pm 3.8 \text{ Ma}$ . In both cases, the titanite grains contain a large amount of common Pb. There are also titanite phases corresponding to the metamorphic events that occurred in the region.

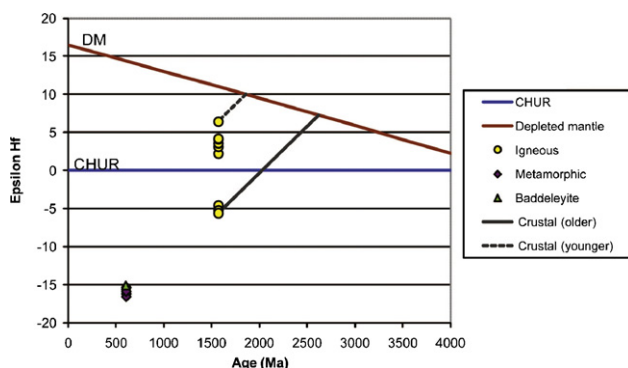


**Fig. 8.** Lu-Hf diagram Epsilon Hf(*i*) vs. age plot of sample CAP-10-08. Depleted mantle (DM) growth curve from Bodet and Schärer (2000). CHUR, chondritic uniform reservoir. All Hf isotope data were calculated using a decay constant of  $1.93 \times 10^{-11} \text{ year}^{-1}$  (Blichert-Toft and Albarède, 1997)  $^{176}\text{Lu}$  decay constant from Scherer et al. (2001). To calculate initial epsilon Hf values, we used the ages determined by U-Pb LA-ICP-MS concordant age of sample CAP-10-08.

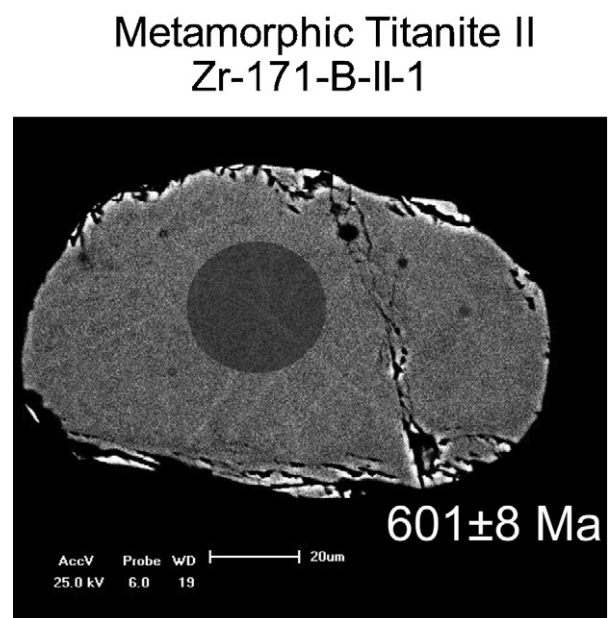
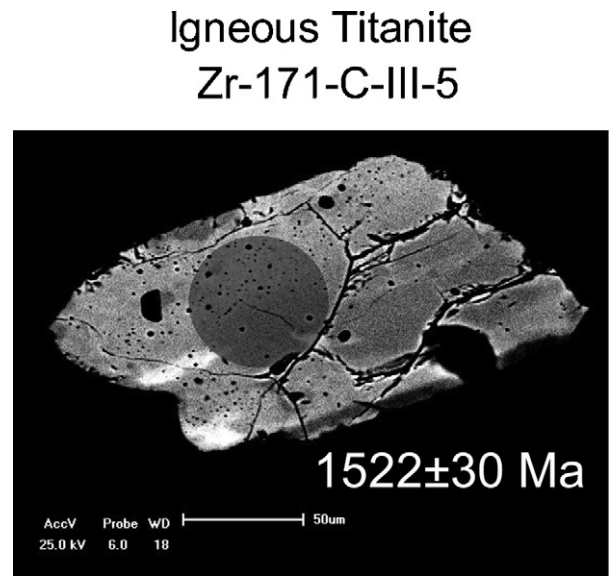


**Fig. 9.** BSE images of the magmatic and metamorphic titanite phases of sample CAP-09-08, analyzed by LA-MC-ICP-MS with indication of spots and obtained U-Pb ages.

## 7. Discussion of results

The primary structures suggest that the Capivari Anorthosite evolved from tholeiitic magma by a mineral fractionation process, which probably occurred by flotation and filter pressing of plagioclase (Philipp et al., in press). The metagabbros and amphibolites have a close relationship with the anorthosite bodies, which show the same comagmatic and concordant igneous banding as the anorthosites. These features suggest a recurrence of tholeiitic magmatism with felsic and mafic rocks. The regular igneous banding associated with the compositional and textural characteristics, as well as the geochemical information, indicate that the anorthosite crystallizes in a stable environment without expressive tectonic activity.

The age of crystallization of the Capivari Anorthosite is well-constrained by the available isotope data because the igneous

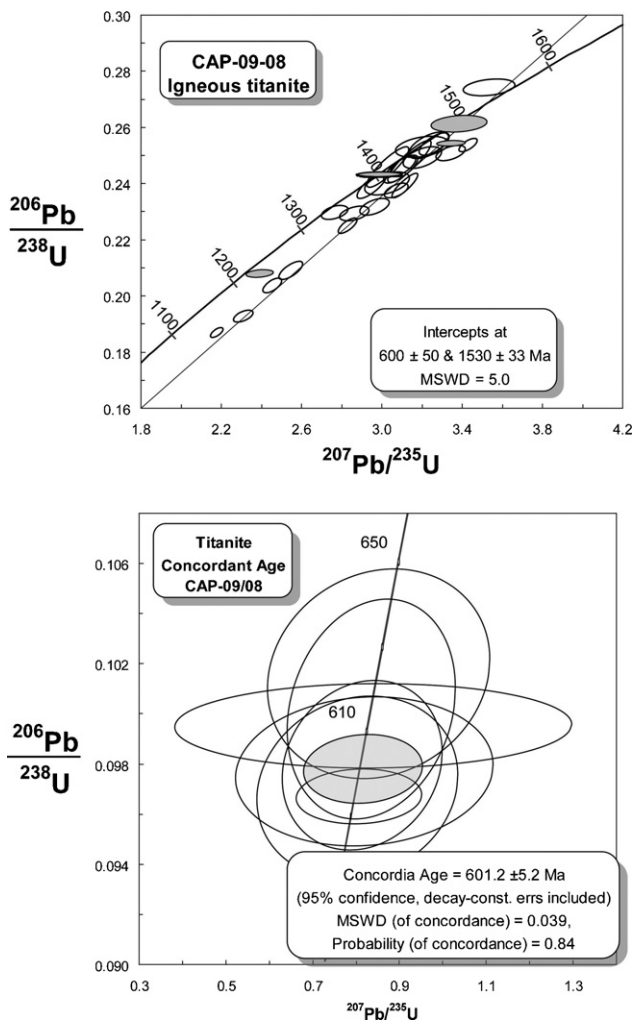


**Fig. 10.** U-Pb LA-MC-ICP-MS titanite results. Concordia diagram for Metagabbro (sample CAP-09-08) of the magmatic titanite phase and the second metamorphic titanite phase (titanite II).

zircons yielded an age of  $1573 \pm 21$  Ma, whereas the igneous titanite of the metagabbro yielded an age of  $1530 \pm 33$  Ma. The younger age of the titanite can be attributed to the lower closing temperature of this mineral compared to zircon. These results can be correlated to a stage of uplift of Capivarita Anorthosite after the crystallization of the complex at 1573 Ma. The present data support the overall temporal distribution of anorthosite complexes in the world. These complexes arose mainly from 1.7 to 1.0 Ga with a major magmatic peak at 1.3 Ga, which is described as the “Goldilocks” scenario for the epoch of massif anorthosites, when the thickness of the crustal lithosphere was not too thin (before 1.8 Ga) and not too thick (after 0.9 Ga) (Morse, 2006).

Additionally, through the analyses of titanite crystal from anorthosite (CAP-010-08), metagabbro (CAP-009-08) and amphibolite (CAP-008-08), where the two mafic tabular bodies cut anorthosite clearly, we were able to determine that they also clearly exhibit relationship of coeval magmatism between the mafic and anorthositic phases. The register of metamorphic events, observed in the Capivarita Anorthosite and comagmatic mafic rocks and the Várzea do Capivarita and Arroio dos Ratos Complexes, represent the latest continental collision events of the Brasiliano Cycle in southernmost Brazil.

We noticed this in the metamorphic processes around 650 Ma and 600 Ma, as was already published for the Dom Feliciano Belt (e.g., Leite et al., 2000; Gross et al., 2006;

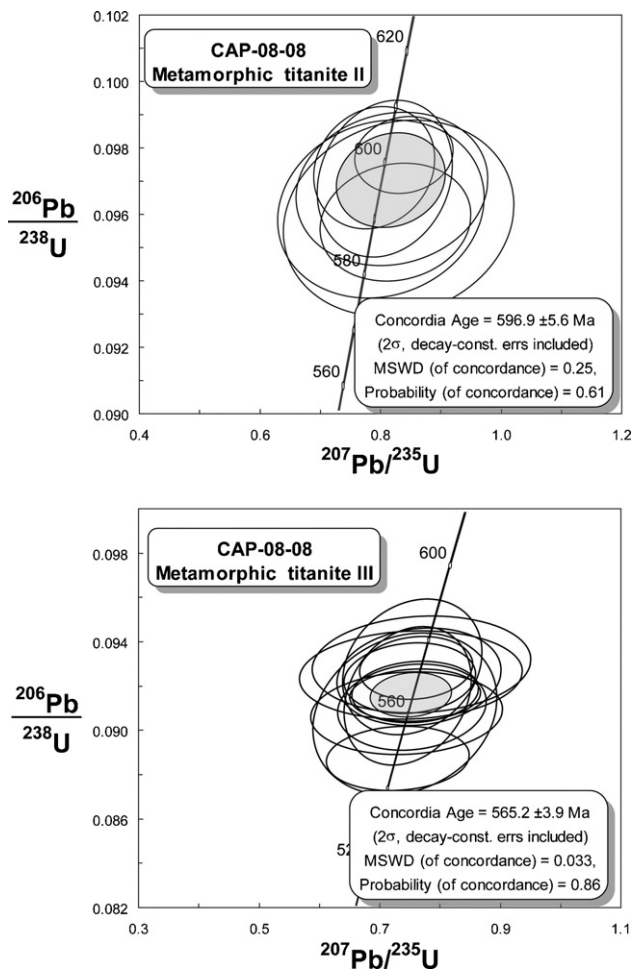


**Fig. 11.** U-Pb LA-MC-ICP-MS titanite results. Concordia diagram for Capivarita Anorthosite (sample CAP-08-08) of two metamorphic titanite phases (titanite II and titanite III).

Silva et al., 2005). A third event (possibly metamorphic or associated with the post-collisional process or even due to the denudation of the Brasiliano Mountains) was dated at  $564 \pm 3.8$  Ma.

These data favor the working hypothesis that the Capivarita Anorthosite and related mafic rocks were generated and positioned during an anorogenic period in the cratonic area at 1.57 Ga, which was situated between the two main orogenesis periods of southern Brazil, the Transamazonian (Paleoproterozoic) and Brasiliano (Neoproterozoic to Eopaleozoic) and represents a period of stabilization for cratonic areas in most of South American Platform. Therefore, the metamorphic ages correspond to the regional metamorphic peak during the collisional event of the Brasiliano Cycle at the margin of the Rio de La Plata Craton ( $\sim 650$  Ma), and the thermal metamorphism corresponds to the generation of late to post-orogenic granites such as Encruzilhada do Sul ( $\sim 600$  Ma). In our case, the Capivarita Anorthosite is a crustal fragment of a stable cratonic area overthrust during the Pan-African-Brasiliano Cycle in the granitic-gneissic terrane situated to the east of the DFB, which is known as the Pelotas Batholith (e.g., Granitic Batholiths in Fig. 1A).

The presence of a Mesoproterozoic crust in the Dom Feliciano Belt is very restricted in Uruguay and southern Brazil (Fig. 1). A-Type Rapakivi granites, such as the Ilescas Granites formed at  $1784 \pm 5$  Ma, were described by Campal and Schipilov (1995) and are exposed in the Nico Perez Terrane, DFB, Uruguay. The Mesoproterozoic ages related to during which the granite-gneissic rocks

formed at  $1063 \pm 37$  Ma in the Punta del Este Terrane (Preciozzi et al., 1999; Basei et al., 2000) are also described for the southernmost portion of the Dom Feliciano Belt. The occurrence of ages between 1.5 and 1.6 Ga in the DFB in Southern Brazil is recorded by detrital zircons in the Metamorphic Porongos Complex, the Neoproterozoic terrane exposed west of the Capivarita Complex (Fig. 1), as shown by Basei et al. (2008). More recently, Gaucher et al. (2010), based on LA-MC-ICP-MS zircon ages, described a volcano-sedimentary sequence deposited between 1.4 and 1.5 Ga exposed in the southernmost part of the DFB (Uruguay) as cratonic cover on the Rio de La Craton.

The 1.5 Ga magmatic age in the domains of the Pan-African-Basílico Belts and Rio de la Plata in southern South America suggest that most of continental areas were stable during the earlier Mesoproterozoic. This stability is probably related to the supercontinent fragmentation, which we can observe from the intraplate magmatism from the 1.57 Ga Capivarita Anorthosite (southern Brazil), 1.5–1.4 Ga Parque UTE and Mina Verdún groups (Nico Perez Terrane, Uruguay) and 1.59 Ga anorogenic mafic dykes in Tandilia, Argentina (Iacumin et al., 2001).

A-type granite gneissic bodies formed from  $1498 \pm 12$  Ma to  $1503 \pm 12$  Ma and are interpreted as an expression of intraplate magmatism based on field relationships and geochemical data. They are also described as part of the exotic Mudorib Complex in the Pan-African Kaoko Belt (Luft et al., 2010), which was tectonically juxtaposed during the Pan-African orogeny (0.65–0.56 Ga) between the continental magmatic arch and passive-margin sediments as well as earlier crustal terranes of the Paleoproterozoic to Archean ages.

The Kunene Complex, in SW Angola contains one the largest anorthosite bodies in the world, which formed in an extensional setting at the margin of the Congo Craton during the early Kibaran Cycle, 1.47–1.32 Ga (Mayer et al., 2004).

The presence of anorthosite bodies of different size at the margin of the Rio de la Plata and Congo Paleoplates as well as records of intraplate-related supracrustal sequences and intrusive granitic bodies, formed mainly in early Mesoproterozoic (Calymian Period), may be therefore the records of the Columbian Supercontinent fragmentation in the West Gondwana.

## 8. Conclusions

The detailed petrographic, mineralogical and isotope data bring new insights into the emplacement and tectono-metamorphic ages of the so-called Capivarita Anorthosite, a crustal fragment from the Neoproterozoic to Early Paleozoic Dom Feliciano Belt, which was amalgamated during the assembly of West Gondwana.

The field relationship, as well the textures and microstructures of the meta-anorthosite and subordinate occurrences of garnet anorthosites, metagabbros and amphibolites, show that these rocks are comagmatic, but metamorphosed under upper amphibolites to granulite facies.

Isotope data obtained by the in situ LA-MC-ICPMS method from zircon grains of the anorthositic lithotype yielded the ages of inherited zircons ( $2028 \pm 17$  Ma), igneous zircons ( $1573 \pm 21$  Ma), and metamorphic zircons ( $606.4 \pm 5.9$  Ma). The igneous zircon Th/U ratios varied from 0.30 to 0.77 and the metamorphic ratios varied from 0.07 to 0.17. The crystallization age of the anorthositic magmatism was confirmed by U-Pb age determination on the igneous titanite from metagabbro and showed a clear cogenetic relationship to the anorthosite. The igneous titanite yielded an age of  $1530 \pm 33$  Ma, which is believed to indicate a cooling age at a temperature of 550–600 °C in the Anorthosite Complex.

Two major metamorphic events were also dated by U-Pb in situ dating of zircon, titanite and baddeleyite. The older one occurred at  $651.5 \pm 8.8$  Ma (titanite), which is already well-constrained in the granitic magmatic arc of the DFB, i.e., the collisional age between the Pelota Batholith (eastern sector of the DFB) and the Metamorphic Porongos Complex (central segment of the DFB). The second regional metamorphism, which is associated with the voluminous intrusion of late to post-orogenic granitic magma in the DFB, is dated at  $\sim 600$  Ma (zircon, titanite and baddeleyite). A third metamorphic age at 0.56 Ga was also found in the titanite grains of amphibolites. This age is believed to be that of the last major tectonic event of the region.

Lu-Hf zircon data provide information regarding the magma provenance of anorthosite and suggested a juvenile source for the melt with some degree of Paleoproterozoic crustal contamination. This interpretation was also confirmed by the Nd model ages of 2.0 Ga and low negative epsilon Nd values ( $-2.0$ ) for  $t = 1.57$  Ga, which is interpreted as contribution of juvenile crust with some Paleoproterozoic crustal components.

The present igneous age of 1.57 Ga for the Capivarita Anorthosite at 1 fits very well within the main epoch of anorthosite generation in the world, i.e., the “Goldilocks” Scenario with records between 0.9 and 1.7 Ga (Morse, 2006). The Capivarita Anorthosite is the first igneous occurrence in the DFB, dated at 1.57 Ga as a crustal fragment generated in intraplate conditions. It was later overthrust to the 0.65–0.59 Ga magmatic arc of the DFB, during assembly of West Gondwana. These crustal bodies can be associated with the fragmentation of an earlier supercontinent, the Columbia Supercontinent (e.g., Rogers and Santosh, 2002), before the block's accretion during the Grenville orogeny to form the supercontinent Rodinia.

## Acknowledgements

Field research was supported by CAPES-COFECUB project to MLLF. Laboratory expenses were funded by CNPq (Conselho Nacional de Desenvolvimento Científico e Tecnológico) – Project # 310593/2006-9 to FCJ. We thank the technicians Fabrício Vieira dos Santos, Sandra Anderson Machado and Maurício Dias Souza for helping in the sample preparation.

## Appendix A. Supplementary data

Supplementary data associated with this article can be found, in the online version, at doi:10.1016/j.precamres.2011.01.005.

## References

- Babinski, M., Chemale Jr., F., Hartmann, L.A., Van Schmus, W.R., Silva, L.C., 1996. Juvenile accretion at 750–700 Ma in southern Brazil. Geology 24 (5), 439–442.
- Babinski, M., Chemale Jr., F., Van Schmus, W.R., Hartmann, L.A., Silva, L.C., 1997. U-Pb and Sm-Nd geochronology of the Neoproterozoic granitic-gneissic Dom Feliciano Belt, Southern Brazil. J. S. Am. Earth Sci. 10 (3–4), 263–274.
- Basei, M.A.S., Siga Jr., O., Masquelin, H., Harara, O.M., Reis Neto, J.M., Preciozzi FP, F.P., 2000. The Dom Feliciano Belt and the Rio de la Plata Craton: tectonic evolution and correlation with similar provinces of southwestern Africa. In: Cordani, U.G., Milani, E.J., Thomas Filho, A., Campos, D.A. (Eds.), Proceedings of the 31st International Geological Congress on The Tectonic Evolution of South America. Rio de Janeiro, pp. 311–334.
- Basei, M. A. S., Frimmel, H. E., Nutman, A. P. and Preciozzi, F., 2008. West Gondwana amalgamation based on detrital zircon ages from Neoproterozoic Ribeira and Dom Feliciano belts of South American and comparison with coeval sequences from SW Africa. In: Pankhurst, R.J., Trouw, R.A.J., Brito Neves, B.B. and de Wit, M.J. West Gondwana: pre-Cenozoic correlations across the South Atlantic Region, Geol. Soc. of London, Sp.Pub. 204, pp. 239–256.
- Blichert-Toft, J., Albarède, F., 1997. The Lu-Hf isotope geochemistry of chondrites and the evolution of the mantle–crust system. Earth and Planetary Science Letters 148, 243–258.
- Bodet, F., Schärer, U., 2000. Evolution of the SE Asian continent from U-Pb and Hf isotopes in single grains of zircon and baddeleyite from large rivers. Geochimica et Cosmochimica Acta 64, 2067–2091.

- Bogdanova, S.V., Pashkevic, I.K., Buryanov, V.B., Makarenko, I.B., Orliuk, M.I., Skobelev, V.M., Starostenko, V.I., Legostaeva, O.V., 2004. Tectonophysics 381 (1–4), 5–27.
- Bossi, J., Ferrando, L., Montaña, J., Campal, N., Morales, H., Gancio, F., Schipilov, A., Piñeyro, D., Sprechmann, P., 1998. Carta geológica del Uruguay. In: Escala 1:500.000. Geeditores, Montevideo.
- Butcher, K., Frey, M., 1994. Petrogenesis of Metamorphic Rocks. Springer-Verlag, Berlin, p. 317.
- Campal, N., Schipilov, A., 1995. The Illescas bluish-quartzrapakivi granite (Uruguay-South America): Some geological features. In: Symposium on Rapakivi Granites and related rocks, Belem, Brazil.
- Chemale Jr., F., 2000. Evolução Geológica do Escudo Sul-rio-grandense. In: Holz, M., De Ros, L.F. (Eds.), Geologia do Rio Grande do Sul. CIGO, Porto Alegre, pp. 13–52.
- Chemale Jr., F., Hartmann, L.A., Silva, L.C., 1995. Stratigraphy and Tectonism of the Brasiliano Cycle in Southern Brazil. In: Communication of Geological Survey Namibia, vol. 10, pp. 151–166.
- Duschene, J.C., Auwera, J.V., Liégeois, J.P., Barton, E.S., Clifford, T.N., 2007. Geochemical constraints of the petrogenesis of the O'okiep Koperberg Suite and granitic plutons in Namaqualand South Africa: a crustal source in Namaquan (Grenville) times. Precambrian Res. 153 (1–2), 116–142.
- Dröppel, K., Littmann, S., Romer, R.L., Okrusch, M., 2007. Petrology and isotope geochemistry of the Mesoproterozoic anorthosite and related rocks of Kunene Complex, NW Namibia. Precambrian Res. 156 (1–2), 1–31.
- Fernandes, L.A.D., Tommasi, A., Porcher, C.C., 1990. Esboço estrutural de parte do Batólito de Pelotas—região de Quitéria-Capivarita. Acta Geol. Leopoldina 13, 117–138.
- Fernandes, L.A.D., Tommasi, A.D., Porcher, C.C., 1992. Deformation patterns in the southern Brazilian branch of the Dom Feliciano Belt: A reappraisal. J. S. Am. Earth Sci. 5 (1), 77–96.
- Fernandes, L.A., Tommasi, A., Porcher, C.C., Marques-Toigo, M., Guerra-Sommer, M., Piccoli, A.M., 1988. Mapa Geológico 1:50.000 de Parte Das Folhas Quitéria e Várzea do Capivarita. Instituto de Geociências, UFRGS, Porto Alegre.
- Formoso, M.L.L., 1973. Geologia da folha Capivarita—RS, Anorthosito de Capivarita. Ph.D. Thesis. Instituto de Geociências, Universidade de São Paulo, São Paulo, p. 215.
- Formoso, M.L.L., Carraro, C.C., 1968. Anorthosito de Capivarita, Rio Pardo RS. In: Anais da Academia Brasileira de Ciências, vol. 40, pp. 361–372.
- Gaucher, C., Frei, R., Chemale Jr., F., Frei, D., Bossi, J., Martínez, G., Chiglino, L., Ceruschi, F., 2010. Mesoproterozoic evolution of the Río de la Plata Craton in Uruguay: at the heart of Rodinia? Int. J. Earth Sci., doi:10.1007/s00531-010-0562-x.
- Geringer, G.J., Schoch, A.E., Sukanov, M., Zhuravlev, D., 1998. Geochemical and isotopic characteristics of different types of anorthosite in the Namaqua mobile belt, South Africa. Chem. Geol. 145, 17–46.
- Gross, A.O.M.S., Porcher, C.C., Fernandes, L.A.D., Koester, E., 2006. Neoproterozoic low-pressure/high temperature collisional metamorphic evolution in the Várzea do Capivarita Metamorphic Suite, SE, Brazil: Thermobarometric and Sm/Nd evidence. Precambrian Res. 147, 41–64.
- Hartmann, L.A., Leite, J.A.D., Silva, L.C., Remus, M.V.D., McNaughton, N.J., Groves, D.I., Fletcher, I.R., Santos, J.O.S., Vasconcellos, M.A.Z., 2000. Advances in SHRIMP geochronology and their impact on understanding the tectonic and metallogenetic evolution of southern Brazil. Aust. J. Earth Sci. 47, 829–843.
- Hartmann, L.A., Campal, N., Santos, J.O.S., McNaughton, N.J., Bossi, J., Schipilov, A., Lafon, J.-M., 2001. Archean crust in the Río de la Plata Craton, Uruguay—SHRIMP U-Pb zircon reconnaissance geochronology. J. S. Am. Earth Sci. 14, 557–570.
- Heather, D.J., Dunkin, S.K., 2003. Geology and stratigraphy of King crater, lunar farside. Icarus 163 (2), 307–329.
- Iacumin, M., Piccirillo, E.M., Girardi, V.A.V., Teixeira, W., Bellieni, G., Echeveste, H., Fernández, R., Pinesi, J.P.P., Ribot, A., 2001. Early Proterozoic calc-alkaline and middle proterozoic tholeiitic dyke swarms from central eastern Argentina: Petrology, Geochemistry, Sr-Nd isotopes and tectonic implications. J. Petrol. 42 (11), 2109–2143.
- Kruger, F.J., Geringer, G.J., Havenga, A.T., 2000. The geology, petrology, geochronology and source region character of the layered gabbroitic Oranjekom Complex in the Kibaran Namaqua mobile belt, South Africa. J. Afr. Earth Sci. 30 (3), 675–687.
- Leite, J.A.D., Hartmann, L.A., McNaughton, N.J., Chemale Jr., F., 1998. SHRIMP U/Pb zircon geochronology of Neoproterozoic juvenile and crustal reworked terranes in southernmost Brazil. Int. Geol. Rev. 40, 688–705.
- Leite, J.A.D., Hartmann, L.A., Fernandes, L.A.D., McNaughton, N.J., Soliani, E., Koester, E., Santos, J.O.S., Vasconcellos, M.A.Z., 2000. Zircon U/Pb SHRIMP dating of gneissic basement of the Dom Feliciano Belt, southernmost Brazil. J. S. Am. Earth Sci. 13, 739–750.
- Luft, J.L., Chemale Jr., F., Armstrong, R., 2010. Evidence of 1.7 to 1.8 Ga Collisional Arc in the Kaoko Belt, NW Namibia. Int. J. Earth Sci., doi:10.1007/s00531-010-0591-5.
- Mayer, A., Hoffmann, A.W., Sinigoi, S., Morais, E., 2004. Mesoproterozoic Sm–Nd and U–Pb ages for the Kunene Anorthosite Complex of SW Angola. Precambrian Res. 133 (3–4), 187–206.
- Mallmann, G., Chemale Jr., F., Ávila, J.N., Kawashita, K., Armstrong, R.A., 2007. Isotope geochemistry and geochronology of the Nico Pérez Terrane, Río de La Plata Craton, Uruguay. Gondwana Res. 12, 489–508.
- Morse, S.A., 2006. Labrador massif anorthosites: chasins the liquids and their sources. Lithos 89 (1–2), 202–221.
- Mukherjee, D., Das, S., 2002. Anorthosites, granulites and supercontinent cycle. Gondwana Res. 5 (1), 147–156.
- Passarelli, C.R., Basei, M.A.S., Siga, O., Mc Reath, I., Neto, M.D.C., 2010. Deformation and geochronology of syntectonic granitoids emplaced in the Major Gercino Shear Zone, southeastern South America. Gondwana Res. 17 (4), 688–703.
- Philipp, R.P., Machado, R., 2005. The late Neoproterozoic granitoid magmatism of the Pelotas Batholith, southern Brazil. J. S. Am. Earth Sci. 19 (4), 461–478.
- Philipp, R.P., Formoso, M.L.L., Dussin, I., Chemale Jr., F., Campos, R.S., in press. Estruturas primárias e tectônicas do Anortosito Capivarita, Pântano Grande, RS: significado e implicações para o entendimento da evolução petrológica. Revista Brasileira de Geociências.
- Preciozzi et al., Preciozzi, F., Masquelin, H. and Basei, M.A.S., 1999. The Namaqua/Grenville terrane of eastern Uruguay. In: II South American Symp. on Isotope Geology, Actas. Córdoba (Argentina), pp. 338–340.
- Ramgrab, G.E., Wildner, W., Camozzato, E., 1993. Porto Alegre—Folha SH.22-Y-B. Estado do Rio Grande do Sul. Escala 1:250.000. Programa de Levantamentos Geológicos Básicos do Brasil. CPRM, Brasília, p. 200.
- Ribeiro et al., Ribeiro, M., Bocchi, P.R., Figueiredo, F.P., Tessari, R.I., 1966. Geologia da Quadrícula de Caçapava do Sul. RGS. DNPM/DFPM, Rio de Janeiro, Boletim 127, p. 232.
- Rogers, J.J.W., Santosh, M., 2002. Configuration of Columbia, a Mesoproterozoic Supercontinent. Gondwana Res. 5 (1), 5–22.
- Scherer, E., Munker, C., Mezger, K., 2001. Calibration of the lutetium-hafnium clock. Science 293, 683–687.
- Silva, L.C., McNaughton, N.J., Armstrong, R., Hartmann, L.A., Fletcher, I.R., 2005. The Neoproterozoic Mantiqueira Province and its African connections: a zircon-based U–Pb geochronologic subdivision of the Brasiliano/Pan-African systems of orogens. Precambrian Res. 136, 203–240.
- Takeda, H., Yamaguchi, A., Bogard, D.D., Karouji, Y., Ebihara, M., Ohtake, M., Saiki, K., Arai, T., 2006. Magnesian anorthosites and a deep crustal rock from the farside crust of the moon. Earth Planet. Sci. Lett. 247 (3–4), 171–184.
- Teixeira, W., 1982. Folhas SH.22–Porto Alegre, SI.22–Lagoa Mirim e SH.21–Uruguaiana. Interpretação dos dados radiométricos e evolução geocronológica. Florianópolis, Projeto RADAMBRASIL, Internal report.
- Tessari, R.I., Picada, R.S., 1966. Geologia da quadrícula de Encruzilhada do Sul, RS, Brasil. DNPM/DFPM, Rio de Janeiro. Boletim 124, 1–147.
- Wilson, M., Overgaard, G., 2005. Relationship between the layered series and overlying evolved rocks in the Bjerkreim–Sokndal Intrusion, southern Norway. Lithos 83 (3–4), 277–298.
- Zhai, M., Liu, W., 2003. Paleoproterozoic tectonic history of North China craton: a review. Precambrian Res. 122 (1–4), 183–199.
- Zhao, G., Sun, M., Wilde, S.M., Sanzhong, L., 2004. A Paleo-mesoproterozoic supercontinent: assembly, growth and break-up. Earth Sci. Rev. 67 (1–2), 91–123.